UNIVERSIDAD DE CHILE
FACULTAD DE CIENCIAS FíSICAS Y MATEMÁTICAS
DEPARTAMENTO DE INGENIERÍA ELÉCTRICA

FINITE-TIME COOPERATIVE CONTROL STRATEGIES FOR THE ECONOMIC OPERATION OF HYBRID AC/DC MICROGRIDS

TESIS PARA OPTAR AL GRADO DE DOCTOR EN INGENIERÍA ELÉCTRICA
EN COTUTELA CON LA UNIVERSIDAD DE NOTTINGHAM

MANUEL DARÍO MARTÍNEZ GÓMEZ

PROFESOR GUÍA:
MARCOS ORCHARD CONCHA

PROFESOR CO-GUÍA:
SERHIY BOZHKO

MIEMBROS DE LA COMISIÓN:
CÉSAR SILVA JIMÉNEZ
MARCO RIVERA ABARCA
PATRICIO MENDOZA ARAYA

Este trabajo ha sido parcialmente financiado por ANID/Doctorado Nacional 2019-21191757

SANTIAGO DE CHILE
2023

RESUMEN DE LA TESIS PARA OPTAR
AL GRADO DE DOCTOR EN INGENIERÍA ELÉCTRICA
POR: MANUEL DARÍO MARTÍNEZ GÓMEZ
FECHA: 2023
PROFESOR GUÍA: MARCOS ORCHARD CONCHA
PROFESOR CO-GUÍA: SERHIY BOZHKO

ESTRATEGIAS DE CONTROL COOPERATIVO EN TIEMPO FINITO PARA LA OPERACIÓN ECONÓMICA DE MICRO-REDES HÍBRIDAS AC/DC

Este trabajo desarrolla una estrategia de control distribuido que garantice una operación óptima y estable de múltiples micro-redes híbridas AC/DC interconectadas. El enfoque de aplicación se encuentra en la operación aislada de micro-redes en baja tensión con equipos generadores distribuidos (DGs) de energía renovable con conversores de potencia. Para la interconexión entre micro-redes, se emplean conversores de interconexión (ILCs). El sistema estudiado se divide en partes correlativas a capítulos: (i) micro-red AC/DC con un ILC, (ii) micro-red AC/DC con un clúster de ILCs, y (iii) multi-micro-red AC/DC con clústeres de ILCs. El esquema de control propuesto en cada caso es distribuido y cooperativo y se implementa en base a una formulación del despacho económico óptimo. Los diseños son compatibles con las acciones de control secundario y terciario mientras incorporan algoritmos de tiempo finito para mejorar convergencia y desacoplamientos. Además, se proponen controladores multipropósito que permitan resguardar la operación saturada de micro-redes, balancear la potencia entre ILCs en un mismo clúster, y evitar la operación saturada de clústeres de ILCs. Los resultados experimentales y de simulación muestran una adecuada respuesta de los controladores propuestos permitiendo cumplir los objetivos de control simultáneamente de acuerdo a la priorización asignada.

RESUMEN DE LA TESIS PARA OPTAR
AL GRADO DE DOCTOR EN INGENIERÍA ELÉCTRICA
POR: MANUEL DARÍO MARTÍNEZ GÓMEZ
FECHA: 2023
PROFESOR GUÍA: MARCOS ORCHARD CONCHA
PROFESOR CO-GUÍA: SERHIY BOZHKO

FINITE-TIME COOPERATIVE CONTROL STRATEGIES FOR THE ECONOMIC OPERATION OF HYBRID AC/DC MICROGRIDS

This work develops a distributed control strategy that guarantees optimal and stable operation of multiple interconnected hybrid AC/DC microgrids. The strategy's application focuses on the isolated operation of low-voltage microgrids with distributed generators of renewable energy sources with power converters. For the interconnection between microgrids, interlinking converters (ILCs) are used. The studied system is divided into parts correlative to chapters: (i) AC/DC microgrid with an ILC, (ii) AC/DC microgrid with a cluster of ILCs, and (iii) AC/DC multi-microgrid with clusters of ILCs. The control scheme proposed in each case is distributed and cooperative and is implemented based on a formulation of the optimal economic dispatch. The designs are compatible with the secondary and tertiary control actions while incorporating finite-time algorithms to improve convergence and decoupling. In addition, multipurpose controllers are proposed that allow safeguarding the saturated operation of microgrids, balancing the power between ILCs in the same cluster, and avoiding the saturated operation of clusters of ILCs. The experimental and simulation results show an adequate response of the proposed controllers, allowing them to meet the control objectives simultaneously according to the assigned prioritisation.

Dedicado especialmente a mi gran hermano, quien me brinda una eterna compañía, a mi mamá, quien me ha entregado todo lo necesario para salir adelante, siempre, y a mi papá, quien desde arriba me ayuda y ve orgulloso como avanzo en esta etapa de mi vida. Gracias

Acknowledgements

I would like to special thank my two supervisors, Prof. Marcos Orchard and Prof. Serhiy Bozhko. Despite the short time that I spent with you, both gave me the confidence and courage to address the advancement of this PhD project.

In addition, I would like to acknowledge the help that I received from the research groups where I participated during the different stages of my PhD. I should start by thanking Enrique Espina and Prof. Roberto Cardenas, who received me and gave me the first guidelines regarding microgrid systems at the University of Chile. Then, I appreciate the support received from my senior PhD mates, Claudio Burgos, Juan Sebastián Gómez and Jacqueline Llanos. I shall not forget to mention the long conversations and mutual support offered by my former laboratory mates, Alex Navas and Erwin Rute. I also would like to thank the PEMC group at the University of Nottingham, who brought me a warm welcome and an unforgettable stay.

I thank my family who were always there for me: my mother Alba and brother Pablo, as well as my partner, Macarena. Finally, I kindly appreciate the pieces of advice received from my friend Prof. Manuel Manriquez.

Table of Content

List of Figures

List of Tables

List of Abbreviations

BESS	Battery Energy Storage System
DAPI	Distributed Averaging Proportional-Integral
DG	Distributed Generator
DNO	Distributed Network Operator
EMS	Energy Management System
ESS	Energy Storage System
IC	Incremental Cost
ILC	Interlinking Converter
LV	Low Voltage
MAS	Multi-Agent System
MG	Microgrid
PI	Proportional-Integral
PLL	Phase-Locked-Loop
RES	Renewable Energy Source
SoC	State-of-Charge
VSC	Voltage-Source Converter

Chapter 1

Introduction

The rapid expansion of small-scale renewable energy sources (RESs), as well as environmental concerns and economic factors, are driving a paradigm shift in power generation. In such a scenario, the traditional centralised electrical system will tend to integrate new modular groups of generation and load, so-called Microgrids (MGs) [5]. Inside MGs, the RESs are placed near the consumption and controlled locally — being known as Distributed Generators (DGs). MGs are defined as autonomous power networks, which can operate either connected or disconnected from the utility grid [6]; the autonomy of MGs is a desirable feature for future networks due to the fact that it improves the reliability of the system in case of failures in the grid-side. In general, MGs comprise a mixture of synchronous generators and voltage-source converters (VSC). Also, the MG infrastructure can be classified as AC, DC, and AC/DC. MGs could be interconnected, so there is flexibility in the implementation, which can adapt to any existing and required topology. The operation of an interconnected AC/DC MG is possible due to an Interlinking Converter (ILC), which allows energy transfer between AC and DC sides.

Regarding the applications, the hybrid AC/DC MG is a promising topology for the energisation of remote/rural communities as well as high-power industrial processes — both being Low-Voltage (LV) MGs, in general. Naturally, AC/DC MGs combine the advantages of both AC and DC MGs, by re-utilising most of the existing AC infrastructure while lowering the overall costs. The additional DC-side network is used to interface DC-based RESs with Energy Storage Systems (ESSs), reducing energy conversion steps in the process [7]. Additionally, the ILCs in the system can perform grid support features such as economic management [8] and AC unbalanced compensation [9].

In this line of development, new topologies, called meshed AC/DC multi-MG are commencing to rise. This kind of topology represents the generalisation of MGs implementations and enhances their flexibility, robustness, and energy management. Particularly, this thesis addresses the meshed AC/DC multi-MG with multiple ILCs for the interconnection between

the MGs. In this topology, clusters of ILCs are formed to provide different paths for the power flow, which improves the reliability of the system but increases its complexity.

Despite the benefits that AC/DC MGs could potentially have, the coordination between AC and DC subgrids adds a new challenge. For the islanded operation, complex control strategies are required for the DGs to cooperate, and simultaneously ensure an appropriate power-sharing for the entire multi-MG system, considering frequency and voltage restoration, as well as economic and operational constraints. Also, in order to guarantee the former, a communication scheme is mandatory; this carries additional obstacles that should be studied thoroughly for successful implementations.

First attempts in the control of AC/DC MGs mainly focus on decentralised algorithms [7, 10,11]. However, in that kind of approach, the AC and DC controllers are designed separately, and the economic dispatch cannot be implemented. The economic dispatch problem in MGs can be solved centralised as a result of an optimisation problem [12] but being susceptible to single-point failure, reducing the reliability of the system to undesirable levels. As an alternative solution, researchers have studied distributed control strategies for the economic dispatch in AC/DC MGs [13, 14] — The distributed control strategies are difficult to design but can achieve an adequate trade-off between performance and reliability.

Motivated by the above, in this thesis proposal, the main issues related to the control of LV converter-based islanded AC/DC multi-MGs are addressed, and novel control strategies for the economic dispatch are proposed based on the cooperative control of multi-agent systems (MAS) [15]. In the proposal, the power-sharing of DGs is regulated according to the MG's incremental cost (IC), which is obtained by shared information from neighbours. The ICs of AC and DC MGs are synchronised through ILCs inside the communication topology. Each ILC includes an average power compensation term to perform a multi-objective control. Overall, the control over DGs and ILCs is performed by means of finite-time protocols and observer-based dynamics. This scheme allows efficient compensation for achieving the economic dispatch without extensive communication infrastructure while operating on the same time scale as conventional secondary control.

1.1 Problem Statement

Multi-MGs are a flexible and promising solution for the transition of electrical power systems towards smart grids. Applied in this context, the MGs are expected to cope with specific challenges related to the flexible integration of DGs and the efficient use of RESs. In terms of implementation, meshed hybrid AC/DC multi-MGs with multiple clusters of ILC are a flexible and scalable solution, but are particularly complex to realise in isolated conditions. Among the main difficulties observed in the control of this kind of MGs for residential/industrial usage are the high stochasticity of loads and a reduced power capacity per DG. Therefore the DGs inherently require an adequate power flow between subgrids, allowing them to fulfil the demanded power while respecting operational and economical constraints. For these reasons, a detailed discussion about relevant problems in the islanded operation of

AC/DC MGs is made as follows:

1.1.1 Safety and economic operation in AC/DC MGs

Current trends in the control of ILCs mainly focus on decentralised algorithms [11,16], where normalised droop curves guide the power to be transferred by the ILC [10]. For example, in [17], a decentralised economic dispatch is proposed incorporating DGs and the ILC, but the droop curves of every DG need to be changed to cost-based curves, which is not practical in most situations since it requires knowledge of the maximum IC of a DG in the MG. In addition, the majority of works on decentralised control concentrate their efforts on separately developing the secondary control on each side (AC and DC) regardless of the ILC, which may lead to an inaccurate power distribution [18]. As a result, these approaches cannot guarantee an economically optimal operation since the ILC disown the IC of the DGs. Also, decentralised approaches could not guarantee the optimal operation since inequality constraints are implicit and the Karush-Kuhn Tucker conditions may not be met [19,20].

Another restriction that should be considered in economic dispatch in AC/DC MGs is to regulate the average power between MGs. Achieving an equal IC usually disturbs the power balance objective. This may cause the saturation of a MG since the average power generated in one side MG may be greatly different from the other side MG. Particularly, this issue is present in AC/DC MGs with a high-capacity ILC (or group of ILCs), emphasised when the IC greatly differs from one MG to another. A common reason for λ variation is the regulation of SoC in BESSs-based DGs; Another source of changes in the IC values is the market price for energy; In the grid-connected operation of one MG, the MG might buy energy depending on the availability of its RESs and consumption profile [12,21], changing the MG IC dramatically. Therefore, the average power regulation must be considered to avoid MG saturations, potential line congestions and extend the useful life of assets. To the best of the author's knowledge, there are no works reported in the literature that take into account ICs and average power for the ILC.

Regarding the power distribution, some studies have little addressed the effects of the secondary control over AC/DC MGs in literature [8,14,16,18,22,23]. Works such as [18,23,24] have proposed distributed control strategies for the power transfer between AC and DC MGs through the ILC. In [25], the economic dispatch is developed by means of an auxiliary variable consensus, which implements secondary control actions to the ILC. However, the implementation of this strategy is not trivial since cost-based droop curves are required for every DG. In [14], a unified distributed IC strategy for single AC/DC MGs is performed, however sufficient conditions for stability and the parameters design are not provided. Also, this work does not validate the strategy experimentally. Overall, available distributed control schemes are still unattractive given the limited functionality that they bring to the operation of the ILC at the cost of investing in communication lines.

1.1.2 Coordination of ILCs in an AC/DC MG under economic dispatch

For achieving an optimal operation, all the ILCs need to know the state of the other ILCs in the system to balance the power transfers. This is seamlessly achieved by means of centralised control or full-connected graphs. However, the cost of investing in new communication lines is prohibitive in real-world applications; mainly due to distances and amount of communication links. To solve this, decentralised control has been proposed to deal with the coordination of ILCs in a cluster [26, 27], however, this solution relied on steady-state deviations of voltage and frequency variables to operate. A hybrid solution using decentralised control with an upper-level centralised control is proposed in [28], improving resiliency compared with pure centralised approaches, but inheriting the disadvantages of centralised control.

Recent literature has proposed distributed control for the coordination of ILCs. In [29], a consensus algorithm is applied to ensure a power balance of droop-based ILCs, in the proposal a load condition estimation is fed to a leader ILC unit whereas the followers synchronise their power ratings. Later, [30] proposed a control law that simultaneously achieves a power-sharing of the subgrids and the ILC cluster by using a two-term consensus protocol; an enlarged communication matrix is created to this end. However, previous developments do not provide accurate measurements during transient states. Furthermore, a control solution is required by which the power balancing between ILCs in a cluster could be performed without affecting the IC consensus.

1.1.3 Coordination of DGs and ILCs in an AC/DC multi-MG

Control over interconnected MGs implies a high level of coordination between the DGs that it comprises, involving greater implementation difficulties compared to single AC/DC MGs. Specifically for multi-MG AC/DC interconnected by ILCs, the literature has proposed some solutions based on control by droop curves [31]. Purely decentralised control strategies, as in [31], are possible to realise, however, they are dependent on voltage or frequency deviations. This kind of solution is not attractive since errors are induced by the restoration of these variables to nominal values (secondary control). Moreover, a decentralised control scheme is not acceptable for a system that wants to have the ability to interconnect with the power grid.

Complementary to the above, in works such as [24, 32–34] researchers proposed a combined droop control with a distributed control layer for AC/DC multi-MGs. In [32], the authors realise a PI control over the difference of voltage and frequency deviations measured against weighted received measurements from neighbours. However, this control scheme requires knowledge of the number of ILCs to yield, so variations in this number may cause inappropriate behaviour. In [24], a power-sharing is realised by using a consensus protocol of errors of MG power measurements sent to each ILC. In [33], a similar algorithm to [24] is proposed but enlarged. A robust controller that incorporates secondary control variables is used for simultaneous restoration and power-sharing; in this approach, the ILCs participate in the secondary control regulation of the AC side. The authors in [33] proposed a consensus of ICs performed by the ILCs. In this work, authors communicate each ILC link (cluster)

to share local error estimations obtained by the difference between ICs variables from the subgrids. Nonetheless, this and all the previous strategies discussed in this paragraph are limited to single ILCs by cluster.

Combining the aforementioned problems, this thesis proposes a distributed finite-time control combining actions of DGs and ILC to coordinate a global IC. The hypotheses, objectives, and methodology are presented below.

1.2 Hypotheses

The proposed hypotheses which sustain the development of this thesis are the following:

(i) The global economic operation of a single AC/DC MG can be obtained by applying a distributed controller of IC variables received from interconnected MGs into the ILC. Also, a consensus of observed average MG powers can be included in the strategy to compound a multi-objective control algorithm, capable of equalising the ICs and safeguarding saturation/congestion of MGs. The regulation between control objectives can be realised by arbitrary or adaptive weights.

(ii) The global economic operation of an AC/DC multi-MG with clusters of ILCs can be obtained without directly communicating the clusters of ILCs. Furthermore, a control strategy can be constructed by incorporating additional control goals creating a multi-objective control that simultaneously allows the equalising of ICs between subgrids, and power balancing between ILCs in a cluster while avoiding (whenever possible) the saturation of any subgrid or ILC.

(iii) The consensus between clusters of ILCs can be established as an operational constraint to regulate the power flow in a meshed AC/DC multi-MG. In order to apply this control action, trade-off weights can be assigned in a consensus of the average power of ILC clusters to adjust the ILC's power reference.

(iv) The application of finite-time algorithms in the distributed controllers of the ILCs achieves the global economic dispatch in a finite number of steps. In particular, there exists a Lyapunov-Krasovskii candidate for the ILC dynamics that guarantees finite-time stability.

1.3 Objectives

1.3.1 General objective

The main objective of this doctoral thesis is to propose, design, analyse and validate a novel distributed control strategy for the economic operation of isolated AC/DC multi-MGs considering the fulfilment of defined power saturation constraints. The proposed control strategy will be able to coordinate the ILCs and clusters of ILCs reducing the investments of dedicated/additional communication links.

1.3.2 Specific objectives

Within the framework of this work, the following specific objectives are proposed:

(i) To analyse and discuss the control methods proposed in the literature through an extensive review. Special attention is focused on AC/DC MGs, distributed control and its application to MGs. Comparisons are made regarding the proposed method of this thesis.

(ii) To design a distributed finite-time control strategy for the ILC that guarantees optimal power-sharing and a reliable operation of AC/DC MGs.

(iii) To design a distributed finite-time control strategy for the ILC that guarantees optimal power-sharing, coordination with other ILCs and a reliable operation of a AC/DC multi-MG.

(iv) To validate via simulations, in terms of dynamic response and power-sharing, the performance of the proposed controllers.

(v) To build an experimental prototype of a hybrid AC/DC MG for validating the proposed controllers. Specifically, the construction of a DC MG setup and a reconfiguration of existing AC MG infrastructure.

1.4 Main Contributions

The contributions of this thesis are as follows:

(i) A novel distributed finite-time control in the ILC for the economic dispatch of hybrid AC/DC MGs. The proposed strategy combines the consensus of ICs and average MG powers to add flexibility to the ILC, avoiding saturation, and then operation outside safety limits, of interfaced MGs. A Lyapunov-Krasovskii candidate is derived that ensures the finite-time convergence of the proposed controller in the AC/DC MG.

(ii) A distributed dynamic average consensus protocol for the ILC power-sharing in an AC/DC MG with multiple ILCs is developed. The proposed controller achieves the synchronisation of powers while providing an alternative source for local power estimations. An estimation methodology for the total power transferred by the ILC cluster is suggested as well as an estimation for the local ILC power. Also, a novel anti-windup is proposed to reduce the steady-state errors of the control scheme under communication delays.

(iii) A distributed control scheme for the economic dispatch in meshed AC/DC multi-MGs is presented. The proposal achieves the global economic dispatch using local information of ILCs, so it does not rely on direct communications between ILC clusters. Also, power operational constraints of DGs, MGs, ILCs and clusters of ILCs are included using some communication channels to create a multi-purpose and multi-objective control. It is demonstrated that trade-off weights can adjust the prioritisation to avoid the saturation of MGs or clusters of ILCs.

1.4.1 Journal publications extracted from the thesis

(1) **Martínez-Gómez, M.**, Orchard, M., Bozhko, S. "Dynamic Average Consensus for Power Balancing of a Cluster of Interlinking Converters in AC/DC Microgrids under Economic Dispatch and Delays" (2023). IEEE Transactions on Smart Grid, 14, 5, pp. 4137-4140. (*from Chapter 4*).

(2) **Martínez-Gómez, M.**, Navas, A., Orchard, M., Bozhko, S., Burgos-Mellado, C., Cardenas, R. "Multi-Objective Finite-Time Control for the Interlinking Converter on Hybrid AC/DC Microgrids" (2021). IEEE Access, 9, pp. 116183 - 116193. (*from Chapter 3*).

(3) Espina, E., Llanos, J., Burgos-Mellado, C., Cárdenas, R., **Martínez-Gómez, M.**, Sáez, D. "Distributed control strategies for microgrids: An overview" (2020). IEEE Access, 8, pp. 193412-193448. (*from Chapter 2*).

1.4.2 Journal publications related to this thesis

(4) **Martínez-Gómez, M.**, Burgos-Mellado, C., Morales-Paredes, H., Gómez, J., Verma, A., Bonaldo, J. "Distributed Control Scheme for Clusters of Power Quality Compensators in Grid-Tied AC Microgrids" (2023). Sustainability, 15, 22, art. no. 15698.

1.4.3 Conference publications extracted from the thesis

(1) **Martínez-Gómez, M.**, Burgos-Mellado, C., Cardenas, R. "Distributed Control for a Cost-based Droop-free Microgrid" (2020). IEEE 21st Workshop on Control and Modeling for Power Electronics, COMPEL 2020, art. no. 9265722.

(2) **Martínez-Gómez, M.**, Cardenas, R., Navas, A., Rute, E. "A Multi-Objective Distributed Finite-Time Optimal Dispatch of Hybrid Microgrids" (2020). 46th Annual Conference of the IEEE Industrial Electronics Society, IECON 2020, art. no. 9254375, pp. 3755-3760.

(3) **Martínez-Gómez, M.**, Cardenas, R. "Finite-Time Second-Order Cooperative Control for the Economic Dispatch in DC Microgrids" (2020). 46th Annual Conference of the IEEE Industrial Electronics Society, IECON 2020, art. no. 9254353, pp. 1596-1601.

(4) Espina, E., Burgos-Mellado, C., Gomez, J.S., Llanos, J., Rute, E., Navas, A., **Martínez-Gómez, M.**, Cardenas, R., Saez, D. "Experimental Hybrid AC/DC-Microgrid Prototype for Laboratory Research" (2020). 22nd European Conference on Power Electronics and Applications, EPE ECCE 2020, art. no. 9215751.

1.4.4 Incoming publications

A list of pending/incoming publications related to this thesis is presented next.

- "Distributed Coordination for the Economic Dispatch in Hybrid and Meshed Multi-Microgrids" (2024). in preparation.

- "Small-Signal Modelling for the Evaluation of Distributed Control Strategies on Hybrid AC/DC Microgrids" (2024). in preparation.

1.5 Research Method

The thesis uses a quantitative methodology, based on data collection —through simulations and experimental development— and analysis of these through their waveforms. In addition, the employed methodology uses common elements of the automatic control area, such as the theoretical verification of convergence and stability. In particular, the methodology of this thesis subdivides the development into different MG topologies, which cumulatively converge finally in a complex multi-MG topology (which is of most interest to study). At each stage of methodological development, similar techniques are used to perform modelling, convergence testing, stability study, and simulation validation. In the modelling used for convergence and stability tests, a mathematical modelling of the dynamics associated with both the communications infrastructure and the electrical system that make up the studied MG topologies has been followed.

The methodology used by this thesis sustains its form thanks to the work carried out by other scientific documents of interest in the area, such as [13,35–38]. In these references, the mathematical modelling that is closely related to the MG topology predominates. In [35,37], the microgrid is modelled from its basic components, including the internal dynamics of the power converters that are assumed to make up the distributed generation sources. In these works, the rotating reference frame (or RRF) axis transformation is incorporated into the modelling, which is a fundamental step to be able to study the dynamic behaviour of a system of parallel operation of multiple generators, since these must be synchronised.

Although both works differ slightly in the way of performing the linearisation, they provide some insights into how to analyse the stability of the modelled system, where the use of linearisations is distinguished to obtain representative state variables. In particular, due to the completeness presented, what is exposed in [35] is taken for the basic modelling of this doctoral thesis regarding internal control of converters and droop control (omitting its development in the content of this document).

Regarding secondary control, different works in the literature have addressed its study, in which it is common to see evidence of convergence of the protocols proposed for synchronisation (consensus). In works such as [36,38], formal mechanisms are established to model the physical dynamics of the MG in a distributed and linear differential way, making possible the application of consensus theory. This allows the methodology to inherit analysis tools used in the distributed control literature, such as large-signal stability using Lyapunov-Krasovskii candidates. As described in [15], MAS, which presents dynamics that can be modelled as a linear protocol, can be studied in a similar way to classical control systems in state variables thanks to the construction of matrices (such as the Laplacian matrix) that take into account the connectivity of the agents (or power converters in the case of this doctoral thesis). This modelling is based on graph theory and will be explained in more detail in Chapter 2.

Considering the above descriptions, the overall methodology for this PhD thesis is summarised in Fig. 1.1; it consists of different steps that consider modelling and formulation of the control system, design of the control parameters, construction of simulation models and experimental prototypes.

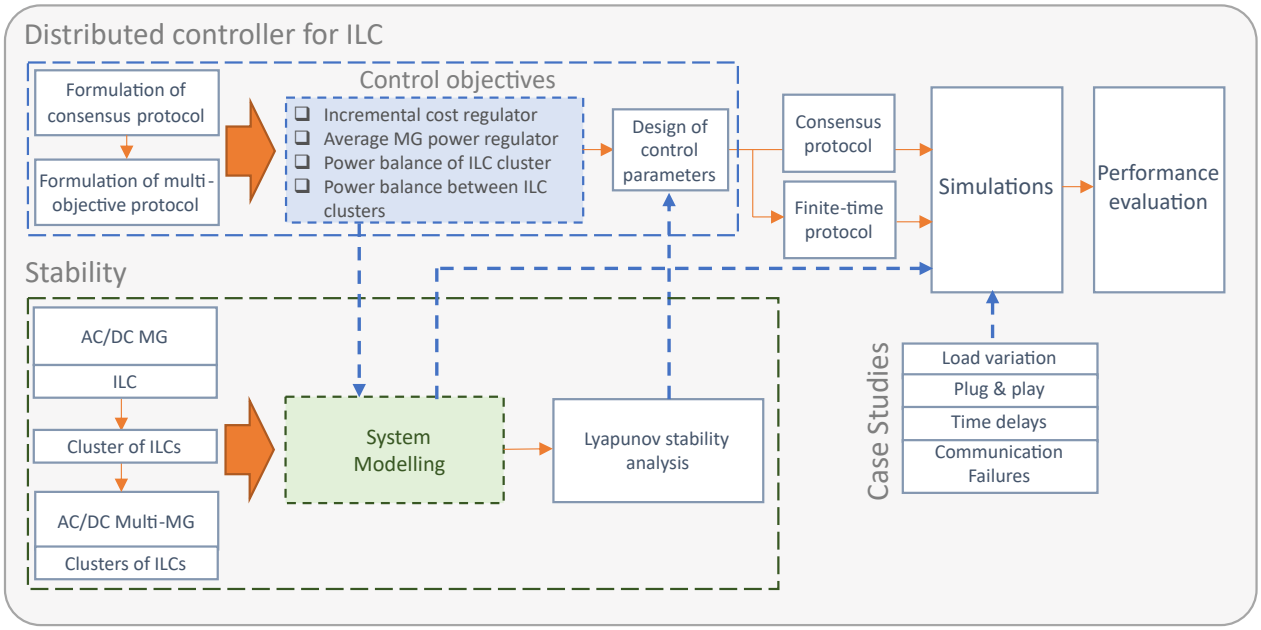

Figure 1.1: Methodology of research proposal.

1.6 Thesis Structure

The rest of the thesis is organised as follows: in Chapter 2 the literature review is presented; the fundamentals of AC/DC MG topologies and their control are described, with a focus on distributed and cooperative control techniques. A general classification of AC/DC MG topologies is made taking into account the number of ILCs. Also, different features inside the MG controllers are highlighted making comparisons where relevant. Chapter 3 describes the design and validation of a novel distributed finite-time controller for the ILC in an AC/DC MG. There are explained the fundamental problems to be solved for an economical and safe operation, then, it was derived that MG saturations can be avoided by using a new trade-off weighting parameter. Also, to enhance the control goals decoupling and accelerate the convergence, the finite-time protocol was verified. Chapter 4 presents an enlarged MG topology compared with Chapter 3, where multiple ILCs are used to interface the AC and DC subgrids. In this chapter, a novel dynamic consensus protocol is presented to realise the power-sharing inside an ILC cluster. Differently from the reported approaches, the proposed controller uses a distributed observer which gives a better average power estimation of the ILC cluster during transient states. Also, a novel anti-windup is proposed to deal with steady-state errors of the distributed observer in the face of transport delays. In Chapter 5, a more generalised MG topology is studied, which is a meshed AC/DC multi-MG with clusters of ILCs. The control goals presented in previous chapters are used in a unified multi-objective formulation. Additionally, a new control goal for balancing the power between clusters of ILCs is presented and studied; this new control goal is analogous to the MG saturation objective presented in Chapter 3. All of the control goals are tested through simulations to analyse their performance. Finally, in Chapter 6, the conclusions of this thesis as well as future research areas are discussed.

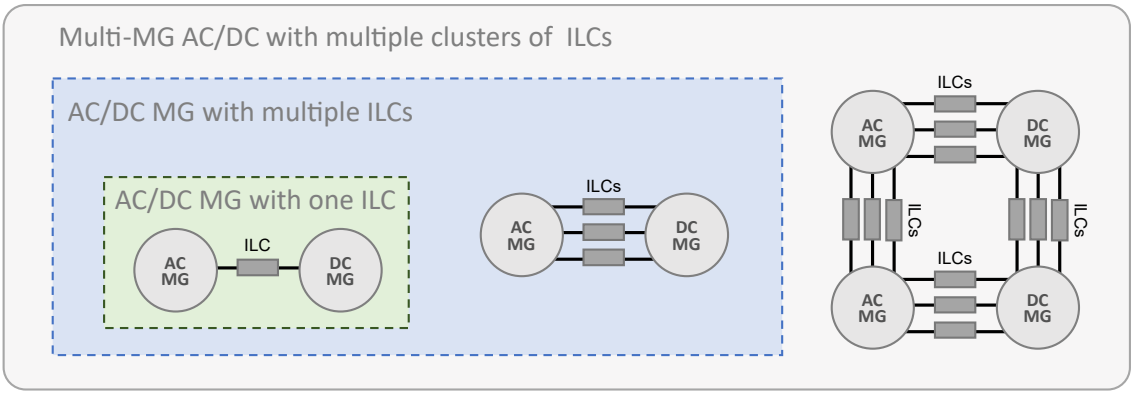

(a)

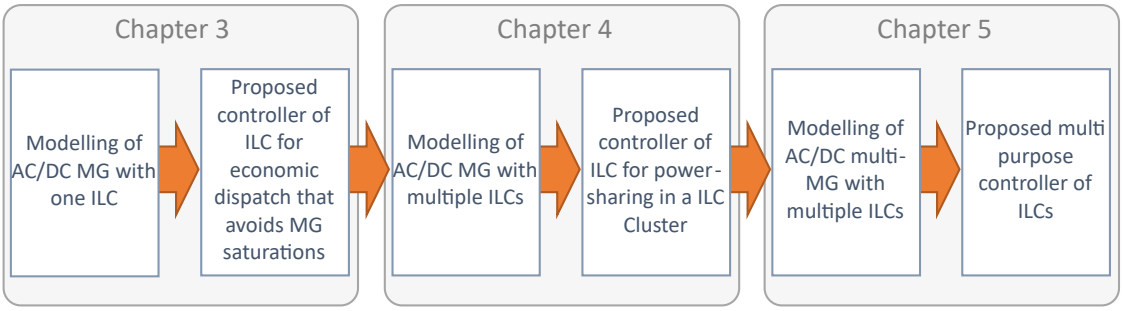

(b)

Figure 1.2: Guideline schematic of thesis structure. (a) MG topologies studied. (b) Relationship between activities taken in each MG topology concerning chapters.

Chapter 2

Literature Review

Content partially published on [1]. Creative Commons license.

This chapter presents the fundamentals of hybrid AC/DC MGs control and the state-of-the-art in cooperative control protocols and its applications to MGs.

2.1 Fundamentals of Hybrid AC/DC MGs

Hybrid MGs are made up of two or more interfaced MGs with an optional grid-connection bus. The basic scheme is an AC MG interconnected to a DC MG by means of one ILC [7]. Nonetheless, other works in the area have proposed the use of multiple ILCs to give greater flexibility and resilience to the system [26, 27, 39, 40]. An example of islanded hybrid MG is given by Fig. 2.1.

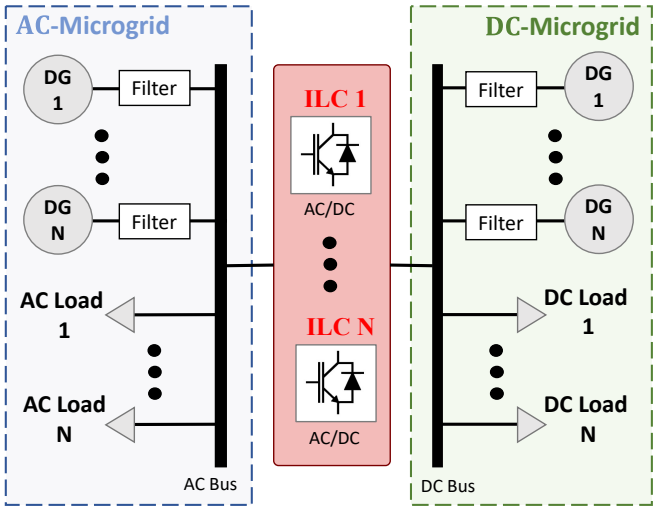

Figure 2.1: A generalised isolated hybrid MG structure.

The topology for ILCs is commonly based on one VSC on each side of a DC-link. However, there are also three-port topologies where the ILC incorporates a Battery Energy Storage System (BESS) [10]. The main objective of the ILC is to transfer active power between MGs through the DC-Link; In particular, the power transfer supports the balance between generated and demanded powers. By transferring excess power from one MG to another, the ILC helps the DGs to be used more efficiently and within their operating limits.

2.1.1 Topologies of AC/DC multi-MGs

MGs can be interconnected with more than one subgrid, creating the so-called AC/DC Multi-MG [24, 41]. It is worth-noting that in the literature, there are fundamentally three types of multi-MGs: (i) AC multi-MG [42–44], (ii) DC multi-MG [45, 46], and (iii) AC/DC multi-MG [24, 31, 33, 34, 47, 48]. In the first two types of MGs, an AC or DC MG is divided into several sections by means of controlled isolation switches. Also, the coordination between subgrids is made by designated MG agents (which involves an additional layer of communications). For the AC/DC multi-MGs, topologies using different numbers of AC and DC subgrids have been proposed. In [33], a single AC MG is interconnected to multiple DC subgrids through ILCs. In [24, 34], a more generalised topology is utilised where several AC and DC subgrids are interconnected by ILCs. A special case is used in [31], where a single DC bus interconnects several AC and DC subgrids. In [47], the topology of meshed AC/DC multi-MG is used in an upper-level robust optimisation for dispatch scheduling of energy resources.

Related to the previous categorisation, the topologies that incorporate more than one ILC can be identified into three main groups: AC/DC MGs with multiple ILCs (shown in Chapter 4), AC/DC multi-MGs, and AC/DC multi-MGs with multiple ILCs (shown in Chapter 5. In the conventional AC/DC MG topology, only 2 MGs are interfaced whereas in an AC/DC multi-MG multiple interlinks are available to transfer power between MGs. Fig. 2.2 represents a comparison between a multi-MG generated by divisions and a generalised AC/DC multi-MG. Note that in Fig. 2.2b there is more than one path for the power to flow from one MG to another, then the topology in Fig. 2.2b can be also called meshed AC/DC multi-MG.

In the approaches [42–46] (Fig. 2.2a), where AC or DC MGs are divided into clusters through controllable isolation switches, the idea is to autonomously manage the power flow in specific zones but these approaches requires an additional layer of communications between MG agents. However, this kind of approach did not have the advantages of AC/DC MG topologies. The meshed AC/DC multi-MG (Fig. 2.2b) has advantages over other multi-MG structures studied in the literature; the additional AC/AC and DC/DC ILCs provide flexibility to the system, allowing each MG to operate with its own voltage and frequency (only for AC MGs) levels. Also, the more links to transfer the power, the more efficient the power flow could be. However, such a level of flexibility comes at the cost of complex control infrastructure and algorithms.

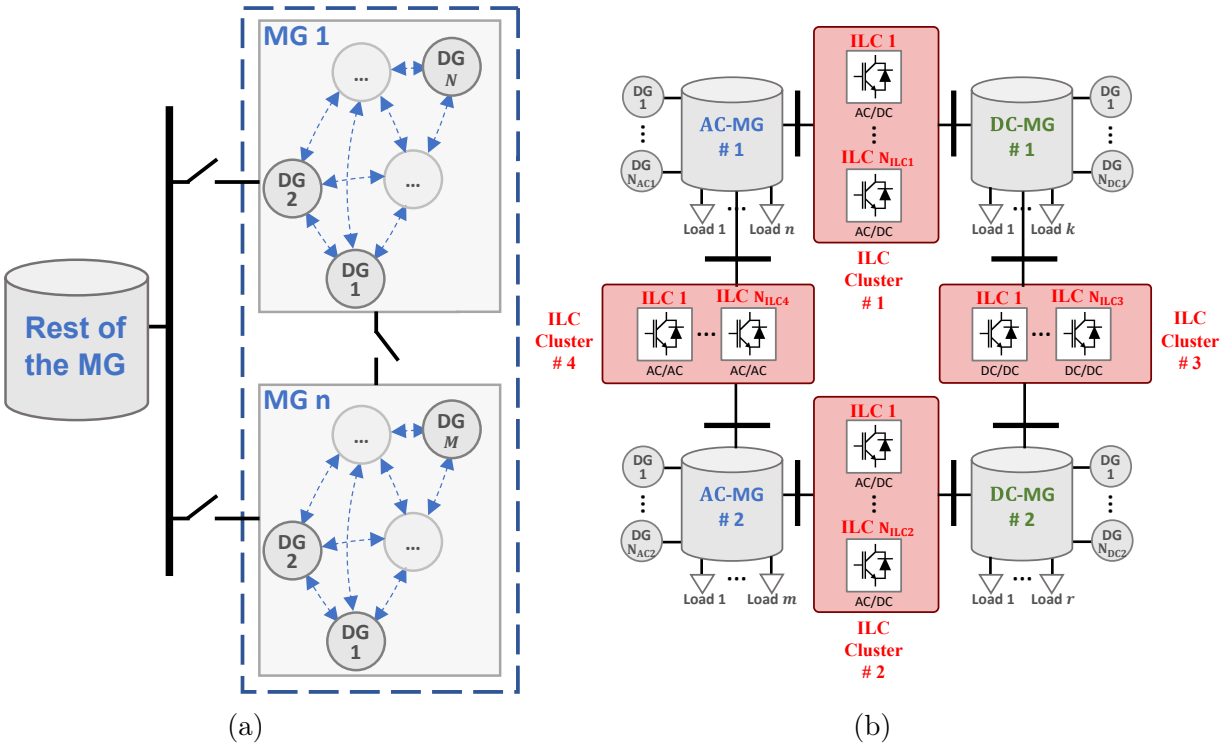

Figure 2.2: Comparison of multi-MG topologies in literature. (a) Conventional AC (or DC) multi-MG. (b) Generalised (meshed) AC/DC multi-MG with multiple ILCs.

2.2 Fundamentals of AC/DC MGs Control

Early works on control over the ILC were centralised [7,11], but decentralised approaches have obtained popularity recently [10,17,49,50]. For the control of DGs, researchers have proposed a hierarchical structure [51,52], which consists of three levels of control: primary, secondary and tertiary. The agreed hierarchical structure is resumed in Fig. 2.3. Explanations on the structure of the hierarchical control of MGs will be given in the next subsections.

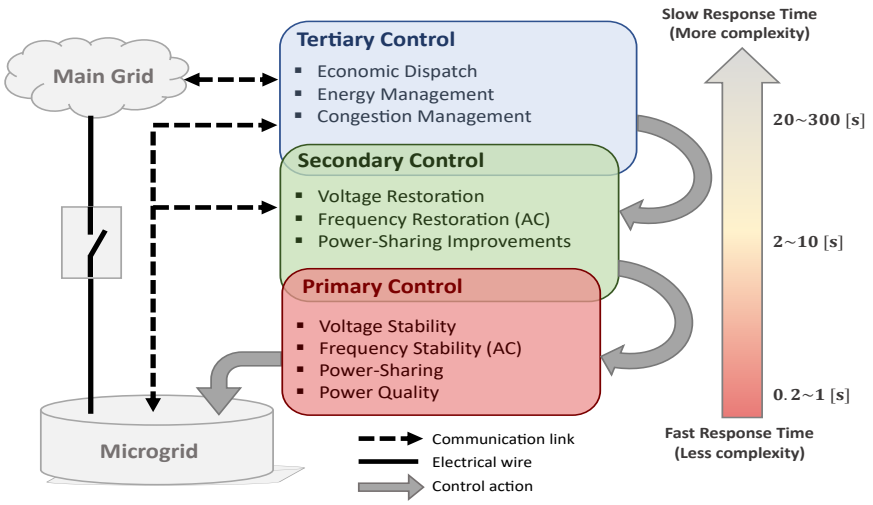

Figure 2.3: Hierarchical control of MGs. Reproduced from [1].

2.2.1 Primary control

In the primary control level, it is controlled the power supplied between DGs to obtain a desired power-sharing [53] . To do this, a virtual droop characteristic is introduced into each converter that mimics the governor of synchronous generators in traditional power systems [35]. Conventionally, a decentralised linear relationship is applied to each DG based on a simplified model of the power flow [52]. The relations used for the decentralised primary control dynamics (also called "droop" dynamics) for each MG are the following [51, 52, 54]:

$$\left.\begin{aligned} E_d &= E^* - nQ \ , \\ \omega &= \omega^* - mP \ , \end{aligned}\right\} \text{for AC MG} \tag{2.1}$$

$$\left.\begin{aligned} E &= E^* - rI \ , \\ \text{(or)} \quad E &= E^* - mP \ , \end{aligned}\right\} \text{for DC MG} \tag{2.2}$$

where E_d and ω are the converter output voltage magnitude and frequency, E^* and ω^* are the voltage and frequency reference nominal values, P, Q and I are the measured active power, reactive power and current, and n, m and r are the droop coefficients. The demonstration for the obtention of the above equations is presented in the Appendix B.

The application of (2.1) and (2.2) introduce deviations from nominal values. This is depicted in Fig. 2.4 for the AC MG case — For DC MGs, the deviations are analogous.

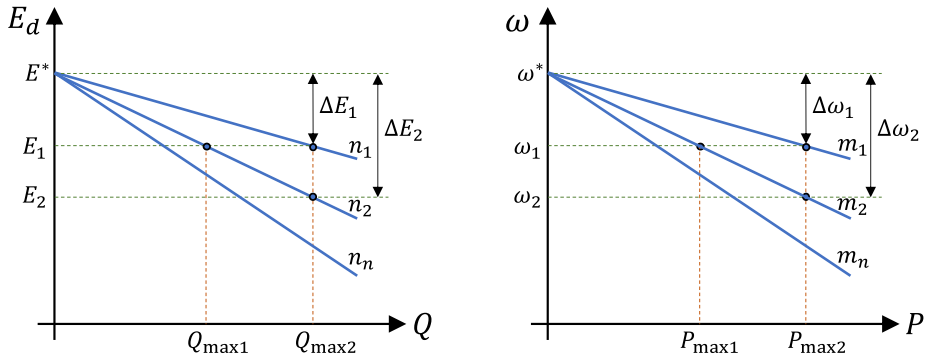

Figure 2.4: Droop deviations over AC MG. Reproduced from [1].

Regarding the implementation, a low-pass filter is required to yield the measurement of the converter's power output. This filter accomplishes two tasks, the decoupling from the internal voltage control loop and the elimination of high-frequency oscillations, such as the converters' switching noise and voltage harmonics [55]. Further details about the power measurement in droop-controlled MGs are given in the Appendix B.

2.2.2 Secondary control

This control level is in charge of the restoration of nominal values of the variables deviated by the primary control. Conventionally, these control actions are performed centralised, where every unit communicates their measurements to obtain average values of voltage and frequency to restore. For every DG, the controller uses a proportional-integral (PI) algorithm to give the control actions. The closed-loop dynamic is represented by [51]:

$$\left.\begin{aligned} \delta E_i &= k_p^E \left(E^* - E_i\right) + k_i^E \int_0^t \left(E^* - E_i\right) d\tau \ , \\ \delta \omega_i &= k_p^\omega \left(\omega^* - \omega_i\right) + k_i^\omega \int_0^t \left(\omega^* - \omega_i\right) d\tau + \Delta\omega_S \ , \end{aligned}\right\} \text{for AC MG} \tag{2.3}$$

$$\left.\begin{aligned} \delta E_i &= k_p^E \left(E^* - E_i\right) + k_i^E \int_0^t \left(E^* - E_i\right) d\tau \ , \end{aligned}\right\} \text{for DC MG} \tag{2.4}$$

where δE^* and $\delta\omega^*$ are compensation control actions additively applied to (2.1) and (2.2). E^* and ω^* are reference nominal values, E_i and ω_i are local measurements of the ith DG, and k_p^E, k_i^E, k_p^ω and k_i^ω are control parameters. The parameter $\Delta\omega_S$ is only active when the MG is connected to the main grid, and it depends on a Phase-Locked-Loop (PLL) measurement. It is important to mention that, due to the control actions of (2.3) or (2.4), the restoration affects the power-sharing. For this reason, some approaches incorporate a power equalisation loop in the secondary control to maintain the sharing ratio. Also, some works even include the Energy Management System (EMS) as part of the secondary control [53]. However, this thesis considers the EMS as part of the tertiary control, so it will be presented in the next subsection.

2.2.3 Tertiary control

The tertiary control looks for the optimal operation of islanded or grid-connected MGs. For islanded MGs, the optimal operation is achieved through the EMS, which can be defined as an optimisation problem that simultaneously solves the economic dispatch and unit commitment problems [55]. The economic dispatch goal is to schedule the power output of each DG such that the total cost of generation (C_{total}) is minimised. The economic dispatch optimisation problem involves generation costs, power losses, and power constraints. Conventionally, the economic dispatch is realised centralised [12, 56], but decentralised control has been also used [57–60]. The traditional optimisation problem of the economic dispatch is given by:

$$\min \sum_{i=1}^{n} C_i\left(P_i\right) \qquad \text{subject to,} \qquad \begin{aligned} C_i(P_i) &= \alpha_i P_i^2 + \beta_i P_i + \gamma_i \ , \\ C_{total} &= \textstyle\sum_{i=1}^{n} C_i(P_i) \ , \\ P_D &= \textstyle\sum_{i=1}^{n} P_i \ , \\ P_i^{\min} &\leq \quad P_i \quad \leq P_i^{\max} \ , \end{aligned} \tag{2.5}$$

where $C_i(P_i)$ is the generation cost function of i-th DG, α_i, β_i, γ_i are coefficients associated to the cost function, P_i is the generated power and P_D is the total demanded power. The formulation (2.5) has inequality constraints that are usually changed to equality constraints through Lagrange's theory [20, 61], so it can be solved by quadratic programming [62]. The Lagrange function of (2.5) can be constructed as

$$\mathbb{L}\left(P_i, \lambda, \sigma_i^+, \sigma_i^-\right) = \sum_{i=1}^{n} C_i\left(P_i\right) + \lambda\left(P_D - \sum_{i=1}^{n} P_i\right) + \sum_{i=1}^{n} \sigma_i^+ (P_i - P_i^{\max}) + \sum_{i=1}^{n} \sigma_i^- (P_i^{\min} - P_i), \tag{2.6}$$

where $\lambda, \sigma_i^+, \sigma_i^-$ are Lagrange multipliers.

The calculation of σ_i^+ and σ_i^- could be done by [20]

$$\dot{\sigma}_i^+ = \frac{k_3}{k_1}\max\left(0,\ P_i - P_i^{\max} + \frac{k_2}{k_3}\sigma_i^+\right) - \frac{k_2}{k_1}\sigma_i^+ , \tag{2.7a}$$

$$\dot{\sigma}_i^- = \frac{k_3}{k_1}\max\left(0,\ P_i^{\min} - P_i + \frac{k_2}{k_3}\sigma_i^-\right) - \frac{k_2}{k_1}\sigma_i^- , \tag{2.7b}$$

where k_1, k_2 and k_3 are positive constants.

Analytically, the solution of the economic dispatch using (2.6) find the IC of generation, which is given by the stationary condition as:

$$\frac{\partial \mathbb{L}}{\partial P_i} = \frac{\partial C_i(P_i)}{\partial P_i} - \lambda + \sigma_i^+ - \sigma_i^- = 0 . \tag{2.8}$$

Under economic operation, the Karush-Kuhn-Tucker optimality conditions are accomplished, so the IC of all DG units should be equal to the optimal Lagrange multiplier, i.e.

$$\lambda = \lambda_i = 2\alpha_i P_i + \beta_i + \sigma_i^+ - \sigma_i^- , \forall\ i = 1, 2, .., n , \tag{2.9}$$

and $n = |\mathcal{N}|$ is the number of DGs [63]. From this fact, the power reference of the i-th DG can be obtained by [64]:

$$P^* = \frac{\lambda - \beta_i}{2\alpha_i} . \tag{2.10}$$

The power reference in (2.10) can be implemented in a conventional PI controller as

$$\delta P = k_p^P (P_i^* - P) + k_i^P \int_0^t (P_i^* - P)\, d\tau , \tag{2.11}$$

which gives a compensation to be applied into (2.1) or (2.2).

The main disadvantage of centralised control for economic dispatch is that the optimisation problem, and then the control algorithm, is dependent on the MG topology (parameters or number of active DGs). For the decentralised formulations, the droop characteristics in (2.1) (or (2.2)) are modified according to economic variables. In [57], droop coefficients are selected according to offline stability analysis and centralised dispatch optimisation. The researchers in [58,59] proposed a cost function droop with stability-designed droop coefficients to perform a decentralised economic dispatch control. In [60], a decentralised economic dispatch is performed based on IC droop curves; In this case, the droop coefficients are proportional to the conventional ones.

Alternative formulations are distributed controllers, that use local and neighbour information to create the control actions [63, 65]. This kind of controller will be addressed in the next section.

2.3 Fundamentals of Distributed Control

Depending on the communication topology, a control strategy could be centralised, decentralised, or distributed [66]. The distributed control strategies are the newest methodology, which considers local controllers with communications between them. Distributed control usually employs more communication links than centralised control, but its infrastructure is more reliable against failures. Also, the length and bandwidth requirement of the communication links is shorter than the centralised approach [67, 68]. Disadvantages of distributed control are the complexity of control algorithms and convergence time.

The research of distributed control has developed three main approaches [67, 68]: Cooperative Control, which is based on the consensus theory, or synchronisation, of MAS with defined dynamics [15, 69, 70], Distributed Optimisation, also known as Decomposition-Based Technique, which shares information between units to solve local optimisation problems [71], and (Intelligent) Agent Control, which consists of autonomous local agents that perform control actions based on local goals and information from neighbours and environment, usually involving Machine-Learning techniques [66, 72, 73].

The focus of this work is the application of MGs of the cooperative control of MAS, through consensus theory, here-in-on referred to as *Distributed Control*.

2.3.1 Distributed cooperative control of MAS

The control of networked dynamic systems was first introduced in the 50's decade [74], and since then it has been applied for the control of sensors and industrial processes. To apply the cooperative control actions, local controllers (agents) need to communicate their information (state variables) to neighbours, so establishing a communication topology is a fundamental requirement. Depending on the structure of the communications network, there are different behaviours for the convergence of the states [15, 69]. Because of this, structures called *Graphs* are defined to analyse the dynamics of communication. More explanations about the graph theory are given in the Appendix C.

The convergence speed of the states is related to the communication topology and depends, at the same time, on the algorithms (or protocols) used by each agent [15, 74]. There are different dynamic models to perform distributed control protocols, depending mainly on the process representation. For research, major development areas have been identified as linear and non-linear consensus [75].

2.3.2 Linear consensus protocols

Asymptotic consensus is the most studied kind of protocol [76, 77], which is the basis on which other techniques and improvements are developed. Linear protocols perform a distributed state feedback control law, in which the tracking error is calculated by comparing the local and neighbouring state values. In terms of modelling, the conventional first-order linearised

consensus can be described as follows (see more details in Appendix C):

$$u_i = -\sum\nolimits_{j\in\mathcal{N}_i} a_{ij}(x_i - x_j)\,. \tag{2.12}$$

The obtained consensus value is given by the average of initial states $x_i(0)$. Eq. (2.12) is distributed according to the configuration of the communication links (given by a_{ij}).

Conversely to the conventional single-integrator dynamics, references [78, 79] formulate the agent dynamics as dependant on the control input u_i and the state x_i. The matrix representation of such a generalised system is given by

$$\begin{aligned} \dot{X}_i(t) &= AX_i(t) + BU_i(t)\,, \\ Y_i(t) &= CX_i(t)\,, \end{aligned} \tag{2.13}$$

where X_i, U_i and Y_i are vectors of the state variables, control inputs and control outputs of the i-th agent, respectively. Matrices A, B and C are assumed stabilisable and detectable. Authors in [78] claimed that this generalisation is useful for modelling dynamic systems, performing a robust *dynamic consensus* as a linear combination of individual inputs. By considering a one-dimensional MAS and by following the steps in [79], authors can construct the following observer-based consensus protocol

$$\bar{x}_i = x_i + \int_0^t \sum_{j\in\mathcal{N}_i} a_{ij}(\bar{x}_j - \bar{x}_i)d\tau\,, \tag{2.14}$$

where $\bar{x}_i$ and $\bar{x}_j$ are estimated average values. This kind of protocol allows the state to be estimated with only neighbouring measurements.

2.3.3 Finite-time consensus protocols

Finite-time consensus is a trending improvement applied for MAS that reports a robust and accelerated convergence when compared with linear consensus [80–82]. First studies of cooperative control of MAS using finite-time protocols were carried out in [80], showing how non-uniform gradient flows achieve consensus in finite-time. Subsequently, the works [81, 82] extended the study about finite-time controllers for MAS, considering directed and undirected, time-variant or invariant adjacency matrices.

Basically, the finite-time protocols implement a Lipschitz continuous distributed state feedback control law. The idea of finite-time stabilisation is to direct the states of the system towards their equilibrium more quickly by modifying the state feedback of conventional algorithms; It can be considered the finite-time protocol as a general case of the linear protocols [83, 84]. Additionally, according to control system analyses, finite-time control ensures convergence in a finite number of steps [85], and it exhibits better rejection of disturbances and better robustness against uncertainties when compared with conventional strategies (based on asymptotic convergence) [86].

To design the state feedback, a discontinuous function is incorporated. In addition, the resulting feedback is weighted by the magnitude of the state itself to adjust the "continuity" of the controller, and thus find the best parameters to improve the convergence. For a system of the form $\dot{x}_i = u_i$, it is defined the finite-time distributed state feedback, u_i, as:

$$u_i = -c \sum_{j \in \mathcal{N}_i} a_{ij} \operatorname{sign}(x_j - x_i) |x_j - x_i|^{\alpha} , \tag{2.15}$$

where a_{ij} is the communication matrix coefficient between agents i and j, $|\cdot|$ represents the absolute value function, and $\operatorname{sign}[\cdot]$ is the signum function. For convenience, it is denoted $\operatorname{sig}[x]^{\alpha} = \operatorname{sign}(x)|x|^{\alpha}$. Providing $c > 0$ and $0 < \alpha < 1$, the finite-time convergence can be demonstrated and the convergence time is given by [82]:

$$T \leq \frac{1}{c(1-\alpha)} \left(V(x_0)\right)^{1-\alpha} , \tag{2.16}$$

where $V(x_0)$ is a Lyapunov-Krasovskii candidate function. The convergence depends on c and α which are tunning parameters. In the Appendix D of this document, one can find the proof of convergence for first-order systems under consensus algorithms with finite-time feedback control. Second-order models are also applicable to the protocols shown in (2.15) [84].

2.4 Consensus Trends Applied to MGs

Consensus algorithms have become part of MG control strategies by virtue of the advances in networked systems control theory. Since the last decade, authors have proposed distributed control strategies relying on the sharing information for the implementation of tertiary [13, 20, 63, 65, 77, 87–104], secondary [36, 105–111] and primary control [112–117]. The control objectives used in distributed control strategies are to achieve optimal dispatch [77], to improve the sharing of both active and reactive powers [118], to restore frequency and voltage [110], and to share imbalances and harmonics among power converters [119].

Investigative efforts have been made to control DC MGs in a distributed manner. In [120, 121], a distributed secondary control is performed but assuming a completely connected graph topology. Subsequently, in [106] a scheme based on consensus theory on multi-agent systems is successfully implemented for controlling average voltage and currents for an equal power-sharing through adaptive droop coefficients. In [107], the authors use a similar topology but with the current consensus directly compensating into the voltage loop. Later, in [122], authors proposed a transient dynamics improvement for [106]; they employ a double consensus loop of virtual resistance and average current to change adaptively the droop coefficients. Other works have drawn on qualities of consensus theory to improve convergence and resilience in secondary control of DC MGs [123–125], e.g. using finite convergence algorithms. However, none of these schemes focused on developing the economic dispatch.

For AC MGs, research followed a similar trend, with [36] proposing a consensus protocol for secondary control. The consensus protocols inside the voltage and frequency loops are constructed based on a linear model obtained by means of the input-output feedback-linearisation technique. In [126], the authors studied further details about the inclusion of

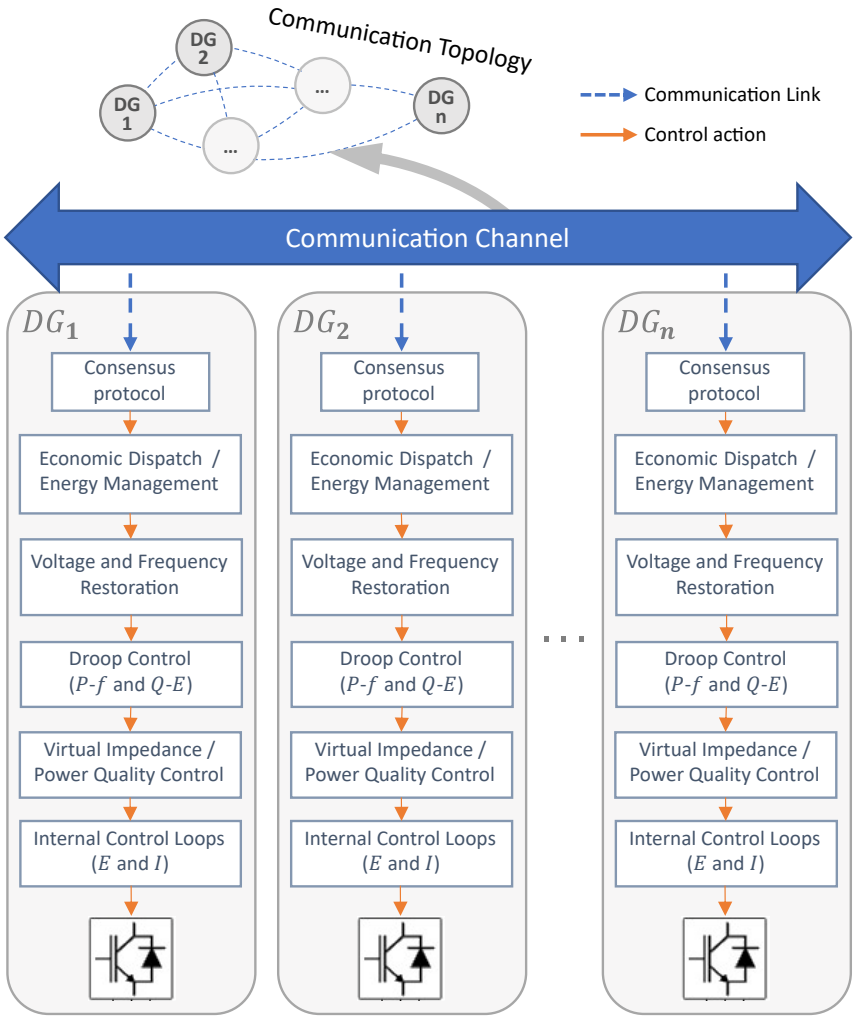

Figure 2.5: Distributed control architecture of an MG. Adapted from [1].

power-sharing features in the previous formulation. Later, a slightly different approach was made by [110], where a distributed-proportional-integral (DAPI) controller was elaborated. This distributed protocol uses the error in the average frequency of the MG as an auxiliary variable to perform the frequency restoration. This controller also incorporates the reactive power-sharing in the voltage loop, proposing a trade-off parameter for the voltage restoration weight. Another work proposed a cooperative controller replacing the frequency droop [113]. The authors drew from the converter's phase dynamics to avoid additional integrators in the frequency restoration loop, allowing a faster secondary control response without frequency measurements. This approach also benefits from the voltage observer proposed in [106]. Following a similar path, in [127] a multi-functional controller was made by the combination of [113] and [110]. The controller realises all of the previous control actions, i.e. voltage and frequency restoration along with active and reactive power-sharing. A fundamental part of this control design is the incorporation of two distributed observers, for voltage and active power. Indeed, in the literature (see [107,113,128,129]), authors have applied (2.14) to depict average voltage observers in MGs. Observers have also been applied to active power [127], IC [102] and State of Charge (SoC) of batteries [130], in distributed control strategies of MGs.

Regarding economic operation, in [63, 95] secondary controllers are proposed to apply the IC in consensus algorithms with an optimiser to solve the economic dispatch. However, the use of optimisers requires a high computing capacity to work in short periods of time. In [61, 88] the IC consensus is used as a deviation for an integral controller applied to the frequency loop of AC MGs. Subsequently, in [19, 20], another IC consensus was proposed based on the DAPI structure. This approach focuses on solving a power-constraint economic dispatch, and it incorporates a congestion management consensus term. In [101] and [102], a distributed IC observer is implemented to realise tertiary control in DC MGs. The approach in [101] adaptively modifies the droop coefficients using a consensus, as in [107] but with average ICs. This controller is reliable, but it does not address improvements for transient dynamics. In [102], a global power imbalance estimation is required to achieve the economic dispatch, which is estimated through a secondary current regulator. However, the tertiary control of IC needs to be decoupled from the secondary current regulator for stable operation, lacking in transient dynamics for the IC as a result. Furthermore, like [61, 95], it does not restore the voltages near nominal values.

Reference	**MG Type**	**Power-Sharing**	**Economic Dispatch**	**Enhanced Transients***	**Secondary Restoration**	**Topology Knowledge**
Ref. [36]	AC	✓			✓	
Ref. [110]	AC	✓			✓	
Ref. [116]	AC	✓		✓		✓
Ref. [118]	AC	✓		✓	✓	
Ref. [88, 90]	AC		✓			
Ref. [20]	AC		✓		✓	
Ref. [108]	DC	✓			✓	✓
Ref. [106]	DC	✓			✓	
Ref. [122]	DC	✓		✓	✓	
Ref. [99]	DC		✓			
Ref. [102, 104]	DC		✓		✓	
Ref. [18, 23, 24]	AC/DC	✓			✓	
Ref. [49]	AC/DC		✓		✓	✓
Ref. [13, 14]	AC/DC		✓		✓	
PhD proposal	AC/DC	✓	✓	✓	✓	

*referring to improvements made by changes to the loop with the power/current dynamics.

Table 2.1: Summary of distributed control strategies applied to MGs.

2.4.1 Convergence improvements in MGs

In terms of research effort, in the last two decades, the emphasis has been on the development of consensus protocols, and for this reason, many alternatives have been proposed for enhancing its performance [75, 131–133], i.e.: consensus with constraints, event-triggered consensus, finite-time consensus, delay-robust consensus.

In order to improve the convergence speed, in [105] an integral-proportional secondary control strategy based on the *signum* function has been proposed for the control of isolated AC MGs. This work laid the foundations for subsequent works such as [38, 111, 118, 134–136] that apply variants of the *signum* function to perform the feedback protocol of the consensus algorithms, forming more complete control strategies under the finite-time convergence. In [123, 124, 136] finite-time protocols for consensus applications are investigated for DC MGs. In [123], the finite-time protocol includes an input-saturation restriction. That strategy is compared against that reported in [107], and it is claimed that the proposed methodology achieves a slightly better response time with less overshoot. In [124], a finite-time controller for average-voltage regulation is combined with a second-order consensus of the SoC of a BESS. It is claimed that this methodology improves the current sharing within a finite settling time.

Other strategies to improve consensus are related to optimising communication channel usage. Limiting the rate of shared information required for DGs leads to benefits that have been reported in the literature [137–139]. One of the first works that applied this concept to MGs was [140]. In this work, self-triggered aperiodic communication is utilised for coordinating the consensus control actions. This aperiodic communication reduces the data transmission rates required among DGs. For the implementation, point-to-point communication was considered between neighbouring units and the next time instant for information transmission and control update is precalculated depending on a power error threshold.

A problem regarding the communications in distributed control is the time delays, which deteriorate and slow the convergence. The effect of delays have been studied in distributed secondary control of MGs [37, 124, 141–143]. In [37], a small-signal analysis of distributed secondary control is performed to study the time delays in AC MGs. Later on, this work was expanded in [143] to the DC MGs. Overall, there are no clear methodologies proposed for directly coping with communication issues, with the obvious exception of robust consensus designs.

A robust distributed secondary control strategy was proposed in [144] to consider the uncertainty in the communication links (between DGs), through an iterative learning mechanic. The authors claim that the controller proposed in [144] guarantees the control objectives even if all DGs are subject to internal uncertainties and external noises including initial voltage and/or frequency resetting errors and measurement disturbances. The latter topic is also addressed in [145].

Other variations of the distributed control structure have been studied for dealing with delays and uncertainty. For instance, in [146–148], predictive control with consensus protocols has been proposed to yield secondary control. However, the theory behind these controllers outreaches the scope of this thesis (focused on non-optimisation cooperative control).

A summary of consensus protocols applied to MGs is presented in Table 2.2

Protocol	**Features**	**MG Type**	**References**
Linear	They have the typical advantages and characteristics associated with linear systems. They can be described by linear differential equations and analysed using linear control tools. They could have sub-optimal performance when applied to non-linear systems.	DC	Power-sharing [106–108, 143, 149–151] Economic dispatch [99, 100, 102, 104, 152, 153]
		AC	Power-sharing [108, 110, 113, 126, 127, 154] Economic dispatch [20, 88, 90, 155]
Finite-Time	It is claimed that they can achieve a faster dynamic performance than that achieved by using linear consensus, and relatively good disturbance rejection capabilities. However, they may introduce chattering in the response.	DC	Power-sharing [45, 46, 123–125, 135, 156]
		AC	Power-sharing [38, 89, 105, 118, 152, 157] [158] Economic dispatch [89]
Other non-linear	Typically based on sliding control algorithms. It is claimed that they are reliable to model uncertainties and disturbances, and they introduce a reduced level of chattering when compared to that introduced by finite-time protocols.	DC	Power-sharing [159]
		AC	Power-sharing [158, 160–162] [163–166] [167].

Table 2.2: Summary of different consensus protocols applied to MGs.

2.5 Discussion

This chapter reviewed the fundamentals related to the cooperative control of MGs giving context to the advances in theories and strategies for the control of AC/DC MGs. The developments in the consensus theory allow MGs to implement, every time more, advanced and complex techniques to ensure efficient control over the critical variables. Regarding the control of ILCs, the literature depicts linear approximations (droop) for most of the power transfer dynamics, relying on steady-state deviations of frequency or voltage; few works have included an additional control layer with consensus algorithms, but the functionalities/decision-making capabilities of the ILC are still limited. In the current literature, cooperative control strategies that achieve economic dispatch in multi-MG systems are insufficiently explored. Therefore, there are research gaps regarding the dynamic performance of different distributed cooperative control methods applied to generalised multi-MGs with multiple interconnections.

Chapter 3

Multi-objective and Distributed Finite-time Control for the Interlinking Converter in a Hybrid AC/DC Microgrid

Content partially published on [2]. Creative Commons license.

3.1 Introduction

In this chapter, the proposed control strategy for a single AC/DC MG is described. Particularly, this chapter proposes a distributed coordination between generators by means of a finite-time controller for the MG's ILC, which ensures an economic operation while taking care of the MG power utilisation. The latter implies that a multi-objective control is performed by the ILC, which uses shared variables of ICs and average powers from distributed generators on AC and DC sides. Also, an adaptive weighting method is proposed to adjust the control effort regarding the average power utilisation of a side MG. For simplicity, it is assumed only one ILC, but the strategy can be extendable to multiple ILCs (as shown in Chapter 4). The controller's performance is verified through simulations and experimental setups. Results show that the proposed strategy is able to perform a trade-off between the two control objectives while achieving a finite-time convergence even though communication delays exist.

3.1.1 Problem statement

For the control of the hybrid AC/DC MG, the problem to be solved consists of simultaneously ensuring economic power-sharing and a reliable operation for all the DGs. For the economic dispatch coordination, both subgrids (AC and DC) need to agree on the most cost-effective use of DGs. This is done by means of the equal IC principle [50]. However, this is not an easy task because the optimal power distribution is not only economical; it also needs to avoid the saturation of DGs, and, consequently, of MGs. The saturations originate because,

occasionally, the IC variables suffer variations, and the difference between the ICs of the AC and DC MGs is significant. Common reasons for such variations of ICs are the disconnection of DGs, the power-sharing of ESSs based on the State of Charge (SoC) [51], and the market price for energy in grid-connected operations [21].

3.1.2 Motivation

The literature about hybrid AC/DC MG topologies has not sufficiently explored the distributed control in the ILCs for economic dispatch. Some approaches exist, such as [14, 25], but they have not properly discussed the interaction dynamics of ILCs and DGs to this end. The work in [30] give some details about communication matrices considering ILCs but focuses on the controller design and system dynamics with the goal of power-sharing instead of economic dispatch; moreover, it lacks definitions and stability proofs.

In terms of the ILC's control, the sole regulation of ICs in situations where significant differences exist between the subgrids may lead the ILC to leave an MG without energy reserves, which are critical for dealing with generation-demand balancing, especially during transient states. Thus, if a saturated subgrid increases its load, it will need to obtain power from the other subgrid through the ILC, which is a slow process that might deteriorate the transient dynamics. To the best of the author's knowledge, this problem has not been addressed in the control area of AC/DC MGs, with the exception of [28], where an attempt to avoid MG's saturation is indirectly introduced by means of a safety operation limit of 0.95 imposed in the power boundaries of the ILC's operation mode. Nonetheless, this method constantly reduces the power capacity of the ILC; also, it requires a fixed topology, so it is not effective in the plug & play operation of DGs.

Motivated by this, this chapter introduces a novel multi-objective formulation for the optimal dispatch of hybrid AC/DC MGs with MG saturation constraints.

3.1.3 Contributions and organisation

The contributions of this chapter can be summarised as follows:

- A finite-time communication-based control for the ILC is proposed, which guarantees the economic dispatch of a hybrid AC/DC MG. A Lyapunov candidate is then derived, which models the AC/DC MG as a graph of error signals and demonstrates the system's convergence.

- A multi-objective formulation for the ILC is proposed. An average power term is added to the ILC's controller to manage the saturation of MGs. A proof of convergence is also developed, showing that the system can simultaneously reach equilibrium in IC and average power, providing a trade-off weighting gain.

- Experimental and simulation validations of the proposed multi-objective finite-time

controller for the ILC are realised. They show the behaviour of the ILC's controller under different conditions.

The rest of the chapter is organised as follows. In Section 3.2, the formulation of the economic dispatch problem is presented as well as the definitions for communication network, distributed control protocol, and design of control parameters. The design of the distributed control for the ILC is presented along with a Lyapunov convergence analysis. Section 3.3, explains the formulation of economic dispatch with MG saturation constraint. It includes the design and proof of convergence of a multi-objective distributed control. In Section 3.4, a time delay stability analysis is conducted regarding the distributed control protocols described in previous sections. In Section 3.5, case studies are described with the system and control parameters. In Section 3.6, the results are presented and discussed, followed by the conclusions in Section 3.7.

3.2 Design of a Distributed Control Strategy for the Interlinking Converter

3.2.1 Formulation of economic dispatch in a hybrid AC/DC MG

In a hybrid AC/DC MG with an ILC, such as the one shown in Fig. 3.1, the power interaction between the side MGs (also named subgrids) is realised solely by the ILC. Under this premise, the power transferred by the ILC becomes a demand disturbance for each MG, modifying the generated power and thus the IC of the DGs.

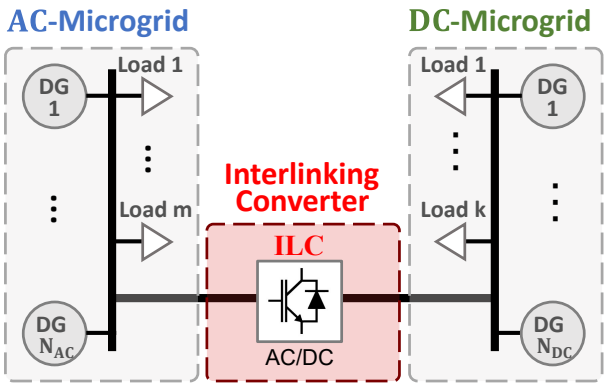

Figure 3.1: Example of a hybrid AC/DC MG with one ILC.

In order to optimise the energy resources in the hybrid AC/DC MG, the ILC can be controlled such that it synchronises the ICs of all the DGs, achieving a global economic dispatch. Thus, based on the developments made for the AC MG by [20,61,64], the optimisation problem that describes the economic dispatch in a hybrid AC/DC MG can be written as

$$\min_{\boldsymbol{P}} \left\{ \sum_{i=1}^{N_{\rm AC}} C_i(P_i) + \sum_{i=1}^{N_{\rm DC}} C_i(P_i) \right\} \quad \text{subject to,} \quad \begin{array}{c} C_i(P_i) = a_{ci}P_i^2 + b_{ci}P_i + c_{ci} \ , \\ P_i^{\min} \leq P_i \leq P_i^{\max} \ , \\ -P_{\rm ILC}^{\max} \leq P_{\rm ILC}(\boldsymbol{P}) \leq P_{\rm ILC}^{\max} \ , \\ P_D^{\rm AC} + P_{\rm ILC}(\boldsymbol{P}) = \sum_{j\in\mathcal{N}_{\rm AC}} P_j \ , \\ P_D^{\rm DC} - P_{\rm ILC}(\boldsymbol{P}) = \sum_{j\in\mathcal{N}_{\rm DC}} P_j \ , \end{array} \tag{3.1}$$

where $C_i(P_i)$ is a quadratic cost function for the i-th generator with parameters a_{ci}, b_{ci} and c_{ci}. $\mathcal{N}_{\rm AC}$ and $\mathcal{N}_{\rm DC}$ are the group of DGs in the AC and DC MGs, whereas $N_{\rm AC} = |\mathcal{N}_{\rm AC}|$ and $N_{\rm DC} = |\mathcal{N}_{\rm DC}|$ are the number of DGs in the AC and DC MGs, respectively. Also, $P_{\rm ILC}(\boldsymbol{P})$ is a function that describes the power transfer by the ILC, with $\boldsymbol{P} = (P_1, P_2, ..., P_{N_{\rm sys}})$ and $N_{\rm sys}$ the total number of DGs ($N_{\rm AC}$ plus $N_{\rm DC}$) in the system. $P_{\rm D}^{\rm AC}$ and $P_{\rm D}^{\rm DC}$ are the demanded powers of the subgrids. The sign of the $P_{\rm ILC}(\boldsymbol{P})$ terms in (3.1) suggests a positive value for a power transferring from the DC to AC MG.

Arranging (3.1), one can get

$$\min_{\boldsymbol{P}} \left\{ \sum_{i=1}^{N_{\rm sys}} C_i(P_i) \right\} \quad \text{subject to,} \quad \begin{array}{c} C_i(P_i) = a_{ci}P_i^2 + b_{ci}P_i + c_{ci} \ , \\ P_i^{\min} \leq \ P_i \ \leq P_i^{\max} \ , \\ -P_{\rm ILC}^{\max} \leq P_{\rm ILC}(\boldsymbol{P}) \leq P_{\rm ILC}^{\max} \ , \\ P_{\rm D}^{\rm AC} + P_{\rm D}^{\rm DC} - \sum_{j\in\mathcal{N}_{\rm sys}} P_j = 0 \, , \end{array} \tag{3.2}$$

where $\mathcal{N}_{\rm sys} = \{\mathcal{N}_{\rm AC} \cup \mathcal{N}_{\rm DC}\}$. It can be seen that the power balancing constraints can be merged by summing them, cancelling $P_{\rm ILC}(\boldsymbol{P})$ in the process (resulting in the same constraint for power balance than [168]). From (3.2), the inequality constraints can be converted into a set of equality constraints, producing a Lagrangian function of the form

$$\begin{aligned} \mathbb{L}\left(P_i, \sigma_i^+, \sigma_i^-, \Lambda^+, \Lambda^-, \lambda\right) &= \sum_{i=1}^{N_{\rm sys}} C_i(P_i) + \sum_{i=1}^{N_{\rm sys}} \sigma_i^+(P_i - P_i^{\max}) + \sum_{i=1}^{N_{\rm sys}} \sigma_i^-(P_i^{\min} - P_i) \\ &+ \Lambda^+\left(P_{\rm ILC}(\boldsymbol{P}) - P_{\rm ILC}^{\max}\right) + \Lambda^-\left(- P_{\rm ILC}^{\max} - P_{\rm ILC}(\boldsymbol{P})\right) + \lambda\left(P_{\rm D}^{\rm AC} + P_{\rm D}^{\rm DC} - \sum_{i=1}^{N_{\rm sys}} P_i\right), \end{aligned} \tag{3.3}$$

where λ, σ_i^+, σ_i^-, Λ^+, and Λ^- are Lagrange multipliers. Analogously to σ_i^+ and σ_i^- in (2.5), Lagrange multipliers Λ^+ and Λ^- are defined to adjust for the power constraint violations on the ILC.

With those definitions, the derivative of Lagrange's function takes the form

$$\frac{\partial}{\partial P_i}\mathbb{L} = \frac{\partial C_i\left(P_i\right)}{\partial P_i} + \sigma_i^+ - \sigma_i^- + (\Lambda^+ - \Lambda^-)\frac{\partial P_{\rm ILC}(\boldsymbol{P})}{\partial P_i} - \lambda \ , \tag{3.4}$$

where $\frac{\partial P_{\rm ILC}(\boldsymbol{P})}{\partial P_i}$ is the sensibility of the ILC to the variation of P_i. Using (3.4) for analysing the stationary optimality condition, it gives:

$$\frac{\partial}{\partial P_i}\mathbb{L} = 0 \quad \Leftrightarrow \quad \lambda = \frac{\partial C_i\left(P_i\right)}{\partial P_i} + \sigma_i^+ - \sigma_i^- + (\Lambda^+ - \Lambda^-)\frac{\partial P_{\rm ILC}(\boldsymbol{P})}{\partial P_i} \ . \tag{3.5}$$

The term $\frac{\partial P_{\mathrm{ILC}}(\boldsymbol{P})}{\partial P_i}$ could be obtained analytically by assuming an ILC controller and then analysing the whole electrical system model of the hybrid AC/DC MG, e.g., using a small-signal analysis. However, it is evident that if the ILC does not have sufficient power capacity for the power transfers (by violating the inequality constraints), we have $\Lambda^+ > 0$, and the global synchronisation of ICs cannot be reached. Still, it can be argued that the economic dispatch (minimum cost of operation respecting the power constraints) could be reached.

When the ILC has enough power capability for the power transfers, i.e., $\{\Lambda^+, \Lambda^-\} = 0$, then, the stationary optimality condition can be revised as follows:

$$\frac{\partial}{\partial P_i}\mathbb{L}\left(P_i, \sigma_i^+, \sigma_i^-, \lambda\right) = 0 \Leftrightarrow \lambda = \frac{\partial C_i\left(P_i\right)}{\partial P_i} + \sigma_i^+ - \sigma_i^- \,. \tag{3.6}$$

From (3.6), it can be noted that all the DGs must have the same IC (λ) to accomplish the global economic dispatch (other optimality conditions can be proved as in [20]). Provided that each MG implements its own economic dispatch optimisation, a distributed control based on the works [20, 169] can be assumed on each side (more details about distributed control in each subgrid are given in Section 3.2.5). As a result, the ICs in each MG are obtained locally by the DGs as

$$\lambda_i^{\mathrm{AC}} = 2a_{ci}P_i + b_{ci} + \sigma_i^+ - \sigma_i^- \,, \tag{3.7a}$$

$$\lambda_j^{\mathrm{DC}} = 2a_{cj}P_j + b_{cj} + \sigma_j^+ - \sigma_j^- \,, \tag{3.7b}$$

where the condition $\lambda_i^{\mathrm{AC}} = \lambda_j^{\mathrm{DC}}\ \forall\ i \in \mathcal{N}_{\mathrm{AC}} \wedge j \in \mathcal{N}_{\mathrm{DC}}$ must be held for the global economic dispatch. Therefore, the goal of the ILC is to equalise the ICs of (3.7).

From this point, a distributed control strategy is designed for this purpose, which generates the required power reference P^*_{ILC}. The power reference for the internal control loops of the ILC can be calculated by directly comparing the ICs of (3.7). Hence, concerning reliability and accuracy, it is proposed a distributed scheme where the DGs send their IC measurements to the ILC. Because the control actions taken by the ILC affect the IC dynamics of the AC and DC subgrids, the whole hybrid AC/DC MG can be viewed and analysed as a multi-agent system with a graph $\mathcal{G}_{\mathrm{sys}}$. Fundamentals of graph theory are summarized in the Appendix C.

In the next subsection, definitions for the global communication network of hybrid AC/DC MG are provided.

3.2.2 Communication network

For simplicity, the communication between MGs is implemented only through the ILC, i.e. DGs of different subgrids cannot communicate directly. The proposed communication topology for the hybrid MG can be represented as a combination of graphs, such as $\mathcal{G}_{\text{sys}} := \mathcal{G}_{\text{AC}} \cup \mathcal{G}_{\text{DC}} \cup \mathcal{G}_{\text{ILC}}$. Each subgrid's graph contains its communicated nodes (or DGs), and can be expressed as $\mathcal{G}(A^{\text{AC}})$ or $\mathcal{G}(A^{\text{DC}})$. Also, $\mathcal{G}_{\text{ILC}} := (\mathcal{N}^*, E^{\text{ILC}}, A^{\text{ILC}})$ with $\mathcal{N}^* \subset (\mathcal{N}_{\text{AC}} \cup \mathcal{N}_{\text{DC}} \cup \mathcal{N}_{\text{ILC}})$ represents the communication graph between the side MGs and the ILC. Fig. 3.2 summarises the communication scheme considered by this work. In this chapter, the communication scheme assumes only one ILC ($N_{\text{ILC}} = 1$), but it can be extended to multiple ILCs, as it will be shown in Chapter 4.

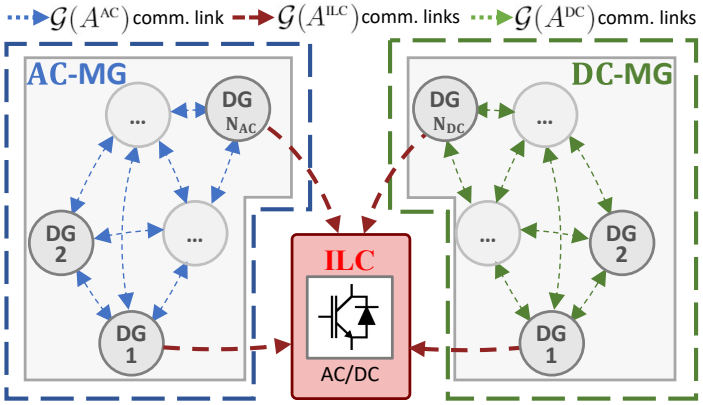

Figure 3.2: Cyber-physical system representing a hybrid AC/DC MG. The ILC is an agent that solely receives information, and it can indirectly (by a physical power transfer) connect the AC and DC graphs. Reproduced from [2].

The former gives $\{A^{\text{ILC}}\} = \{a^{\text{ILC}}_{\text{AC}\,i} \cup a^{\text{ILC}}_{\text{DC}\,j} \cup a^{\text{ILC}}_{\text{ILC}\,k} \,/\, i \in \mathcal{N}_{\text{AC}} \wedge j \in \mathcal{N}_{\text{DC}} \wedge k \in \mathcal{N}_{\text{ILC}}\}$ where $\boldsymbol{a}^{\text{ILC}}_{\text{AC}}$, $\boldsymbol{a}^{\text{ILC}}_{\text{DC}}$ and $\boldsymbol{a}^{\text{ILC}}_{\text{ILC}}$ are vectors that represent the communication between the ILC and the DGs in the AC and DC subgrids, and with the system's ILCs, respectively.

This communication topology allows the subgraphs $\mathcal{G}_{\text{AC}}$ and $\mathcal{G}_{\text{DC}}$ operate independently when the ILC ($\mathcal{G}_{\text{ILC}}$) is disconnected, or when one side stops communicating to the ILC.

3.2.3 Distributed control of ILC for economic dispatch

Provided that each MG (AC or DC) can regulate and share its DG's IC through a distributed control (described in Section 3.2.5), a PI controller for equalising these ICs can be constructed for the ILC as

$$P^*_{\text{ILC}} = k^P_p(u_{\text{ILC}}) + k^P_i \int_0^t (u_{\text{ILC}})d\tau\,, \tag{3.8}$$

where P^*_{ILC} is the power reference to be transferred between MGs, u_{ILC} is the input error of IC, k^P_p and k^P_i are control parameters. The reference P^*_{ILC} is used to produce the current references, by means of a division scheme [24], for the internal control loops of the ILC (the control of the internal loops can be performed following the procedure described in [10] or

[24]). Due to the physical limitations of the ILC, saturation is implemented on the controller's output along with an anti-windup algorithm on the integrator. Thus, Lagrange's multipliers Λ^+ and Λ^- are not required to be designed.

Given the communication matrix A^{ILC}, one can estimate the control input for the ILC controller as

$$u_{\text{ILC}} = c_L \left(\sum_{i=1}^{N_{\text{AC}}} a_{\text{AC}i}^{\text{ILC}} \lambda_i - \sum_{j=1}^{N_{\text{DC}}} a_{\text{DC}j}^{\text{ILC}} \lambda_j \right) . \tag{3.9}$$

Then, a finite-time algorithm has been added to (3.9) based on [38, 82] for a faster convergence and small disturbance rejection. Moreover, the finite-time convergence along with the PI structure of (3.8) provide robustness in the face of disturbances due to variation of parameters or not modelled dynamics. Hence, the resulting controller is given by:

$$u_{\text{ILC}} = c_L \sum_{i=1}^{N_{\text{AC}}} \sum_{j=1}^{N_{\text{DC}}} \text{sig} \left[a_{\text{AC}i}^{\text{ILC}} \lambda_i - a_{\text{DC}j}^{\text{ILC}} \lambda_j \right]^{\alpha_L} , \tag{3.10}$$

where $c_L > 0$ and $\alpha_L \in (0, 1)$ are parameters for regulating the convergence speed. Eq. (3.10) performs the error between averaging IC measurements between AC and DC MGs. The order of terms in (3.10) suggests a positive value for a power transferring from the DC to AC MG; u_{ILC} is negative otherwise.

Remark 1 The controller developed in (3.8) can include, without negative effects, a decentralised droop dynamics as reported in the works [18, 170]. If designed properly, the power flow originated by droop dynamics will be compensated by the distributed control of (3.8), acting as the second layer in the ILC used in [18].

The proposed protocol in (3.10), (3.8) gives the following result.

Theorem 1 *Consider the control protocol described in* (3.10) *and* (3.8) *implemented by the ILC of a hybrid AC/DC MG. Under a balanced graph with a spanning tree in the AC and DC sub-MGs, the ICs synchronise in finite-time* $t_f \leq \frac{V(0)^{1-p}}{M(1-p)} \; \forall \; M > 0$ *and* $0 < p < 1$.

Proof. It is assumed that $N = N_{\text{AC}} = N_{\text{DC}}$ and $\boldsymbol{a}_{\text{AC}}^{\text{ILC}} = \boldsymbol{a}_{\text{DC}}^{\text{ILC}}$ for the sake of simplicity. This allows the ICs to be paired, and the tracking error to be constructed as $e_i^{\lambda} = \lambda_i^{\text{AC}} - \lambda_i^{\text{DC}}$. Also, assuming an initial steady-state condition in the AC/DC MG, i.e., no load impacts, the activation of the controller in (3.10) will drive the ILC to have a dynamics defined by

$\dot{e}_i^\lambda = c_L \sum_{j=1}^N a_{ij} \text{sig}\left[e_j^\lambda - e_i^\lambda\right]^{\alpha_L}$ with

$$[a_{ij}]_{N\times N} \simeq \begin{bmatrix} 0 & a_{\text{AC1}}^{\text{ILC}} a_{\text{AC2}}^{\text{ILC}} & \dots & a_{\text{AC1}}^{\text{ILC}} a_{\text{AC}N}^{\text{ILC}} \\ a_{\text{AC2}}^{\text{ILC}} a_{\text{AC1}}^{\text{ILC}} & 0 & & a_{\text{AC2}}^{\text{ILC}} a_{\text{AC}N}^{\text{ILC}} \\ \vdots & & \ddots & \vdots \\ a_{\text{AC}N}^{\text{ILC}} a_{\text{AC1}}^{\text{ILC}} & a_{\text{AC}N}^{\text{ILC}} a_{\text{AC2}}^{\text{ILC}} & \dots & 0 \end{bmatrix}. \tag{3.11}$$

It is worth noting that ICs are given by (3.7) and that Lagrange multipliers σ_i^+ and σ_i^- are obtained by (2.7) using a sufficiently fast feedback loop. This means that these dynamics can be neglected by the global IC dynamics.

Let $V = \frac{1}{2} e^\lambda (e^\lambda)^T$ be a Lyapunov candidate, with $e^\lambda = (e_1^\lambda, \dots, e_N^\lambda)$, then

$$\dot{V} = (e^\lambda)^T \dot{e}^\lambda = \sum_{i,j=1}^N c_L e_i^\lambda a_{ij} \text{sig}\left[e_j^\lambda - e_i^\lambda\right]^{\alpha_L}. \tag{3.12}$$

From (*Lemma 2* [38]), one has

$$\dot{V} \leq -\frac{1}{2} \left(\sum_{i,j=1}^N (c_L a_{ij})^{\frac{2}{1+\alpha_L}} (e_j^\lambda - e_i^\lambda)^2 \right)^{\frac{1+\alpha_L}{2}}. \tag{3.13}$$

By defining $A^\lambda = [(c_L a_{ij})^{(2/(1+\alpha_L))}]$, it results in

$$\dot{V} \leq -\frac{1}{2} \left((e^\lambda)^T L(A^\lambda)\, e^\lambda \right)^{\frac{1+\alpha_L}{2}}. \tag{3.14}$$

From (*Lemma 3* [38]), one has

$$2(e^\lambda)^T L(A^\lambda)\, e^\lambda \geq 2\, \gamma_2 \left(L(A^\lambda) \right) (e^\lambda)^T e^\lambda > 0\,, \tag{3.15}$$

with $\gamma_2(L(A^\lambda))$ as the second eigenvalue of $L(A^\lambda)$. Recalling $2V = (e^\lambda)^T e^\lambda$ and replacing (3.15) into (3.14), it gives

$$\begin{aligned} \dot{V} &\leq -\frac{1}{2} \left(4\gamma_2(L(A^\lambda))V \right)^{\frac{1+\alpha_L}{2}} \\ &\leq -2^{\alpha_L} \gamma_2(L(A^\lambda))^{\frac{1+\alpha_L}{2}} V^{\frac{1+\alpha_L}{2}} \\ &\leq -MV^p\,, \end{aligned} \tag{3.16}$$

where $M = 2^{\alpha_L} \gamma_2(L(A^\lambda))^{(1+\alpha_L)/2}$ and $p = (1+\alpha_L)/2$ are positive constants as long as $c_L > 0$ and $\alpha_L \in (0,1)$. Therefore, (3.16) satisfies (*Lemma 1* [38]), i.e. $V(t)$ reaches zero at finite time t_f. ■

3.2.4 Parameters for the proposed IC controller

Since the IC of each MG is received from several DGs (for reliability purposes), the communication vectors of the ILC need to apportion the information for generalised compatibility (any number of communicating DGs per MG). Hence, the weights of the communication vector for the ILC respecting the AC MG are designed as

$$a_{\mathrm{AC}\,i}^{\mathrm{ILC}} = \begin{cases} \frac{1}{N_{\mathrm{AC}}^{\mathrm{ILC}}}\,, & \text{if } i\text{-th DG communicates}\,, \\ 0\,, & \text{otherwise}\,, \end{cases} \tag{3.17}$$

where $N_{\mathrm{AC}}^{\mathrm{ILC}}$ is the number of active nodes in the AC MG sending information to the ILC. The weights for the communication vector $\boldsymbol{a}_{\mathrm{DC}}^{\mathrm{ILC}}$ can be derived analogically.

The PI controller of power in the ILC is tuned assuming a unit plant, decoupled from the ILC's inner current controller and the subgrids' IC consensus. The design control bandwidth is selected as $\omega_{\mathrm{ILC}} = \min(\omega_{\mathrm{sec}}^{\mathrm{AC}}, \omega_{\mathrm{sec}}^{\mathrm{DC}})$, where $\omega_{\mathrm{sec}}^{\mathrm{AC}}$ and $\omega_{\mathrm{sec}}^{\mathrm{DC}}$ are the secondary control bandwidths applied into the AC and DC MGs, respectively.

3.2.5 Distributed control of DGs for economic dispatch

The distributed control for DGs can be chosen based on already published methods, like [20, 36, 106, 108, 110]. In particular, the thesis' author studied and developed a variation of the former papers to achieve voltage and frequency restoration while an IC consensus is performed.

For the DC MG, the structure of the i-th DG's secondary control can be defined as:

$$E_i^{\mathrm{ref}} = E_{\mathrm{DC}}^{*} - m^{\mathrm{DC}} P_i + \delta E_i^1 + \delta E_i^2\,, \tag{3.18}$$

$$\left.\begin{aligned} \delta E_i^1 &= k_p^E \left(u_i^E\right) + k_i^E \int_0^t \left(u_i^E\right) d\tau\,, \\ u_i^E &= E_{\mathrm{DC}}^{*} - \overline{E}_i\,, \\ \overline{E}_i &= E_i + \int_0^t \left(\sum_{j=1}^{N_{\mathrm{DC}}} a_{ij}\, \mathrm{sig}\left[\overline{E}_j - \overline{E}_i\right]^{\nu^1} \right) d\tau\,, \end{aligned}\right\} \text{Average voltage regulator} \tag{3.19}$$

$$\left.\begin{aligned} \delta E_i^2 &= k_p^{\lambda}(u_i^{\lambda}) + k_i^{\lambda} \int_0^t (u_i^{\lambda}) d\tau\,, \\ u_i^{\lambda} &= c_{\lambda}^{\mathrm{AC}}\, \mathrm{sig}\left[\sum_{j=1}^{N_{\mathrm{DC}}} a_{ij}\left(\lambda_j - \lambda_i\right) \right]^{\nu^2}\,, \end{aligned}\right\} \text{Incremental cost regulator} \tag{3.20}$$

where E_i, and P_i are the output voltage and power of the i-th DG in the DC MG, E_{DC}^{*} is the MG reference voltage, m^{DC} is the droop gain, $\{k_p^E, k_i^E, k_p^{\lambda}, k_i^{\lambda}\} > 0$ are parameters of PI controllers, $c_{\lambda}^{\mathrm{DC}} > 0$ is a convergence speed parameter. Parameters $\{\nu^1, \nu^2\} \in (0, 1)$ regulate the finite-time convergence.

The control scheme is resumed in Fig. 3.3, where $G^E_{\mathrm{DC}}(s)$ and $G^\lambda_c(s)$ are PI controllers.

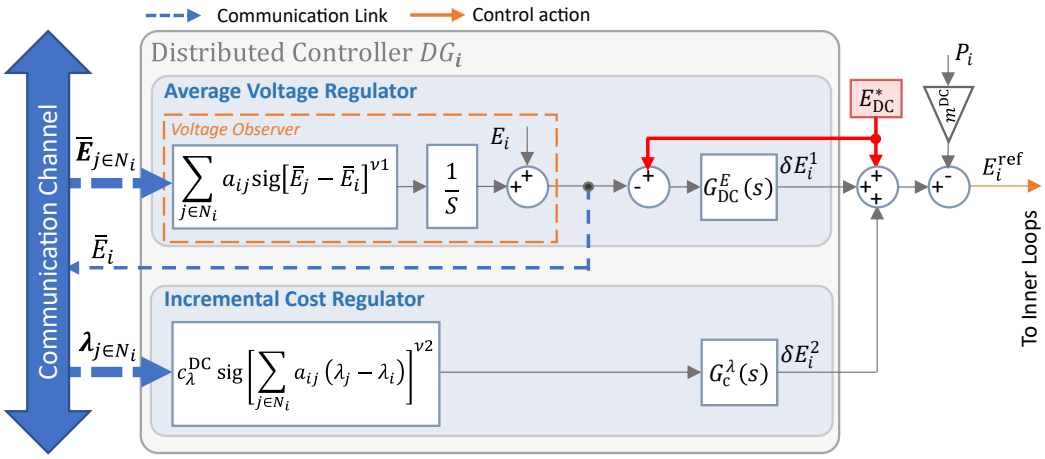

Figure 3.3: Distributed controller for DGs in DC MG.

For the AC MG, the DGs have the following secondary control loops:

$$E_{di}^{\mathrm{ref}} = E^*_{\mathrm{AC}} - n^{\mathrm{AC}} Q_i + n_d^{\mathrm{AC}} \dot{Q}_i + \delta E_i^1 + \delta E_i^2 \ , \tag{3.21}$$

$$\left.\begin{aligned} \delta E_i^1 &= k_p^E \left(u_i^E\right) + k_i^E \int_0^t \left(u_i^E\right) d\tau \ , \\ u_i^E &= E^*_{\mathrm{AC}} - \overline{E}_i \ , \\ \overline{E}_i &= E_{di} + \int_0^t \left(\sum_{j=1}^{N_{\mathrm{AC}}} a_{ij} \ \mathrm{sig}\left[\overline{E}_j - \overline{E}_i\right]^{\mu^1} \right) d\tau \ , \end{aligned}\right\} \ \text{Average voltage regulator} \tag{3.22}$$

$$\left.\begin{aligned} \delta E_i^2 &= k_p^Q (u_i^Q) + k_i^Q \int_0^t (u_i^Q) d\tau \ , \\ u_i^Q &= c_Q \sum_{j=1}^{N_{\mathrm{AC}}} a_{ij} \left(\frac{Q_j}{Q_j^{\max}} - \frac{Q_i}{Q_i^{\max}} \right) \ , \end{aligned}\right\} \ \text{Reactive power regulator} \tag{3.23}$$

$$\omega_i = \omega^* - m^{\mathrm{AC}} P_i + m_d^{\mathrm{AC}} \dot{P}_i + \delta\omega_i^1 + \delta\omega_i^2 \ , \tag{3.24}$$

$$\left.\begin{aligned} \delta\omega_i^1 = c_\omega \int_0^t \left((\omega^* - \omega_i) + \sum_{j=1}^{N_{\mathrm{AC}}} a_{ij} \left(\delta\omega_j^1 - \delta\omega_i^1\right) \right) \ , \end{aligned}\right\} \ \text{Frequency regulator} \tag{3.25}$$

$$\left.\begin{aligned} \delta\omega_i^2 = c_\lambda^{\mathrm{AC}} \int_0^t \mathrm{sig} \left[\sum_{j=1}^{N_{\mathrm{AC}}} a_{ij} \left(\lambda_j - \lambda_i\right) \right]^{\mu^2} \ , \end{aligned}\right\} \ \text{Incremental cost regulator} \tag{3.26}$$

where E_{di} is the voltage in the direct axis of a d-q reference frame, $\overline{E}_i$, ω_i, P_i, Q_i are the local average voltage, frequency, active and reactive powers of the i-th DG in the AC MG,

respectively. E^*_{AC} is the MG's voltage reference whereas ω^* is the MG's frequency reference. n^{AC} and m^{AC} are the voltage and frequency droop gains. n_d^{AC} and m_d^{AC} are damping factors to improve transient dynamics. Also, $k_p^E > 0$ and $k_i^E > 0$ are the parameters of a PI controller with input is u_i^E, $k_p^Q > 0$ and $k_i^Q > 0$ are the parameters of a PI controller whose input is u_i^Q. $0 < \{\mu^1, \mu^2\} < 1$ are finite-time fractional exponents, and $\{c_Q, c_\omega, c_\lambda^{\text{AC}}\} > 0$ are convergence speed gains.

The control scheme is resumed in Fig. 3.4, where $G^E_{\text{AC}}(s)$ and $G^Q_c(s)$ are PI controllers.

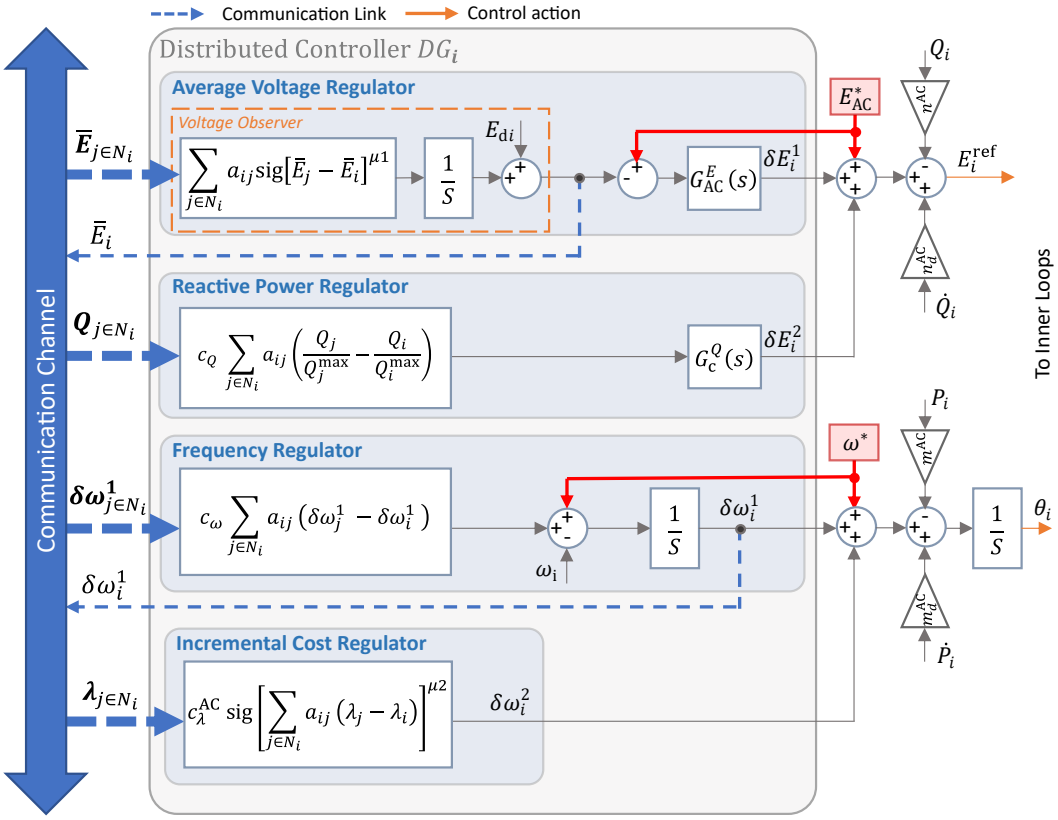

Figure 3.4: Distributed controller for DGs in AC MG.

The convergence proof of the asymptotic form of (3.19) and (3.20) is analogous to [106], with IC instead of current. For the finite-time consideration, [123] performed a similar stability analysis. The convergence of (3.22) and (3.23) was demonstrated in [112, 127]. In steady-state, the consensus protocols of (3.22) and (3.23) achieve an average voltage value for the MG equals to reference E^* while distributing the reactive power between DGs. The asymptotic convergence of (3.25) was demonstrated in [110]. The finite-time convergence of (3.26) was demonstrated in [171] based on [38] and [20]. The asymptotic version of the convergence proof of (3.26) was demonstrated in [127] but using the consensus variable of power instead of IC. In steady-state, the consensus protocols of (3.25) and (3.26) achieve the synchronisation of the DG's frequencies to ω^* while distributing the DG's active power according to the local cost functions, i.e., the synchronisation of IC is also achieved.

Since the convergence advantage of finite-time algorithms in secondary control is minor compared with the impact in the system's dynamic caused by the parameter selection of the ILC control, $\{\nu^1, \nu^2, \mu^1, \mu^2\} = 0$ will be taken for the sake of simplicity in the rest of this thesis. A similar case is presented with the damping terms n_d^{AC} and m_d^{AC} since they only improve transient dynamics of primary control and can be omitted if there is an appropriate virtual impedance loop or similar technique to decouple between active and reactive power.

More details about the formulation of primary control and distributed secondary control for DGs are given in Appendix B and Appendix F, respectively.

3.3 Design of a Multi-Objective Distributed Control Strategy for the Interlinking Converter

Based on the previous formulation, an additional control goal can be incorporated into (3.10) if the average power of each MG is considered [172]. The idea behind this is to regulate a trade-off between an economic and safety operation. Occasionally, the IC suffers variations, and the difference between the ICs of the AC and DC MGs could be significant. Under these circumstances, the balancing of ICs performed by (3.10) can lead to improper operation (saturation) of some generators. It is worth noting that the economic dispatch indiscriminately modifies the power generated by DGs, so MG saturations may occur.

Undoubtedly, imposing power constraints on the subgrids can help to reserve energy in the dispatchable DGs. These reserves are crucial for dealing with local transients [53]. Also, saving in the generated average power of a MG may directly reduce the lines' utilisation and increase the useful life of assets. In particular, line congestions might appear when a MG is forced to operate near its maximum power capacity (e.g. 1.0 [p.u]). The former can be verified considering a linearised relation for line congestion (based on [20])

$$I_l(P) \approx I_l^0 + \sum_{i=1}^{N} P_i G_{l\,i} \approx I_l^0 + \overline{G}_l \frac{1}{N} \sum_{i=1}^{N} P_i \,, \tag{3.27}$$

$$I_l(\overline{P}) \approx I_l^0 + \overline{G}_l \overline{P} \,, \tag{3.28}$$

where I_l is current in line l, I_l^0 is a constant, G_{li} is the participation index of the i-th DG to the l-th line, $\overline{G}_l$ is the average participation index of DGs to the l-th line, and $\overline{P}$ is the average power of the MG's DGs. Then, the normalised MG's average congestion could be approximated as [172]

$$\text{Sat}_{\text{Avg}}^{\text{MG}}(\overline{P}) = \frac{1}{L} \sum_{l=1}^{L} \frac{I_l(\overline{P})}{I_l^{\max}} \approx \sum_{l=1}^{L} \frac{I_l^0}{L I_l^{\max}} + \overline{P} \sum_{l=1}^{L} \frac{\overline{G}_l}{L I_l^{\max}} \approx \kappa_1 + \kappa_2 \overline{P} \,, \tag{3.29}$$

where κ_1 and κ_2 are constants that depend on the MG's topology. Therefore, it is suggested that the MG's average power linearly increases/decreases the utilisation of the distribution lines, which can congest and consequently damage part of the MG's infrastructure.

The aforementioned reasons call for additional compensation for the ILC controller. By controlling the average power of the MG, one could prevent the over-stress of cheaper generators of the hybrid MG. Also, avoidance of potential distribution line congestions is possible without knowledge of the MG topology.

The estimation of an MG average power is feasible to obtain by means of a distributed observer of power performed in every DG [127]. This kind of observer can be constructed as follows:

$$\overline{P}_i = P_i + \kappa_c \int_0^t \left(\sum_{j \in \mathcal{N}_i} a_{ij} \ \text{sig} \left[\overline{P}_j - \overline{P}_i \right]^{\beta} \right) d\tau \,, \tag{3.30}$$

where $\overline{P}_i$ is the average power estimation realised by the i-th DG in a MG, P_i is the measured power of the local DG. The coefficients $\kappa_c > 0$ and $0 < \beta < 1$ regulate the convergence rate.

The use of (3.30) gives rise to the development of control compensations to safeguard the MG's operation, which will be discussed in the next subsections.

3.3.1 Formulation of economic dispatch in a hybrid AC/DC MG with subgrid power saturation

Based on (3.1), a formulation of the economic dispatch optimisation including a constraint about the subgrids saturation is given by:

$$\min_{\boldsymbol{P}} \left\{ \sum_{i=1}^{N_{\text{sys}}} C_i(P_i) \right\} \quad \text{subject to,} \quad \begin{aligned} C_i(P_i) &= a_{ci} P_i^2 + b_{ci} P_i + c_{ci} \,, \\ P_i^{\min} &\leq P_i \leq P_i^{\max} \,, \\ -P_{\text{ILC}}^{\max} &\leq P_{\text{ILC}}(\boldsymbol{P}) \leq P_{\text{ILC}}^{\max} \,, \\ 0 &\leq \overline{P}_{\text{AC}}(\boldsymbol{P}) \leq \overline{P}_{\text{AC}}^{\max} \,, \\ 0 &\leq \overline{P}_{\text{DC}}(\boldsymbol{P}) \leq \overline{P}_{\text{DC}}^{\max} \,, \\ P_{\text{D}}^{\text{AC}} + P_{\text{D}}^{\text{DC}} &- \textstyle\sum_{j \in \mathcal{N}_{\text{sys}}} P_j = 0 \,, \end{aligned} \tag{3.31}$$

where $\overline{P}_{\text{AC}}(\boldsymbol{P}) = \sum_{i=1}^{N_{\text{AC}}} \frac{P_i}{N_{\text{AC}}}$ and $\overline{P}_{\text{DC}}(\boldsymbol{P}) = \sum_{i=1}^{N_{\text{DC}}} \frac{P_i}{N_{\text{DC}}}$ are the average powers among DGs in the AC and DC MGs, $\overline{P}_{\text{AC}}^{\max}$ and $\overline{P}_{\text{DC}}^{\max}$ are the defined maximum values for the AC and DC MGs that preserve the energy reserves, e.g., defined by a DNO. Moreover, the Lagrangian function results in

$$\begin{aligned} \mathbb{L}\left(P_i, \sigma_i^+, \sigma_i^-, \Lambda^+, \Lambda^-, \nu_{\text{AC}}, \nu_{\text{DC}}, \lambda\right) &= \sum_{i=1}^{N_{\text{sys}}} C_i(P_i) + \sum_{i=1}^{N_{\text{sys}}} \sigma_i^+ (P_i - P_i^{\max}) + \sum_{i=1}^{N_{\text{sys}}} \sigma_i^- (P_i^{\min} - P_i) \\ &+ \Lambda^+ \left(P_{\text{ILC}}(\boldsymbol{P}) - P_{\text{ILC}}^{\max} \right) + \Lambda^- \left(-P_{\text{ILC}}^{\max} - P_{\text{ILC}}(\boldsymbol{P}) \right) + \nu_{\text{AC}} \left(\overline{P}_{\text{AC}}(\boldsymbol{P}) - \overline{P}_{\text{AC}}^{\max} \right) \\ &+ \nu_{\text{DC}} \left(\overline{P}_{\text{DC}}(\boldsymbol{P}) - \overline{P}_{\text{DC}}^{\max} \right) + \lambda \left(P_{\text{D}}^{\text{AC}} + P_{\text{D}}^{\text{DC}} - \sum_{i=1}^{N_{\text{sys}}} P_i \right) \,, \end{aligned} \tag{3.32}$$

where ν_{AC} and ν_{DC} are Lagrange multipliers for the MG power saturation constraints.

The proof of stationary optimality condition of (3.32) gives

$$\begin{aligned}\frac{\partial}{\partial P_i}\mathbb{L} =& \frac{\partial C_i\left(P_i\right)}{\partial P_i} + \sigma_i^+ - \sigma_i^- + (\Lambda^+ - \Lambda^-)\frac{\partial P_{\mathrm{ILC}}(\boldsymbol{P})}{\partial P_i} + \frac{\nu_x}{N_x} - \lambda = 0 \\ \Leftrightarrow \quad & \lambda = \frac{\partial C_i\left(P_i\right)}{\partial P_i} + \sigma_i^+ - \sigma_i^- + (\Lambda^+ - \Lambda^-)\frac{\partial P_{\mathrm{ILC}}(\boldsymbol{P})}{\partial P_i} + \frac{\nu_x}{N_x}\,,\end{aligned} \tag{3.33}$$

where ν_x represents ν_{AC} if $i \in \mathcal{N}_{\mathrm{AC}}$ or ν_{DC} if $i \in \mathcal{N}_{\mathrm{DC}}$. Accordingly, N_x represents the number of DGs in the AC or DC MGs. Then, assuming sufficient power capacity in the ILC, we have

$$\lambda = \frac{\partial C_i\left(P_i\right)}{\partial P_i} + \sigma_i^+ - \sigma_i^- + \frac{\nu_x}{N_x}\,, \tag{3.34}$$

where $\nu_{\mathrm{AC}} \geq 0$ and $\nu_{\mathrm{DC}} \geq 0$ are placed in order to reserve power capacity in their corresponding MG, i.e., avoid saturations. It can be seen from (3.34) that values greater than zero in ν_{AC} and ν_{DC} will deviate the global IC, moving the IC of its corresponding MG independently from the other MG. Then, the ILC cannot ensure the synchronisation between the AC and DC sides (similar to the case of Λ^+ and Λ^+ multipliers). A solution to this could be incorporating the MG saturation constraints (ν_{AC} and ν_{DC}) locally in the DGs of each subgrid (similar idea to what was done in [20] for the AC MG). This solution could keep the synchronisation between AC and DC ICs while increasing the global IC to avoid MG saturations. However, this kind of implementation is beyond the scope of this thesis.

Alternatively, from (3.1), one can put an additional control goal instead of a constraint to restrict the MG saturations. As mentioned in the previous paragraph, to avoid an MG saturation the ILC can reduce its power transfer, inevitably deteriorating the synchronisation of ICs. Then, the ILC can perform one of the following to incorporate a new goal to avoid MG saturations by reducing the control action related to the IC balancing: (i) calculate a weighting factor "g", i.e., $\min\left\{g(\overline{P}_{\mathrm{AC}}, \overline{P}_{\mathrm{DC}})\sum_{i=1}^{N_{\mathrm{sys}}} C_i(P_i)\right\}$, or (ii) sum a term "$g$", i.e., $\min\left\{\sum_{i=1}^{N_{\mathrm{sys}}} C_i(P_i) + g(\overline{P}_{\mathrm{AC}}, \overline{P}_{\mathrm{DC}})\right\}$. Both methods could be equally effective provided a proper tunning process for the parameters of the function $g(\overline{P}_{\mathrm{AC}}, \overline{P}_{\mathrm{DC}})$.

This thesis will be focused on the application of the second method (a form of regularisation). This method adds a new term, $g(\overline{P}_{\mathrm{AC}}, \overline{P}_{\mathrm{DC}})$, which includes a weighting factor, h, to regulate the trade-off concerning the original objective function. For the implementation, the new term is chosen such that is equalises the average power values of the side MGs. This will give a reference from where the ILC will deviate from the global IC to support the saturation of both subgrids equally. Thus, for this case, the objective function to minimise is given by

$$\sum_{i=1}^{N_{\mathrm{sys}}} C_i(P_i),\ + g(\overline{P}_{\mathrm{AC}}, \overline{P}_{\mathrm{DC}}) = \sum_{i=1}^{N_{\mathrm{sys}}} C_i(P_i) + h\left(\sum_{i=1}^{N_{\mathrm{AC}}} \frac{P_i}{N_{\mathrm{AC}}} - \sum_{i=1}^{N_{\mathrm{DC}}} \frac{P_i}{N_{\mathrm{DC}}}\right)\,. \tag{3.35}$$

Providing different h coefficients for the AC and DC MGs can provide more flexibility in the control design (prioritising the power reserves of one MG). Then, the optimisation

problem can be formulated as

$$\min_{\boldsymbol{P}} \left\{ \sum_{i=1}^{N_{\text{sys}}} C_i(P_i) + h_{\text{AC}} \sum_{i=1}^{N_{\text{AC}}} \frac{P_i}{N_{\text{AC}}} - h_{\text{DC}} \sum_{i=1}^{N_{\text{DC}}} \frac{P_i}{N_{\text{DC}}} \right\}$$

subject to,

$$\begin{aligned} C_i(P_i) &= a_{ci} P_i^2 + b_{ci} P_i + c_{ci} \ , \\ P_i^{\min} \leq\ & P_i \ \leq P_i^{\max} \ , \\ -P_{\text{ILC}}^{\max} \leq P_{\text{ILC}}(\boldsymbol{P}) &\leq P_{\text{ILC}}^{\max} \ , \\ P_{\text{D}}^{\text{AC}} + P_{\text{D}}^{\text{DC}} - \textstyle\sum_{j \in \mathcal{N}_{\text{sys}}} P_j &= 0 \ , \end{aligned} \tag{3.36}$$

with the Lagrangian function

$$\begin{aligned} \mathbb{L}\left(P_i, \sigma_i^+, \sigma_i^-, \Lambda^+, \Lambda^-, h_{\text{AC}}, h_{\text{DC}}, \lambda\right) &= \sum_{i=1}^{N_{\text{sys}}} C_i(P_i) + h_{\text{AC}} \sum_{i=1}^{N_{\text{AC}}} \frac{P_i}{N_{\text{AC}}} - h_{\text{DC}} \sum_{i=1}^{N_{\text{DC}}} \frac{P_i}{N_{\text{DC}}} \\ &+ \sum_{i=1}^{N_{\text{sys}}} \sigma_i^+ (P_i - P_i^{\max}) + \sum_{i=1}^{N_{\text{sys}}} \sigma_i^- (P_i^{\min} - P_i) + \Lambda^+ \left(P_{\text{ILC}}(\boldsymbol{P}) - P_{\text{ILC}}^{\max} \right) \\ &+ \Lambda^- \left(P_{\text{ILC}}^{\min} - P_{\text{ILC}}(\boldsymbol{P}) \right) + \lambda \left(P_{\text{D}}^{\text{AC}} + P_{\text{D}}^{\text{DC}} - \sum_{i=1}^{N_{\text{sys}}} P_i \right) . \end{aligned} \tag{3.37}$$

Then, the stationary optimality condition gives

$$\begin{aligned} \frac{\partial}{\partial P_i} \mathbb{L} =& \frac{\partial C_i\left(P_i\right)}{\partial P_i} + \frac{h_x}{N_x} + \sigma_i^+ - \sigma_i^- + (\Lambda^+ - \Lambda^-) \frac{\partial P_{\text{ILC}}(\boldsymbol{P})}{\partial P_i} + -\lambda = 0 \\ \Leftrightarrow \quad \lambda =& \frac{\partial C_i\left(P_i\right)}{\partial P_i} + \sigma_i^+ - \sigma_i^- + (\Lambda^+ - \Lambda^-) \frac{\partial P_{\text{ILC}}(\boldsymbol{P})}{\partial P_i} + \frac{h_x}{N_x} \ , \end{aligned} \tag{3.38}$$

where $h_x = h_{\text{AC}}$ if $i \in \mathcal{N}_{\text{AC}}$, else $h_x = -h_{\text{DC}}$ if $i \in \mathcal{N}_{\text{DC}}$.

Note the similarities of (3.38) with (3.33). Due to this fact, the formulation in (3.36) also produces a de-synchronisation of ICs between the AC and DC sides. However, it will be applied in the rest of the chapter to produce the necessary control actions to avoid the subgrids' saturation by sacrificing the precision of the global IC consensus.

3.3.2 Distributed multi-objective control for economic dispatch and power regulation

The multi-objective control design of the ILC begins by adding a compensation term u_{ILC} into the control input of (3.8). This new term yields the difference between the average power of AC and DC MGs informed by the DGs. Also, because of the inherent trade-off between IC and average power regulation, a weight is added to regulate the average power balancing.

The resulting controller is given by:

$$
\begin{aligned}
P^{*}_{\mathrm{ILC}} &= k^{P}_{p}(u_{\mathrm{ILC}} + u^{'}_{\mathrm{ILC}}) + k^{P}_{i}\int_{0}^{t}(u_{\mathrm{ILC}} + u^{'}_{\mathrm{ILC}})d\tau\ , \\
u^{'}_{\mathrm{ILC}} &= c_{P}\sum_{i=1}^{N_{\mathrm{AC}}}\sum_{j=1}^{N_{\mathrm{DC}}}\mathrm{sig}\left[h_{\mathrm{AC}}\,a^{\mathrm{ILC}}_{\mathrm{AC}i}\overline{P}_{i} - h_{\mathrm{DC}}\,a^{\mathrm{ILC}}_{\mathrm{DC}j}\overline{P}_{j}\right]^{\alpha_{P}}\ ,
\end{aligned}
\tag{3.39}
$$

where c_P is a scaling coefficient, α_P is a fractional exponent for convergence, h_{AC} and h_{DC} are weights regulating the trade-off in the control objective, and $\overline{P}_i$ and $\overline{P}_j$ are the average power estimation of the i-th DG in the AC MG and the j-th DG in the DC MG, respectively. For implementation, (3.39) is simplified by $\alpha_P = 1$, giving a conventional asymptotic protocol and avoiding unnecessary chattering. The proposed control scheme is resumed in Fig. 3.5, where $G^{P}_{c}(s)$ represents a PI controller transfer function with a logic to clamp the output in case of a complete loss of communications.

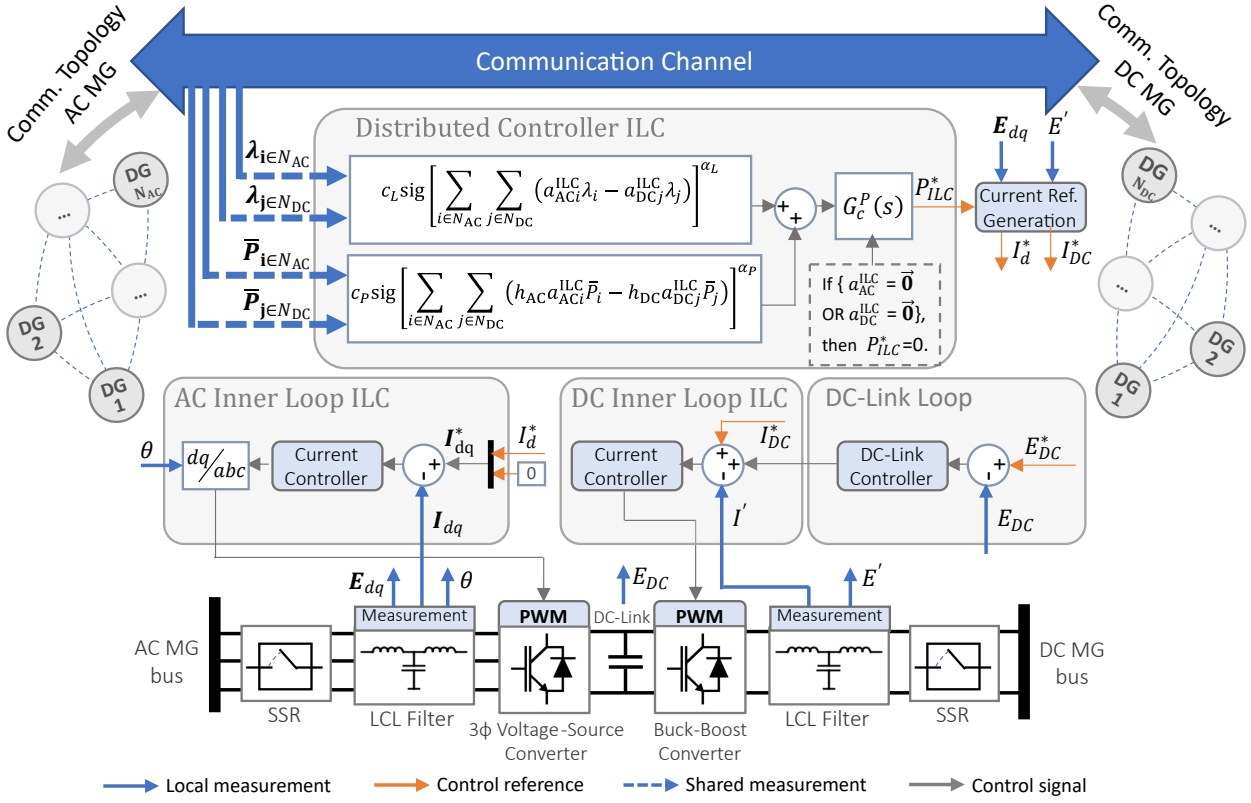

Figure 3.5: Proposed control scheme for the ILC. Adapted from [2].

Remark 2 Noting that differently from [23], under economic dispatch the normalised powers of DGs are not longer representative of the MG's power utilisation. Therefore, the implementation of (3.30) is required by every DG. Just sending normalised powers to the ILC could provide an accurate measurement of MG's utilisation if and only if all DGs of an MG communicate their local measurements (a fully connected graph), which is not a realistic nor attractive scenario of communication investments.

The use of (3.39) by the ILC gives rise to the following result

Theorem 2 *Consider the control protocol described in* (3.39) *implemented by the ILC of a hybrid MG. Under a balanced graph with a spanning tree in the AC and DC sub-MGs, the IC synchronizes in a proportion given by the average power difference at a finite-time* $t_f \leq \frac{V(0)^{1-p}}{M(1-p)}$ $\forall$ $M > 0$ *and* $0 < p < 1$.

Proof. Based on Theorem 1, the tracking errors are defined as $e_i^{\lambda} = \lambda_i^{\mathrm{AC}} - \lambda_i^{\mathrm{DC}}$ and $e_i^{P} = h_{\mathrm{AC}}\overline{P}_i^{\mathrm{AC}} - h_{\mathrm{DC}}\overline{P}_i^{\mathrm{DC}}$. For simplicity, it is assumed $\alpha_L = \alpha_P$. Also, the dynamics of the power observers $\overline{P}_i^{\mathrm{AC}}$ and $\overline{P}_i^{\mathrm{DC}}$ can be viewed as constants by the ILC, provided a high gain κ_c and a low ω_{ILC}. Then, let $V = V_\lambda + V_P = 1/2\,(e^{\lambda}(e^{\lambda})^T + e^{P}(e^{P})^T)$ be a Lyapunov candidate; by following the steps of Theorem 1 (*Lemma 2* [38] and *Lemma 3* [38]), one can get

$$\begin{aligned}
\dot{V} &\leq -\frac{1}{2}\left(\sum_{i,j=1}^{N}(c_L a_{ij})^{\frac{2}{1+\alpha_L}}(e_j^{\lambda}-e_i^{\lambda})^2\right)^{\frac{1+\alpha_L}{2}} - \frac{1}{2}\left(\sum_{i,j=1}^{N}(c_P a_{ij})^{\frac{2}{1+\alpha_L}}(e_j^{P}-e_i^{P})^2\right)^{\frac{1+\alpha_L}{2}} \\
\dot{V} &\leq -2^{\alpha_L}\left(\gamma_1(L(A^{\lambda}))^{\frac{1+\alpha_L}{2}}V_{\lambda}^{\frac{1+\alpha_L}{2}} + \gamma_2(L(A^{P}))^{\frac{1+\alpha_L}{2}}V_{P}^{\frac{1+\alpha_L}{2}}\right) \\
\dot{V} &\leq -MV^{p},
\end{aligned} \tag{3.40}$$

where $A^P = [(c_P a_{ij})^{(2/(1+\alpha_P))}]$, $p = (1+\alpha_L)/2$, $M = 2^{\alpha_L}\gamma^p$, and

$$\gamma = \frac{\left(\gamma_1\left(L(A^{\lambda})\right)\right)^2 + \left(\gamma_2\left(L(A^{P})\right)\right)^2 - \left|\left(\gamma_1\left(L(A^{\lambda})\right)\right)^2 - \left(\gamma_2\left(L_P\right)\right)^2\right|}{2\left(\left(\gamma_1\left(L(A^{\lambda})\right)\right)^2 + \left(\gamma_2\left(L(A^{P})\right)\right)^2\right)^{\frac{1}{2}}}.$$

where $\gamma_1(\cdot)$ and $\gamma_2(\cdot)$ are the first and second eigenvalues of their corresponding matrices.

Coefficients p and M are positive $\Leftrightarrow$ $\{c_L, c_P\} \in (0,\infty)$ and $\{\alpha_L, \alpha_P\} \in (0,1)$, which completes the proof. ■

3.3.3 Parameters for the proposed multi-objective controller

The parameters of the PI controller are the same as in the previous section. Regarding the weight used for the trade-off between control goals, values around [0,1] are recommended. Fine-tuning can be conducted through offline Pareto optimality studies [53, 173]. However, since this control action is only required when power is near the specified boundaries, h coefficients can be calculated online with an adaptive formula depending on the MG saturation. For this purpose, this work proposes an activation function with an exponential shape given by

$$h(\overline{P}_x) = k_h^1 \, e^{\left(k_h^2 \, \overline{P}_x\right)} , \tag{3.41}$$

where the sub-index x represents either the AC or DC MG. The form of (3.41) is selected because it gives a smooth and gradual increase in the average power balance when $\overline{P}_x \rightarrow 1$. The parameters of (3.41) are selected such that $h(1.0) = 0.9$, i.e. nearly 90% of the ILC capacity is employed for average power balance when a MG is at maximum capacity. This behaviour is illustrated in Fig. 3.6.

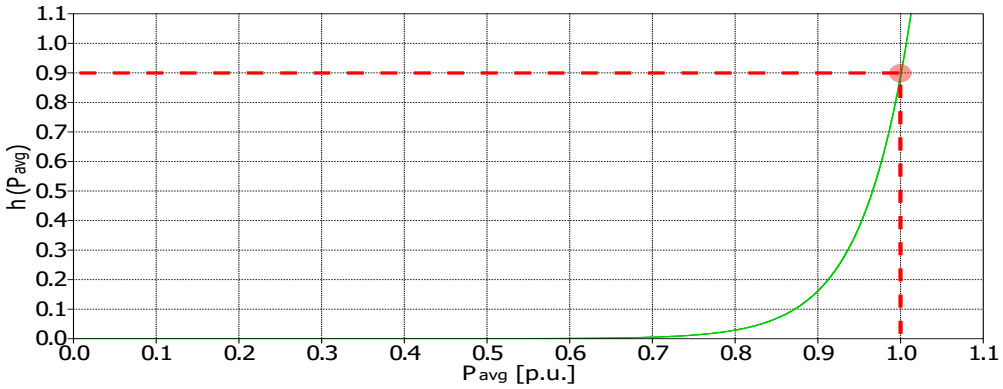

Figure 3.6: Weight function for average power regulation. Adapted from [2].

Concerning the transient state dynamics, it is worth noting that (3.41) has a dependency on the average estimation of each subgrid, which consequently depends on the DG's powers and their communications. Such dependency can be avoided by providing the same conditions described in Theorem 2.

3.4 Time Delay Stability Analysis

The convergence proofs of Theorem 1 and Theorem 2 settled the ground for the simulation tests coming in the next sections. However, the occurrence of time delays needs to be addressed first, which is one of the more disturbing issues in communications systems (e.g., it disturbs stability more than communication losses do). Time delays in distributed control, using single-integrator dynamics, generally slow down the convergence time and increase the transient state oscillations (overshoot) of the consensus variable in all agents. In normal operations, time delays are assumed to be small and bounded. As demonstrated in (*Theorem 10* [76]), fixed and homogeneous time delays $\tau < \tau_{\max}$ provide global asymptotic stability. $\tau_{\max} = \frac{\pi}{2\gamma_{\max}(L(A))}$ where $\gamma_{\max}(L(A))$ is the maximum eigenvalue of the system's

Laplacian matrix. It is worth noting that these conditions are reasonable to assume so that no further control actions should be taken when time delays are present.

Despite this fact, the use of distributed observers, like the one in (3.30), gives rise to different results. Works like [174–176] have identified issues with the dynamic average consensus when affected by disturbances and time delays, even with constant input reference values. Indeed, the issue can be mathematically demonstrated when considering the sampling of different time instants. Based on (3.30), we have:

$$\overline{P}_i(t) = \begin{cases} P_i(t) + \int_0^t \sum_{j=1}^N a_{ij}(\overline{P}_j(0) - \overline{P}_i(t_n^i))dx & \text{if } 0 < t \leq \tau \ , \\ P_i(t) + \int_0^t \sum_{j=1}^N a_{ij}(\overline{P}_j(t_n^j - \tau) - \overline{P}_i(t_n^i))dx & \text{if } t > \tau \ , \end{cases} \tag{3.42}$$

where t_n^i is the most recent sampled instant by the i-th agent immediately before running the updating rule, and the initial condition $\overline{P}_j(0) = 0 \ \forall j \in \mathcal{N}$ (see [78, 174]) must be met for achieving consensus to the true average value, i.e., $\text{Lim}_{t\to\infty} \left\| (1/N) \sum_{j=1}^N P_j(t) - \overline{P}_i(t) \right\| = 0$. From (3.42), it can be seen that for $0 < t \leq \tau$ the integrator increases without limits since it receives incorrect deviations (i.e., it accumulates $P_i(t)$ plus a real value). During this time period, $\overline{P}_i(t)$ gets deteriorated and shared with other neighbours, propagating cumulative errors throughout the network. If $P_i(t)$ is constant during this time period, we can get by iterating

$$\overline{P}_i(t) = \left(1 - \sum_{j=1}^N a_{ij}\right)^s P_i \ , \ \text{ for } 0 < t \leq \tau \ , \text{ and } s = t/T_s \text{ (number of samples)} \ , \tag{3.43}$$

which shows how the average deviates without even receiving neighbour measurements.

A numerical verification of this is conducted in Appendix E using constant and a triangular wave input. The results confirm what was announced by [174]. To the best of the author's knowledge, unfortunately, the dynamic average consensus used in the literature of MGs (e.g. [107, 127]) did not compensate for the steady-state deviations caused by time delay; they simply did not address this situation, presumable because their control bandwidth is designed to be sufficiently slow. This last statement can be true to some extent with the results of [174], i.e., the steady-state errors are proportional to time delays and small in well-connected topologies.

Therefore, considering the fact that steady-state errors only reduce the average value, and the application of power observer given in this chapter, in which the power observers are used in an exponential activation function, the effect of time delays can be negligible for small delays ($\tau < 500$[ms]) so no countermeasures will be taken.

3.5 Case Studies

Performance evaluations of the proposed controllers are made through experimental tests and simulations. The experimental tests were conducted in a laboratory environment with a small hybrid MG testbed in order the validate the controllers in (2.15) and (3.39). Subsequently, simulations were yielded to further analyse the behaviour of the ILC in the face of communication delays and changes in the trade-off policy. The simulation environment was necessary to allow the load impacts of different simulations to occur at the same time-step — this permits the waveforms to be overlapped and presented in the same chart for detailed analysis. Also, the simulated MG represents an extended version of the experimental testbed MG, with extra DGs and loads. Three cases are explored, both in the aforementioned experimental and simulated environments. These cases of study are the following:

Case 1. Load changing operation

This is a base case for all the tests. The response of the ILC's controller is studied under controlled load impacts, first at the DC MG and then at the AC MG. The impacts' magnitudes are described in Table 3.1. Cases 2 and 3 subdue the hybrid MG to the same load impacts as Case 1.

Case 2. Communication delayed operation

The ILC's controller is subject to constant time delays in all its communication links. For the experimental tests, it is used a constant delay τ of 400 [ms]. The values of delay τ used for simulations are 125, 250 and 500 [ms]. Also, the DG1 of AC MG loses communication at some point prior to the AC load impacts.

Case 3: Multi-objective operation

The behaviour of the ILC's controller is studied under different values of h_{AC} and h_{DC}. For experimental tests, the adaptive formula (3.41) is used. For the simulations, values of h_{AC} and h_{DC} equals to 0, 0.2, 0.4, and the adaptive formula (3.41) are used.

Details about the simulated and experimental settings are now provided.

3.5.1 Simulated MG

The simulations are performed in the software PLECS. The hybrid MG used for simulations is shown in Fig. 3.7; it incorporates 5 DGs and 3 loads per MG. The electrical parameters of the system are based on the testbed hybrid MG [3] and are listed in Table 3.1. Control parameters are shown in Tables 3.2-3.3; details about droop and secondary control gains used by the DGs are given in Appendix F.

The economic function parameters in DC MG are 1/2 of the ones shown in Table 3.2. The power constraints for the converters are the following; $P_i^{\max} = 1$ [kW] $\forall\, i \in \mathcal{N}_{\text{sys}}$, $Q_i^{\max} = 0.25$ [kVAR] $\forall\, i \in \mathcal{N}_{\text{AC}}$ and $P_{\text{ILC}}^{\max} = 5$ [kW]. The ILC has the communication vectors $\boldsymbol{a}_{\text{AC}}^{\text{ILC}} = (1, 0, 0, 0, 1)$ and $\boldsymbol{a}_{\text{DC}}^{\text{ILC}} = (1, 0, 0, 1, 0)$.

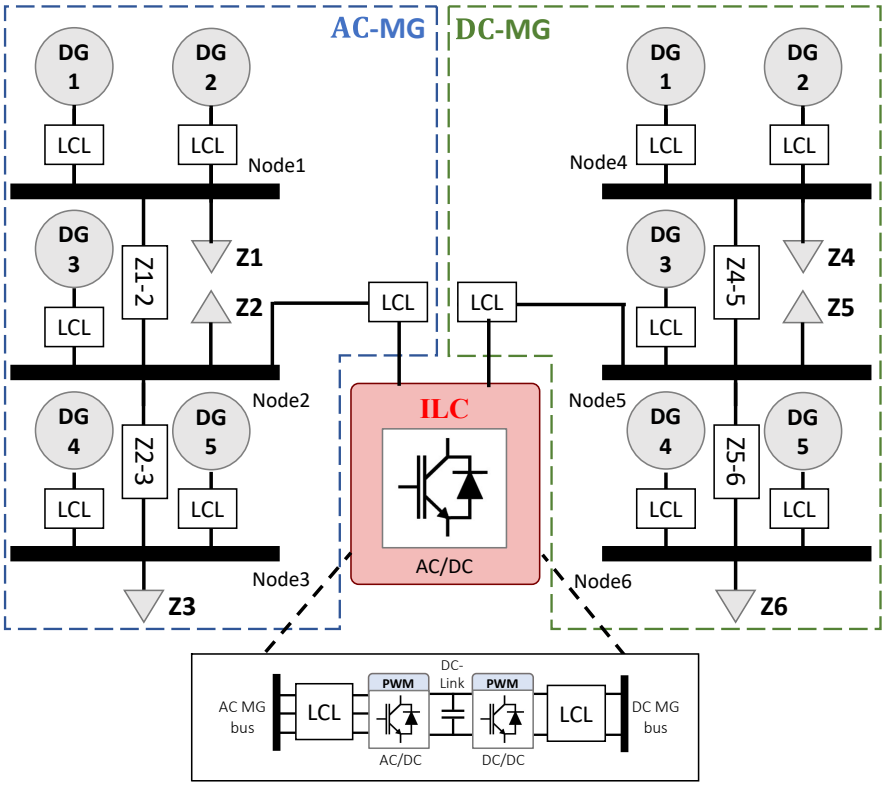

Figure 3.7: Simulated hybrid MG structure. The ILC block represents the AC/DC converter depicted in Fig.3.5. Adapted from [2].

Parameter	Value	Parameter	Value
Nom. Freq.	50 [Hz]	Line R1-2	1 [mΩ]
Nom. Volt. AC	120 [$V_{1\Phi}$]	Line R2-3	1 [mΩ]
Load Z1	15 [Ω]	Line L1-2	2.50 [mH]
Load Z2	33 [Ω]	Line L2-3	2.50 [mH]
Load Z3	12 [Ω]		
Nom. Volt. DC	100 [V]	Line R4-5	0.17 [Ω]
Load Z4	11 [Ω]	Line R5-6	0.50 [Ω]
Load Z5	8 [Ω]	Line L4-5	2.50 [mH]
Load Z6	16 [Ω]	Line L5-6	2.50 [mH]

Table 3.1: System parameters of hybrid MG.

For the tests, a load impact on the DC side is introduced with the connection of Z6. Subsequently, a second and a third load impacts take place on the AC MG; the AC load impacts correspond to the connection and disconnection of Z1.

Param.	DG1	DG2	DG3	DG4	DG5
a_{ci} [\$/kW^2]	0.264	0.444	0.400	0.500	0.250
b_{ci} [\$/kW]	0.067	0.111	0.100	0.125	0.063
c_{ci} [\$]	51.00	31.00	78.00	42.00	51.00

Table 3.2: Economic function parameters in AC MG.

Parameter	Value	Parameter	Value
k_p^P	0.25	α_L	0.70
k_i^P	1.57	α_P	1.00
c_L	1000	k_h^1	1x10^{-7}
c_P	4000	k_h^2	16

Table 3.3: Control parameters of the ILC.

3.5.2 Experimental setup

The testbed MG topology used for experimental validations is a reduced version of the one shown in Fig. 3.7, with the absence of Z3 and Z5. The generation is composed of DG1 and DG4 (renamed as DG2) on the AC side and DG1, DG3 (renamed as DG2) and DG4 (renamed as DG3) on the DC side. The DGs are emulated through industrial modular equipment of the Triphase brand; it consists of multiple 15 [kVA] back-to-back converters with a 16 [kHz] real-time embedded measurement and control system [3]. The experimental AC and DC MG distribution systems are built in separate racks as shown in Fig. 3.8. Details inside the DG's emulators are shown in Fig. 3.9.

Control parameters for the DGs and power constraints are the same used by simulations. The control parameters for the ILC are the same as Table 3.3, except $k_i^P = 0.78$ and $\alpha_L = 0.5$. For the communication, the ILC has the vectors $a_{\text{AC}}^{\text{ILC}} = (1, 1)$ and $a_{\text{DC}}^{\text{ILC}} = (1, 0, 1)$.

Figure 3.8: Components of experimental testbed hybrid AC/DC MG, described in [3]. Reproduced from [2].

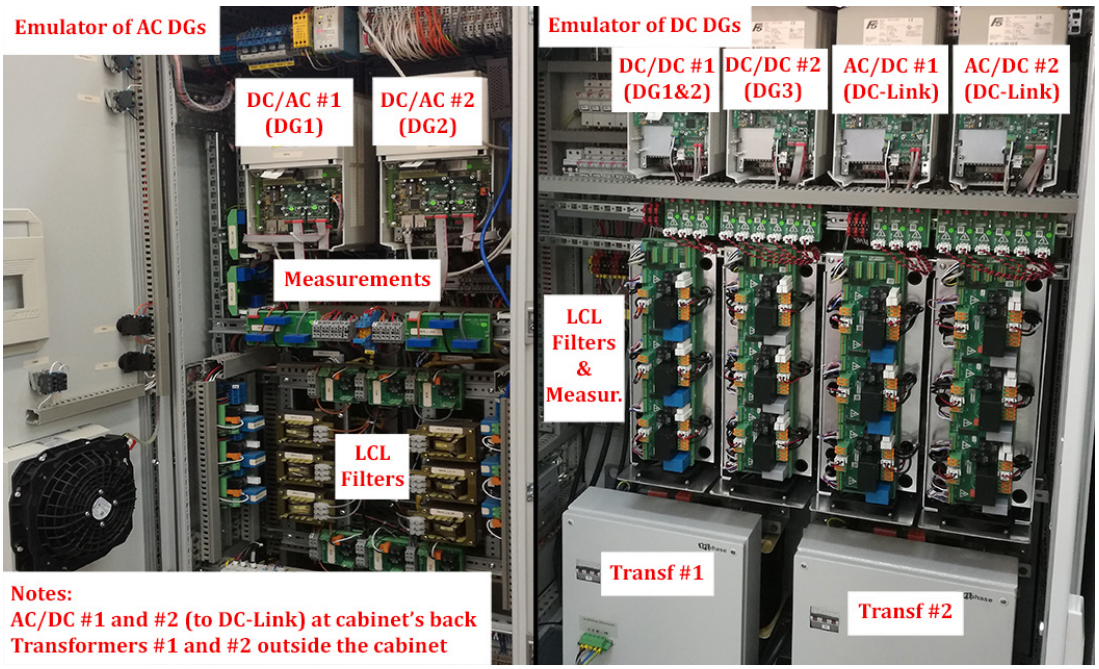

Figure 3.9: Detailed view of equipment and configuration of DG's emulators. Reproduced from [2].

3.6 Results

3.6.1 Experimental results

Case 1. Load changing operation

The results under load changes are presented in Fig. 3.10, Fig. 3.11 and Fig. 3.12. From Fig. 3.10 and Fig. 3.11, adequate operation under load impacts can be seen in the AC and DC side MGs. At $t = 8$ [s], the ILC controller is activated, showing a smooth transient on both sides; then, at $t = 19$ [s], the first load impact occurs in the DC MG accompanied by another small transient. For both cases, the system quickly stabilises to seamlessly find its economic operation point within a 2 [s] time span. For the instant $t = 30$ [s], the effect of the load impact that occurred on the AC side can be seen, with a more pronounced transient than in the DC case. Finally, at $t = 43$ [s], a second load impact is seen in the AC MG of equal magnitude but opposite sign to the previous one. Both impact loads recover in about three seconds, roughly doubling the settling time of the DC side's load impact.

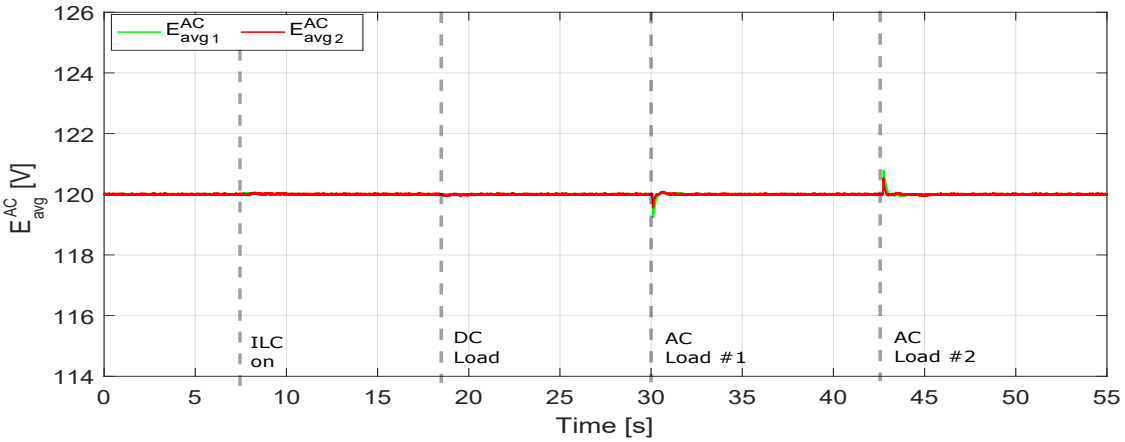

(a)

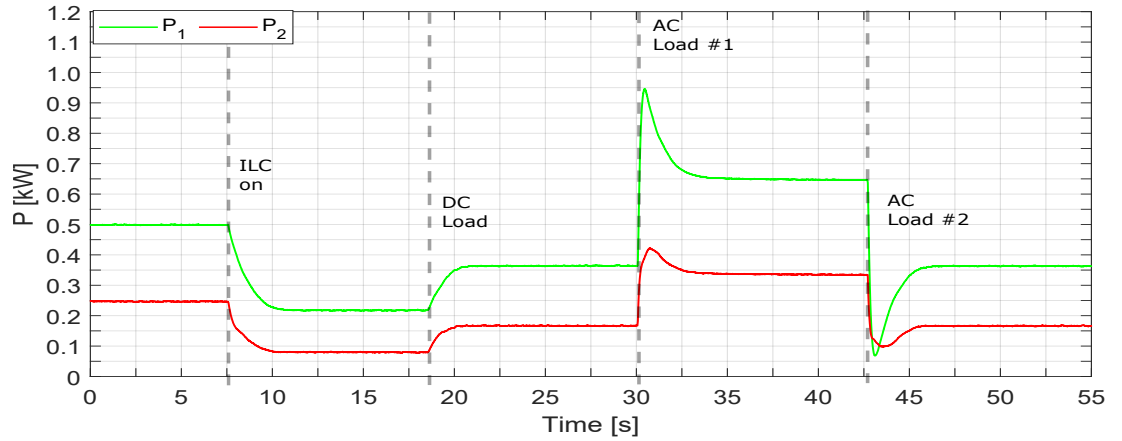

(b)

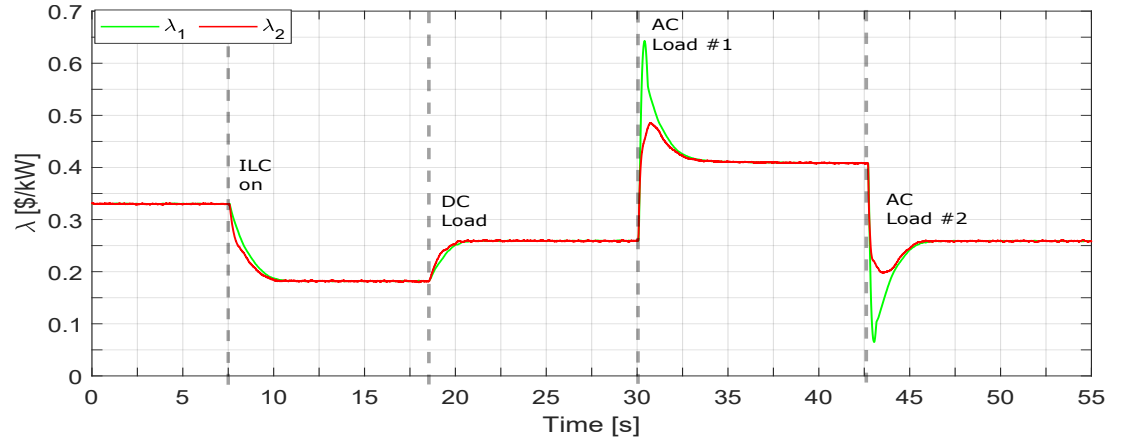

(c)

Figure 3.10: MATLAB data logging of the experimental waveforms of AC MG under controller in (3.39) and h-coefficient in (3.41). (a) Average voltage of DGs. (b) Active power of DGs. (c) IC of DGs. Adapted from [2].

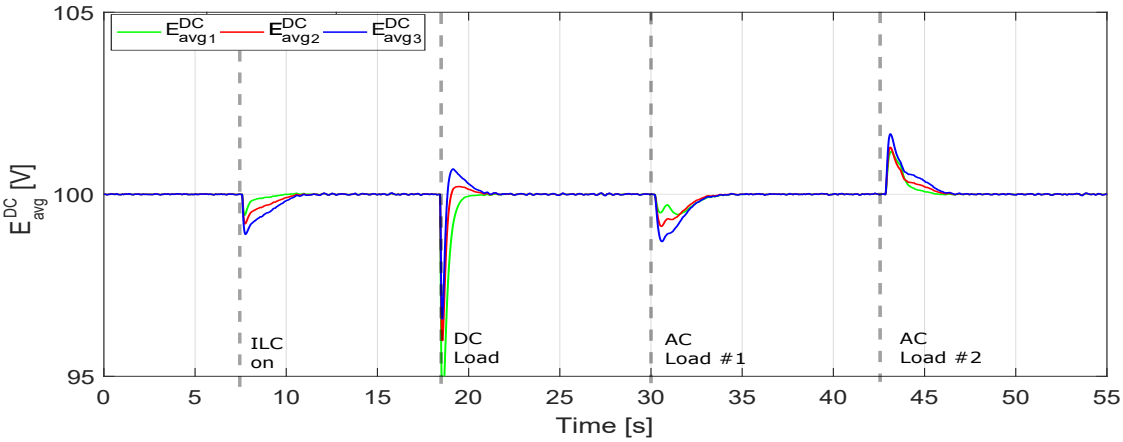

(a)

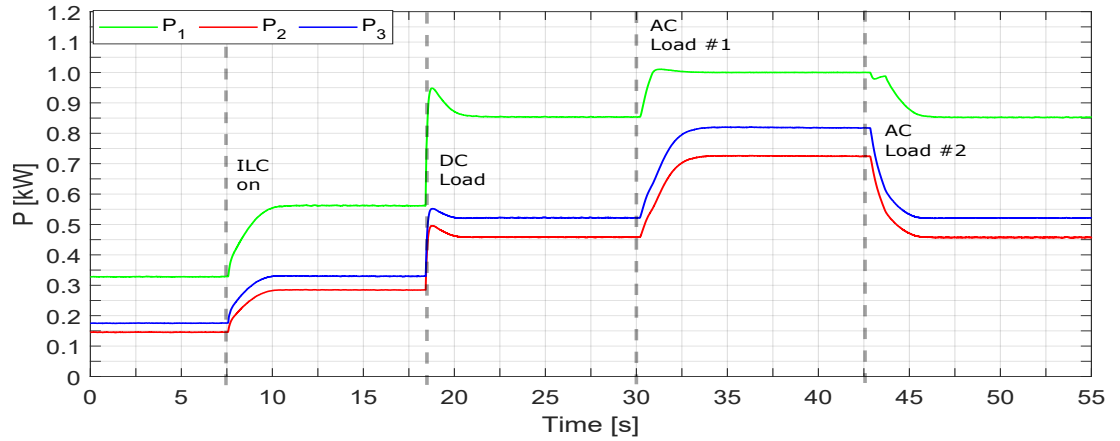

(b)

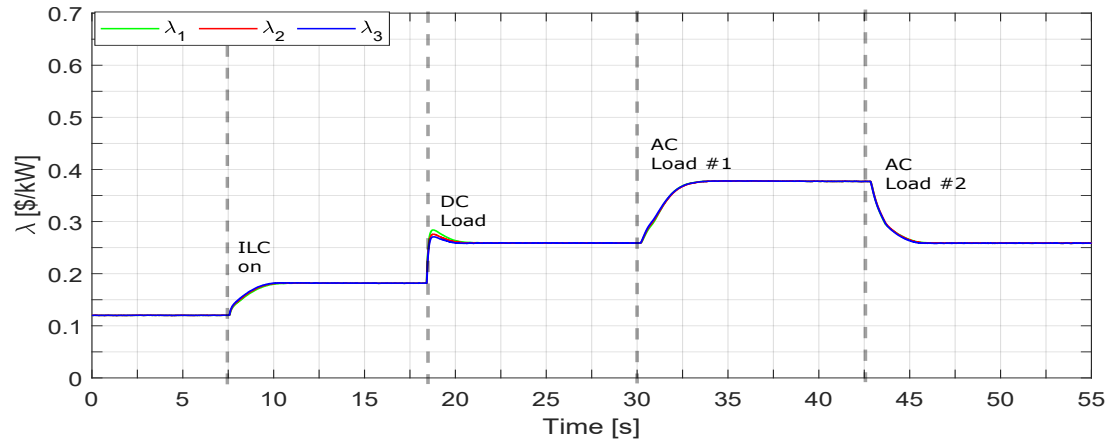

(c)

Figure 3.11: MATLAB data logging of the experimental waveforms of DC MG under controller in (3.39) and h-coefficient in (3.41). (a) Average voltage of DGs. (b) Active power of DGs. (c) IC of DGs. Adapted from [2].

On the IC waveforms in Fig. 3.12, it can be seen that the ILC quickly equates the ICs, within the described settling times of the previous paragraph. The authors acknowledge missing information from the ILC on the initial transient $t \in (7, 10)$. The stored data was held for 2.5 seconds by the ILC before updating. However, as seen in the previous figures, the real system followed a seamless and damped transient during this period, reaching a steady-state value where the ICs are equalised. Between $t = 30$ [s] and $t = 43$ [s] it can be seen that the DC MG is near 80% of its capacity, so the IC balancing of the ILC is relaxed. After $t = 43$ [s], the IC balancing recovers its fitness. The results show that the ILC is capable of acting near the IC consensus bandwidth of the subgrid's secondary control, ensuring an optimal operation of the AC/DC MG at almost all times (except during the short transients).

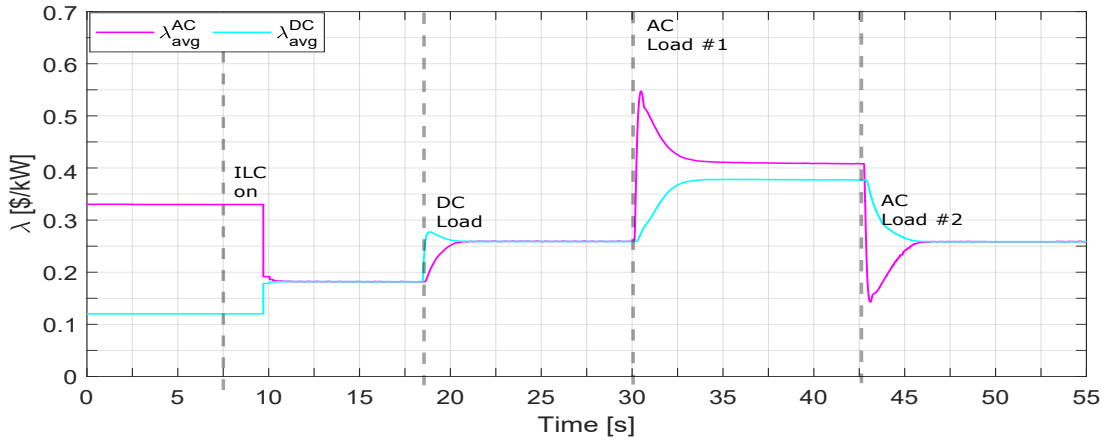

(a)

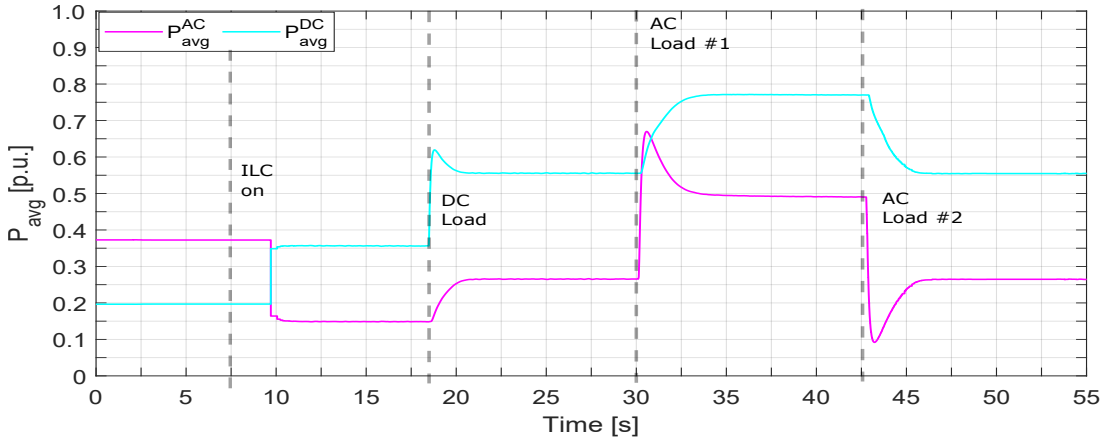

(b)

Figure 3.12: MATLAB data logging of the experimental waveforms of the ILC under controller in (3.39) and h-coefficient in (3.41). (a) Average calculation of ICs. (b) Average calculation of average powers. Adapted from [2].

3.6.2 Simulation results

Case 1. Load changing operation

The results for the proposed control scheme under simulation are shown in Fig. 3.13, Fig. 3.14, Fig. 3.15 and Fig. 3.16. Also, a brief comparison is presented in Fig. 3.17, showing the performance of the ILC's controller regarding finite-time convergence.

The secondary control variables of DGs are shown in Fig. 3.13, Fig. 3.14 and Fig. 3.16. From Fig. 3.13a and Fig. 3.13b, it can be seen the voltage levels of the DGs in AC and DC MGs restored near nominal values after the activation of secondary voltage control at t= 0.3 [s]. It can be highlighted that there exist small deviations in the steady-state between DGs; this behaviour was expected since there is an inherent trade-off concerning power and voltage regulation in the subgrids (due to the resistive/inductance ratio in the line feeders and composition of the overall MG). Another perspective about the performance of voltage restoration can be seen in Fig. 3.14a and Fig. 3.14b, where average value calculations $\overline{E}_i$ (using observers in (3.19) and (3.22)) are presented. The average voltages reach consensus to the reference value after a short transient. As for the frequency, Fig. 3.13c also show a restoration to the nominal value. In this case, the frequency restoration was activated at t= 1.0 [s]. Finally, in Fig. 3.14c the secondary reactive power-sharing is depicted. It was activated simultaneously with the secondary voltage control, at t= 0.3 [s]. It can be seen that reactive power achieves a consensus but for values close to zero; this is mostly because the proposed MG topology did have resistive loads, mainly.

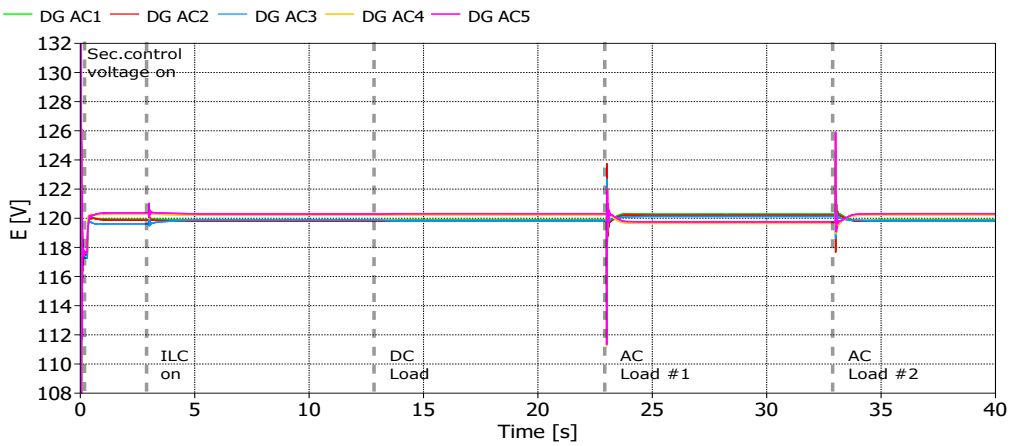

(a)

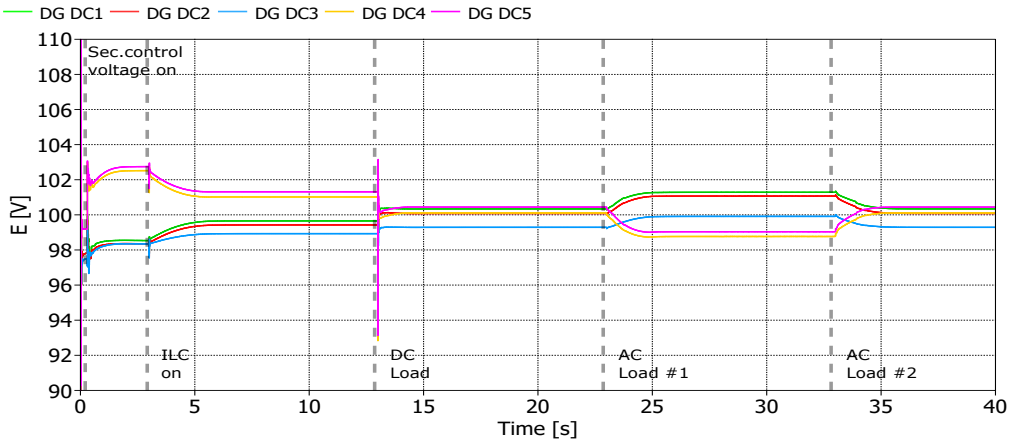

(b)

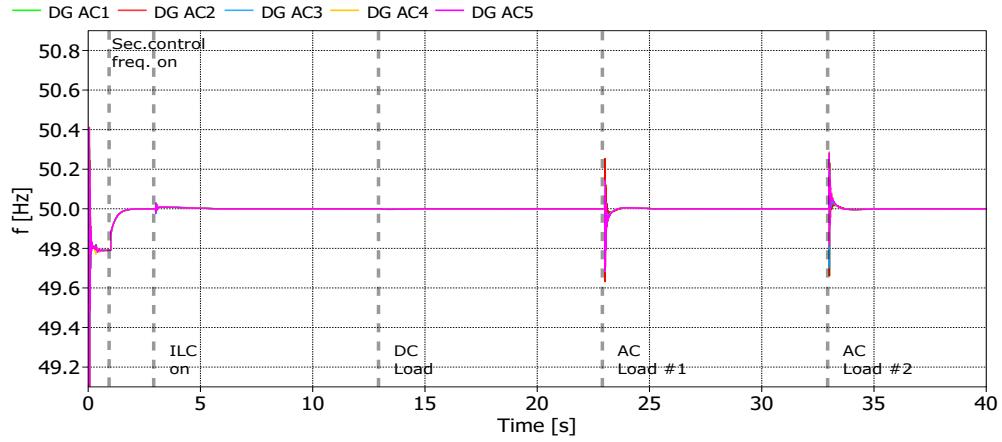

(c)

Figure 3.13: Simulation results of the hybrid MG under load changing conditions. (a) DG's voltages at AC subgrid. (b) DG's voltages at DC subgrid. (c) DG's frequency.

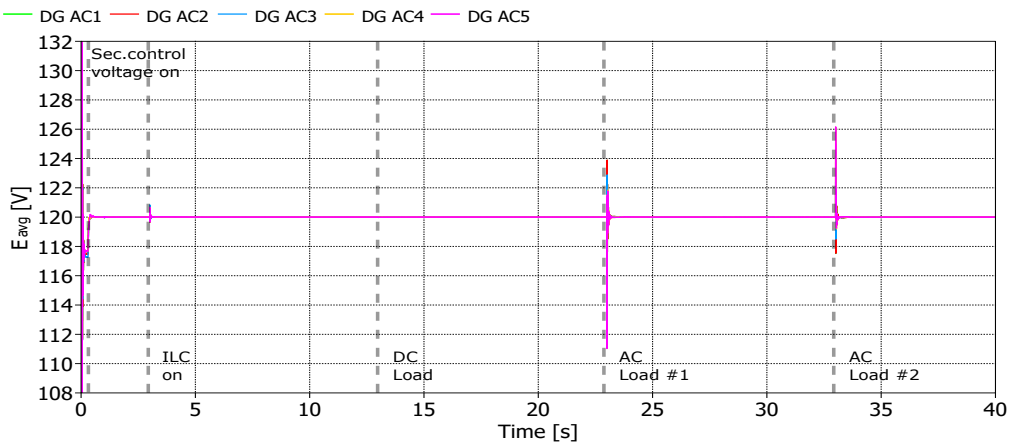

(a)

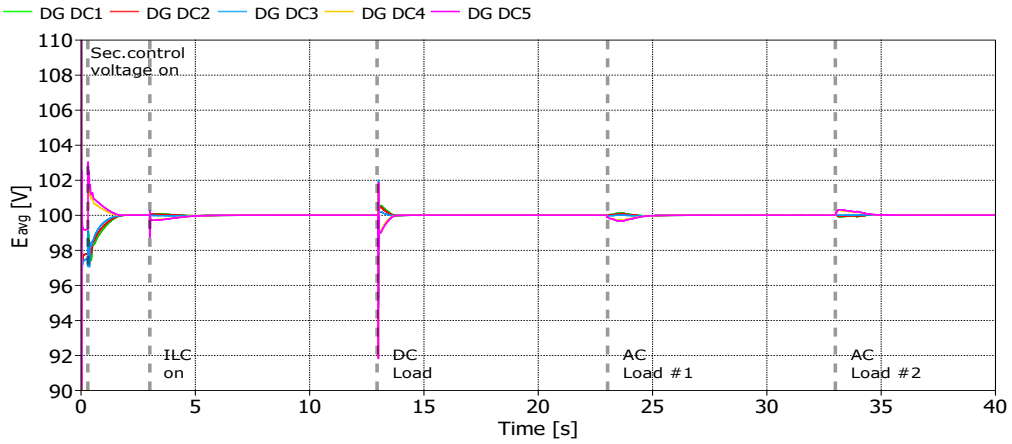

(b)

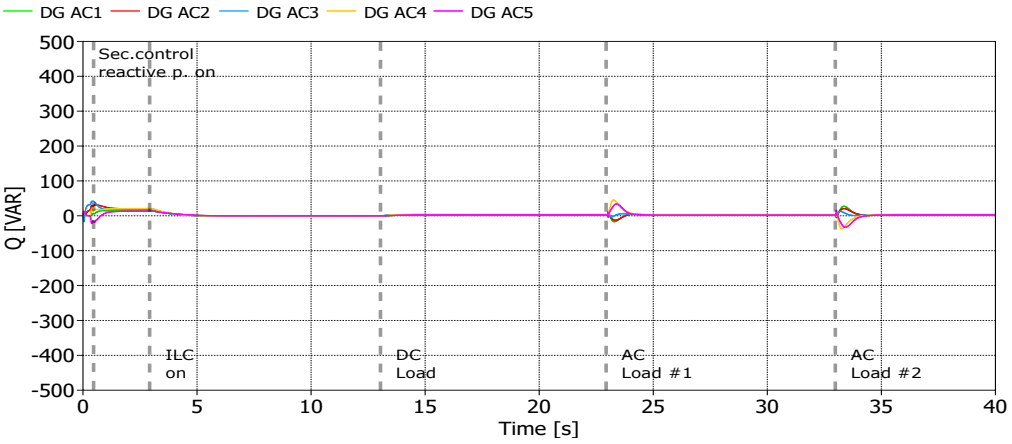

(c)

Figure 3.14: Simulation results of the hybrid MG under load changing conditions. (a) DG's average voltages at AC subgrid. (b) DG's average voltages at DC subgrid. (c) DG's reactive power.

Results for the variables measured by the ILC are presented in Fig. 3.15. From Fig. 3.15a, it can be seen that the average estimations of IC per subgrid reached a consensus after the activation of the ILC control, at t= 3 [s]. This means that the hybrid AC/DC MG is operating at the cheapest cost. Transient states can be observed for every major event of the simulation. The duration of the transient states is related to the control parameters of the ILC (control bandwidth). During these transients, the combined effects of the IC consensus of secondary control and the ILC control action can be observed. It is worth noting that a faster control bandwidth for the ILC could result in transient state oscillations due to coupling with the aforementioned IC consensus of the secondary control of DGs.

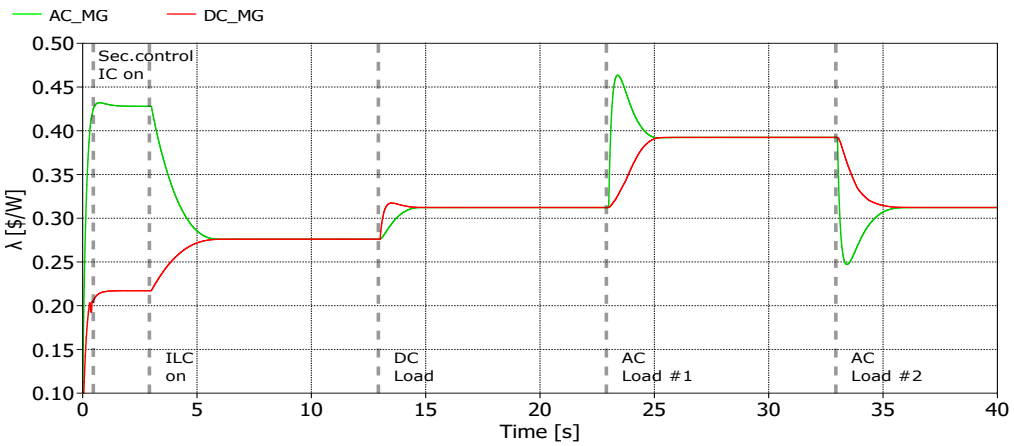

(a)

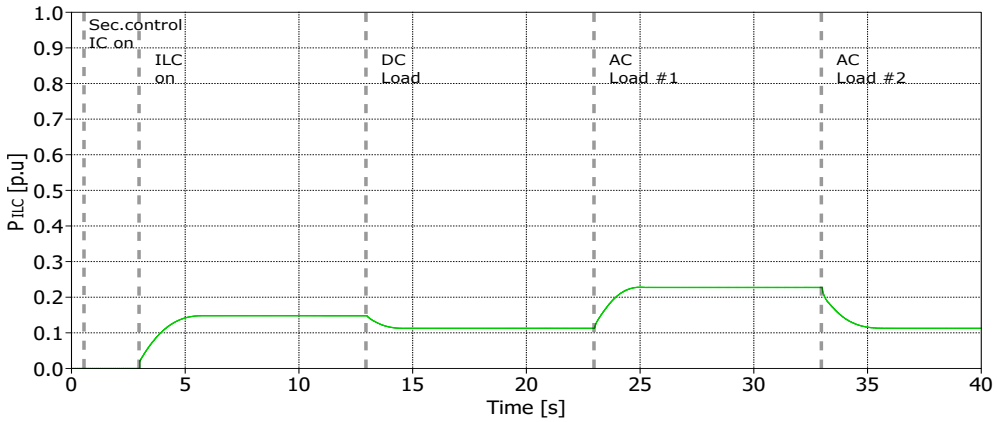

(b)

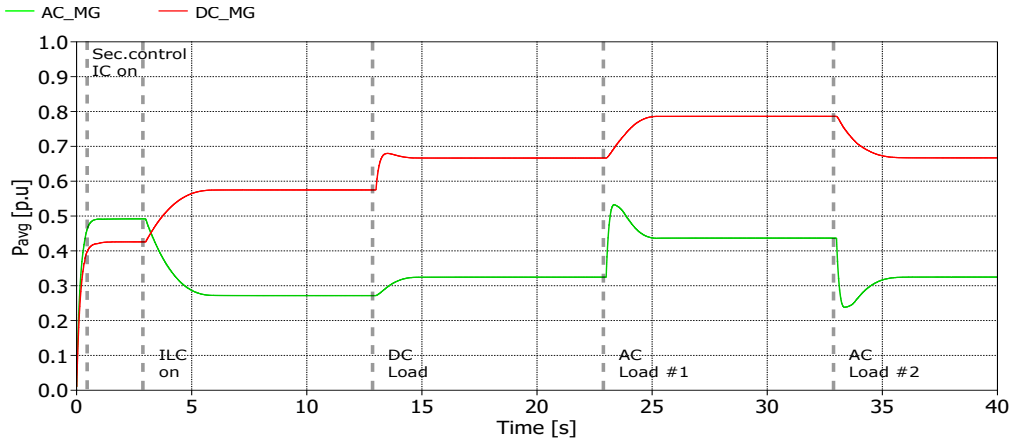

(c)

Figure 3.15: Simulation results of the hybrid MG under load changing conditions. (a) Average IC of MGs. (b) Power of ILC. (c) Average power of MGs.

The behaviour of the ICs along the hybrid MG system can be better perceived by the curves of Fig. 3.16. After the secondary control of IC is activated, DGs inside each MG achieve consensus. Then, with the ILC activation, all DGs continuously achieve consensus at new equilibrium points, despite the transients caused by load impacts. This behaviour will be true provided the DGs and the ILC is not saturated in power.

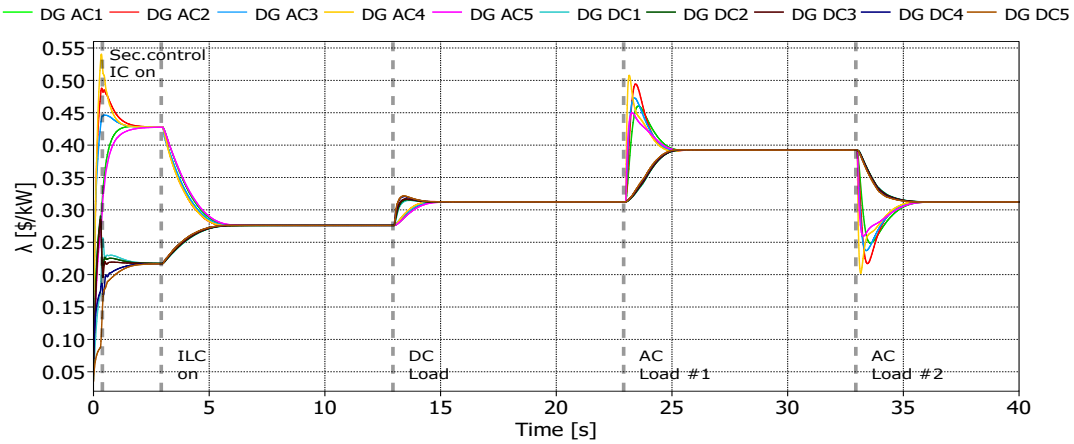

Figure 3.16: Simulation results of the DG's ICs at hybrid MG in Case 1.

A short comparison is presented in Fig. 3.17 where the performance of the ILC with and without the finite-time convergence is depicted. It can be seen that when the finite time is deactivated, i.e., the exponent α_L=1, the consensus of ICs takes more time. The finite-time consensus achieves a reduced cost of operation in the hybrid AC/DC MG faster. However, this benefit is in the long term since the savings (proportional to the area between the curves) are small in each transient state.

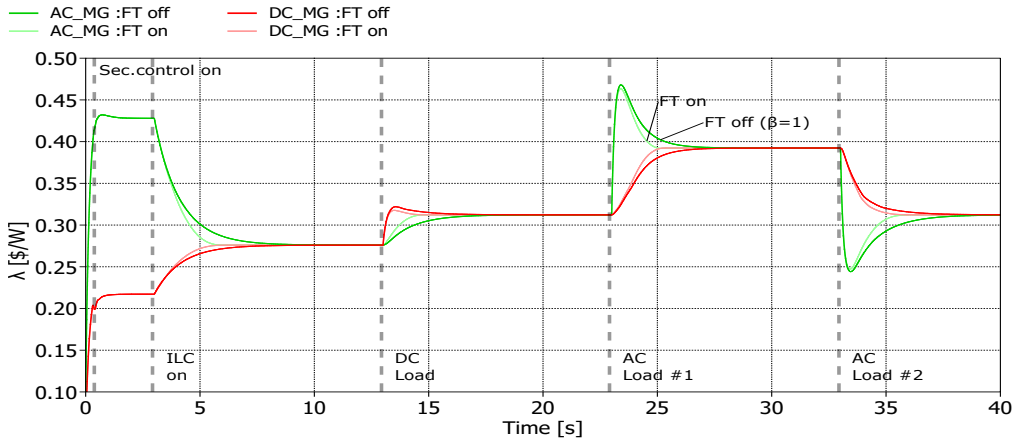

(a)

Figure 3.17: Comparison of ILC controller's performance with and without finite-time convergence.

Case 2. Communication delayed operation

Fig. 3.18 shows the ILC signals under the presence of 500 [ms] time delays in the communication between DGs and the ILC. Also, a communication loss with DG1 is simulated at t=28[s]. In this case study, the impact loads of the AC side are produced at t=23[s] (Z1 is connected) and t=33 [s] (Z1 is disconnected). Overall, an oscillatory response can be seen caused by large delays in the finite-time protocol; nevertheless, this effect can be neglected by reducing the ILC's control bandwidth or increasing the α_L exponent — i.e. the finite-time convergence speed can be reduced to avoid system instability. At t = 28 [s] the communication of DG1 in the AC MG is lost, however, it does not affect the controller performance in any form (provided there is another DG in the same MG communicating). Therefore, given the ILC's control bandwidth and the weighting structure used for communication vectors, a resilient behaviour is seen, being able to operate under large delays even if it loses some of its communication links.

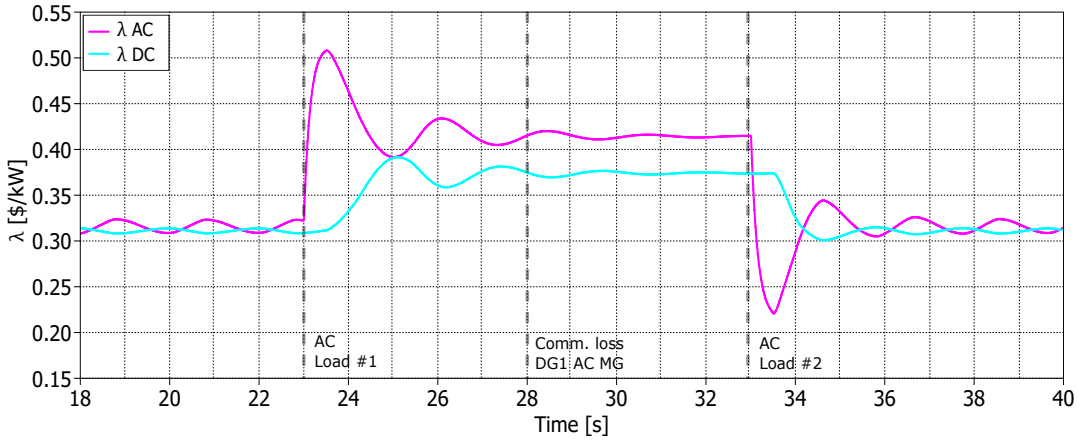

(a)

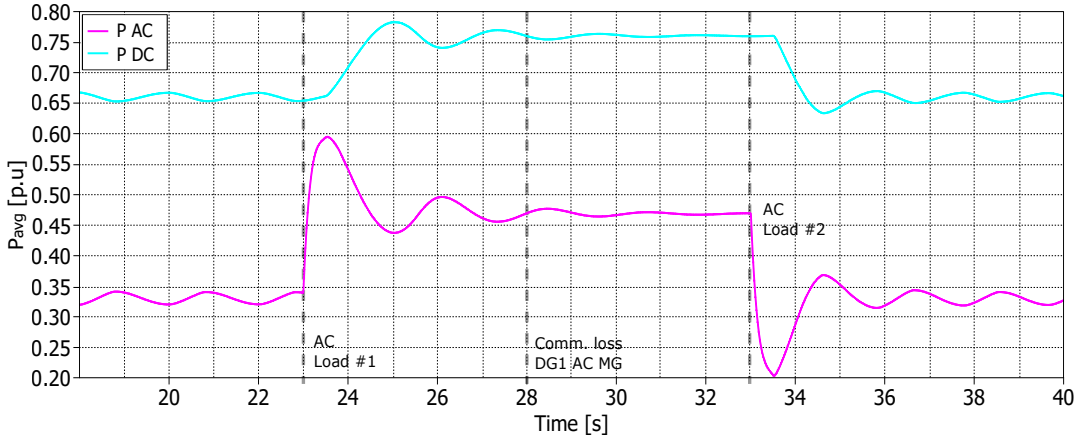

(b)

Figure 3.18: Simulation results of the ILC under 500 [ms] time-delay. (a) Average IC of MGs. (b) Average power of MGs.

Fig. 3.19 shows how the ILC's settling time increases as the transport delay does. In general, the ILC responds adequately to delays $\tau < \tau_{\max}$, where $\tau_{\max} \approx 785$ [ms] by using (3.11) and the procedure described in [76]. The magnitude of the transport delay deteriorates the transient state damping and settling time in proportion. As for the steady-state values, the delays do not alter these values. It is worth noting that for high delays (>500 [ms]), an oscillatory behaviour can be seen in the steady state but it will decrease slowly over time as the simulation runs.

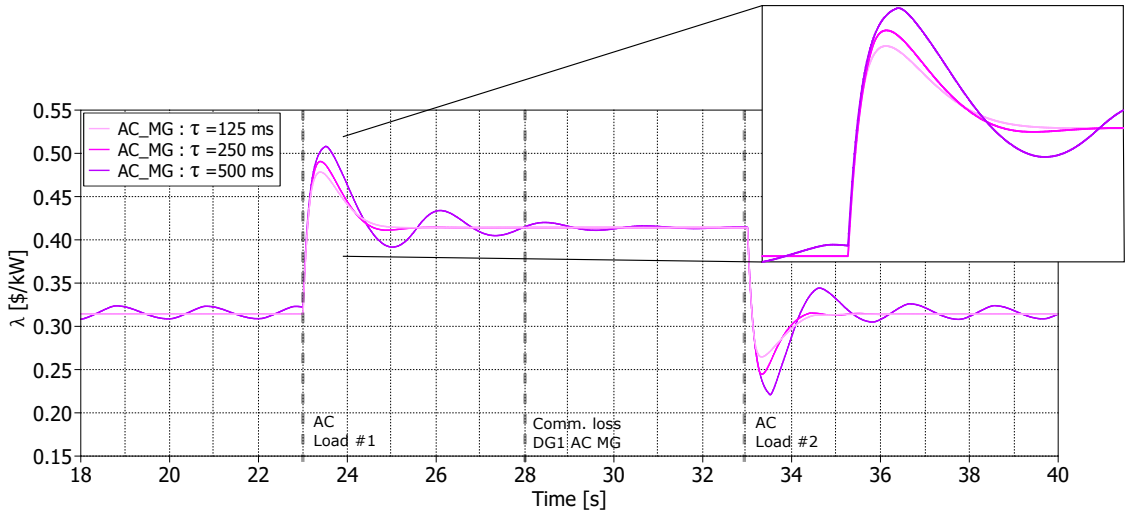

(a)

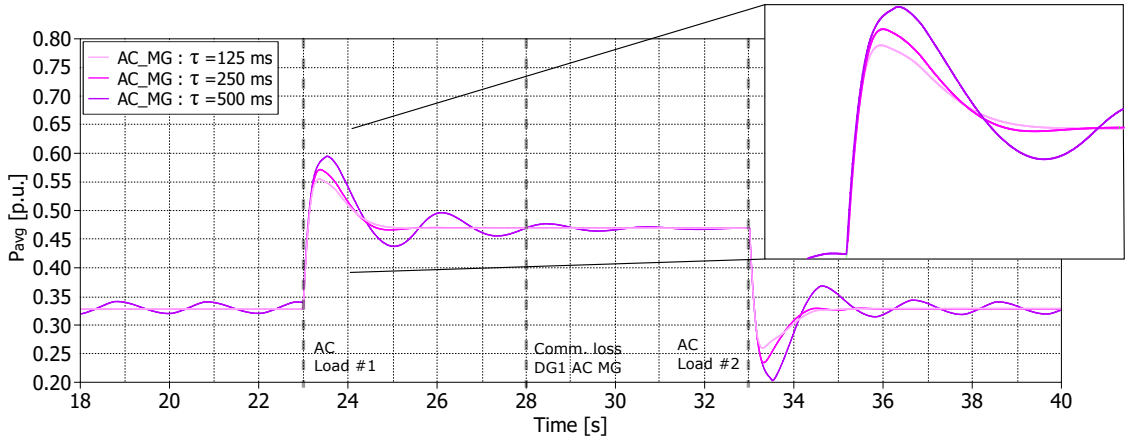

(b)

Figure 3.19: Simulation results of the ILC under different time-delays. (a) Average IC in AC MG. (b) Average power in AC MG. Adapted from [2].

Case 3. Multi-objective operation

Fig. 3.20 presents the results under different h coefficients. It can be seen that the choice of such coefficients gives rise to variations on ICs and average power ratings between MGs. The higher the h coefficient, the greater the deviation of ICs is. Also, it is shown that the regulation of ICs is very sensitive to the h weight parameter; hence, this suggests that only small values should be used when it is strictly necessary. Evidently, using the adaptive formula in (3.41) gives better results, allowing the operation of one of the MGs to be safeguarded above 80 %, maintaining an appropriate trade-off between the control objectives.

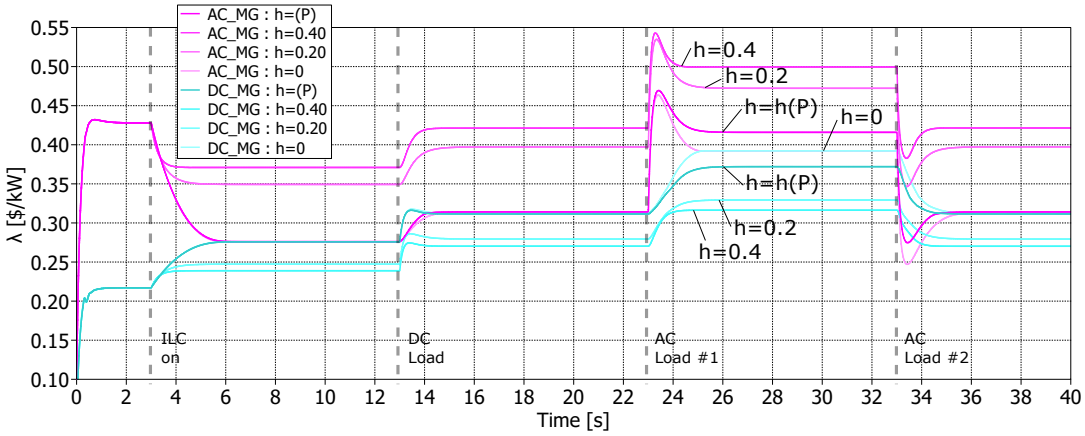

(a)

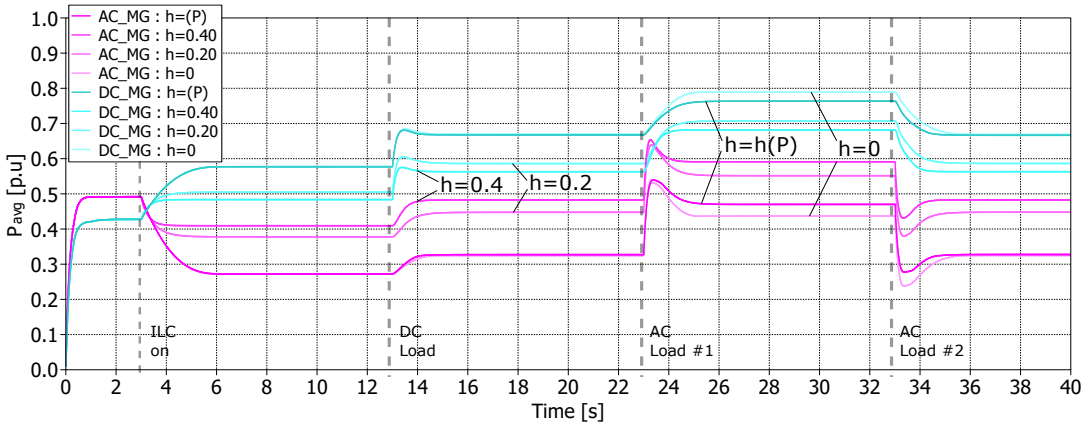

(b)

Figure 3.20: Simulation results of the ILC under different h-coefficients. (a) Average IC of MGs. (b) Average power of MGs. Reproduced from [2].

3.7 Discussion

This chapter demonstrated through experimental tests and simulations the feasibility of a multi-objective control strategy for the ILC in a hybrid AC/DC MG. The proposed ILC's controller relies only on shared measurements of IC and average power to calculate the power reference to be transferred between subgrids. It has been proven that the proposed protocol is resilient against partial communication failures and transport delays. Also, the protocol can ensure a finite-time convergence of control goals, as demonstrated in Theorems 1 and 2. In terms of the design, the weights for the average power balancing showed to be highly sensitive, encouraging caution in its tuning.

Overall, the multi-objective proposal may be applicable in real MG implementations to avoid the operation outside safety limits; in particular, preventing the saturation of one MG while ensuring a fast and decoupled operation. Conversely, to decentralised approaches for the ILC, the proposed strategy allows the application of secondary control on the AC and DC subgrids.

Limitations of the proposed method for controlling the ILC are mainly related to communications; the tuning of finite-time parameters in the presence of large delays is complex and limited due to stability issues. Also, the complete loss of communications with one subgrid clamps the ILC's output to zero (as it is programmed). Future research can be conducted to develop a distributed controller for the ILC that copes with data and communication losses, ensuring a sub-optimum economic operation. Furthermore, using the proposed controllers for enlarged topologies such as meshed hybrid AC/DC MGs with multiple subgrids and multiple ILCs are open research lines to follow. In the next chapters, extensions of the proposal will be presented in more complex MG topologies.

Chapter 4

Dynamic Average Consensus for Power Balancing of a Cluster of Interlinking Converters in AC/DC Microgrids under Economic Dispatch and Delays

4.1 Introduction

The application of consensus algorithms for the economic dispatch in AC/DC MGs can be extended to AC/DC MGs with multiple ILCs. For this reason, this chapter presents proposals based on Chapter 1 for cooperative control in AC/DC MG with multiple ILCs. Particularly, this chapter presents a consensus algorithm for ILC power-sharing (an extension of (3.39)). The proposed algorithm is a novel application of dynamic average consensus with a distributed anti-windup for dealing with steady-state errors from communication delays.

The proposed controller consists of a PI control that balances the ICs received from neighbouring units while achieving equal power-sharing between ILCs. One of the controllers uses an observer (dynamic average consensus) for estimating the average power of the ILC cluster; this method represents an alternative formulation to conventional single-integrator consensus. An anti-windup with reset scheme is proposed to reduce steady-state errors in the presence of fixed time delays. Stability analyses are also presented, as well as simulations. Both show that the proposed controller successfully balances the power between ILCs being comparable with similar approaches in the literature.

4.1.1 Problem statement

For real-world implementations, instead of a single ILC, clusters of ILCs are getting attention due to their scalability in power capacity. An exemplification of AC/DC MG with multiple ILCs is depicted in Fig. 4.1. In this system, the power transfer between the subgrids is made by the ILC cluster of N_{ILC} ILCs. In such a cluster, multiple ILCs need to be coordinated.

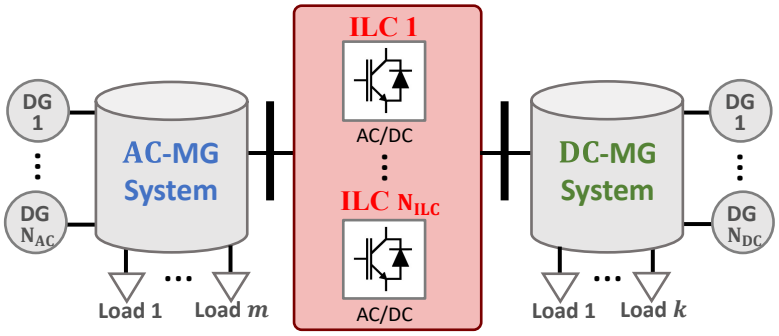

Figure 4.1: Generic hybrid MG with a cluster of ILCs. Reproduced from [2].

In the AC/DC MG with multiple ILCs topology, shown in Fig. 4.1, there must be clear coordination in order not to generate unnecessary power flows between the ILCs. Unnecessary power flow inside a cluster of ILCs produces currents that induce power losses but do not contribute to net power transfers [30]. As in the previous chapter, it is necessary that the control scheme for economic dispatch coordination incorporate power restrictions. In particular, restrictions related to the maximum power provided by each DG, ILC and MG. Additionally, this chapter includes a general term for hard constraints in power that might come from a distributed network operator to reduce distribution line congestions when the ILCs are located at different buses in the subgrids.

4.1.2 Motivation

Conventionally, the control of ILCs is made by decentralised droop curves, producing that the MG's power dispatch relies on the controllers (centralised or distributed) of DGs [1, 16]. For multiple ILCs, the work in [26] was one of the first examples to coordinate the ILC cluster using a droop strategy that equally shared the power. Distributed control has been proposed for the coordination of ILCs [24, 29, 30, 176], improving resiliency compared with centralised approaches and accuracy compared with droop control. In [24], a global power-sharing in an AC/DC MG with multiple subgrids is done by using a PI controller with a consensus algorithm between droop errors of ILCs (not in a cluster). The concept was also applied in [29], where a consensus control has been used for the power-sharing of multiple ILCs in a cluster. Also, a loading condition calculation loop is performed to compensate based on frequency and voltage deviations from droop control. Similarly, [30] carried out a consensus of power between ILCs and DGs for global power-sharing; this strategy assumes cross communications between DGs of different subgrids.

Concerning the consensus algorithms, used for coordinating ILCs, [30] uses single-integrator dynamics with a proportional controller whereas [24, 29] and [176] modify the dynamics by including proportional-integral (PI) gains. Moreover, [176] explored the use of a distributed observer for adjusting droop gains inside the ILC cluster.

To the best of the author's knowledge, dynamic average consensus algorithms can be applied as an alternative to conventional consensus. Reported works in the control of DGs (see observers in secondary control [1]) show dynamic average consensus dealing with trade-offs that conventional consensus could not solve on its own. Also, dynamic average consensus could give each ILC access to a local measurement estimation during transient states, facilitating the development of resilient cyber-attack methods, like the Kalman filter in [177]. Despite the fact that dynamic average consensus is sensible to communication delays, it is mathematically possible to compensate for this (as [178] and [176] anticipated).

In addition, all of the reported works in distributed ILC power-sharing look after the global power-sharing of the AC/DC MG. Thus, interactions with global economic dispatch performed distributedly have not been sufficiently explored.

Motivated by this, this chapter introduces a consensus algorithm in the multi-objective formulation of (3.8), and a different approach with a power observer (by dynamic average consensus) with a PI control that uses a novel anti-windup algorithm that reduces the effects of time-delays.

4.1.3 Contributions and organization

In the proposed scheme, the ILCs perform the power balancing inside the cluster by comparing the local power measurement against the observed average power. In addition, the ILCs also perform a control action related to the economic dispatch between AC and DC subgrids and a local power constraint. This approach looks after the simultaneous convergence of both control goals giving robust access to the average power of the ILC cluster.

The contributions of this work are summarised as follows:

- A distributed control for the coordination of a cluster of ILCs is proposed using a power observer. The control is jointly implemented with an economic dispatch protocol. Large-signal and steady-state stability are provided.

- A novel anti-windup algorithm with a reset scheme is proposed to reduce steady-state errors when communication delays exist in the dynamic average consensus.

- A case study of hybrid AC/DC MG with a cluster of ILCs is simulated and evaluated under different conditions.

The rest of the chapter is organised as follows. In Section 2, the formulation of the economic dispatch with multiple ILCs is developed. Then, a formulation of economic dispatch with ILC power-sharing and power constraints is developed. In this section also the design of the proposed controller with and without dynamic average consensus is described along with stability proof. A novel anti-windup is proposed to deal with communication delays. Section 3 presents the cases of study and system parameters. Section 4 has the results and discussions. Finally, Section 5 presents the chapter summary discussion.

4.2 Design of a Distributed Control Strategy for a Cluster of Interlinking Converters in a Hybrid AC/DC Microgrid

4.2.1 Formulation of economic dispatch in an AC/DC MG with multiple ILCs

Based on (3.1), let $\boldsymbol{P}$ be the vector with the powers of all the DGs in a hybrid AC/DC MG, then, the economic dispatch optimisation can be written as

$$\min_{\boldsymbol{P}} \left\{ \sum_{i=1}^{N_{\rm AC}} C_i(P_i) + \sum_{i=1}^{N_{\rm DC}} C_i(P_i) \right\} = \min_{\boldsymbol{P}} \left\{ \sum_{i=1}^{N_{\rm sys}} C_i(P_i) \right\} \tag{4.1}$$

subject to,

$$C_i(P_i) = a_{ci}P_i^2 + b_{ci}P_i + c_{ci} \quad \forall\ i \in \mathcal{N}_{\rm sys} = \{\mathcal{N}_{\rm AC} \cup \mathcal{N}_{\rm DC}\}\ , \tag{4.1a}$$

$$P_i^{\min} \leq\ P_i\ \leq P_i^{\max} \quad \forall\ P_i \in \boldsymbol{P},\ i \in \mathcal{N}_{\rm sys}\ , \tag{4.1b}$$

$$-\ P_{{\rm ILC},j}^{\max} \leq\ P_{{\rm ILC},j}(\boldsymbol{P})\ \leq P_{{\rm ILC},j}^{\max} \quad \forall\ j \in \mathcal{N}_{\rm ILC}\ , \tag{4.1c}$$

$$P_D^{\rm AC} - \sum_{i=1}^{N_{\rm AC}} P_i = \sum_{l=1}^{N_{\rm ILC}} P_{{\rm ILC},l}(\boldsymbol{P})\ , \tag{4.1d}$$

$$P_D^{\rm DC} - \sum_{i=1}^{N_{\rm DC}} P_i = -\sum_{l=1}^{N_{\rm ILC}} P_{{\rm ILC},l}(\boldsymbol{P})\ , \tag{4.1e}$$

where $C_i(P_i)$ is a quadratic cost function for the i-th DG, with parameters a_{ci}, b_{ci} and c_{ci}. $P_{\rm D}^{\rm AC}$ and $P_{\rm D}^{\rm DC}$ are the demanded powers of the AC and DC subgrids, $N_{\rm AC}$ and $N_{\rm DC}$ are the number of DGs in the AC and DC subgrids, and $N_{\rm ILC}$ is the number of ILCs.

When summing the power demand constraints equations, the term with $P_{{\rm ILC},l}$ disappears due to the symmetry in the power flow (similar to what was shown in Chapter 3). Then, based on (3.3), the same type of Lagrange multipliers can be defined, resulting in the Lagrangian function

$$\mathbb{L}\left(P_i,\sigma_i^+,\sigma_i^-,\Lambda_j^+,\Lambda_j^-,\lambda\right)=\sum_{i=1}^{N_{\text{sys}}}C_i(P_i)+\sum_{i=1}^{N_{\text{sys}}}\sigma_i^+(P_i-P_i^{\max})+\sum_{i=1}^{N_{\text{sys}}}\sigma_i^-(P_i^{\min}-P_i)$$
$$+\sum_{j=1}^{N_{\text{ILC}}}\Lambda_j^+\left(P_{\text{ILC}j}(\boldsymbol{P})-P_{\text{ILC}j}^{\max}\right)+\sum_{j=1}^{N_{\text{ILC}}}\Lambda_j^-\left(P_{\text{ILC}j}^{\min}-P_{\text{ILC}j}(\boldsymbol{P})\right)+\lambda\left(P_{\text{D}}^{\text{AC}}+P_{\text{D}}^{\text{DC}}-\sum_{i=1}^{N_{\text{sys}}}P_i\right). \tag{4.2}$$

The stationary optimality condition can be checked as follows.

$$\begin{aligned}\frac{\partial}{\partial P_i}\mathbb{L}&=\frac{\partial C_i\left(P_i\right)}{\partial P_i}+\sigma_i^+-\sigma_i^-+\sum_{j=1}^{N_{\text{ILC}}}\left(\Lambda_j^+-\Lambda_j^-\right)\frac{\partial P_{\text{ILC}j}(\boldsymbol{P})}{\partial P_i}-\lambda=0\\ \Leftrightarrow\quad\lambda&=\frac{\partial C_i\left(P_i\right)}{\partial P_i}+\sigma_i^+-\sigma_i^-+\sum_{j=1}^{N_{\text{ILC}}}\left(\Lambda_j^+-\Lambda_j^-\right)\frac{\partial P_{\text{ILC}j}(\boldsymbol{P})}{\partial P_i}\ .\end{aligned} \tag{4.3}$$

Eq. (4.3) allow us to infer that the ICs have similar dynamics to (3.5) obtained in Chapter 3.

Remark 3 It is worth noting that differently from Chapter 3, the ICs of the side MGs can synchronise even if there are multipliers Λ_j^+ or Λ_j^- different to zero; this is true if and only if there is, at least, one ILC that is not saturated, i.e., $\prod_{j=1}^{N_{\text{ILC}}}\Lambda_j^+\Lambda_j^-=0$.

4.2.2 Formulation of economic dispatch in an AC/DC MG with multiple ILCs and ILC power-sharing

In order to analyse the effect of including the power-sharing between the ILCs, we can add equality constraints as follows.

$$\min_{\boldsymbol{P}}\left\{\sum_{i=1}^{N_{\text{sys}}}C_i(P_i)\right\} \tag{4.4}$$

subject to,

$$C_i(P_i)=a_{ci}P_i^2+b_{ci}P_i+c_{ci}\quad\forall\ i\in\mathcal{N}_{\text{sys}}\ , \tag{4.4a}$$
$$P_i^{\min}\leq\ P_i\ \leq P_i^{\max}\quad\forall\ P_i\in\boldsymbol{P},\ i\in\mathcal{N}_{\text{sys}}\ , \tag{4.4b}$$
$$-P_{\text{ILC},j}^{\max}\leq\ P_{\text{ILC},j}(\boldsymbol{P})\ \leq P_{\text{ILC},j}^{\max}\quad\forall\ j\in\mathcal{N}_{\text{ILC}}\ , \tag{4.4c}$$
$$P_D^{\text{AC}}+P_D^{\text{DC}}-\sum_{i=1}^{N_{\text{sys}}}P_i=0\ , \tag{4.4d}$$
$$\frac{P_{\text{ILC},l}(\boldsymbol{P})}{P_{\text{ILC},l}^{\max}}-\frac{P_{\text{ILC},j}(\boldsymbol{P})}{P_{\text{ILC},j}^{\max}}=0\quad\forall\ l,j\in\mathcal{N}_{\text{ILC}}\ . \tag{4.4e}$$

The Lagrangian function is

$$\begin{aligned}\mathbb{L}\left(P_i,\sigma_i^+,\sigma_i^-,\Lambda_j^+,\Lambda_j^-,\lambda\right) &= \sum_{i=1}^{N_{\text{sys}}} C_i(P_i) + \sum_{i=1}^{N_{\text{sys}}} \sigma_i^+(P_i - P_i^{\max}) + \sum_{i=1}^{N_{\text{sys}}} \sigma_i^-(P_i^{\min} - P_i) \\ &+ \sum_{j=1}^{N_{\text{ILC}}} \Lambda_j^+ \left(P_{\text{ILC}j}(\boldsymbol{P}) - P_{\text{ILC}j}^{\max}\right) + \sum_{j=1}^{N_{\text{ILC}}} \Lambda_j^- \left(P_{\text{ILC}j}^{\min} - P_{\text{ILC}j}(\boldsymbol{P})\right) + \lambda \left(P_{\text{D}}^{\text{AC}} + P_{\text{D}}^{\text{DC}} - \sum_{i=1}^{N_{\text{sys}}} P_i\right) \\ &+ \sum_{l=1}^{N_{\text{ILC}}} \sum_{\substack{j=1 \\ j\neq l}}^{N_{\text{ILC}}} \frac{w_{jl}}{2} \left(\frac{P_{\text{ILC},l}(\boldsymbol{P})}{P_{\text{ILC},l}^{\max}} - \frac{P_{\text{ILC},j}(\boldsymbol{P})}{P_{\text{ILC},j}^{\max}}\right),\end{aligned} \tag{4.5}$$

where w_{jl}, such that $w_{jl} = -w_{lj}$, are the Lagrange multipliers for the new equality constraints (ILC power-sharing).

Then, the stationary optimality condition gives

$$\begin{aligned}\frac{\partial}{\partial P_i}\mathbb{L} &= \frac{\partial C_i\left(P_i\right)}{\partial P_i} + \sigma_i^+ - \sigma_i^- + \sum_{j=1}^{N_{\text{ILC}}} \left(\Lambda_j^+ - \Lambda_j^-\right) \frac{\partial P_{\text{ILC}j}(\boldsymbol{P})}{\partial P_i} - \lambda \\ &\quad + \sum_{l=1}^{N_{\text{ILC}}} \sum_{\substack{j=1 \\ j\neq l}}^{N_{\text{ILC}}} \frac{w_{jl}}{2} \left(\frac{1}{P_{\text{ILC},l}^{\max}} \frac{\partial P_{\text{ILC},l}(\boldsymbol{P})}{\partial P_i} - \frac{1}{P_{\text{ILC},j}^{\max}} \frac{\partial P_{\text{ILC},j}(\boldsymbol{P})}{\partial P_i}\right) = 0 \\ \Leftrightarrow \quad \lambda &= \frac{\partial C_i\left(P_i\right)}{\partial P_i} + \sigma_i^+ - \sigma_i^- + \sum_{j=1}^{N_{\text{ILC}}} \left(\Lambda_j^+ - \Lambda_j^-\right) \frac{\partial P_{\text{ILC}j}(\boldsymbol{P})}{\partial P_i} \\ &\quad + \sum_{l=1}^{N_{\text{ILC}}} \sum_{\substack{j=1 \\ j\neq l}}^{N_{\text{ILC}}} \frac{w_{jl}}{2} \left(\frac{1}{P_{\text{ILC},l}^{\max}} \frac{\partial P_{\text{ILC},l}(\boldsymbol{P})}{\partial P_i} - \frac{1}{P_{\text{ILC},j}^{\max}} \frac{\partial P_{\text{ILC},j}(\boldsymbol{P})}{\partial P_i}\right).\end{aligned} \tag{4.6}$$

The latter formulation can also be performed by changing the constraints in (4.4e) by a new control goal. In this case, due to the fact that ILCs get closer to the ILC cluster average power when they share power, a tracking error concerning the average power is selected as a control goal. This is done by means of a penalty function, similar to what was made in Chapter 3 with the multi-objective formulation. The former leads to the formulation

$$\min_{\boldsymbol{P}} \left\{ \sum_{i=1}^{N_{\text{sys}}} C_i(P_i) + w \sum_{j=1}^{N_{\text{ILC}}} \left(\overline{P}_{\text{ILC}}(\boldsymbol{P}) - \frac{P_{\text{ILC},j}(\boldsymbol{P})}{P_{\text{ILC},j}^{\max}}\right) \right\} \tag{4.7}$$

subject to,

$$C_i(P_i) = a_{ci}P_i^2 + b_{ci}P_i + c_{ci} \quad \forall\, i \in \mathcal{N}_{\text{sys}}\,, \tag{4.7a}$$

$$P_i^{\min} \leq\ P_i\ \leq P_i^{\max} \quad \forall\, P_i \in \boldsymbol{P},\ i \in \mathcal{N}_{\text{sys}}\,, \tag{4.7b}$$

$$-P_{\text{ILC},j}^{\max} \leq\ P_{\text{ILC},j}(\boldsymbol{P})\ \leq P_{\text{ILC},j}^{\max} \quad \forall\, j \in \mathcal{N}_{\text{ILC}}\,, \tag{4.7c}$$

$$P_D^{\text{AC}} + P_D^{\text{DC}} - \sum_{i=1}^{N_{\text{sys}}} P_i = 0\,, \tag{4.7d}$$

where w is a global weighting factor to adjust the prioritisation of the control goal, and $\overline{P}_{\text{ILC}}(\boldsymbol{P}) = \left(\sum_{l=1}^{N_{\text{ILC}}} \frac{P_{\text{ILC},l}(\boldsymbol{P})}{N_{\text{ILC}} P_{\text{ILC},l}^{\max}}\right)$. It will be seen in this chapter that for $w > 0$ the system will seamlessly and simultaneously achieve the synchronisation of DG's ICs and ILC's normalised powers.

The Lagrangian function is

$$\begin{aligned}
\mathbb{L}\left(P_i, \sigma_i^+, \sigma_i^-, \Lambda_j^+, \Lambda_j^-, \lambda\right) &= \sum_{i=1}^{N_{\text{sys}}} C_i(P_i) + w \sum_{j=1}^{N_{\text{ILC}}} \left(\overline{P}_{\text{ILC}}(\boldsymbol{P}) - \frac{P_{\text{ILC},j}(\boldsymbol{P})}{P_{\text{ILC},j}^{\max}}\right) \\
&+ \sum_{j=1}^{N_{\text{ILC}}} \Lambda_j^+ \left(P_{\text{ILC}j}(\boldsymbol{P}) - P_{\text{ILC}j}^{\max}\right) + \sum_{j=1}^{N_{\text{ILC}}} \Lambda_j^- \left(P_{\text{ILC}j}^{\min} - P_{\text{ILC}j}(\boldsymbol{P})\right) + \lambda \left(P_{\text{D}}^{\text{AC}} + P_{\text{D}}^{\text{DC}} - \sum_{i=1}^{N_{\text{sys}}} P_i\right) \\
&+ \sum_{i=1}^{N_{\text{sys}}} \sigma_i^+ (P_i - P_i^{\max}) + \sum_{i=1}^{N_{\text{sys}}} \sigma_i^- (P_i^{\min} - P_i)\,.
\end{aligned} \tag{4.8}$$

Conversely to (4.5), in (4.8) there is only one parameter w, which simplifies the implementation.

The stationary optimality condition gives

$$\begin{aligned}
\frac{\partial}{\partial P_i}\mathbb{L} &= \frac{\partial C_i\left(P_i\right)}{\partial P_i} + \sigma_i^+ - \sigma_i^- + \sum_{j=1}^{N_{\text{ILC}}} \left(\Lambda_j^+ - \Lambda_j^-\right) \frac{\partial P_{\text{ILC}j}(\boldsymbol{P})}{\partial P_i} - \lambda \\
&\quad + w \sum_{j=1}^{N_{\text{ILC}}} \left(\sum_{l=1}^{N_{\text{ILC}}} \frac{1}{N_{\text{ILC}} P_{\text{ILC},l}^{\max}} \frac{\partial P_{\text{ILC},l}(\boldsymbol{P})}{\partial P_i} - \frac{1}{P_{\text{ILC},j}^{\max}} \frac{\partial P_{\text{ILC},j}(\boldsymbol{P})}{\partial P_i}\right) = 0 \\
\Leftrightarrow \quad \lambda &= \frac{\partial C_i\left(P_i\right)}{\partial P_i} + \sigma_i^+ - \sigma_i^- + \sum_{j=1}^{N_{\text{ILC}}} \left(\Lambda_j^+ - \Lambda_j^-\right) \frac{\partial P_{\text{ILC}j}(\boldsymbol{P})}{\partial P_i} \\
&\quad + w \sum_{j=1}^{N_{\text{ILC}}} \left(\sum_{l=1}^{N_{\text{ILC}}} \frac{1}{N_{\text{ILC}} P_{\text{ILC},l}^{\max}} \frac{\partial P_{\text{ILC},l}(\boldsymbol{P})}{\partial P_i} - \frac{1}{P_{\text{ILC},j}^{\max}} \frac{\partial P_{\text{ILC},j}(\boldsymbol{P})}{\partial P_i}\right).
\end{aligned} \tag{4.9}$$

4.2.3 Formulation of economic dispatch in an AC/DC MG with multiple ILCs, ILC power-sharing and hard power constraints

Let us introduce a variant of the optimisation problem in (4.7), where hard power constraints are defined for specific ILCs. This can be understood as temporary technical requirements by a DNO. Then, the extended optimisation problem takes the form

$$\min_{\boldsymbol{P}} \left\{ \sum_{i=1}^{N_{\text{sys}}} C_i(P_i) + w \sum_{j=1}^{N_{\text{ILC}}} \left(\overline{P}_{\text{ILC}}(\boldsymbol{P}) - \frac{P_{\text{ILC},j}(\boldsymbol{P})}{P_{\text{ILC},j}^{\max}} \right) \right\} \tag{4.10}$$

subject to,

$$C_i(P_i) = a_{ci} P_i^2 + b_{ci} P_i + c_{ci} \quad \forall\, i \in \mathcal{N}_{\text{sys}} \,, \tag{4.10a}$$

$$P_i^{\min} \leq \; P_i \; \leq P_i^{\max} \quad \forall\, P_i \in \boldsymbol{P},\; i \in \mathcal{N}_{\text{sys}} \,, \tag{4.10b}$$

$$-P_{\text{ILC},j}^{\max} \leq \; P_{\text{ILC},j}(\boldsymbol{P}) \; \leq P_{\text{ILC},j}^{\max} \quad \forall\, j \in \mathcal{N}_{\text{ILC}} \,, \tag{4.10c}$$

$$P_D^{\text{AC}} + P_D^{\text{DC}} - \sum_{i=1}^{N_{\text{sys}}} P_i = 0 \,, \tag{4.10d}$$

$$P_{\text{ILC}k}(\boldsymbol{P}) - P_{\text{ILC}k}^{\text{ref}} = 0 \quad \forall\, k \in \mathcal{N}_k \subseteq \mathcal{N}_{\text{ILC}} \,, \tag{4.10e}$$

where $P_{\text{ILC}k}^{\text{ref}}$ is the power reference defined for the k-th ILC selected from a group of $\mathcal{N}_k$ ILCs. It is worth noting that $-P_{\text{ILC},k}^{\max} \leq \; P_{\text{ILC},k}^{\text{ref}} \; \leq P_{\text{ILC},k}^{\max}$. With such a system, the KKT's stationary condition is proven by fulfilling

$$\begin{aligned}
\frac{\partial}{\partial P_i}\mathbb{L} &= \frac{\partial C_i\left(P_i\right)}{\partial P_i} + \sigma_i^+ - \sigma_i^- + \sum_{j=1}^{N_{\text{ILC}}} \left(\Lambda_j^+ - \Lambda_j^-\right) \frac{\partial P_{\text{ILC}j}(\boldsymbol{P})}{\partial P_i} + \sum_{k=1}^{N_{\text{k}}} z_k \frac{\partial P_{\text{ILC}j}(\boldsymbol{P})}{\partial P_i} - \lambda \\
&\quad + w \sum_{j=1}^{N_{\text{ILC}}} \left(\sum_{l=1}^{N_{\text{ILC}}} \frac{1}{N_{\text{ILC}} P_{\text{ILC},l}^{\max}} \frac{\partial P_{\text{ILC},l}(\boldsymbol{P})}{\partial P_i} - \frac{1}{P_{\text{ILC},j}^{\max}} \frac{\partial P_{\text{ILC},j}(\boldsymbol{P})}{\partial P_i} \right) = 0 \\
\Leftrightarrow \quad \lambda &= \frac{\partial C_i\left(P_i\right)}{\partial P_i} + \sigma_i^+ - \sigma_i^- + \sum_{j=1}^{N_{\text{ILC}}} \left(\Lambda_j^+ - \Lambda_j^-\right) \frac{\partial P_{\text{ILC}j}(\boldsymbol{P})}{\partial P_i} + \sum_{k=1}^{N_{\text{k}}} z_k \frac{\partial P_{\text{ILC}k}(\boldsymbol{P})}{\partial P_i} \\
&\quad + w \sum_{j=1}^{N_{\text{ILC}}} \left(\sum_{l=1}^{N_{\text{ILC}}} \frac{1}{N_{\text{ILC}} P_{\text{ILC},l}^{\max}} \frac{\partial P_{\text{ILC},l}(\boldsymbol{P})}{\partial P_i} - \frac{1}{P_{\text{ILC},j}^{\max}} \frac{\partial P_{\text{ILC},j}(\boldsymbol{P})}{\partial P_i} \right),
\end{aligned} \tag{4.11}$$

where z_k are the Lagrange multipliers associated with the hard constraints of power.

4.2.4 Communication network

For the distributed control design, a communication network is required, similarly to Chapter 3. A communicated AC/DC MG involves agents which may be DGs or ILCs [2, 29, 30]. Then, the communications allow the AC/DC MG to be viewed and analysed as a multi-agent system with a graph $\mathcal{G}_{\text{sys}} := \; \mathcal{G}_{\text{AC}} \; \cup \; \mathcal{G}_{\text{DC}} \; \cup \; \mathcal{G}_{\text{ILC}}$ [2]. The subgraphs $\mathcal{G}_{\text{AC}}$ and $\mathcal{G}_{\text{DC}}$ are the same explained in Chapter 3 and can operate independently when the ILC cluster ($\mathcal{G}_{\text{ILC}}$) is disconnected, or when one side stops communicating to the ILC cluster. It is defined

$\mathcal{G}_{\text{ILC}} := (\mathcal{N}^*, E^{\text{ILC}}, A^{\text{ILC}})$ where $\mathcal{N}^* \subset (\mathcal{N}_{\text{AC}} \cup \mathcal{N}_{\text{DC}} \cup \mathcal{N}_{\text{ILC}})$ is the number of communicated agents, E^{ILC} is the set of edges (agents) that are communicated; communicated agents include ILCs and DGs. In a general form, considering symmetry in the communications (bidirectional flow of information), the communication matrix of the AC/DC MG system can be represented by

$$A^{\text{sys}} = \begin{bmatrix} A^{\text{AC}} & 0_{N_{\text{AC}}\times N_{\text{ILC}}} & 0_{N_{\text{AC}}\times N_{\text{DC}}} \\ 0_{N_{\text{ILC}}\times N_{\text{AC}}} & 0_{N_{\text{ILC}}\times N_{\text{ILC}}} & 0_{N_{\text{ILC}}\times N_{\text{DC}}} \\ 0_{N_{\text{DC}}\times N_{\text{AC}}} & 0_{N_{\text{DC}}\times N_{\text{ILC}}} & A^{\text{DC}} \end{bmatrix} + A^{\text{ILC}}, \tag{4.12}$$

where A^{AC}, A^{DC} and A^{ILC} are the communication matrices of the subgraphs $\mathcal{G}_{\text{AC}}$, $\mathcal{G}_{\text{DC}}$ and $\mathcal{G}_{\text{ILC}}$, respectively. Particularly, the communication matrix A^{ILC} can be represented by

$$A^{\text{ILC}} = \begin{bmatrix} 0_{N_{\text{AC}}\times N_{\text{AC}}} & [a_{\text{AC}}^{\text{ILC}}] & 0_{N_{\text{AC}}\times N_{\text{DC}}} \\ [a_{\text{AC}}^{\text{ILC}}]^{\text{T}} & [a_{\text{ILC}}^{\text{ILC}}] & [a_{\text{DC}}^{\text{ILC}}]^{\text{T}} \\ 0_{N_{\text{DC}}\times N_{\text{AC}}} & [a_{\text{DC}}^{\text{ILC}}] & 0_{N_{\text{DC}}\times N_{\text{DC}}} \end{bmatrix}, \tag{4.13}$$

where

$$a_{\text{AC}}^{\text{ILC}} = \begin{bmatrix} a_{\text{AC1}}^{\text{ILC1}} & \cdots & a_{\text{AC}N_{\text{AC}}}^{\text{ILC1}} \\ \vdots & \vdots & \vdots \\ a_{\text{AC1}}^{\text{ILC}N_{\text{ILC}}} & \cdots & a_{\text{AC}N_{\text{AC}}}^{\text{ILC}N_{\text{ILC}}} \end{bmatrix}, \tag{4.14}$$

$$a_{\text{DC}}^{\text{ILC}} = \begin{bmatrix} a_{\text{DC1}}^{\text{ILC1}} & \cdots & a_{\text{DC}N_{\text{DC}}}^{\text{ILC1}} \\ \vdots & \vdots & \vdots \\ a_{\text{DC1}}^{\text{ILC}N_{\text{ILC}}} & \cdots & a_{\text{DC}N_{\text{DC}}}^{\text{ILC}N_{\text{ILC}}} \end{bmatrix}, \tag{4.15}$$

$$a_{\text{ILC}}^{\text{ILC}} = \begin{bmatrix} a_{\text{ILC1}}^{\text{ILC1}} & \cdots & a_{\text{ILC}N_{\text{ILC}}}^{\text{ILC1}} \\ \vdots & \vdots & \vdots \\ a_{\text{ILC1}}^{\text{ILC}N_{\text{ILC}}} & \cdots & a_{\text{ILC}N_{\text{ILC}}}^{\text{ILC}N_{\text{ILC}}} \end{bmatrix}. \tag{4.16}$$

Also, there are defined $\boldsymbol{a}_{\text{AC}}^{\text{ILC}i} = \left(a_{\text{AC1}}^{\text{ILC}i},\ \ldots\ ,\ a_{\text{AC}N_{\text{AC}}}^{\text{ILC}i}\right)$, $\boldsymbol{a}_{\text{DC}}^{\text{ILC}i} = \left(a_{\text{DC1}}^{\text{ILC}i},\ \ldots\ ,\ a_{\text{DC}N_{\text{DC}}}^{\text{ILC}i}\right)$ and $\boldsymbol{a}_{\text{ILC}}^{\text{ILC}i} = \left(a_{\text{ILC1}}^{\text{ILC}i},\ \ldots\ ,\ a_{\text{ILC}N_{\text{ILC}}}^{\text{ILC}i}\right)$ as vectors that represent the communication of the i-th ILC with the DGs in the AC subgrid, DC subgrid, and with the system's ILCs, respectively.

Remark 4 It is worth noting that for a symmetrical AC/DC MG, i.e., the same number of AC DGs and DC DGs, the system communication matrix can be written as

$$A^{\text{sys}} = \begin{bmatrix} 1 & 0 & 0 \\ 0 & 0 & 0 \\ 0 & 0 & 0 \end{bmatrix} \otimes A^{\text{AC}} + \begin{bmatrix} 0 & 0 & 0 \\ 0 & 0 & 0 \\ 0 & 0 & 1 \end{bmatrix} \otimes A^{\text{DC}} + A^{\text{ILC}}, \tag{4.17}$$

where $\otimes$ represents the Kronecker product.

Remark 5 Differently from the definition given in [30], the proposed matrix A^{sys} defined in (4.12) suggests that DGs of different MGs cannot communicate directly between them.

4.2.5 Distributed control using consensus

The control over the power flow of an individual ILC can be described as compensation of an error signal depending on the average information received of ICs, supporting the IC consensus implemented by the subgrids [2]. For the inclusion of more ILCs, balancing control actions should be added. Then, inspired by [29,30] and [2], the following protocol is proposed:

$$P^*_{\text{ILC}i} = (u_{\text{L}i} + u_{\text{R}i})G^P_{\text{PI}}(s) + u_{\text{C}i}\ , \tag{4.18}$$

$$u_{\text{L}i} = c_L \left(\sum_{l=1}^{N_{\text{AC}}} \frac{a^{\text{ILC}i}_{\text{AC}l}}{N^{\text{ILC}}_{\text{AC}}} \lambda_l - \sum_{j=1}^{N_{\text{DC}}} \frac{a^{\text{ILC}i}_{\text{DC}j}}{N^{\text{ILC}}_{\text{DC}}} \lambda_j \right)\ , \tag{4.19}$$

$$u_{\text{C}i} = c_C \left(\frac{1}{s} \sum_{j=1}^{N_{\text{ILC}}} a^{\text{ILC}}_{\text{ILC}ij} \left(\frac{P_{\text{ILC}j}}{P^{\text{max}}_{\text{ILC}j}} - \frac{P_{\text{ILC}i}}{P^{\text{max}}_{\text{ILC}i}} \right) \right)\ , \tag{4.20}$$

$$u_{\text{R}i} = c_{Ri} \left(P^{\text{ref}}_{\text{ILC}i} - \frac{P_{\text{ILC}i}}{P^{\text{max}}_{\text{ILC}i}} \right)\ , \tag{4.21}$$

where $P^*_{\text{ILC}i}$ is the power reference for the internal control loop of the i-th ILC ($P_{\text{ILC}i} \approx P^*_{\text{ILC}i}$ in real-world scenario), $P^{\text{ref}}_{\text{ILC}i}$ is a hard constraint of desired power (e.g. from a network operator with or without direct communication with the ILC), u_{L} is the local error estimation for power transfer, same as in (3.9), u_{C} represents the error from the balancing of the cluster of ILCs, u_{R} is the local error from the hard constraint, $G^P_{\text{PI}}(s) = k^P_p + k^P_i/s$ is a PI controller. The parameters c_L, c_{Ri} and c_C regulate the convergence speed of their corresponding compensation action. Also, provided a binary-defined adjacency matrix, $N^{\text{ILC}}_x = \boldsymbol{a}^{\text{ILC}i}_x \cdot \mathbf{1}_{N_x}$ is equal to the active nodes sending information to the i-th ILC, with x representing the AC or DC side, and $\mathbf{1}_{N_x}$ representing a vector of ones with length N_x.

It is clear that the combination of u_{Ri} and u_{Ci} in the closed loop resembles a consensus algorithm with a leader agent [15]. In this case, multiple leaders would fight to impose their local power references while the remaining ILCs would try to get closer to the leaders. Thus, references $P^{\text{ref}}_{\text{ILC}i}$ might lead to reducing the total power transferred between the subgrids, i.e., the de-synchronisation of ICs. A solution to avoid this issue is to remove the ILCs with designated power references from the ILC power-sharing communication algorithm (they could be optionally removed from IC consensus as well). Otherwise, with one ILC with a defined power reference included in the system, all the ILC clusters will try to reach that power reference, most likely counteracting the effect of (4.19). With more than two ILCs with defined power references, the problem to be solved by the local controllers becomes complex, especially when $P^{\text{ref}}_{\text{ILC}i} \neq P^{\text{ref}}_{\text{ILC}j} \forall i, j \in \mathcal{N}_k$.

Equation (4.18) represents the basis by which further analyses will be conducted in this chapter. The next sections will present modifications of (4.18) and simulation comparisons.

The proposed protocol in (4.18)-(4.20) gives the following result.

Theorem 3 *Consider the control protocol described in* (4.18)-(4.20) *implemented by the ILCs of a hybrid AC/DC MG. Under a balanced graph with a spanning tree in the AC and DC sub-MGs, and between the ILCs, the ILCs globally synchronise the IC while sharing their power rating asymptotically.*

Proof. Lets assume $N = N_{\text{AC}} = N_{\text{DC}}$ and $a_{\text{AC}}^{\text{ILC}} = a_{\text{DC}}^{\text{ILC}}$ for the sake of simplicity. Assuming also an initial steady-state condition in the MG, i.e., no load impacts, the activation of the controller in (4.18) will drive the ILC cluster to have a power dynamics as follows: the IC dynamics can be expressed as $u_{\text{L}i} \approx \dot{e}_i^{\lambda} = c_L \sum_{j=1}^{N} a_{ij} \left(e_j^{\lambda} - e_i^{\lambda}\right)$ [2], with $e_j^{\lambda} = \lambda_l - \lambda_k \ \forall \ l \in \mathcal{N}_{\text{AC}}, k \in \mathcal{N}_{\text{DC}}$, and $L(A)$ balanced. For the ILC power-sharing, we define $e_i^C = \sum_{j=1}^{N_{\text{ILC}}} \frac{P_{\text{ILC}j}}{N_{\text{ILC}}} - P_{\text{ILC}i}$. Then, $\dot{e}_i^C = c_C \sum_{j=1}^{N_{\text{ILC}}} a_{\text{ILC}ij}^{\text{ILC}} \left(e_j^C - e_i^C\right)$. Concerning the power constraints of Λ^+ and Λ^-, they can be assumed achieved and perceived *instantaneous* by the much slower IC dynamics (due to their implementation as part of saturation with anti-windup as explained in Chapter 3).

For the hard constraint of power, the local power is modified to reach the designated value $P_{\text{ILC}i}^{\text{ref}}$ each sampling time. Therefore, if the ILCs with defined power references are not excluded from the communication protocol of ILC power-sharing, the ILC power-sharing dynamics get modified to $e_i^C = e_i^R \approx P_{\text{ILC}i}^{\text{ref}} - \frac{P_{\text{ILC}i}}{P_{\text{ILC}i}^{\max}}$ and $\dot{e}_i^C \approx c_C \sum_{j=1}^{N_{\text{ILC}}} a_{\text{ILC}ij}^{\text{ILC}} \left(e_j^C - e_i^C\right) + c_C \kappa_{Ri} e_i^C$, where $\boldsymbol{\kappa}_R$ is a binary N_{ILC} sized vector whose elements are $\kappa_{Ri} = c_{Ri}$ if the i-th ILC has a hard constraint of power (basically, a leader unit) and $\kappa_{Ri} = 0$ otherwise.

Let $V = V_L + V_C = 1/2 \left(\boldsymbol{e}^{\lambda} R (\boldsymbol{e}^{\lambda})^{\text{T}} + \boldsymbol{e}^C Y (\boldsymbol{e}^C)^{\text{T}}\right)$ be a Lyapunov candidate function, with R and Y positive-definite matrices, $\boldsymbol{e}^{\lambda} = (e_1^{\lambda}, \ldots, e_N^{\lambda})$, and $\boldsymbol{e}^C = (e_1^C, \ldots, e_{N_{\text{ILC}}}^C)$. Following similar steps than *Theorem 1* [36], the components $\dot{V}_L$ and $\dot{V}_C$ can be proved non-increasing provided $c_L, c_C > 0$ and that there is a spanning tree in the communication matrices. Therefore, $\dot{V} < M \in \mathbb{R}$. However, only $e_i^{\lambda} + e_i^C = 0$ can be guaranteed in steady-state. This is so if and only if $P_{\text{ILC}i}^{\text{ref}} = P_{\text{ILC}j}^{\text{ref}} \forall i, j \in \mathcal{N}_k$. If $\boldsymbol{\kappa}_R = \mathbf{0}$ (or equivalently $c_{Ri} = 0 \, \forall i \in \mathcal{N}_k$) is selected to avoid interference with the convergence of the IC consensus and the ILC power-sharing, $\boldsymbol{e}^{\lambda}$ and $\boldsymbol{e}^C$ converge to zero asymptotically, which completes the proof. ■

4.2.6 Distributed control using dynamic average consensus

From (4.18), an alternative formulation for the power-sharing inside a cluster of ILCs can be made by using a dynamic average consensus. In this case, the idea is to locally estimate the average power of the ILC cluster ($\overline{P}_{\text{ILC}i}$) for using it as a reference in a PI controller. The estimation of the ILC cluster power can be a more useful consensus variable compared with ILC power when accessed by a DNO for further decision-making, or for implementing cyber attack detection schemes. The use of dynamic average consensus in ILCs responds to an effort to provide robust and flexible control to the ILC power-sharing control loop. This is important when different control goals are settled into the ILC, e.g. economic dispatch, ILC power-sharing and other power constraints. This technique will allow the same result as

(4.18) but with more decoupling capabilities.

The analogy of this is the voltage control loop of DGs in MGs. Authors recognise that there are trade-offs; then, for example, equal voltage regulation and reactive power-sharing are unfeasible in MGs with inductive lines (the general case) [51,110,127,179]. To solve these trade-offs in distributed control, on the one hand, some works (see examples in [110, 179]) proposed to relax the voltage restoration (convert it on a soft constraint) so the voltages did not converge to the same reference value. The problems with this are the definition of the restriction gain (which is sensible with systems stability) and the fact that there is little control over how far from the reference the voltage of DGs can go. On the other hand, other authors deal with the trade-off in voltage control using average values (through dynamic average consensus) [107, 127]. The tunning process of the observer is simple, and, in most cases, a unitary gain performs seamlessly.

Hence, the proposed protocol using a dynamic average consensus is given by:

$$P^{*}_{\mathrm{ILC}i} = (u_{\mathrm{L}i} + u_{\mathrm{C}i} + u_{\mathrm{R}i})G^{P}_{\mathrm{PI}}(s)\ , \tag{4.22}$$

$$u_{\mathrm{L}i} = c_L \left(\sum_{i=1}^{N_{\mathrm{AC}}} \frac{a^{\mathrm{ILC}}_{\mathrm{AC}i}}{N^{\mathrm{ILC}}_{\mathrm{AC}}} \lambda_i - \sum_{j=1}^{N_{\mathrm{DC}}} \frac{a^{\mathrm{ILC}}_{\mathrm{DC}i}}{N^{\mathrm{ILC}}_{\mathrm{DC}}} \lambda_j \right)\ , \tag{4.23}$$

$$u_{\mathrm{C}i} = c_C \left(\overline{P}_{\mathrm{ILC}i} - \frac{P_{\mathrm{ILC}i}}{P^{\max}_{\mathrm{ILC}i}} \right)\ , \tag{4.24a}$$

$$\overline{P}_{\mathrm{ILC}i} = \frac{P_{\mathrm{ILC}i}}{P^{\max}_{\mathrm{ILC}i}} + c^{'}_{C} \frac{1}{s} \sum_{j=1}^{N_{\mathrm{ILC}}} a^{\mathrm{ILC}}_{\mathrm{ILC}ij} (\overline{P}_{\mathrm{ILC}j} - \overline{P}_{\mathrm{ILC}i})\ , \tag{4.24b}$$

$$u_{\mathrm{R}i} = c_{Ri} \left(P^{\mathrm{ref}}_{\mathrm{ILC}i} - \frac{P_{\mathrm{ILC}i}}{P^{\max}_{\mathrm{ILC}i}} \right)\ , \tag{4.25}$$

where $\overline{P}_{\mathrm{ILC}i}$ comes from a distributed observer and stands for the average power of the ILC cluster. Indeed, the total power transferred by the ILC cluster can be estimated by using the average power as $P^{\mathrm{Total}}_{\mathrm{ILC}} = N_{\mathrm{ILC}}\overline{P}_{\mathrm{ILC}i}$. Noting that with (4.18) the total power can be directly estimated by $P^{\mathrm{Total}}_{\mathrm{ILC}} = N_{\mathrm{ILC}}P_{\mathrm{ILC}i}$, but with a loss of accuracy in transient states. Also, the local power could be estimated using the available average power. This is yielded by: (i) $\widehat{P}^{1}_{\mathrm{ILC}i} = P^{\max}_{\mathrm{ILC}i}\overline{P}_{\mathrm{ILC}i}$ (from (4.20)), and (ii) $\widehat{P}^{2}_{\mathrm{ILC}i} = P^{\max}_{\mathrm{ILC}i}\big(\overline{P}_{\mathrm{ILC}i} - \frac{c^{'}_{C}}{s}\sum a^{\mathrm{ILC}}_{\mathrm{ILC}ij}(\overline{P}_{\mathrm{ILC}j} - \overline{P}_{\mathrm{ILC}i})\big)$ (from (4.24)).

Remark 6 Differently from [29, 30] and (4.20), the proposed algorithm in (4.24) involves more control parameters but allows flexibility and access to the average power of the ILC cluster, which will be used in the next chapter.

The proposed protocol in (4.22)-(4.24) gives the following result.

Theorem 4 *Consider the control protocol described in* (4.22)-(4.24) *implemented by the ILCs of a hybrid AC/DC MG. Under a balanced graph with a spanning tree in the AC and DC sub-MGs, and between the ILCs, the ILCs globally synchronise the IC while sharing their power rating asymptotically, even though hard constraints of power are imposed on some of the ILCs.*

Proof. Taking the same assumptions than Theorem 3, with the ILC power-sharing error defined as $e_i^C = \overline{P}_{\text{ILC}i} - \frac{P_{\text{ILC}i}}{P_{\text{ILC}i}^{\max}} \equiv \overline{P}_{\text{ILC}i} - \sum_{j=1}^{N_{\text{ILC}}} \frac{P_{\text{ILC}j}(0)}{N_{\text{ILC}} P_{\text{ILC}j}^{\max}}$, where $P_{\text{ILC}j}(0)$ are the initial values of ILC power when the protocol (4.24) is activated. Then, $\dot{e}_i^C = c_C c_C^{'} \sum_{j=1}^{N_{\text{ILC}}} a_{\text{ILC}ij}^{\text{ILC}} \left(e_j^C - e_i^C\right)$. For the power constraint, $e_i^R = P_{\text{ILC}i}^{\text{ref}} - \frac{P_{\text{ILC}i}}{P_{\text{ILC}i}^{\max}}$. A high value of c_{Ri} could ensure a fast local action, so $e_i^R = 0$ in view of the IC and ILC power-sharing loops. Moreover, conversely, to Theorem 3, the local power modification does not alter the ILC power-sharing. The remaining ILCs adjust their power ratings to get close to the ILC power average, but this value does not have specific bounds that prohibit the zero error in a steady state. The former independency between e_i^λ, e_i^C and e_i^R is not true when the condition in Remark 3 is not fulfilled.

When the simplification $e^R = 0$ is not met (there is no decoupling), we have

$$e_i^R = P_{\text{ILC}i}^{\text{ref}} - \frac{P_{\text{ILC}i}}{P_{\text{ILC}i}^{\max}} = (P_{\text{ILC}i}^{\text{ref}} - \overline{P}_{\text{ILC}i}) + e_i^C \ . \tag{4.26}$$

Then,

$$\dot{e}_i^R = -\dot{\overline{P}}_{\text{ILC}i} + \dot{e}_i^C \approx 0 \ . \tag{4.27}$$

Similarly to Theorem 3, let V be a Lyapunov candidate function such that $V = V_L + V_C + V_R = 1/2 \left(\boldsymbol{e}^\lambda R (\boldsymbol{e}^\lambda)^{\text{T}} + \boldsymbol{e}^C Y (\boldsymbol{e}^C)^{\text{T}} + \boldsymbol{e}^R Z (\boldsymbol{e}^R)^{\text{T}}\right)$ with R, Y and Z positive-definite matrices, $\boldsymbol{e}^\lambda = (e_1^\lambda, \ldots, e_N^\lambda)$, $\boldsymbol{e}^C = (e_1^C, \ldots, e_{N_{\text{ILC}}}^C)$, and $\boldsymbol{e}^R = (e_1^R, \ldots, e_{N_{\text{ILC}}}^R) \cdot \boldsymbol{\kappa}_R^{\text{T}}$. Also, $\boldsymbol{\kappa}_R$ is defined as in Theorem 3. Therefore, following the steps of *Theorem 1* [36], $\dot{V} < M \in \mathbb{R}$, i.e., the IC error $(\boldsymbol{e}^\lambda)$ converge asymptotically, which completes the proof. ■

4.2.7 Steady-state stability

Provided a steady-state operation, by using the proposed controller in (4.22), similarly to [127], one can get

$$\begin{aligned}\Delta \boldsymbol{P}_{\mathrm{ILC}}^{\mathrm{ss}} =& K_{\mathrm{e}}(t_0) + K_{\mathrm{P}}\left(\overline{\boldsymbol{P}}_{\mathrm{ILC}}^{\mathrm{ss}} - \boldsymbol{P}_{\mathrm{ILC}}^{\mathrm{ss}} - K^{\mathrm{red}} c_L L(A) \boldsymbol{e}^{\lambda}\right) \\ &+ K_{\mathrm{I}}\left(\overline{\boldsymbol{P}}_{\mathrm{ILC}}^{\mathrm{ss}} - \boldsymbol{P}_{\mathrm{ILC}}^{\mathrm{ss}} - K^{\mathrm{red}} c_L L(A) \boldsymbol{e}^{\lambda}\right)(t - t_0)\,, \end{aligned} \tag{4.28}$$

where K_{P} and K_{I} are diagonal matrices carrying the proportional and integral gains, $K_{\mathrm{e}}(t_0)$ is a column vector that carries the controller's output at $t = t_0$, $\boldsymbol{e}^{\lambda} = \left(e_1^{\lambda}, \ldots, e_N^{\lambda}\right)^{\mathrm{T}}$ is the same described in Theorem 1, and K^{red} is a $N_{\mathrm{ILC}} \times N$ reduction matrix that represents how the compensation of errors $\boldsymbol{e}^{\lambda}$ is distributed between the ILCs; a necessary condition is that $\mathbf{1}_{N_{\mathrm{ILC}}} K^{\mathrm{red}} = \mathbf{1}_N$. In the steady state, the time-dependent part of (4.28) is zero; thus, one can have

$$\left\langle \boldsymbol{P}_{\mathrm{ILC}}^{\mathrm{ss}} \right\rangle \mathbf{1}_{N_{\mathrm{ILC}}}^{\mathrm{T}} - \boldsymbol{P}_{\mathrm{ILC}}^{\mathrm{ss}} = K^{\mathrm{red}} c_L L(A) \boldsymbol{e}^{\lambda}\,, \tag{4.29}$$

where $\left\langle \boldsymbol{P}_{\mathrm{ILC}}^{\mathrm{ss}} \right\rangle$ represents the average value of state vector $\boldsymbol{P}_{\mathrm{ILC}}^{\mathrm{ss}} = \left(\frac{P_{\mathrm{ILC1}}^{\mathrm{ss}}}{P_{\mathrm{ILC1}}^{\max}}, \ldots, \frac{P_{\mathrm{ILC}N_{\mathrm{ILC}}}^{\mathrm{ss}}}{P_{\mathrm{ILC}N_{\mathrm{ILC}}}^{\max}}\right)^{\mathrm{T}}$. If all the DGs initially share the same IC, then $\left\langle \boldsymbol{P}_{\mathrm{ILC}}^{\mathrm{ss}} \right\rangle \mathbf{1}_{N_{\mathrm{ILC}}}^{\mathrm{T}} = \boldsymbol{P}_{\mathrm{ILC}}^{\mathrm{ss}}$. Otherwise, multiplying both sides of (4.29) from the left by $\mathbf{1}_{N_{\mathrm{ILC}}}$ gives

$$\mathbf{1}_{N_{\mathrm{ILC}}} \left\langle \boldsymbol{P}_{\mathrm{ILC}}^{\mathrm{ss}} \right\rangle \mathbf{1}_{N_{\mathrm{ILC}}}^{\mathrm{T}} - \mathbf{1}_{N_{\mathrm{ILC}}} \boldsymbol{P}_{\mathrm{ILC}}^{\mathrm{ss}} = \mathbf{1}_{N_{\mathrm{ILC}}} K^{\mathrm{red}} c_L L(A) \boldsymbol{e}^{\lambda}\,. \tag{4.30}$$

Recalling the necessary condition for K^{red}, one can get on the right side of (4.30) that

$$\mathbf{1}_{N_{\mathrm{ILC}}} K^{\mathrm{red}} c_L L(A) \boldsymbol{e}^{\lambda} = c_L (\mathbf{1}_N L(A) \boldsymbol{e}^{\lambda}) = 0_{N_{\mathrm{ILC}}}^{\mathrm{T}} \tag{4.31}$$

due to the bidirectional communications assumed. Therefore, $\left\langle \boldsymbol{P}_{\mathrm{ILC}}^{\mathrm{ss}} \right\rangle \mathbf{1}_{N_{\mathrm{ILC}}}^{\mathrm{T}} = \boldsymbol{P}_{\mathrm{ILC}}^{\mathrm{ss}}$, which completes the system stability proof.

4.2.8 Robustness of controller under fixed communication delays

As demonstrated in Chapter 3, [174] and [178], the dynamic average consensus has bounded errors in steady-state due to communication delays. The steady-state errors originate because of the local updating of variable $\overline{P}_{\mathrm{ILC}i}$ during $0 < t < \tau$, where there is still non-available information from neighbours (initial values of $\overline{P}_{\mathrm{ILC}j}$ are assumed zero). To overcome this, it is proposed to clamp to zero the inputs of the integrator of (4.24b) — like an anti-windup algorithm — during the initial states until information began to arrive from neighbours. Therefore, (4.24) is proposed to be adjusted according to Algorithm 1.

Algorithm 1 clamps to zero the invariant inputs by weighting the communication data. For this purpose, the difference between $\overline{P}_{\mathrm{ILC}j}(t - \tau)$ and $\overline{P}_{\mathrm{ILC}j}(t - \tau - T_k)$ is used to detect the end of the steady-state, where $T_k \in [\tau, \infty)$ is the sampling time and τ is the time delay. Then, the parameters of the communication matrix are multiplied by 0 if there is no new information from neighbours and 1 otherwise. This procedure reduces the error induced during $t < \tau$.

Also, in Algorithm 1, because the anti-windup is not perfect and its precision depends on the relation between T_k and τ, a reset signal S is generated to refresh the cumulative steady-state error after multiple load changes; this signal is activated with a boolean flag signal st that comes from a periodic timer (with sampling time T_{sample} and period $T_{st} >> \tau$). For the design of the parameters, T_k should be close (20-120% tolerance) to τ and T_{st} can be determined according to the knowledge of load variability of the AC/DC MG.

Algorithm 1 Selective Anti-windup with Reset (i-th ILC).

INITIALIZATION $T = 0,\ S = 0,\ st = 0,\ \overline{\boldsymbol{P}}_{\text{ILC}} = \mathbf{0}_{N_{\text{ILC}}}$
STEP 1 Simultaneously execute the functions:
TIMER(T , S , st)
  if $S == 1$, $T \leftarrow 0$, $st \leftarrow 0$, **end if**
  while $T < T_{st}$, $T \leftarrow T + T_{\text{sample}}$, **end while**
  $st \leftarrow 1$
  return st , T
ANTIWIND($\boldsymbol{a}^{\text{ILC}}_{\text{ILC}i}$, $\overline{\boldsymbol{P}}_{\text{ILC}}(t-\tau)$, st)
  for $j = 1, ..., \mathcal{N}_i^{\text{ILC}}$
    if $\left\|\overline{P}_{\text{ILC}j}(t-\tau) - \overline{P}_{\text{ILC}j}(t-\tau-T_k)\right\| > \varepsilon,\ ss_{ij} \leftarrow 1$
   else $ss_{ij} \leftarrow 0$, **end if**
   $a^{\text{ILC}}_{\text{ILC}ij} \leftarrow a^{\text{ILC}}_{\text{ILC}ij} \cdot ss_{ij}$
  end for
  $S \leftarrow \prod_{j=1}^{\mathcal{N}_i^{\text{ILC}}} a_{ij} \cdot st$
  return $\boldsymbol{a}^{\text{ILC}}_{\text{ILC}i}$, S
STEP 2 Reset the integrator of (4.24b) with the rising of S, and multiply u_C by NOT(S) and NOT($\sum_{j=1}^{\mathcal{N}_i^{\text{ILC}}} a^{\text{ILC}}_{\text{ILC}ij} == 0$).
STEP 3 Return to STEP 1.

4.3 Case Studies

The proposed controller is tested in a simulated AC/DC MG in PLECS. The MG is based on [2] and depicted in Fig. 4.2. The electrical parameters of the system are listed in Table 4.1, and the rest of the parameters are based on the ones listed in Chapter 3, Tables 3.1-3.2. The economic cost function parameters of the DC MG are 3/4 the ones listed in Table 3.2 (the ones used for the AC MG). The power ratings for the DGs are the following: $P_i^{\max} = 10$ [kW] $\forall i \in \{1,2,3,4,5\} \subset \mathcal{N}_{\text{AC}}$, $Q_i^{\max} = 3.33$ [kW] $\forall i \in \mathcal{N}_{\text{AC}}$, $P_i^{\max} = 10$ [kW] $\forall i \in \{1,2\} \subset \mathcal{N}_{\text{DC}}$, $P_i^{\max} = 15$ [kW] $\forall i \in \{3,4,5\} \subset \mathcal{N}_{\text{DC}}$.

Parameter	Value	Parameter	Value
Nom. Freq.	50 [Hz]	Nom. Volt. DC	400 [V]
Nom. Volt. AC	220 [$V_{1\Phi}$]	Load Z4	63.15 [Ω]
Load Z1	23.08 [Ω]	Load Z5	63.15 [Ω]
Load Z2	23.08 [Ω]	Load Z6	12.63 [Ω]
Load Z3	7.69 [Ω]		

Table 4.1: System parameters of hybrid MG with multiple ILCs.

The control parameters of the proposed ILC controller are $k_p^P = 0.25$, $k_i^P = 1.57$, $c_L = 1400$, $c_C = 560$, $c_C' = 0.8$, $c_{Ri} = 0$, $\varepsilon = 10^{-3}$, $T_{\text{sample}} = 0.1$[s], $T_k = 0.5$[s] and $T_{st} = 13$[s]. The power constraints for the ILCs are the following: $P_{\text{ILC4}}^{\max} = 10$ [kW], $P_{\text{ILC3}}^{\max} = 1.3P_{\text{ILC4}}^{\max}$, $P_{\text{ILC2}}^{\max} = 0.7P_{\text{ILC4}}^{\max}$, and $P_{\text{ILC1}}^{\max} = 1.1P_{\text{ILC4}}^{\max}$. The ILCs have the communication vectors $a_{\text{AC}}^{\text{ILC1}} = (1,\ 0,\ 0,\ 0,\ 1)$, $a_{\text{AC}}^{\text{ILC2}} = (1,\ 0,\ 0,\ 0,\ 0)$, $a_{\text{AC}}^{\text{ILC3}} = (1,\ 0,\ 0,\ 0,\ 0)$, $a_{\text{AC}}^{\text{ILC4}} = (0,\ 0,\ 1,\ 0,\ 0)$, $a_{\text{DC}}^{\text{ILC1}} = (1,\ 0,\ 0,\ 0,\ 0)$, $a_{\text{DC}}^{\text{ILC2}} = (0,\ 0,\ 1,\ 1,\ 0)$, $a_{\text{DC}}^{\text{ILC3}} = (0,\ 0,\ 0,\ 1,\ 1)$, $a_{\text{DC}}^{\text{ILC4}} = (0,\ 0,\ 0,\ 1,\ 0)$, and the communication matrix

$$[a_{\text{ILC}}^{\text{ILC}}] = \begin{bmatrix} 0 & 1 & 1 & 0 \\ 1 & 0 & 0 & 1 \\ 1 & 0 & 0 & 1 \\ 0 & 1 & 1 & 0 \end{bmatrix}.$$

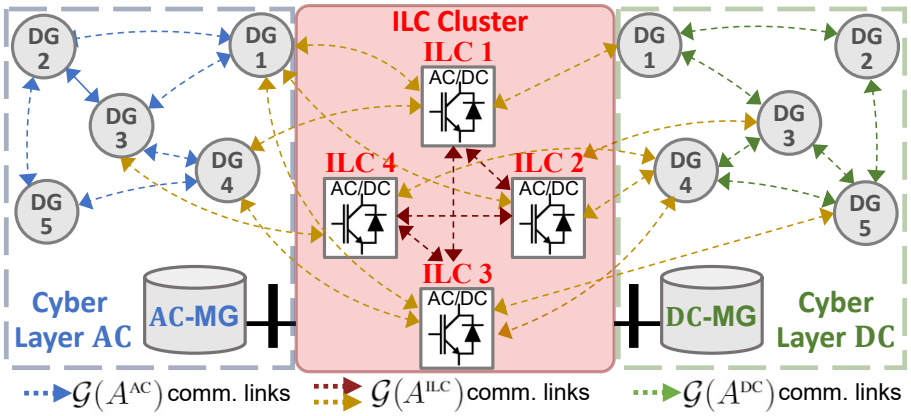

Figure 4.2: Simulated MG topology with communications. Reproduced from [4].

In all of the test scenarios, the MG is subdued to load impacts; first, on the AC side by changing Z3 from 7.69 to 4.69[Ω], then, on the DC side by changing Z6 from 12.63 to 8.47[Ω] and vice versa. There are four groups of simulations analysed:

Case 1. Load changing operation:

This test employs the proposed controller in (4.22) with anti-windup. The performance of the power balancing is analysed under load impacts and constant time delays of 330 [ms]. Also, in this test, in ILC #2, c_{R2}=20 and $P^{\text{ref}}_{\text{ILC2}}$=800[W] to analyse the behaviour of the controller with a fixed power in one of the ILCs.

Case 2. Comparison between controllers' performances:

The same scenario of Case 1 is used to compare the performances of the controllers of both conventional consensus of (4.18) (with a gain of 5) and dynamic consensus of (4.22).

Case 3. Delay in the communications:

This test is conducted to show the performance of (4.22) with and without the anti-windup. Time delays are tested throughout the ILC Cluster graph; values of 0 and 500 [ms] are analysed for the delays (tests with small delays are omitted for briefness). Conversely to Cases 1 and 2, this test is conducted without hard power constraints, i.e., c_{R2}=0.

Case 4. Comparison between average power and local power estimations:

A test is conducted showing the performance of $\overline{P}_{\text{ILC}i}$ estimation using both conventional and dynamic consensus without hard constraints, and 500 [ms] of delays. Also, $P_{\text{ILC}i}$ is compared using the estimators:
(i) $\widehat{P}^1_{\text{ILC}i} = P^{\max}_{\text{ILC}i}\overline{P}_{\text{ILC}i}$, and (ii) $\widehat{P}^2_{\text{ILC}i} = P^{\max}_{\text{ILC}i}\left(\overline{P}_{\text{ILC}i} - \frac{c'_C}{s}\sum a^{\text{ILC}}_{\text{ILC}ij}(\overline{P}_{\text{ILC}j} - \overline{P}_{\text{ILC}i})\right)$.

4.4 Results

Case 1. Load changing operation

The simulation results for Case 1 are shown in Fig. 4.3. From the simulation tests, it can be seen in Fig. 4.3a that the ICs (average real-time estimations) of each subgrid converge asymptotically. Small errors can be observed in the presence of time-delays, $\approx 6\times10^{-3}$[%] at τ=0.5[s], which is negligible when compared with other real-world sources of error, like noise.

Figure 4.3b shows the curves of ILC powers. Similarly to Fig. 4.3a, Fig. 4.3b depicts an appropriate power balancing inside the ILC cluster with minor chattering introduced by the anti-windup. Despite the use of the anti-windup with reset scheme, there are still small steady-state errors due to the time delays, which are $\approx 1.2\times10^{-1}$[%]. The latter exempts the ILC's #2 power, which remains restricted to a fixed amount as it was expected to be.

From Fig. 4.3c, the balance of average powers can be seen. Here, it is possible to advert small oscillations that Algorithm 1 creates, especially at the beginning of the simulation. Several resets can be seen near t=13[s], t=33[s], t=52[s] and t=67[s]. It can be seen that the spikes provoked by the resets in the average power values were not transferred into the ILC powers (4.3b) nor the MGs ICs (4.3a). Also, one can note that even with $\overline{P}_{\text{ILC2}} \neq P_{\text{ILC2}}$, the controller allows convergence in average power and economic dispatch.

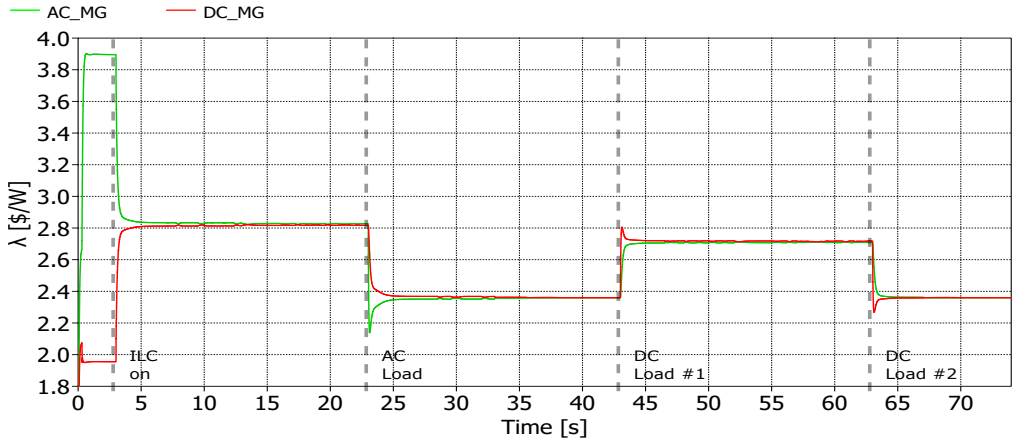

(a)

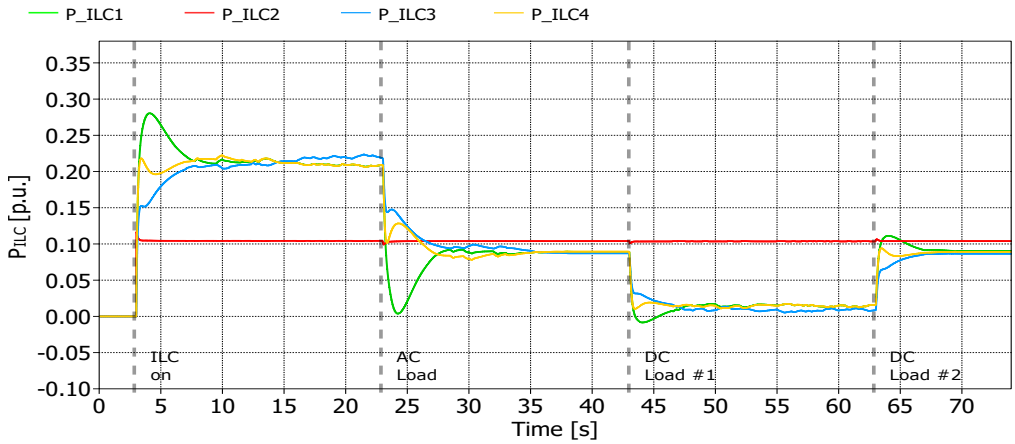

(b)

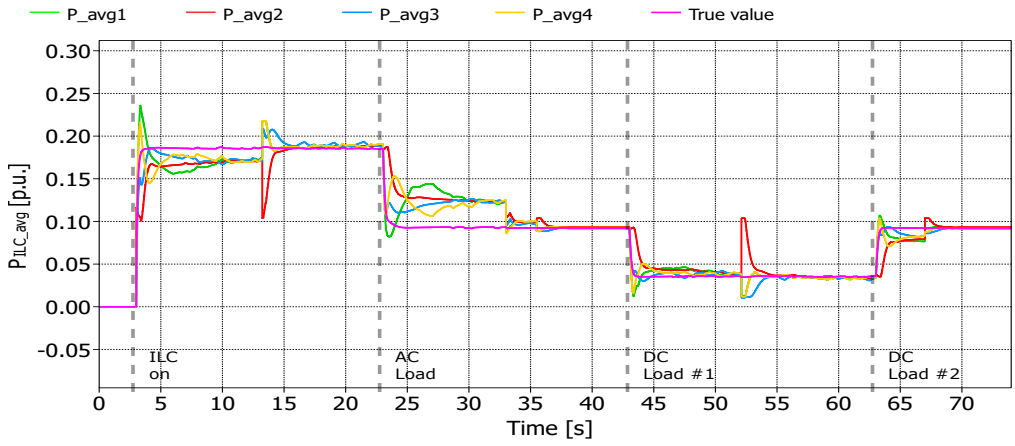

(c)

Figure 4.3: Simulation results for Case 1. (a) Average IC of MGs. (b) Power of ILCs. (c) Average power of ILCs. Adapted from [4].

Case 2. Comparison between controllers' performances

The performance of the system under controllers (4.18) and (4.22) is shown in Fig. 4.4 and Fig. 4.5. In Fig. 4.4, both controllers achieve IC consensus, as can be seen in Fig. 4.4a and Fig. 4.4b, with almost the same settling time due to their analogy in the control parameters. The latter means that the ILC power-sharing of both strategies did not interfere with the IC consensus.

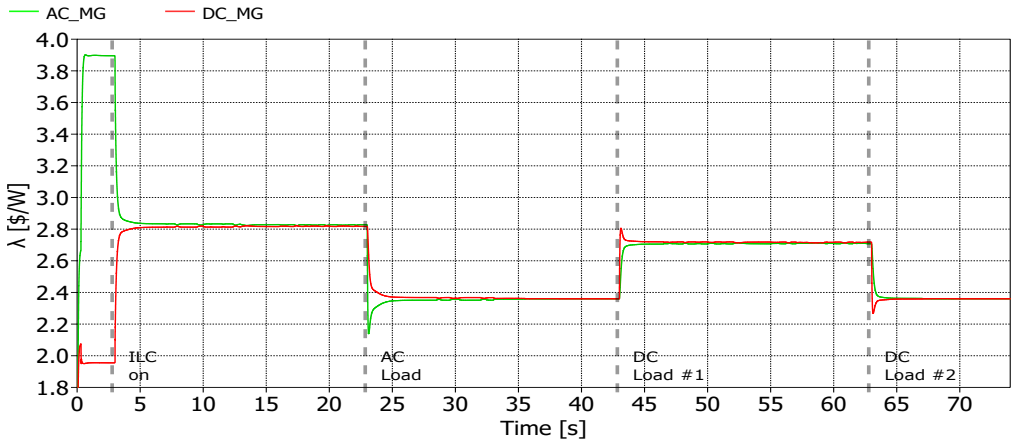

(a)

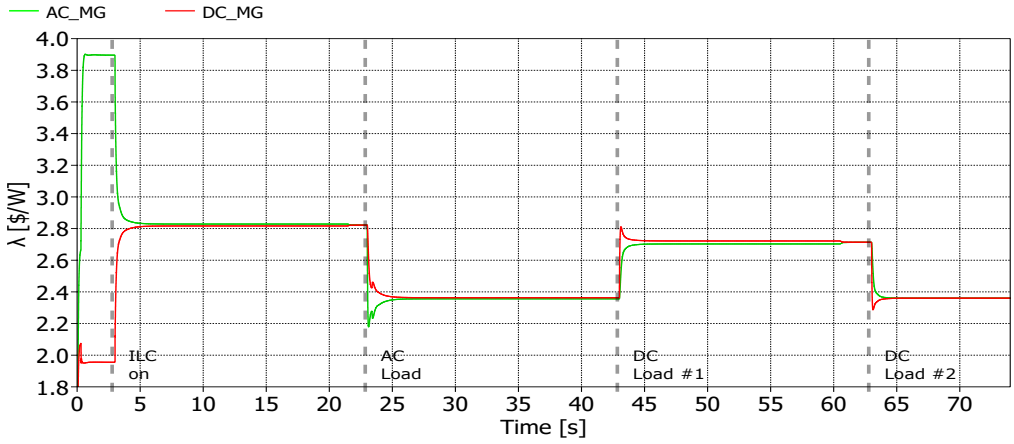

(b)

Figure 4.4: Simulation results for Case 2. (a) Average IC curves, averaged from DGs data of controller in (4.22). (b) Average IC curves, averaged from DGs data of controller in (4.18).

As for the ILC powers, Fig. 4.5b present higher differences in the power consensus's tolerance (more deviations) concerning Fig. 4.5a. Moreover, Fig. 4.5b shows sudden changes in the ILC powers, particularly around t=23[s] and t=63[s]. Those changes of the conventional consensus are undesirable in real applications since they change the value of the ILC #2, which was supposed to keep a constant value. The only visible advantage of the conventional consensus is that under delays (like this condition) the power curves are smoother than the case with the dynamic average consensus. The reason behind this is the non-linear design of the anti-windup that introduces small chattering.

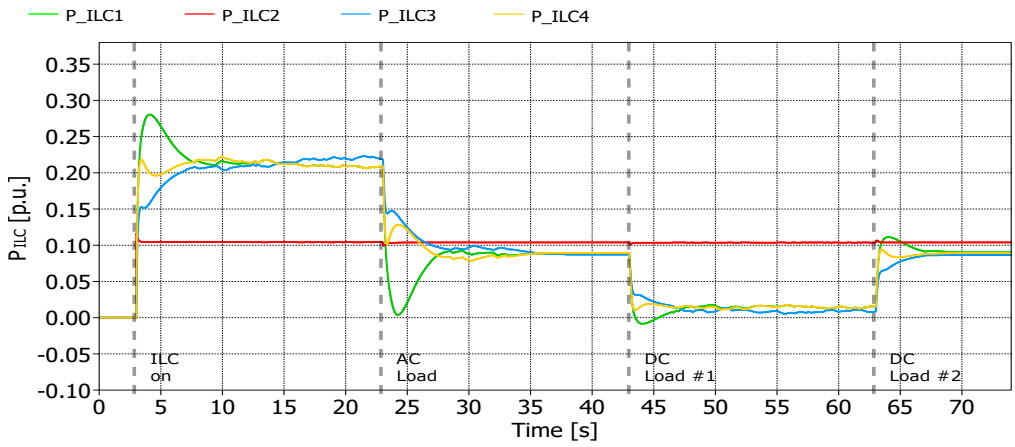

(a)

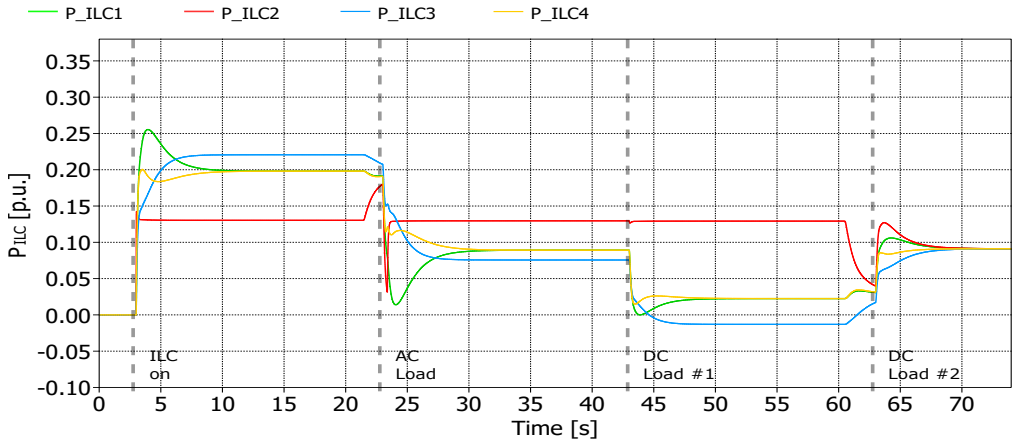

(b)

Figure 4.5: Simulation results for Case 2. (a) Power of ILCs using the controller in (4.22). (b) Power of ILCs using the controller in (4.18).

Case 3. Delay in the communications

A deep performance analysis of Algorithm 1 can be obtained from Fig. 4.6. Here, the proposed controller without anti-windup (red) suffers large steady-state errors, ≈51[%] with τ=0.5[s], when compared with the delay-free case (blue). The controller with anti-windup (green) greatly reduces the gap between the ILC's cluster average power estimations concerning the true average value, with an error of ≈11[%] after the load impact, and ≈1[%] after the reset produced at t=30.5[s]. This result differs from the solution shown in [78] where a delay-robust algorithm achieves consensus between the local estimates $\overline{P}_{\mathrm{ILC}i}$ but with constant deviations proportional to the delays, which are undesirable in this application.

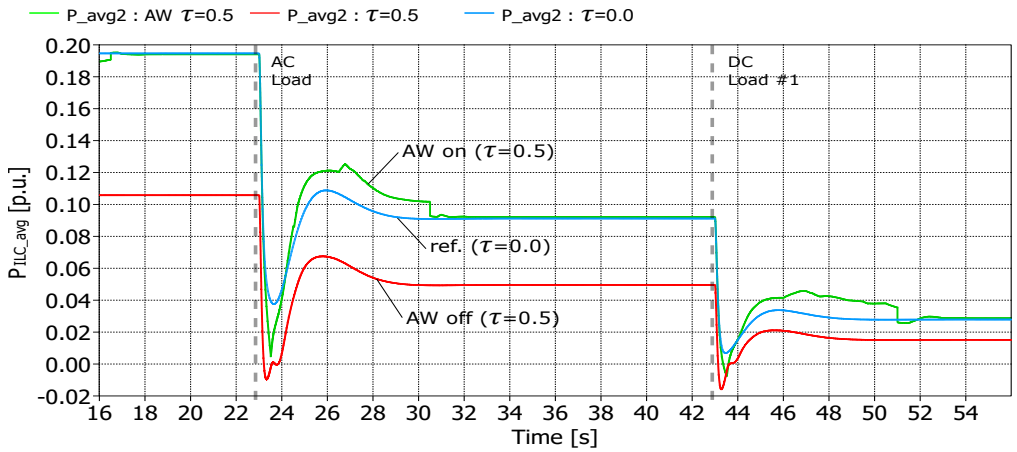

Figure 4.6: Simulation results for Case 3. Comparison of the ILC #2's estimation of ILC average power using the proposed controller with and without anti-windup and different delays. Adapted from [4].

Due to space limitations, analyses concerning the controller robustness against time-varying delays are regarded as future work. However, previous developments, such as [178], allow us to anticipate the convergence of the proposed algorithm given a bounded magnitude of the time delay and its derivative.

Case 4. Comparison between average power and local power estimations

A comparison of average power estimation is given in Fig. 4.7a. It can be seen a similar dynamic performance for both controllers. The controller that uses the observer in (4.24) (green) presents less damping, in general, when compared to conventional consensus (red) which only relies on the local power measurement. Overall, the conventional consensus is barely affected by the delays due to its slow convergence speed (≈7[s]). In the case of the proposed dynamic consensus controller, the anti-windup algorithm successfully worked to compensate for steady-state errors and maintain the quality of the response within acceptable levels.

Fig. 4.7b shows how effective the dynamic consensus can be to estimate the local power. The estimation $\widehat{P}^1_{\mathrm{ILC}i}$ (red) is not accurate during the transients states. However, estimation

$\widehat{P}^2_{\mathrm{ILC}i}$ has a perfect fit with the true value of $P_{\mathrm{ILC}i}$ at almost any time. The anti-windup helps the dynamic consensus to provide an accurate measurement of $\overline{P}_{\mathrm{ILC}i}$ and, consequently, $P_{\mathrm{ILC}i}$ when consensus is reached (steady-state error <2[%]). This estimation can be used for further reliability purposes beyond the scope of this paper.

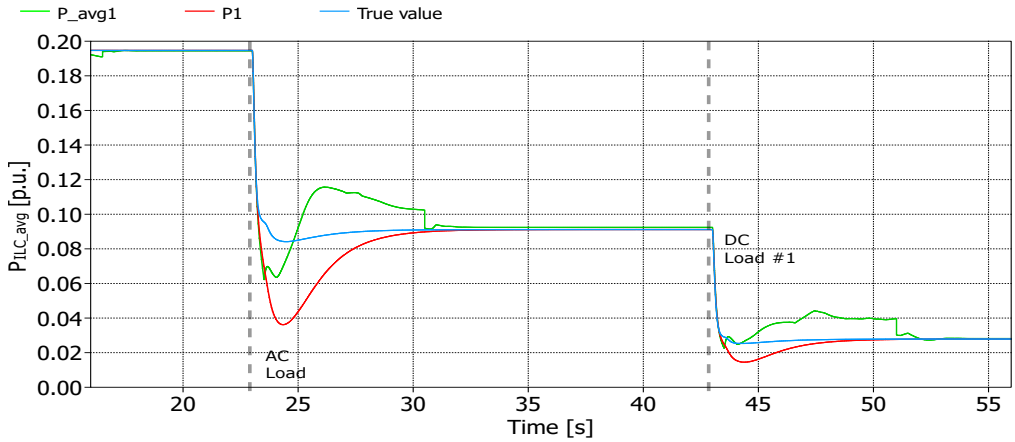

(a)

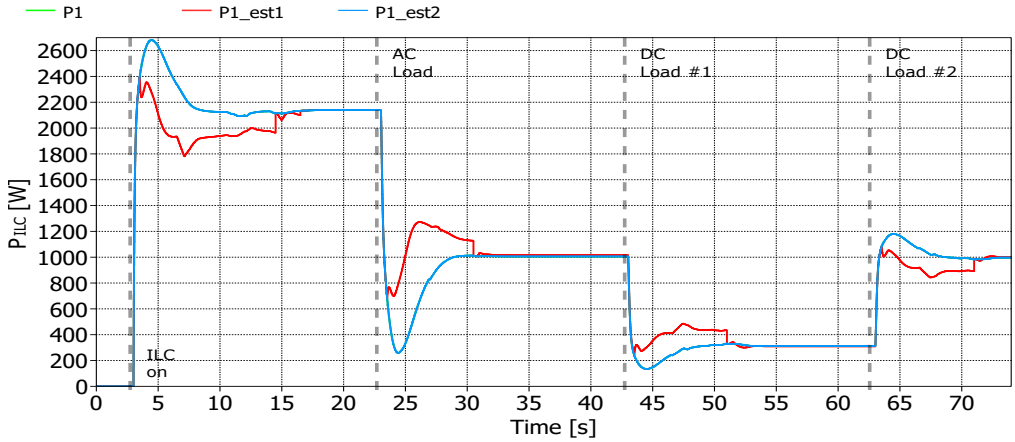

(b)

Figure 4.7: Simulation results for Case 4. (a) Comparison of the ILC #1's estimation of ILC average power using the proposed controller and conventional consensus. (b) Comparison of the ILC #1's estimation of local power with estimators (i) and (ii). Adapted from [4].

4.5 Discussion

This chapter validated the feasibility of dynamic average consensus for power balancing in an ILC cluster of an AC/DC MG. It can be seen that the power balancing using the power observer does not adversely affect the economic dispatch, even though communication delay exists. Moreover, steady-state errors are small and bounded, and they are greatly reduced by the proposed anti-windup algorithm. The latter allows the deployment of the proposed controller without compromising the operation costs of the MG. The proposed controller also makes the average power utilisation of the ILC cluster available from each ILC, which can be used for further decision-making or cyber-attack resilient algorithms.

The anti-windup proposed in this chapter is a necessary item to avoid increasing the MG cost of operation unnecessarily when the ILC power-sharing is pursued. It was shown that compensating the initial errors of the dynamic average consensus (power observer) prevents steady-state errors when time delays are present. The described anti-windup might be the basis by which more complex distributed control strategies using dynamic average consensus could be deployed, not only in MGs' control area.

Limitations of the work are evident where large delays are present. There are chattering issues introduced by the anti-windup to reduce steady-state errors, and issues related to the selection of parameters. There must be some prior knowledge about the range of the time delay's magnitude (especially for selecting T_k and T_{st}). Also, the control design has not included robustness against time-varying delays yet.

Chapter 5

Multi-objective and Distributed Finite-time Control for the Coordination of Interlinking Converters in a Hybrid AC/DC Multi-Microgrid

5.1 Introduction

In this chapter, an extension of the control strategy of the previous chapter is proposed. This chapter proposes a cooperative control scheme for the ILCs in a meshed multi-MG system. The proposed scheme has a main goal to achieve economic dispatch by equalising the IC variables shared by a communication layer between ILCs and subgrids. The strategy performs additional control goals related to the balancing of power inside ILC clusters, and the balancing of average power between ILC clusters and subgrids to avoid saturations. The control scheme uses adjustable weights based on exponential activation functions for dealing with the trade-offs between economic and safety operations. Experiments are conducted through an extensive simulated environment, modelled in PLECS. The results show a successful operation of the proposed controllers, which reduces the investment in communication links while enhancing the reliability of the system. As a result, the use of the proposed control strategy could maintain optimal costs during normal operation and reduce operational costs in the long term by protecting the lifetime of critical MG components.

5.1.1 Problem statement

Within multi-MGs, global control actions, such as power-sharing and optimal dispatch, require a certain level of coordination between the subgrids. In this sense, we have a challenge when defining the communication topology, and dealing with a trade-off between robustness and investment costs. In addition, as mentioned in Chapter 3 and Chapter 4, EMSs for economic dispatch must consider restrictions to guarantee a safe and efficient operation. In

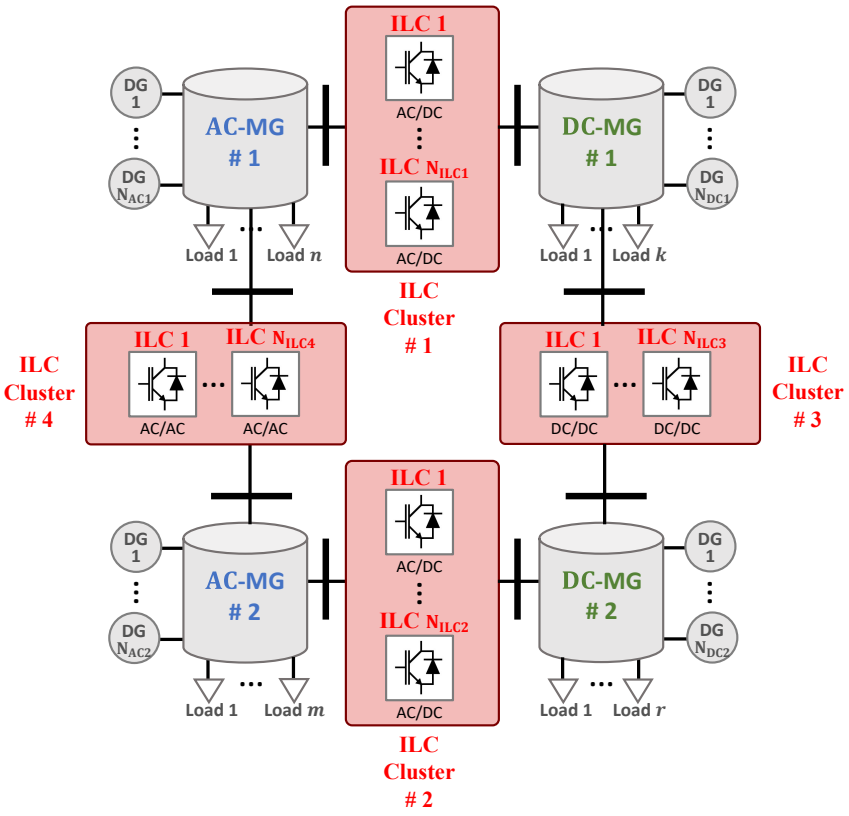

Figure 5.1: Representation of a meshed and hybrid multi-MG with four clusters of ILCs.

this regard, it is required to incorporate local power restrictions specific to each MG into the global coordination of the system. In the case of multi-MG with multiple ILCs, coordination is required within each ILC cluster so that the system operates properly and there is no unnecessary power flows through the system (causing losses), as previously mentioned in Chapter 4; here it is essential to avoid the unnecessary power flow inside a cluster and between clusters of ILCs. Finally, it should be considered to seek to take advantage of the information available by the control strategy, so that the DNO can define additional restrictions and deliver an optimal power flow that adjusts to the needs of the distribution network (multi-MG).

5.1.2 Motivation

The combination of MGs has caught special interest because this brings even more flexibility to the system [180]. One of the research trends concerning MGs is related to its topologies; in particular, hybrid AC/DC MGs have been extensively studied for real applications since they keep the advantages of the DC systems while reusing most of the existing AC power systems [16, 181]. In this regard, some researchers have proposed to enlarge the hybrid MG systems to multi-MGs [31, 41]. In Fig. 5.1, a generic representation of meshed AC/DC Multi-MG is shown.

Some of the advantages of multi-MGs are lower operation costs and higher profits that MG owners (or communities) can receive when compared with single MG systems [41–44, 182].

Also, multi-MG customers can benefit from a more reliable and economical power supply [43]. In terms of the ILC construction, special cases are the ILCs for DC-DC and AC-AC MGs. For such cases, small modifications need to be made compared with the control logic employed in AC/DC ILCs (discussions about the ILC construction are outside the scope of this thesis). It is worth noting that an AC/AC ILC adjusts the MG's voltage and frequency levels; the latter allows the integration of industrial subgrids into a global coordination scheme. Moreover, using ILCs for the interconnection of multiple MGs gives freedom for each MG to operate with its own voltage level and/or frequency.

Despite its potential, the use of meshed topologies with ILCs (like the one shown in Fig. 5.1) is barely covered in the literature (as in [41, 47]). Consequently, there is a lack of studies in the literature about the control design and coordination of such meshed systems.

Until now, meshed topologies with multiple ILCs were considered complex to study and the available literature only focuses on multiple AC MGs partitioned by isolation switches. The potential contribution in this regard is significant because in complex networks, such as the one that is addressed, centralised control and optimisers (which have been the main way of approaching it until now) entail significant disadvantages in terms of costs, reliability and time of execution.

5.1.3 Contributions and organisation

The contributions of this chapter can be summarised as follows:

- The formulation of an economic dispatch optimisation is derived for a meshed hybrid AC/DC multi-MG system with clusters of ILCs. The power balance constraint is proposed using a connectivity matrix and non-linear functions representing the ILC powers as dependent on the power of all the DGs in the system.

- The formulation of an economic dispatch optimisation with multiple objectives is proposed for the meshed hybrid AC/DC multi-MG system with clusters of ILCs. Terms inside the objective function are proposed to regularise the avoidance of MG saturation and ILC power-sharing inside ILC clusters.

- A distributed multi-objective finite-time control for the ILCs is proposed, which guarantees the economic dispatch without communication between ILC clusters. Also, MG saturation and ILC power-sharing are implemented through control loops relying on averaged values of powers from neighbour DGs and other ILCs inside the ILC cluster.

- A novel constraint for the economic dispatch optimisation of meshed hybrid AC/DC multi-MG system is proposed to restrict the saturation of power of ILC clusters. This constraint is implemented as a term in a distributed multi-objective controller, which yields the consensus of average powers of ILCs received from neighbour ILC clusters.

- A case study of meshed hybrid AC/DC multi-MG with clusters of ILCs is simulated and evaluated under different conditions.

The rest of the chapter is organised as follows. In Section 2, the formulation of the economic dispatch problem and distributed control design for the ILC controllers are presented. The design includes multiple control objectives: for IC consensus, MG saturation and ILC power-sharing. In Section 3, the formulation and distributed control design of a novel ILC cluster saturation constraint is performed, which is added to the developments of the previous section. Section 4 describes the case studies, providing details about the simulated system and control parameters. In Section 5, the simulation results are presented and discussed. Finally, a final overall discussion is presented in Section 6, which includes a comparison of the proposed control strategy with the literature.

5.2 Design of Distributed Control for a Meshed Multi-Microgrid with Clusters of Interlinking Converters

Control over the topology of multiple interconnected AC/DC MGs requires the generalisation of the developments made in the first chapters of this thesis. In general, it is hypothesised that the coordination of ILCs can be performed in a distributed manner, allowing optimal global dispatch. This section will propose the application of coordination control for a generalised meshed multi-MG; this topology incorporates several subgrids of AC and DC nature interconnected by clusters of ILCs.

5.2.1 Formulation of economic dispatch in a meshed AC/DC multi-MG

Based on (4.1), let $\boldsymbol{P}$ be the vector with the powers of all the DGs in the multi-MG, then, the economic dispatch optimisation can be written as

$$\min_{\boldsymbol{P}} \left\{ \sum_{i=1}^{N_1^{\mathrm{MG}}} C_i(P_i) + \cdots + \sum_{i=1}^{N_m^{\mathrm{MG}}} C_i(P_i) \right\} = \min_{\boldsymbol{P}} \left\{ \sum_{i=1}^{N_{\mathrm{sys}}} C_i(P_i) \right\} \tag{5.1}$$

subject to,

$$C_i(P_i) = a_{ci}P_i^2 + b_{ci}P_i + c_{ci} \quad \forall\ P_i \in \boldsymbol{P},\ i \in \mathcal{N}_{\mathrm{sys}}\,, \tag{5.1a}$$

$$P_i^{\min} \leq\ P_i\ \leq P_i^{\max} \quad \forall\ P_i \in \boldsymbol{P},\ i \in \mathcal{N}_{\mathrm{sys}}\,, \tag{5.1b}$$

$$-P_{\mathrm{ILC},i}^{\max} \leq\ P_{\mathrm{ILC},i}(\boldsymbol{P})\ \leq P_{\mathrm{ILC},i}^{\max} \quad \forall\ i \in \mathcal{N}_j^{cl},\ j \in \mathcal{N}_{cl}\,, \tag{5.1c}$$

$$P_D^m - \sum_{i=1}^{N_m^{\mathrm{MG}}} P_i = \sum_{j=1}^{N_{cl}} \phi_{mj} \sum_{l=1}^{N_j^{cl}} P_{\mathrm{ILC},l}(\boldsymbol{P}) \quad \forall\ m \in \mathcal{N}_{\mathrm{MG}}\,, \tag{5.1d}$$

where $C_i(P_i)$ is a quadratic cost function for the i-th DG in the m-th MG, with parameters a_{ci}, b_{ci} and c_{ci}. P_{D}^m is the demanded power of the m-th MG, N_{MG} is the number of MGs in the system, N_m^{MG} is the number of DGs in the m-th MG, N_{cl} is the number of ILC clusters,

and N_j^{cl} is the number of ILCs in the j-th cluster. Constraint (5.1d) represents the power balance of the multi-MG. Also, the physical connectivity matrix between ILC clusters and MGs is given by

$$\phi = \overbrace{\begin{bmatrix} \phi_{11} & \dots & \phi_{1j} \\ \vdots & \ddots & \vdots \\ \phi_{m1} & \dots & \phi_{mj} \end{bmatrix}}^{N_{cl}} \Bigg\} N_{\text{MG}} \ , \tag{5.2}$$

such that $\phi_{mj} \in \{1, -1\}$ if there is a connection whereas $\phi_{mj} = 0$ otherwise. The condition $\mathbf{1}_m^T \phi = 0$ must hold, i.e., there is a conservative power flow between ILC clusters. Thereafter, when summing the constraints equations in (5.1d), the term with $P_{\text{ILC},l}$ disappears due to the properties of matrix ϕ.

Given this property of matrix ϕ, the construction of the Lagrange's function has the same form and type of Lagrange multipliers of the Lagrange's function described in (4.2).

Remark 7 The optimisation in (5.1) considers the global economic dispatch, i.e., all the DGs are cooperating to achieve the cheapest operation. This is different from [43], where MGs have their own optimisation and costs for selling their energy.

5.2.2 Formulation of economic dispatch in a meshed AC/DC multi-MG with ILC power-sharing, hard power constraints and sub-grid power saturation

Based on the advancements of the previous subsection and chapters 3 and 4, this section presents a formulation for the global economic dispatch of multiple interconnected MGs with additional control goals. In particular, the regulation of MG saturations (in the form presented in (3.39)) and the ILC power balancing (described in (4.24)) studied along with hard constraints of power in some of the ILCs.

Then, an expanded multi-objective global dispatch optimisation can be expressed as

$$\min_{\boldsymbol{P}} \left\{ J \left(f^1(\boldsymbol{P}), f^2(\boldsymbol{P}), f^3(\boldsymbol{P}) \right) \right\} \tag{5.3}$$

subject to,

$$f^1(\boldsymbol{P}) = \sum_{m=1}^{N_{\mathrm{MG}}} \sum_{i=1}^{N_m^{\mathrm{MG}}} C_i(P_i)\,, \tag{5.3a}$$

$$f^2(\boldsymbol{P}) = \sum_{m=1}^{N_{\mathrm{MG}}} \sum_{\substack{k=1 \\ k\neq m}}^{N_{\mathrm{MG}}} \left(h_{\mathrm{m}} \overline{P}_m^{\mathrm{MG}}(\boldsymbol{P}) - h_{\mathrm{k}} \overline{P}_k^{\mathrm{MG}}(\boldsymbol{P}) \right), \tag{5.3b}$$

$$f^3(\boldsymbol{P}) = \sum_{j=1}^{N_{cl}} \sum_{l=1}^{N_j^{cl}} \left(\overline{P}_j^{cl}(\boldsymbol{P}) - \frac{P_{\mathrm{ILC},l}(\boldsymbol{P})}{P_{\mathrm{ILC},l}^{\max}} \right), \tag{5.3c}$$

$$C_i(P_i) = a_{ci} P_i^2 + b_{ci} P_i + c_{ci} \quad \forall\ P_i \in \boldsymbol{P},\ i \in \mathcal{N}_m^{\mathrm{MG}},\ m \in \mathcal{N}_{\mathrm{MG}}\,, \tag{5.3d}$$

$$P_i^{\min} \leq\ P_i\ \leq P_i^{\max} \quad \forall\ P_i \in \boldsymbol{P},\ i \in \mathcal{N}_m^{\mathrm{MG}},\ m \in \mathcal{N}_{\mathrm{MG}}\,, \tag{5.3e}$$

$$-\ P_{\mathrm{ILC},i}^{\max} \leq\ P_{\mathrm{ILC},i}(\boldsymbol{P})\ \leq P_{\mathrm{ILC},i}^{\max} \quad \forall\ i \in \mathcal{N}_j^{cl},\ j \in \mathcal{N}_{cl}\,, \tag{5.3f}$$

$$\sum_{m=1}^{N_{\mathrm{MG}}} P_{\mathrm{D}}^m - \sum_{m=1}^{N_{\mathrm{MG}}} \sum_{i=1}^{N_m^{\mathrm{MG}}} P_i = 0\,, \tag{5.3g}$$

$$P_{\mathrm{ILC}k}(\boldsymbol{P}) - P_{\mathrm{ILC}k}^{\mathrm{ref}} = 0 \quad \forall\ k \in \mathcal{N}_k \subseteq \mathcal{N}_j^{cl},\ j \in \mathcal{N}_{cl}\,. \tag{5.3h}$$

The functions $\overline{P}_m^{\mathrm{MG}}(\boldsymbol{P})$ and $\overline{P}_j^{cl}(\boldsymbol{P})$ are the per unit average power of the m-th MG and j-th ILC cluster, respectively. The objective function $f^1(\boldsymbol{P})$ represents the original economic dispatch. The objective functions $f^2(\boldsymbol{P})$ and $f^3(\boldsymbol{P})$ represent the additional objectives proposed previously in this work, which are the balancing among the power utilisation of MGs and among ILCs in a cluster, respectively. Coefficients $h_m\ \forall\ m \in \mathcal{N}_{\mathrm{MG}}$ determine the prioritisation in the management of saturation/reserves of MGs.

In order to solve (5.3), assumptions can be made in the objective functions. One way to deal with the simultaneous optimisations is to regularise with weighting parameters (following similar steps to the adopted in Chapter 3 and Chapter 4). These changes give rise to the objective junction:

$$\min_{\boldsymbol{P}} \left\{ f^1(\boldsymbol{P}) + h f^2(\boldsymbol{P}) + w f^3(\boldsymbol{P}) \right\}\,, \tag{5.4}$$

where h and w are weighting parameters regulating the trade-off between control objectives. Moreover, these parameters can be considered variants on the multi-MG power conditions.

Based on (4.8) and (4.11), one has that the derivative of the Lagrange's function is

$$\begin{aligned} \frac{\partial}{\partial P_i}\mathbb{L} =& \frac{\partial C_i\left(P_i\right)}{\partial P_i} + h g^1(\boldsymbol{P}) + w g^2(\boldsymbol{P}) + \sigma^+ - \sigma^- \\ &+ \sum_{j=1}^{N_{cl}} \sum_{l=1}^{N_j^{cl}} (\Lambda_l^+ - \Lambda_l^-) \frac{\partial P_{\mathrm{ILC}l}(\boldsymbol{P})}{\partial P_i} + \sum_{k=1}^{N_k} z_k \frac{\partial P_{\mathrm{ILC}k}(\boldsymbol{P})}{\partial P_i} - \lambda\,, \end{aligned} \tag{5.5}$$

where $g^1(\boldsymbol{P})$ and $g^2(\boldsymbol{P})$ are linear functions which can be calculated based on the results of (3.38) and (4.11).

Then, equalising to zero and solving results in

$$\begin{aligned}\lambda =&\frac{\partial C_i\left(P_i\right)}{\partial P_i}+hg^1(\boldsymbol{P})+wg^2(\boldsymbol{P})+\sigma^+-\sigma^- \\ &+\sum_{j=1}^{N_{cl}}\sum_{l=1}^{N_j^{cl}}(\Lambda_l^+-\Lambda_l^-)\frac{\partial P_{\mathrm{ILC}l}(\boldsymbol{P})}{\partial P_i}+\sum_{k=1}^{N_k}z_k\frac{\partial P_{\mathrm{ILC}k}(\boldsymbol{P})}{\partial P_i}\ .\end{aligned} \tag{5.6}$$

Remark 8 Similarly to Chapter 4, there is a condition that ensures the economic operation. As the single hybrid AC/DC MG case, $\lambda_l = \lambda_k \ \forall \ l,k \in \mathcal{N}_{\mathrm{sys}}$ must be held to achieve the cheapest operation cost. In this case, if $\{h, w\} = \mathbf{0}$, the ICs between all the DGs in the hybrid AC/DC multi-MG are synchronised using (5.6) provided there is at least one ILC without saturation, i.e., $\prod_{j=1}^{N_{cl}}\prod_{l=1}^{N_j^{cl}}\Lambda_l^+\Lambda_l^- = 0$. Also, there must be at least one ILC cluster without a single hard constraint of power in it.

From (5.6), one can see terms that deviate the optimal solution of the conventional economic dispatch. In particular, it is possible to design the weighting parameters h and w such that the system deviates the optimum IC regarding some safety operational criteria, like having energy reserves for an MG failure. Hence, a distributed control scheme can be realised for solving the multi-objective optimisation problem through the incorporation of weighting parameters in each ILC's control loop.

5.2.3 Communication network of a hybrid multi-MG with multiple clusters of ILCs

Concerning the communication topology, the multi-MG with multiple clusters of ILCs can be represented by an equivalent graph $\mathcal{G}_{\mathrm{sys}} := \cup_{i=1}^{N_{\mathrm{MG}}}\ \mathcal{G}_{\mathrm{MG},i}\ \cup_{j=1}^{N_{cl}}\ \mathcal{G}_{cl,j}$ where $\mathcal{G}_{\mathrm{MG},i}$ is the graph of the i-th MG and $\mathcal{G}_{cl,j}$ is the graph of the j-th ILC cluster. Each graph can operate independently in case of clusters' failures. The graphs $\mathcal{G}_{\mathrm{MG},i}$ are analogous to $\mathcal{G}_{\mathrm{AC}}$ and $\mathcal{G}_{\mathrm{DC}}$ of the previous chapters. In addition, $\mathcal{G}_{\mathrm{cl},j} := \ (\mathcal{N}_j^*, E_j^{cl}, A^{cl,j})$ with $\mathcal{N}_j^* \subset (\mathcal{N}_m^{\mathrm{MG}} \cup \mathcal{N}_n^{\mathrm{MG}} \cup \mathcal{N}_j^{cl})$ for any pair of MGs, m and n, connected by the j-th ILC cluster, and $\{A^{cl,j}\} = \cup_{i=1}^{N_j^{cl}}\{\boldsymbol{a}_m^{\mathrm{ILC}i}\}\ \cup_{i=1}^{N_j^{cl}}\ \{\boldsymbol{a}_n^{\mathrm{ILC}i}\}\ \cup_{i=1}^{N_j^{cl}}\ \{\boldsymbol{a}_{\mathrm{ILC}}^{\mathrm{ILC}i}\}$ where $\boldsymbol{a}_m^{\mathrm{ILC}i}$, $\boldsymbol{a}_n^{\mathrm{ILC}i}$ and $\boldsymbol{a}_{\mathrm{ILC}}^{\mathrm{ILC}i}$ are vectors that represent the communication between an ILC and the DGs of the m-th and n-th MGs, and with the other ILCs in the j-th cluster, respectively.

In matrix form, the communication network of the AC/DC multi-MG system can be represented by

$$A^{\mathrm{sys}} = \begin{bmatrix} A^{\mathrm{MMG}} & A_{\mathrm{MMG}}^{\mathrm{ILCs}} \\ A_{\mathrm{MMG}}^{\mathrm{ILCs}} & A_{\mathrm{ILCs}}^{\mathrm{ILCs}} \end{bmatrix}, \tag{5.7}$$

$$A^{\mathrm{MMG}} = \begin{bmatrix} A^m & 0 & \cdots & 0 \\ 0 & \ddots & \ddots & \vdots \\ \vdots & \ddots & \ddots & 0 \\ 0 & \cdots & 0 & A^{N_{\mathrm{MG}}} \end{bmatrix}, \tag{5.8}$$

$$A^{\mathrm{ILCs}}_{\mathrm{MMG}} = \begin{bmatrix} A^{cl,1}_{\mathrm{MG},1} & \cdots & A^{cl,1}_{\mathrm{MG},N_{\mathrm{MG}}} \\ \vdots & \vdots & \vdots \\ A^{cl,N_{cl}}_{\mathrm{MG},1} & \cdots & A^{cl,N_{cl}}_{\mathrm{MG},N_{\mathrm{MG}}} \end{bmatrix}, \tag{5.9}$$

$$A^{\mathrm{ILCs}}_{\mathrm{ILCs}} = \begin{bmatrix} A^{cl,1}_{cl,1} & \cdots & A^{cl,1}_{cl,N_{cl}} \\ \vdots & \vdots & \vdots \\ A^{cl,N_{cl}}_{cl,1} & \cdots & A^{cl,N_{cl}}_{cl,N_{cl}} \end{bmatrix}, \tag{5.10}$$

where A^m is the adjacency matrix of the m-th MG. A^{MMG}, $A^{\mathrm{ILCs}}_{\mathrm{MMG}}$, and $A^{\mathrm{ILCs}}_{\mathrm{ILCs}}$ are the communication matrices describing the communications between DGs, DGs and ILCs, and between ILCs, respectively. Particularly, $A^{cl,j}_{\mathrm{MG},m} = \begin{bmatrix} \boldsymbol{a}^{\mathrm{ILC1}}_m \\ \vdots \\ \boldsymbol{a}^{\mathrm{ILC}N^{cl}_j}_m \end{bmatrix}$ and $A^{cl,k}_{cl,j} = \begin{bmatrix} \boldsymbol{a}^{\mathrm{ILC1}}_{cl,j} \\ \vdots \\ \boldsymbol{a}^{\mathrm{ILC}N^{cl}_k}_{cl,j} \end{bmatrix}$ with $\boldsymbol{a}^{\mathrm{ILC}i}_m = \left(a^{\mathrm{ILC}i}_1, \ \dots \ , \ a^{\mathrm{ILC}i}_{N^{\mathrm{MG}}_m}\right)$ and $\boldsymbol{a}^{\mathrm{ILC}i}_{cl,j} = \left(a^{\mathrm{ILC}i}_{\mathrm{ILC1}}, \ \dots \ , \ a^{\mathrm{ILC}i}_{\mathrm{ILC}N^{cl}_j}\right)$ vectors that represent the communication of the i-th ILC with the DGs in the m-MG and the ILCs of the j-th ILC cluster, respectively. Noting that $A^{cl,j}_{cl,j} = A^{cl,j}_{\mathrm{ILC}} = \begin{bmatrix} \boldsymbol{a}^{\mathrm{ILC1}}_{\mathrm{ILC}} \\ \vdots \\ \boldsymbol{a}^{\mathrm{ILC}N^{cl}_j}_{\mathrm{ILC}} \end{bmatrix}$ with $\boldsymbol{a}^{\mathrm{ILC}i}_{\mathrm{ILC}} = \left(a^{\mathrm{ILC}i}_{\mathrm{ILC1}}, \ \dots \ , \ a^{\mathrm{ILC}i}_{\mathrm{ILC}N^{cl}_j}\right)$. The form of A^{MMG} suggests that no communication between DGs of different MGs is allowed. In this section, the ILCs of different clusters are assumed not communicated, i.e., $A^{cl,i}_{cl,j} = 0$ $\forall \ i \neq j \ \wedge \ i,j \in \mathcal{N}_{cl}$.

The former definitions are used to design a distributed controller in the ILCs of the AC/DC multi-MG.

5.2.4 Distributed multi-objective control using consensus protocol

The distributed control for solving (5.4) is designed as an extension of (4.22). For the i-th ILC in the j-th ILC cluster, which interconnects the m-th MG with the n-th MG of a multi-MG system, the control actions take the form:

$$P^*_{\mathrm{ILC}i} = (u_{\mathrm{L}i} + u_{\mathrm{C}i} + u_{\mathrm{P}i} + u_{\mathrm{R}i}) G^P_{\mathrm{PI}}(s) \ , \tag{5.11}$$

$$u_{\mathrm{L}i} = c_L \sum_{l=1}^{N^{\mathrm{MG}}_m} \sum_{k=1}^{N^{\mathrm{MG}}_n} \mathrm{sig}\left[\frac{a^{\mathrm{ILC}i}_l}{N^{\mathrm{ILC}}_m} \lambda_l - \frac{a^{\mathrm{ILC}i}_k}{N^{\mathrm{ILC}}_n} \lambda_k \right]^{\alpha_L} , \tag{5.12}$$

$$u_{\mathrm{C}i} = c_C \left(\overline{P}^{cl}_{j,i} - \frac{P_{\mathrm{ILC}i}}{P^{\max}_{\mathrm{ILC}i}} \right) , \tag{5.13a}$$

$$\overline{P}^{cl}_{j,i} = \frac{P_{\mathrm{ILC}i}}{P^{\max}_{\mathrm{ILC}i}} + c_C^{'} \frac{1}{s} \sum_{k=1}^{N_j^{cl}} \mathrm{sig}\Big[a^{\mathrm{ILC}i}_{\mathrm{ILC}k} (\overline{P}^{cl}_{j,k} - \overline{P}^{cl}_{j,i}) \Big]^{\alpha_C} , \tag{5.13b}$$

$$u_{\mathrm{P}i} = c_P \sum_{l=1}^{N_m^{\mathrm{MG}}} \sum_{k=1}^{N_n^{\mathrm{MG}}} \mathrm{sig} \left[\frac{a^{\mathrm{ILC}i}_{l}}{N^{\mathrm{ILC}}_{m}} h_m(\overline{P}^{\mathrm{MG}}_{m,l}) \overline{P}^{\mathrm{MG}}_{m,l} - \frac{a^{\mathrm{ILC}k}_{k}}{N^{\mathrm{ILC}}_{n}} h_n(\overline{P}^{\mathrm{MG}}_{n,k}) \overline{P}^{\mathrm{MG}}_{n,k} \right]^{\alpha_P} , \tag{5.14a}$$

$$\overline{P}^{\mathrm{MG}}_{\mathrm{x},l} = \frac{P_l}{P^{\max}_{l}} + \frac{1}{s} \sum_{k=1}^{N_{\mathrm{x}}^{\mathrm{MG}}} a_{\mathrm{x},lk} (\overline{P}^{\mathrm{MG}}_{\mathrm{x},k} - \overline{P}^{\mathrm{MG}}_{\mathrm{x},l}) , \tag{5.14b}$$

$$u_{\mathrm{R}i} = c_{Ri} \left(P^{\mathrm{ref}}_{\mathrm{ILC}i} - \frac{P_{\mathrm{ILC}i}}{P^{\max}_{\mathrm{ILC}i}} \right) , \tag{5.15}$$

where $N^{\mathrm{ILC}}_{m} = \boldsymbol{a}^{\mathrm{ILC}i}_{m} \cdot \mathbf{1}_{N^{\mathrm{MG}}_{m}}$ is the number of DGs of the m-th MG communicating with the i-th ILC (active nodes), provided a binary communication matrix. The term $\overline{P}_{\mathrm{x},l}$ comes from a distributed observer of the l-th DG of the x-th MG and stands for the estimated average power of the MG. Also, $a_{\mathrm{x},lk}$ is the communication weight between DG l and DG k, where $a_{\mathrm{x},lk} \subseteq A^{\mathrm{x}}$ (x could be the MG m or n in the example shown in (5.11)). The terms h_m and h_n are weights that adjust the trade-off between IC balancing and the MG power utilization of the interconnected MGs m and n, respectively. In this case, those coefficients are designed adjustable based on (3.41) of Chapter 3.

5.3 Design of Distributed Control for a Meshed Multi-Microgrid with Balancing of Clusters of Interlinking Converters

From the design of the previous section, a novel ILC cluster balancing objective can be included by adding a new control goal. The ILC cluster power balancing is not a control objective necessary for achieving the economic dispatch, moreover, it increases the global IC by deteriorating the power transfer between MGs. Despite this issue, grid operators might need to induce some reductions on the total power transferred by the clusters of ICs to fulfil specific safety conditions or reduce the system's power losses. It is worth noting that, as demonstrated in Chapter 4, the hard constraints of power in ILCs could lead to the ILC cluster achieving the designated power, providing an increase or reduction in the ILC cluster transferred power. However, a different approach could be taken by inducing a balancing between a group of ILC clusters, which avoids the necessity of power references that may lead the system to saturation if selected inappropriately.

Then, this section studies the feasibility of the implementation of such ILC cluster power balancing control and its effect on the overall system performance. For its formulation, it

is applied the same principle shown in Chapter 3 for the MG saturation, i.e. a formulation relying on an average power observer.

5.3.1 Formulation of economic dispatch in a meshed AC/DC multi-MG with ILC power-sharing, ILC cluster power-sharing, hard power constraints and subgrid power saturation

Similarly to the case of balancing the MG's average power to reduce the MG saturations described in Chapter 3, a control goal can be added to the objective function of 5.4 to perform the balancing of ILC cluster powers. Then, the objective function can be expressed as

$$J\left(f^1(\boldsymbol{P}), f^2(\boldsymbol{P}), f^3(\boldsymbol{P}), f^4(\boldsymbol{P})\right) = f^1(\boldsymbol{P}) + hf^2(\boldsymbol{P}) + wf^3(\boldsymbol{P}) + \Gamma f^4(\boldsymbol{P}) \ , \tag{5.16}$$

where

$$f^4(\boldsymbol{P}) = \sum_{j=1}^{N_{cl}} \sum_{\substack{k=1 \\ k\neq j}}^{N_{cl}} \left(d_j \overline{P}_j^{cl}(\boldsymbol{P}) - d_k \overline{P}_k^{cl}(\boldsymbol{P})\right) \ , \tag{5.17}$$

Γ is a weighting parameter to regulate the control goal of ILC cluster balancing, and $d_j \ \forall \ j \in \mathcal{N}_{cl}$ is a coefficient that determines the prioritisation in the management of saturation/reserves ILC clusters.

Thus, the KKT stationary optimality condition gives

$$\begin{aligned} \lambda =& \frac{\partial C_i\left(P_i\right)}{\partial P_i} + hg^1(\boldsymbol{P}) + wg^2(\boldsymbol{P}) + \Gamma g^3(\boldsymbol{P}) + \sigma^+ - \sigma^- \\ &+ \sum_{j=1}^{N_{cl}} \sum_{l=1}^{N_j^{cl}} (\Lambda_l^+ - \Lambda_l^-) \frac{\partial P_{\mathrm{ILC}l}(\boldsymbol{P})}{\partial P_i} + \sum_{k=1}^{N_k} z_k \frac{\partial P_{\mathrm{ILC}k}(\boldsymbol{P})}{\partial P_i} \ , \end{aligned} \tag{5.18}$$

where $g^3(\boldsymbol{P})$ is a linear function depending on $\frac{\partial P_{\mathrm{ILC}l}(\boldsymbol{P})}{\partial P_i}$.

5.3.2 Distributed multi-objective control with ILC cluster balancing using consensus protocol

In this case, the communication between clusters of ILCs is assumed so that $\boldsymbol{a}_{cl,k}^{cl,j} \neq 0$ for all $k, j \in \mathcal{N}_{cl}$. Then, based on (5.11), the distributed controller for the i-th ILC of the j-th ILC cluster is:

$$P_{\mathrm{ILC}i}^* = (u_{\mathrm{L}i} + u_{\mathrm{C}i} + u_{\mathrm{P}i} + u_{\Gamma i} + u_{\mathrm{R}i}) G_{\mathrm{PI}}^P(s) \ , \tag{5.19}$$

with

$$u_{\Gamma i} = c_\Gamma \operatorname{sign}(\overline{P}_{j,i}^{cl}) \sum_{l=1}^{N_{cl}} \sum_{k=1}^{N_j^{cl}} a_{\mathrm{ILC}k}^{\mathrm{ILC}i} \left(\Gamma_l(\overline{P}_{l,k}^{cl}) \| \overline{P}_{l,k}^{cl} \| - \Gamma_i(\overline{P}_{j,i}^{cl}) \| \overline{P}_{j,i}^{cl} \|\right) \ , \tag{5.20}$$

where c_Γ is a convergence speed parameter, $\overline{P}_{l,k}^{cl}$ is the average power estimation of the l-th cluster estimated by the k-th ILC using (5.13b), and Γ_i is the trade-off weight for the power-sharing of ILC clusters regarding the IC consensus. Similarly to h coefficients described in

Chapter 3, Γ_i can be fixed or adjusted by an activation function of the form $\Gamma_i(\overline{P}_x^{cl}) = k_\Gamma^1 e^{k_\Gamma^2 \overline{P}_x^{cl}}$ where x is an ILC cluster; this ensures that this "penalty" compensation smoothly activates as the maximum power of an ILC cluster is reaching. It can be seen from (5.20) that the ILC clusters' sign is managed. For the effects of the balancing, the subtraction is defined with only positive values. Then, the sign of the local ILC cluster is preserved and reincorporated at the end of the tracking error calculation.

A summary of the multi-objective control strategy for the ILCs using (5.11)-(5.19) is given in the flowchart of Fig. 5.2. It describes the steps involving an arbitrary ILC of the multi-MG system.

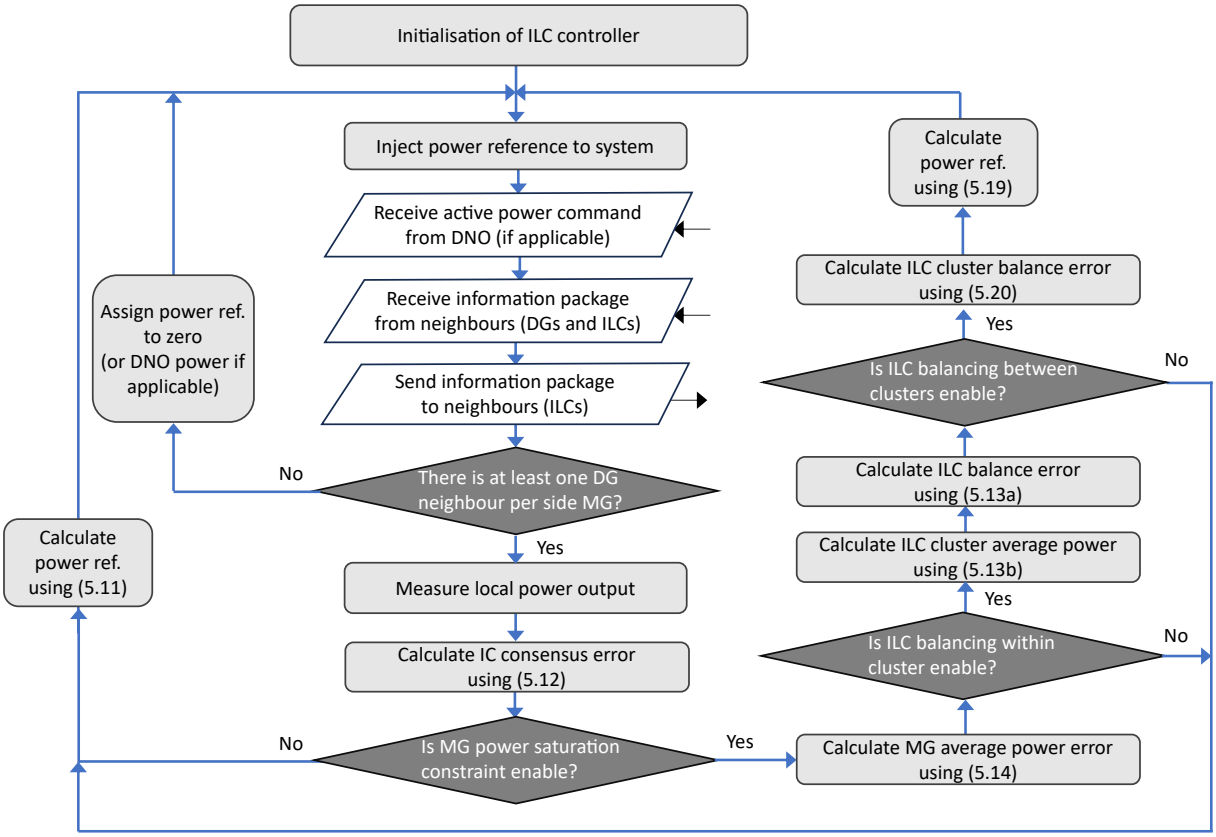

Figure 5.2: Flowchart of the proposed multi-objective control strategy for ILCs in a meshed multi-MG system.

5.4 Case Studies

To analyse the performance of the different proposed terms in the ILC controllers, simulations are carried out on the software PLECS. For the simulations, an AC MG interconnected with 2 DC MGs is analysed; the system is depicted in Fig 5.3, and it is composed of 5 AC DGs, 5 DC DGs, 3 AC loads and 3 DC loads. Also, there are three ILC clusters in the system, so the power flow of a meshed system can be studied. In particular, the system in Fig. 5.3 is similar to Fig. 3.7 used in Chapter 4. In this case, it can be seen that the DC MG is divided in two,

with the DC MG #1 made up of the DG6 and DG7 units, and the DC MG #2 compound of the DG8, DG9 and DG10 units. As for the ILC clusters, Cluster #1 is made of 3 ILCs, whereas Cluster #2 and Cluster #3 are made of 2 ILCs each. Numerical identification of DGs and ILCs has been taken for clarity, which can be seen in Fig 5.3.

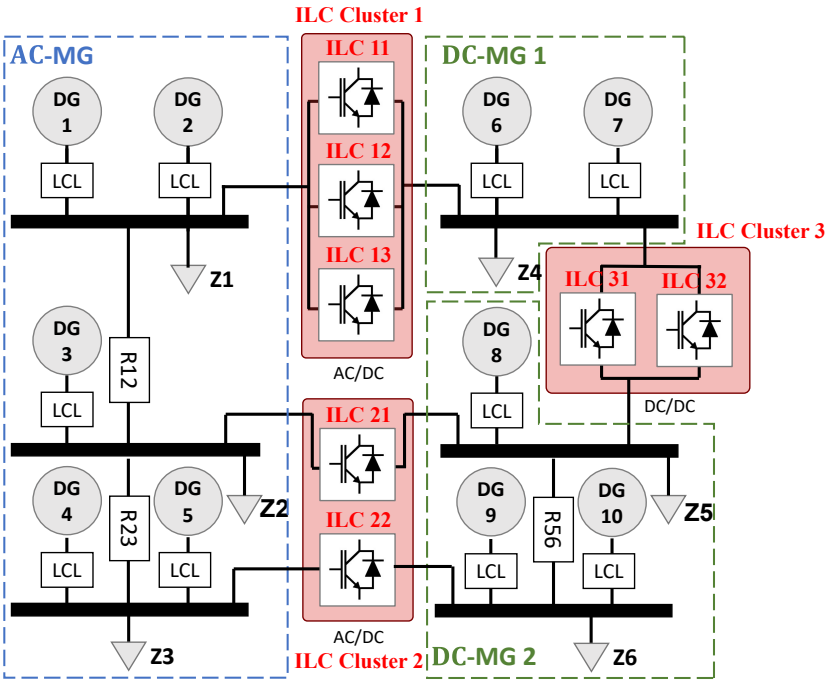

Figure 5.3: Simulated meshed multi-MG system.

The rating magnitude of voltage for the AC MG is 220 [V] per phase, whereas the rating frequency is 50 [Hz]. The rating voltage levels for the DC MG #1 and DC MG #2 are 400 [V] and 370 [V], respectively. The power ratings for the DGs are the following: $P_i^{\max} = 10$ [kW] $\forall i \in \mathcal{N}_{\text{AC}}$, $Q_i^{\max} = 3.33$ [kVAR] $\forall i \in \mathcal{N}_{\text{AC}}$, $P_i^{\max} = 10$ [kW] $\forall i \in \mathcal{N}_{\text{DC}}$. The power capacities of ILCs are: $P_{\text{ILC11}}^{\max} = 11,0$[kW], $P_{\text{ILC12}}^{\max} = 7,7$[kW], $P_{\text{ILC13}}^{\max} = 14,3$[kW], $P_{\text{ILC21}}^{\max} = 10,0$[kW], $P_{\text{ILC22}}^{\max} = 7,0$[kW], $P_{\text{ILC31}}^{\max} = 9,0$[kW], $P_{\text{ILC32}}^{\max} = 6,3$[kW]. The communication matrices and vectors are:

$$A^{\text{AC}} = \begin{bmatrix} 0 & 1 & 1 & 0 & 0 \\ 1 & 0 & 1 & 1 & 0 \\ 1 & 1 & 0 & 1 & 1 \\ 0 & 1 & 1 & 0 & 1 \\ 0 & 0 & 1 & 1 & 0 \end{bmatrix}, A^{\text{DC1}} = \begin{bmatrix} 0 & 1 \\ 1 & 0 \end{bmatrix}, A^{\text{DC2}} = \begin{bmatrix} 0 & 1 & 1 \\ 1 & 0 & 1 \\ 1 & 1 & 0 \end{bmatrix}, \tag{5.21}$$

$$A_{\text{AC}}^{cl,1} = \begin{bmatrix} 1 & 1 & 0 & 0 & 0 \\ 0 & 1 & 0 & 0 & 0 \\ 0 & 1 & 1 & 0 & 0 \end{bmatrix}, A_{\text{DC1}}^{cl,1} = \begin{bmatrix} 1 & 1 \\ 1 & 0 \\ 0 & 1 \end{bmatrix}, A_{\text{DC2}}^{cl,1} = \begin{bmatrix} 0 & 0 & 0 \\ 0 & 0 & 0 \\ 0 & 0 & 0 \end{bmatrix}, \tag{5.22}$$

$$A_{\mathrm{AC}}^{cl,2} = \begin{bmatrix} 0 & 0 & 0 & 1 & 1 \\ 0 & 0 & 0 & 0 & 1 \end{bmatrix}, A_{\mathrm{DC1}}^{cl,2} = \begin{bmatrix} 0 & 0 \\ 0 & 0 \end{bmatrix}, A_{\mathrm{DC2}}^{cl,2} = \begin{bmatrix} 0 & 1 & 1 \\ 0 & 0 & 1 \end{bmatrix}, \tag{5.23}$$

$$A_{\mathrm{AC}}^{cl,3} = \begin{bmatrix} 0 & 0 & 0 & 0 & 0 \\ 0 & 0 & 0 & 0 & 0 \end{bmatrix}, A_{\mathrm{DC1}}^{cl,3} = \begin{bmatrix} 1 & 1 \\ 1 & 1 \end{bmatrix}, A_{\mathrm{DC2}}^{cl,3} = \begin{bmatrix} 1 & 1 & 0 \\ 1 & 1 & 0 \end{bmatrix}, \tag{5.24}$$

$$A_{cl,1}^{cl,1} = \begin{bmatrix} 0 & 1 & 1 \\ 1 & 0 & 1 \\ 1 & 1 & 0 \end{bmatrix}, A_{cl,2}^{cl,1} = \begin{bmatrix} 0 & 0 \\ 0 & 0 \\ 0 & 0 \end{bmatrix}, A_{cl,3}^{cl,1} = \begin{bmatrix} 0 & 0 \\ 0 & 0 \\ 0 & 0 \end{bmatrix}, \tag{5.25}$$

$$A_{cl,1}^{cl,2} = (A_{cl,2}^{cl,1})^{\mathrm{T}}, A_{cl,2}^{cl,2} = \begin{bmatrix} 0 & 1 \\ 1 & 0 \end{bmatrix}, A_{cl,3}^{cl,2} = \begin{bmatrix} 0 & 0 \\ 0 & 0 \end{bmatrix}, \tag{5.26}$$

$$A_{cl,1}^{cl,3} = (A_{cl,3}^{cl,1})^{\mathrm{T}}, A_{cl,2}^{cl,3} = (A_{cl,3}^{cl,2})^{\mathrm{T}}, A_{cl,3}^{cl,3} = \begin{bmatrix} 0 & 1 \\ 1 & 0 \end{bmatrix}. \tag{5.27}$$

The economic function parameters in the DGs of the AC MG are the same as described in Table 3.2. For the DGs in the DC MGs, the values are 3/4 of the ones used in the AC MG. The ILC control parameters are $k_p^P = 0.25$, $k_i^P = 2.35$, $c_L = 1000$, $c_C = 2000$, $c_C^{'} = 5$, $c_P = 0.1P_{\mathrm{ILC}i}^{\max}$, and $c_\Gamma = 3000$. The finite-time gains are $\alpha_L = 0.8$, $\alpha_C = 1.0$, and $\alpha_P = 1.0$. For briefness in the analysis of simulation curves, power references to ILCs are omitted, i.e., $c_{Ri} = 0$; the interested reader is conducted to Chapter 4 to see the behaviour of the economic dispatch and ILC power-sharing with this condition. The remaining parameters of the system in Fig 5.3 mimic the parameters used in Chapter 4.

For the analysis of the performance of the system under challenging operation, i.e., load impacts, saturations and time delays, four sets of cases of study are used to test each control goal. The cases of study are defined as follows:

Case 1.a. Economic dispatch with load impacts

In this test, the ILCs apply the controller of (5.12) for IC synchronisation. Similarly to Chapter 4, the subgrids are subdued to load impacts to analyse the transient and steady-state performance: at t=23[s], Z3 changes from 7.69 to 4.69[Ω], then, at t=43[s], Z6 changes from 12.63 to 8.47[Ω], finally, at t=43[s], Z6 changes again to 12.63 from 8.47[Ω].

Case 1.b. Economic dispatch with load impacts and ILC cluster saturation

In this case, the maximum power capacity of the ILC Cluster #3 is reduced to produce saturation under certain load impacts. The ILCs of Cluster #3 are $P_{\mathrm{ILC31}}^{\max} = 1800$[W] and $P_{\mathrm{ILC32}}^{\max} = 415,8$[W].

Case 1.c. Economic dispatch with load impacts and communication losses

In this test, the economic dispatch is tested when one ILC cluster stops its power transfer. The system starts with the same conditions as Case 1.b., and then the communication between the side MGs and the ILCs in Cluster #3 is interrupted. Under this condition, only two ILC clusters are operative for the economic dispatch. Sufficient power capacity is available in the remaining ILC clusters.

Case 1.d. Economic dispatch with load impacts and communication time delays

In this test, different time delays are incorporated into the communication links between DGs and ILCs. For briefness, homogeneous delays are incorporated for all communication links to see the difference between delay magnitudes. Delays of 0 [s], 0.125[s] and 0.25[s] are analysed using the system of Case 1.b.

Case 2. Economic dispatch with MG saturation and load impacts

The ILCs perform the control actions in (5.12) and (5.14). For the simulation, the maximum power capacity of some ILCs and DGs is reduced to produce the saturation of one MG. Specifically, $P_{\text{ILC31}}^{\max} = 1800$[W], $P_{\text{ILC32}}^{\max} = 415,8$[W], $P_{6}^{\max} = 4400$[W], $P_{7}^{\max} = 4400$[W] and $P_{8}^{\max} = 4000$[W]. Values of 0.2 are used for the parameter h_m of ILCs in Cluster #1, as well as the adjustable expression $h_m(\overline{P})$ of (3.41) but multiplied by 0.1. The same load impacts as previous simulations are used. A time delay of 0.125 [s] is also used.

Case 3.a. Economic dispatch with ILC power-sharing and load impacts

This test incorporates the ILC power balancing action inside the ILC clusters. It uses the same setup as Case 1.b., i.e., without MG saturations but with the new term (5.13) in the ILCs' controller. The test looks to validate the simultaneous synchronisation of global IC and the ILC powers inside a cluster.

Case 3.b. Economic dispatch with MG saturation constraint, ILC power-sharing and load impacts

This test incorporates the ILC power balancing action inside the ILC clusters. Thus, the new term (5.13) is included in the ILCs' controller. The same setup as Case 2 with the adjustable $h_m(\overline{P})$ is used, i.e. there is saturation in DC MG #1 and ILC Cluster #3 with a time delay between DGs and ILCs.

Case 3.c. Economic dispatch with MG saturation constraint, ILC power-sharing and communication losses

This test performs Case 3.b. but with a communication loss between the ILC #11 and the ILC #12.

Case 3.d. Economic dispatch with MG saturation constraint, ILC power-sharing and communication time delays

This test performs Case 3.a. but with a homogeneous communication delay in all of the ILCs. Delay values of 0, 0.125 and 0.25 [s] are used. The same anti-windup with reset scheme of Chapter 4 is implemented to deal with steady-state errors in the distributed power observer. Also, it tested a subcase where the coupling gains of Cluster #3 are reduced by half to evaluate the level of decoupling between control loops.

Case 4.a. Economic dispatch with MG saturation constraint, ILC power-sharing and ILC saturation constraint

This test uses (5.19) in the ILCs. The communication vectors between clusters of ILCs are non-zero, taking the values: $A_{cl,2}^{cl,1} = \begin{bmatrix} 1 & 1 \\ 1 & 1 \\ 1 & 1 \end{bmatrix}$, $A_{cl,3}^{cl,1} = \begin{bmatrix} 1 & 1 \\ 1 & 1 \\ 1 & 1 \end{bmatrix}$ and $A_{cl,3}^{cl,2} = \begin{bmatrix} 1 & 1 \\ 1 & 1 \end{bmatrix}$. The same MG conditions of Case 3.b. are used with a delay of 0.125 [s] included in the ILC power-sharing communications. The tolerance of the anti-windup is slightly reduced compared with Chapter 4 in order to relax high-frequency oscillations, particularly, $\varepsilon = 10^{-4}$. Also, Γ_j values of 0, 0.5 and the adjustable $\Gamma_j(\overline{P}_{\text{ILC}})$ are used simultaneously for all the ILC clusters.

Case 4.b Economic dispatch with MG saturation constraint, ILC power-sharing, ILC saturation constraint and communication losses

In this test, communication losses are included in the communication between Cluster #1 and Cluster #2. To represent the worst-case scenario, all the communication links are disconnected between these two clusters, i.e., $A_{cl,2}^{cl,1} = \begin{bmatrix} 0 & 0 \\ 0 & 0 \\ 0 & 0 \end{bmatrix}$. The rest of the system parameters are the same as Case 4.a. with the adjustable $\Gamma_j(\overline{P}_{\text{ILC}})$.

Case 4.c Economic dispatch with MG saturation constraint, ILC power-sharing, ILC saturation constraint and communication time delays

In this test, delays are included in the cluster communication, which are 0, 0.125 and 0.25 [s]. The simulation setup is the same as in Case 4.a. with the adjustable $\Gamma_j(\overline{P}_{\text{ILC}})$.

5.5 Results

Case 1.a. Economic dispatch with load impacts

Fig. 5.4 and Fig. 5.5 show a summary of the main results for the application of distributed economic dispatch using (5.12) in the ILCs. The system starts with droop control applied by the DGs. Secondary control is activated at t=0.3[s] for voltage restoration and IC consensus whereas the secondary control for frequency restoration is activated at t=1.8[s].

It can be noted from Fig. 5.4a that all the individual ICs of DGs in the multi-MG synchronise to the same value when the ILC control is enabled, at t=3[s], even though there are no direct communications between DGs of different MGs or between ILCs. Also, seamless transitions of ICs during the load impacts can be observed, with the biggest overshoot occurring in the AC MG, during its local load impact at t=23[s]; this is due to the local DG's bandwidth for IC, which is slower by stability purposes than the bandwidth used in the DC side MGs. As for the ILCs' powers, Fig. 5.4b shows a distribution of power which is not directly related to any control goals, instead this distribution of power comes as a result of the power flow that the economic dispatch creates, which depends on the location of DGs, their communication links with ILCs, and their cost functions. Similarly, Fig. 5.4c shows how the combined power of DGs varies over time as a consequence of the economic dispatch. The transient oscillations are reduced compared with Fig. 5.4c because these are curves of average power (among DGs in the same MG). It can be seen that the DC MG #2 has the highest overshoot on average, shown by its load impacts occurring in t=43[s] and t=63[s].

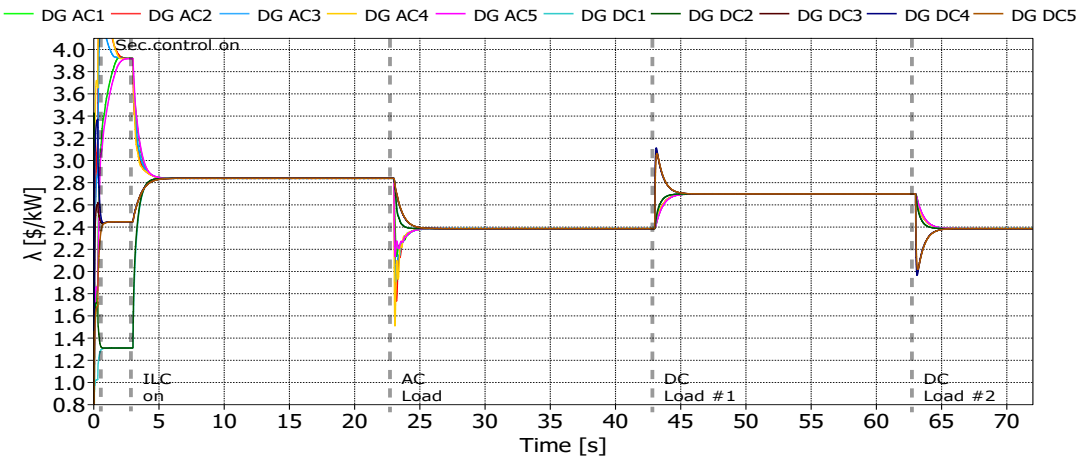

(a)

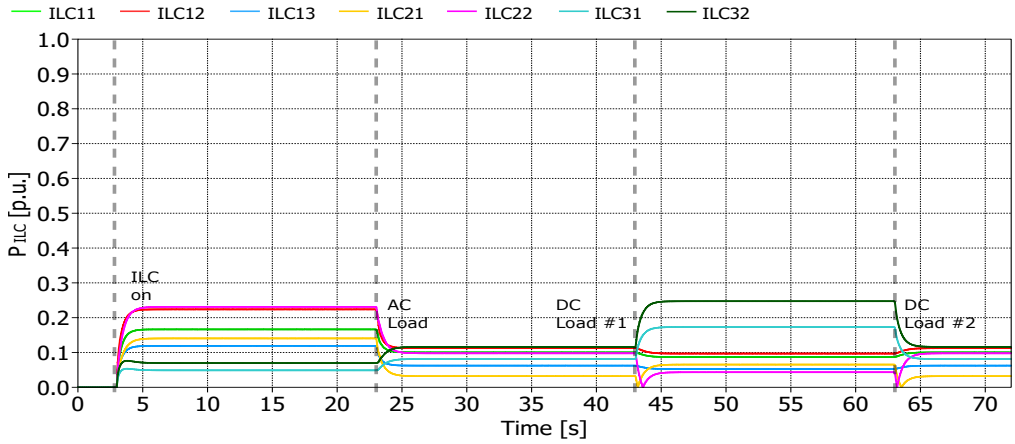

(b)

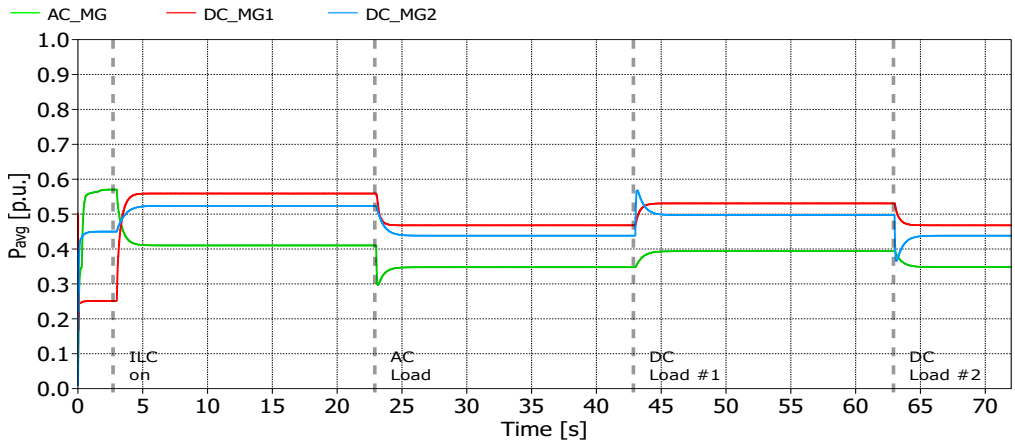

(c)

Figure 5.4: Simulation results for Case 1.a. (a) IC of DGs in multi-MG. (b) Absolute power of ILCs. (c) Average power of MGs.

Additional variables are displayed in Fig. 5.5, where the MGs' average voltages are shown in Fig. 5.5a and Fig. 5.5b whereas the frequency of the only AC MG is shown in Fig. 5.5c. It is worth noting that average voltage estimates are chosen to be graphed instead of individual voltages since they are the secondary control variables used (see (F.4) and (F.7)). It can be seen that the secondary control in each MG is performed seamlessly (each local average voltage reaches its voltage reference) and does not modify nor get modified by the ILC control loop during load impacts. A similar situation is observed for the frequency, where the locally measured frequency stabilises to the reference every time there is a load impact despite the ILCs' power transfers.

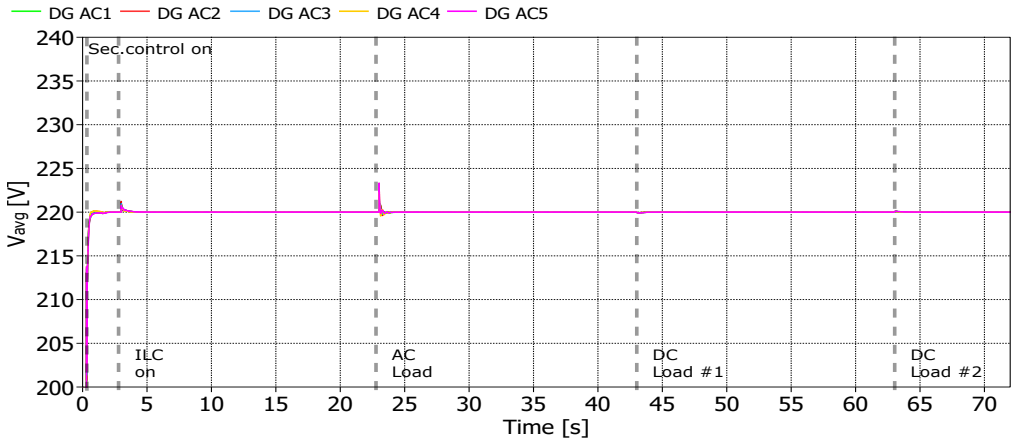

(a)

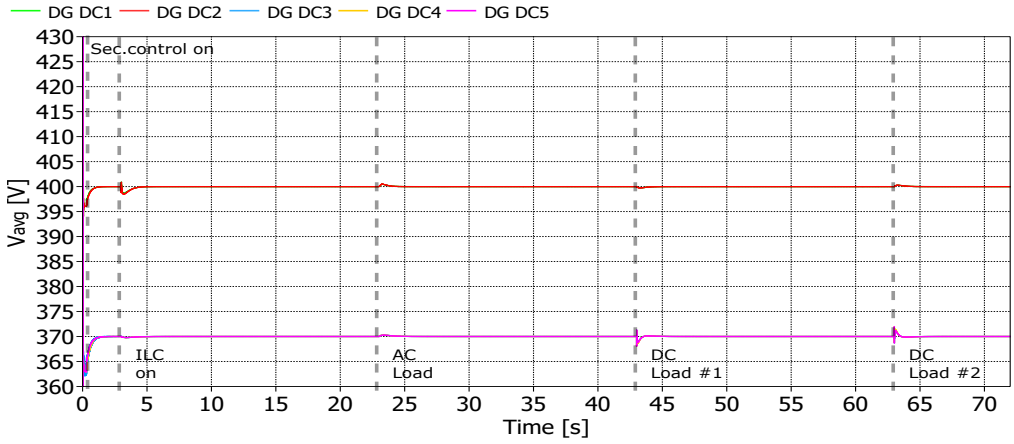

(b)

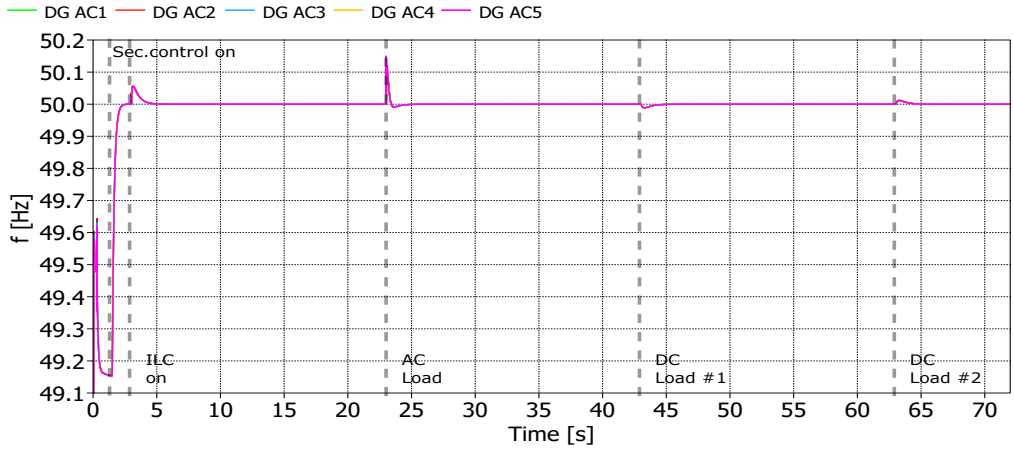

(c)

Figure 5.5: Secondary control variables for Case 1.a. (a) Average voltage magnitude of AC MG. (b) Average voltage magnitude of DC MG #1 and DC MG #2. (c) Frequency of AC MG.

Case 1.b. Economic dispatch with load impacts and ILC cluster saturation

The results for saturation of ILC Cluster #3 are shown in Fig. 5.6. Figure 5.6a illustrates, once again, how the DGs and ILCs manage to equalise the ICs. There are no noticeable differences in the transients and steady-state values compared with Fig. 5.4a. It should be pointed out that the curves in Fig. 5.6a are average IC values, i.e., all the ICs of DGs in each MG are used for an average calculation before plotting; this means that the overshoots in Fig. 5.6a look lower than Fig. 5.4a.

As shown in Fig. 5.6b, since the beginning of the ILC control action, at t=3[s], ILC #32 almost saturates. After the first load impact on the AC side (t=23[s]), ILC #32 saturates and ILC #31 reaches roughly its mid capacity. The situation is more critical after the first load impact in MG DC #2, where both ILC #31 and ILC #32 saturate. In this case, the economic dispatch is still possible due to the meshed multi-MG topology, which has another path to deliver the power transfers. It should be noted that if there is insufficient capacity in any other ILC clusters, there will be desynchronisation in the ICs.

Concerning the average MG powers, shown in Fig. 5.6c, there is a slight alteration in the transient states compared with Fig. 5.4c; mainly, the settling time is increase as some of the power components that were needed to be transferred travelled in a longer path.

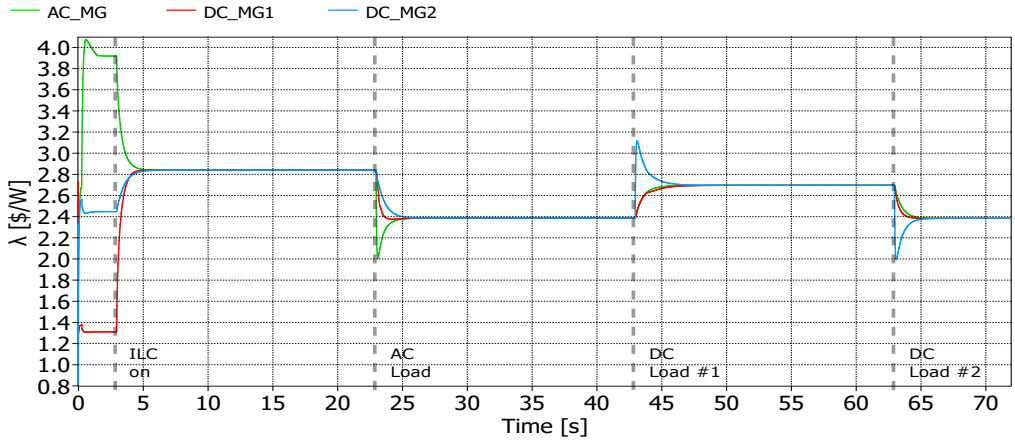

(a)

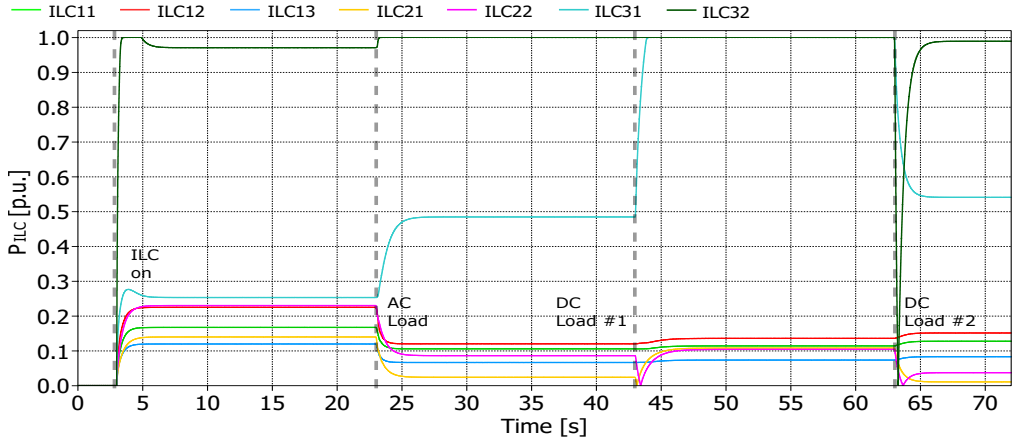

(b)

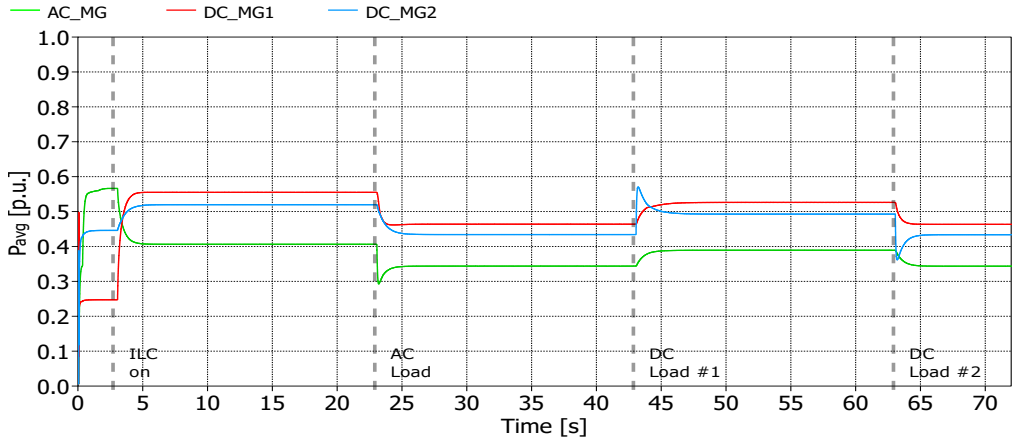

(c)

Figure 5.6: Simulation results for Case 1.b. (a) Average IC of MGs. (b) Absolute power of ILCs. (c) Average power of MGs.

Case 1.c. Economic dispatch with load impacts and communication losses

For this test, where the communications from DGs towards the ILCs in Cluster #3 are lost, the results are presented in Fig. 5.7. Overall, the charts in Fig. 5.7 depicted how the system quickly overcame small disturbances originating from the loss of communications in ILC Cluster #3.

Fig. 5.7a shows that the ILC controller is capable of keeping its consensus of ICs after the communication loss, at t=10[s], reaching the same steady-state values as Case 1.a and Case 1.b. However, the frequency bandwidth of the control is reduced as it has an increased settling time and overshoot. This is mainly because there is one less path for the power to flow (ILC Cluster #3), so it can be seen as a virtual load impact on the rest of ILCs.

In Fig. 5.7b, after t=10[s], all the ILCs achieve new operation points compared with Case 1.b. It is worth remembering that ILC #31 and ILC #32 clamped to zero their power output after t=10[s] as it is programmed to happen when there is no communication from one MG side nor a DNO hard power constraint (command) (see schematic of Fig. 5.2).

In Fig. 5.7c, we can see that the average powers of MGs are restored to the values before the communication loss. Although there is a negligible error in the steady-state values compared with Fig. 5.4c, the rest of the simulation depicts an appropriate response to load impacts. A slower transient is observed, mainly as a consequence of the IC dynamics changes, as described in previous paragraphs.

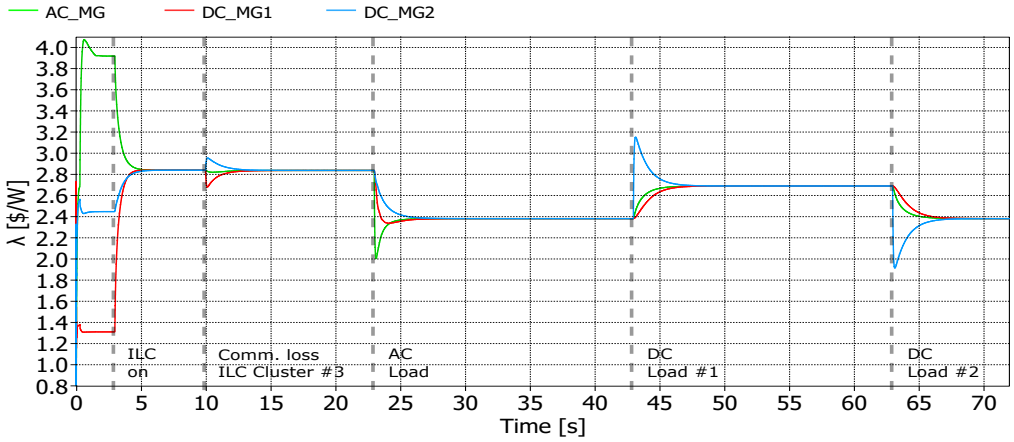

(a)

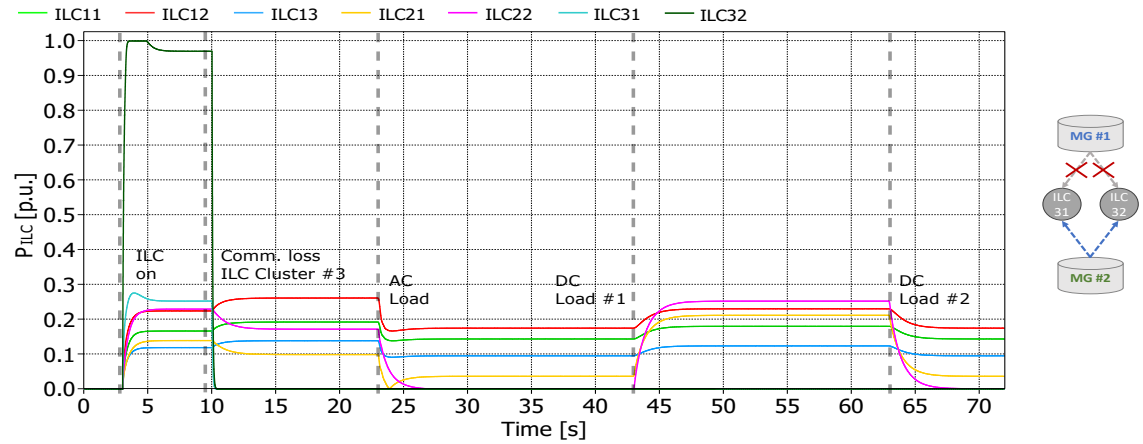

(b)

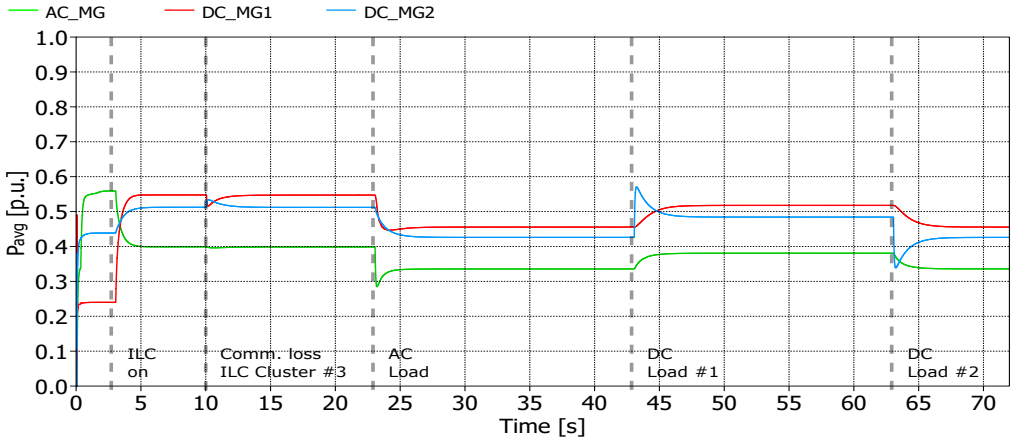

(c)

Figure 5.7: Simulation results for Case 1.c. (a) Average IC of MGs. (b) Absolute power of ILCs. (c) Average power of MGs.

Case 1.d. Economic dispatch with load impacts and communication time delays

Communication delays are analysed for the controller in (5.12) in Fig. 5.8. In Fig. 5.8a, it is shown how time delays slowly increased the ILCs' power overshoot, although the variations are very low. Similar trends are observed in Fig. 5.8b and Fig. 5.8c. In the case of Fig. 5.8b, the delays also induce small steady-state variations in the absolute power of ILCs. The most significant case is ILC #32, especially in $3 < t < 23$ [s], where the difference caused by the 250 [ms] time delay is above 10% concerning the case without delays. For the rest of the ILCs, time delays provoke steady-state deviations of less than 1%.

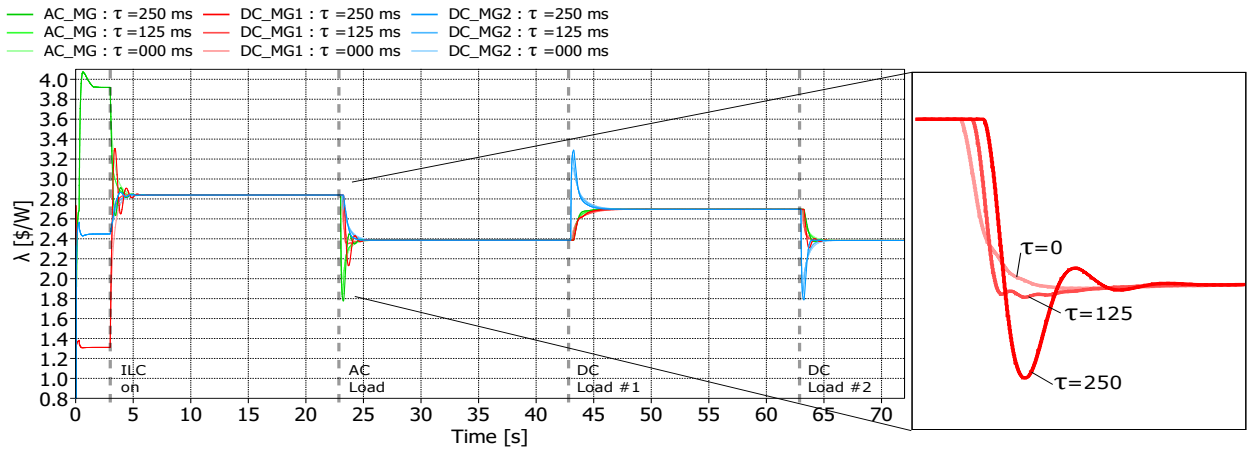

(a)

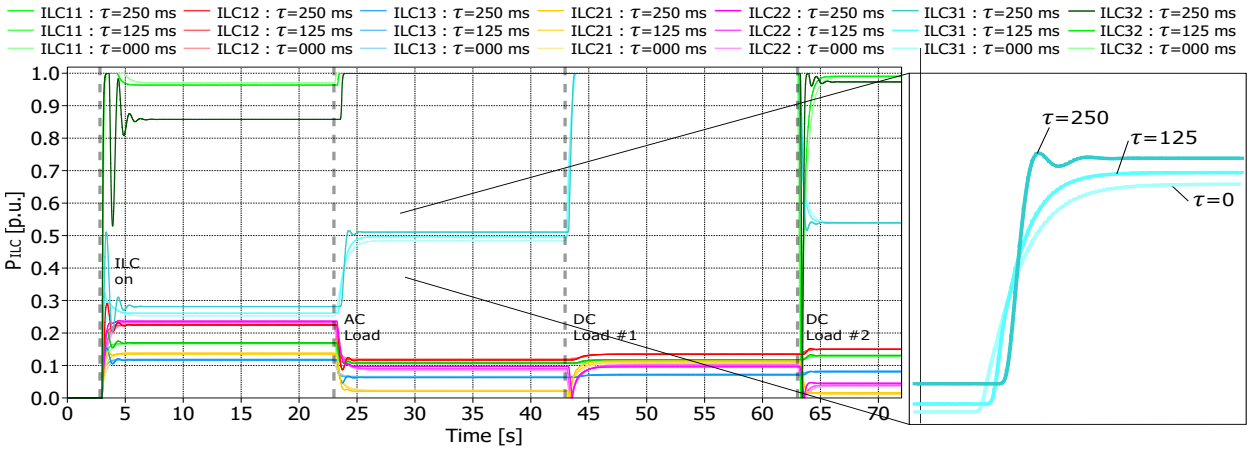

(b)

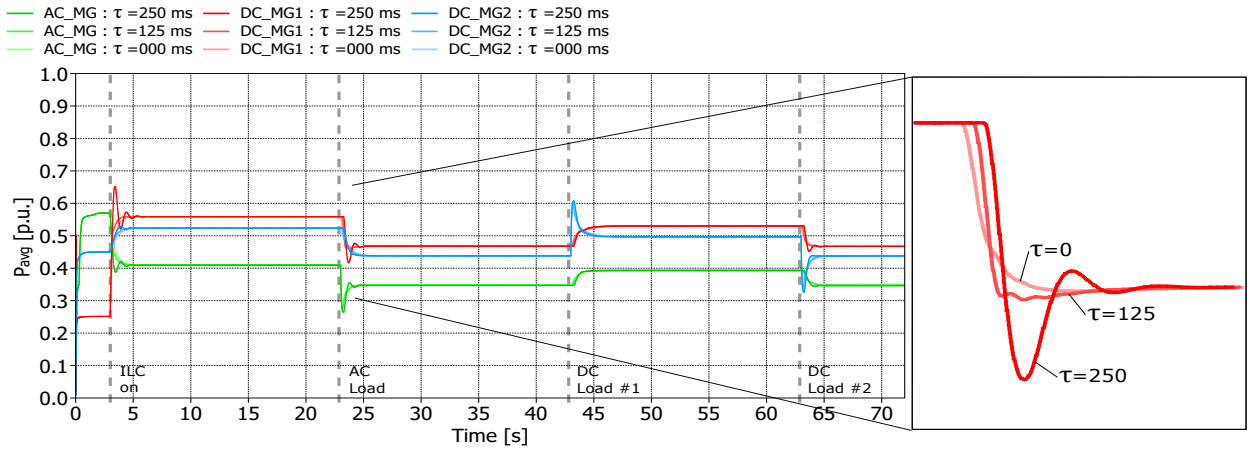

(c)

Figure 5.8: Simulation results for Case 1.d. (a) Average IC of MGs. (b) Absolute power of ILCs. (c) Average power of MGs.

Case 2. Economic dispatch with MG saturation and load impacts

The main results for the multi-objective ILC controller with MG saturations are summarised in Fig. 5.9 and Fig. 5.10. Overall, due to the reduction in the converters' power capacities of DGs, all charts reflect an increase in the overshoot during transient states, i.e. after the activation of the ILCs and load impacts, concerning the results of Case 1.b.

In Fig. 5.9a, it can be seen that after the activation of the saturation constraint, at t=13[s], a higher value for the h_m coefficient (m is the MG number) produces an increase in the transient oscillations of ICs. This phenomenon vanishes after a transient of around 5 [s]. As for the steady-state variations, the ICs show different values compared with Case 1, i.e., there is a de-synchronisation of ICs, similar to what has been seen in Chapter 3. Similar trends regarding the sensibility to h_m and transient state oscillations are observed in the powers of Fig. 5.9c.

In Fig. 5.9b, an increasing behaviour of the absolute powers of ILC #12 and ILC #13 can be seen after t=13[s]. Indeed, in Fig. 5.10, it can be seen that the power of both neutralises each other (different sign), so an equilibrium is reached in the total power transferred by the ILC cluster. However, the power of both ILCs gets saturated, so this behaviour is not ideal for real applications. In the steady-state, Fig. 5.9b shows that the saturated MG (MG DC #1) get reductions in its average power, as expected. The adjustable h_m provides the greater reduction in this case; values of $h_m > 0.4$ could achieve the same reduction in the saturated MG but at the cost of deteriorating the IC synchronisation continuously. The steady-state variations are low for MG AC #1 and MG DC #2, primarily because they do not use more than 80% of their capacity. For ILC Cluster #2 (yellow curves), which does not directly interconnect the saturated MG, the steady-state values are not saturated and the difference between $h = 0.2$ and $h = h(P)$ is insignificant.

The results presented in this case study suggest that the strategy, despite being able to reserve power from saturated MGs, has problems of divergence inside the ILCs of a cluster. This is ineffective since some of the ILCs operate saturated unnecessarily. Therefore, additional control actions should be taken inside the ILC clusters to allow the power constraint to be activated in real-world scenarios.

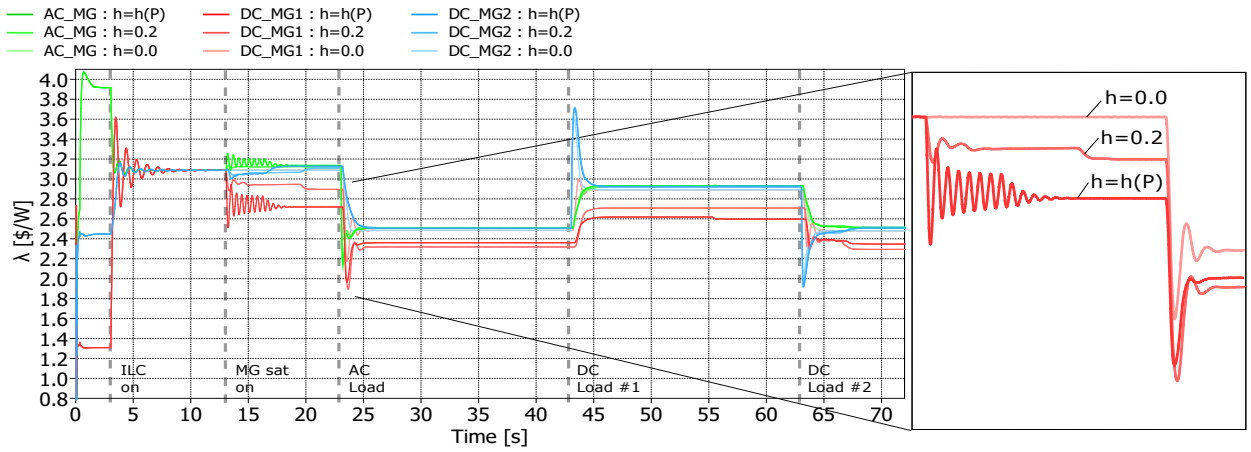

(a)

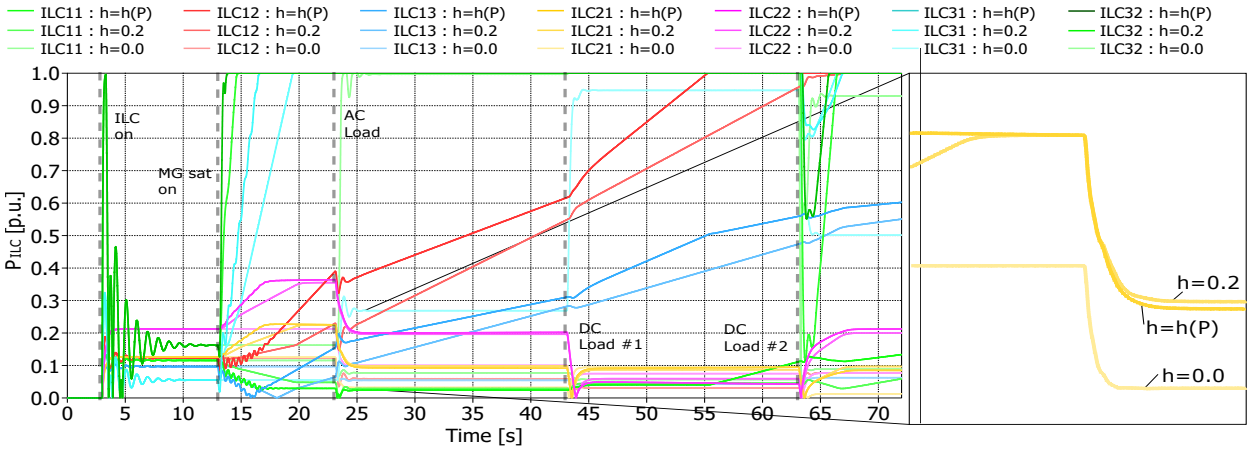

(b)

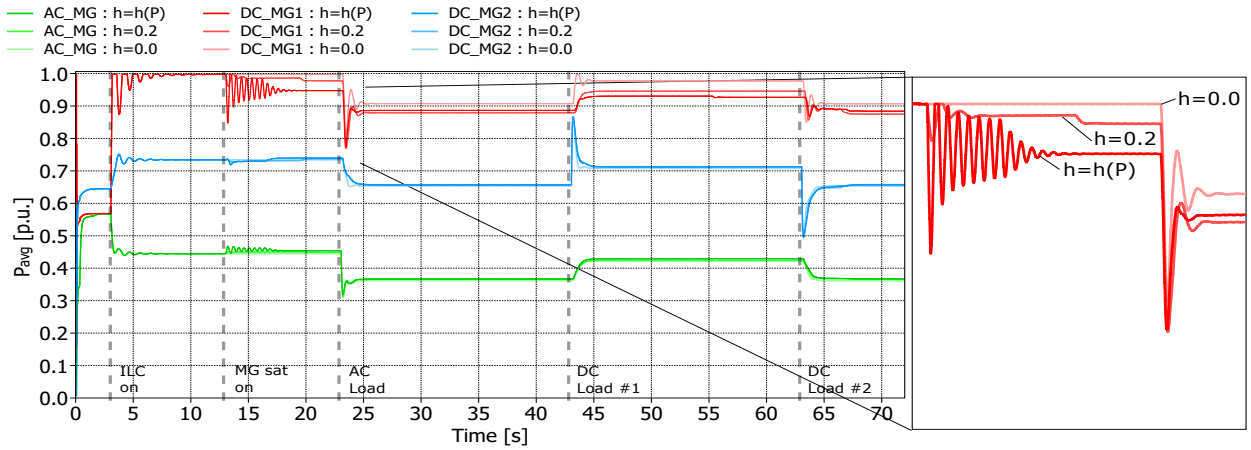

(c)

Figure 5.9: Simulation results for Case 2. (a) Average IC of MGs. (b) Absolute power of ILCs. (c) Average power of MGs.

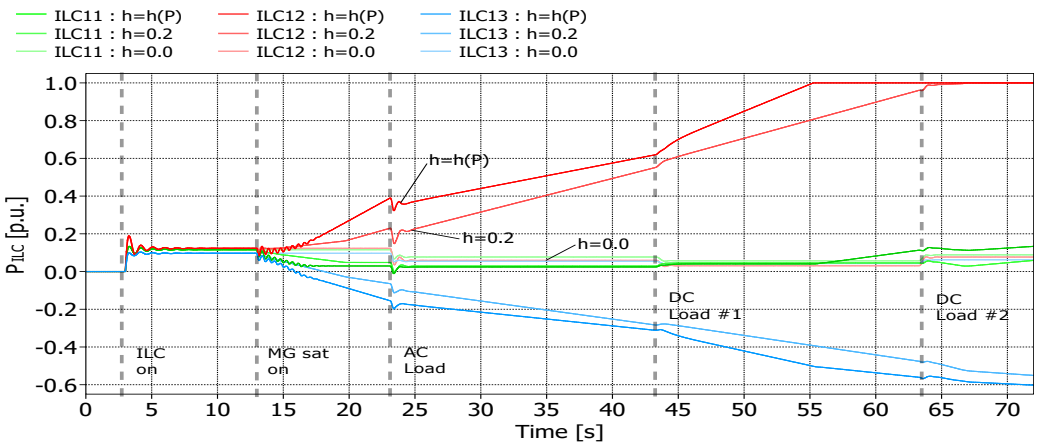

Figure 5.10: Power of ILCs in Cluster #1 during simulation of Case 2.

Case 3.a. Economic dispatch with ILC power-sharing and load impacts

Fig. 5.11 shows the performance of the ILC power balancing in the multi-MG. In Fig. 5.11a, the ICs of the MGs in the system synchronised in the steady-state. The transient state behaviour of ICs slightly changes compared with Fig. 5.6a; the same overshoot and settling time are observed.

The absolute power of ILCs is represented in Fig. 5.11b. It can be seen that the ILCs of each cluster equalise their per unit powers after t=5.5[s], where the ILC power-sharing is activated. It is worth noting that, although there is saturation in Cluster #3, the other ILC clusters behave as expected sharing the power between their ILCs.

No difference is perceived between the curves of average power in Fig. 5.6c and Fig. 5.11c. So it is confirmed that the ILC power-sharing could be executed with a similar bandwidth to the economic dispatch without affecting its performance.

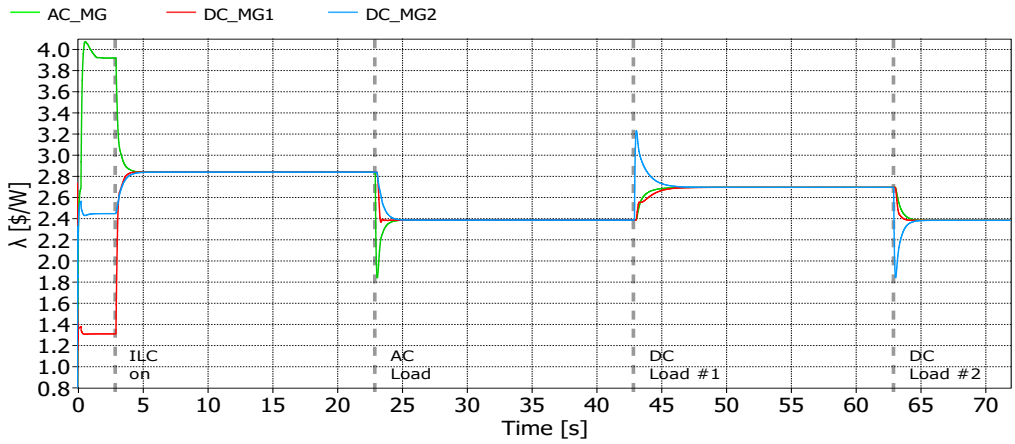

(a)

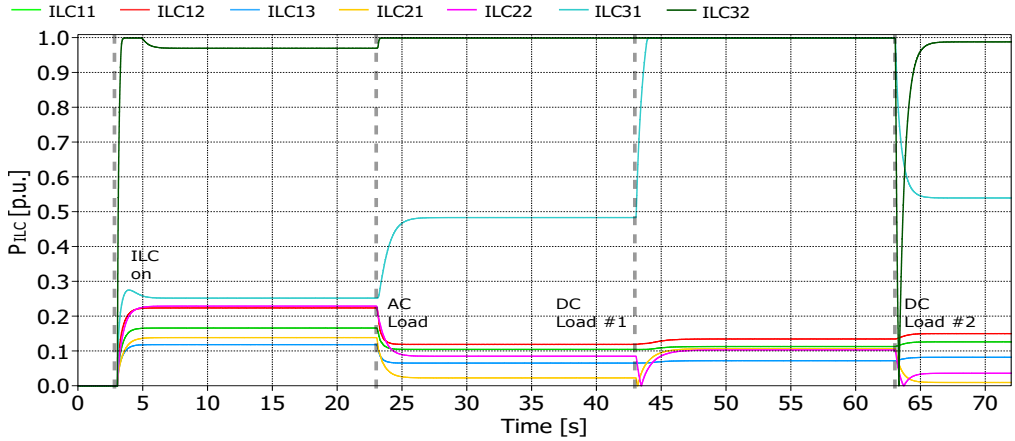

(b)

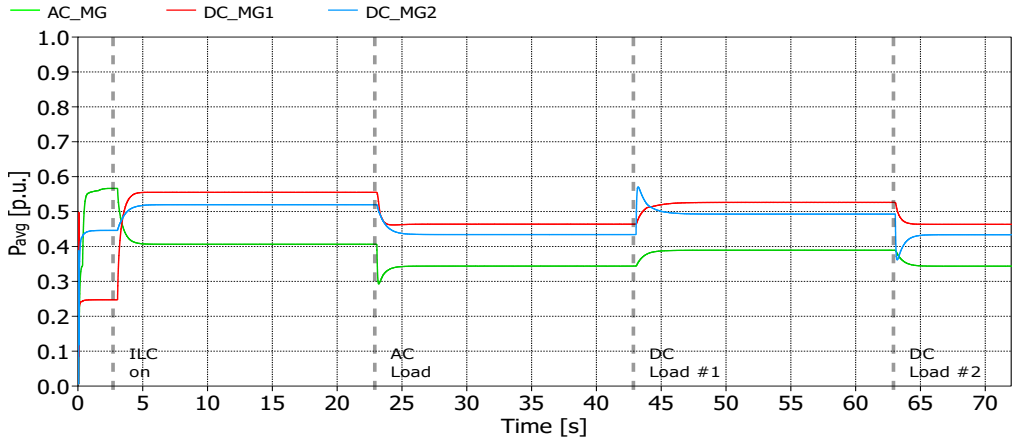

(c)

Figure 5.11: Simulation results for Case 3.a. (a) Average IC of MGs. (b) Absolute power of ILCs. (c) Average power of MGs.

Case 3.b. Economic dispatch with MG saturation constraint, ILC power-sharing and load impacts

Fig. 5.12 and Fig. 5.13 show the performance of the ILC power balancing in the multi-MG with the saturation of DC MG #1. From Fig. 5.12a, it can be seen the same performance for the average ICs compared with Fig. 5.9a with the adjustable h_m coefficient. In general, the ILC power-sharing does not reflect changes in the IC consensus nor the net power flow between MGs. Since its application in t=3[s], there are no visible changes in this case of study.

Based on the response of Fig. 5.9b of Case 2, a different scenario is seen in Fig. 5.12b. The ILC powers are now synchronised after the activation of the ILC power-sharing, at t=3[s], and the consensus values for the ILC clusters are reached (instead of the steady-state values seen in Fig. 5.9b).

The case of the ILC Cluster #1 with the ILC power balancing is depicted in detail in Fig. 5.13. Here, the increasing behaviour of ILC #12 and ILC #13 seen in Case 2 is non-existing. Therefore, the ILC power-sharing aids in solving the problem of saturation of ILCs when there is a saturation of one of the side MGs and the controller of (5.14) is activated.

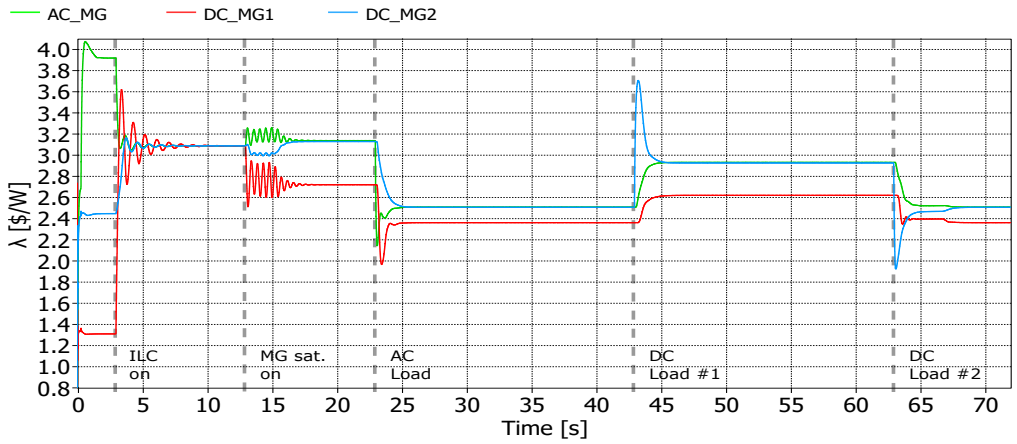

(a)

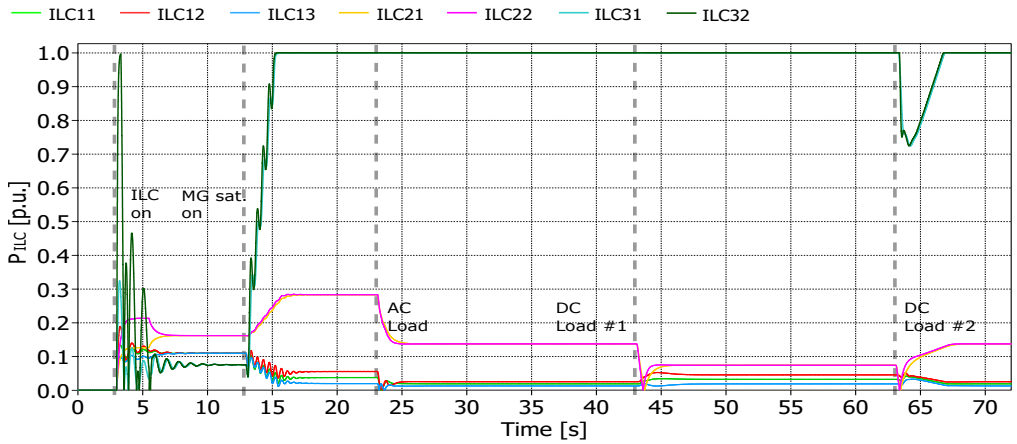

(b)

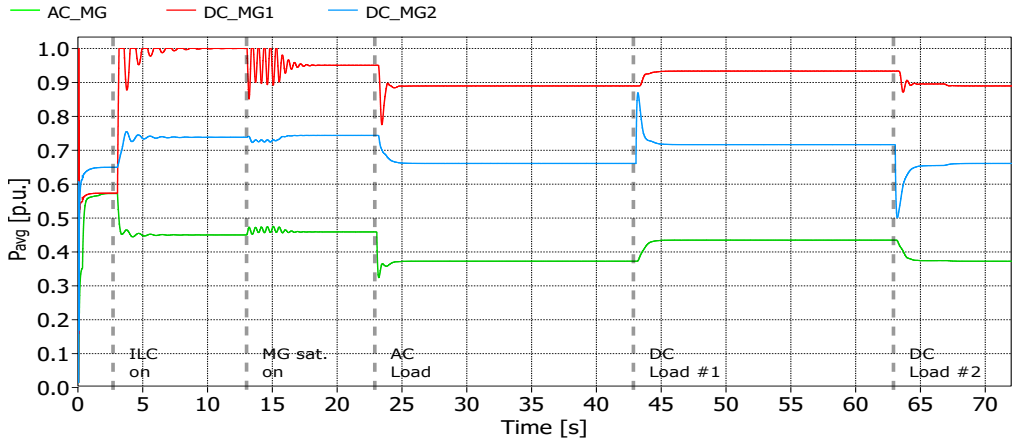

(c)

Figure 5.12: Simulation results for Case 3.b. (a) Average IC of MGs. (b) Absolute power of ILCs. (c) Average power of MGs.

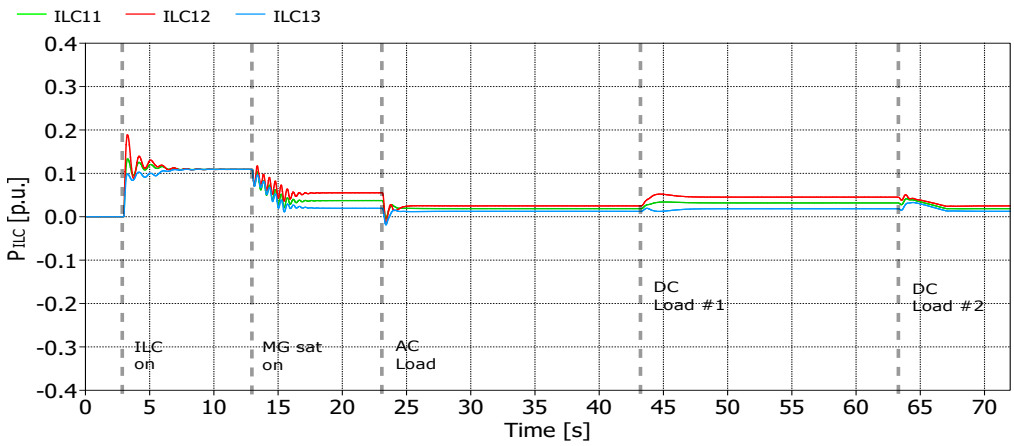

Figure 5.13: Power of ILCs in Cluster #1. during simulation of Case 3.b.

Case 3.c. Economic dispatch with MG saturation constraint, ILC power-sharing and communication losses

The charts in Fig. 5.14 show the results of a communication failure in a communication link between ILCs. In Fig. 5.14a, Fig. 5.14b and Fig. 5.14c, the same trends of Case 3.b. are visualised. Negligible changes can be perceived in the transient states of the power curves of Fig. 5.14b when compared with Fig. 5.12b; particularly, the changes can be seen in the ILCs of Cluster #1, the one where the communication link failure occurred. It can be confirmed that as long as a spanning tree exists in the communication network, the consensus is reached.

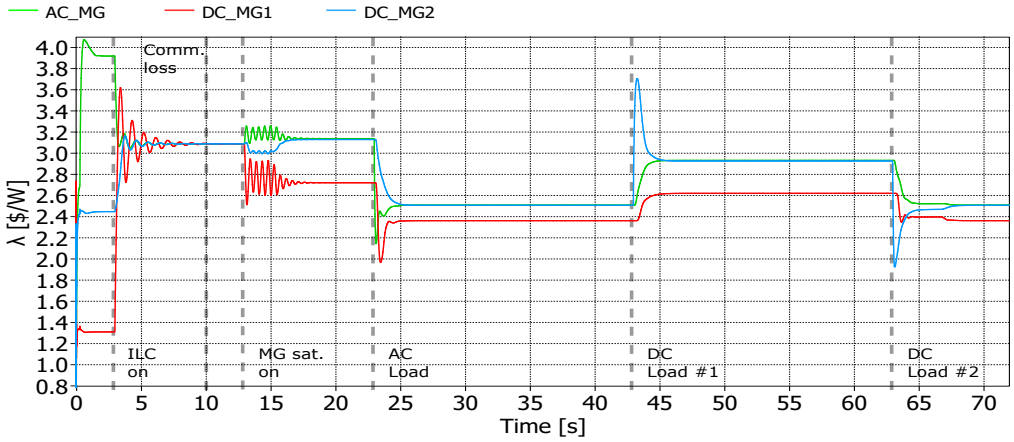

(a)

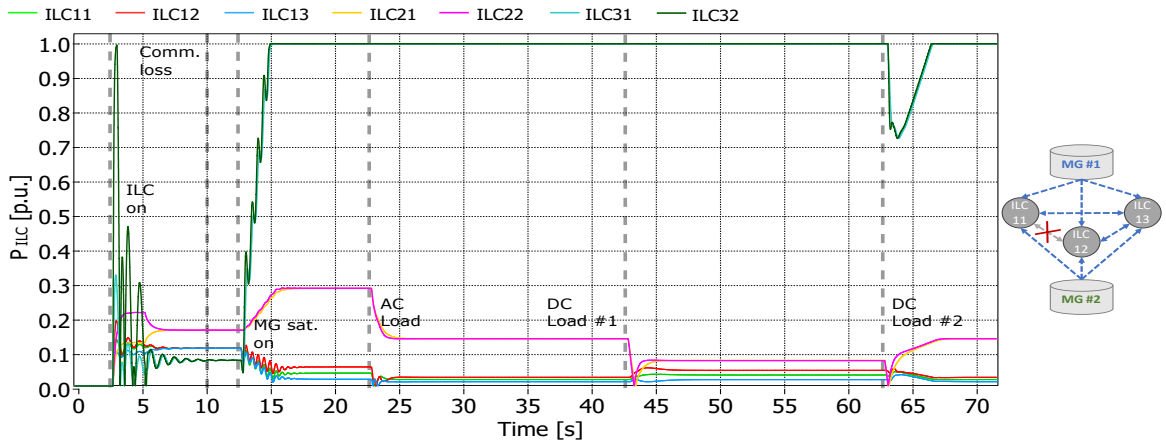

(b)

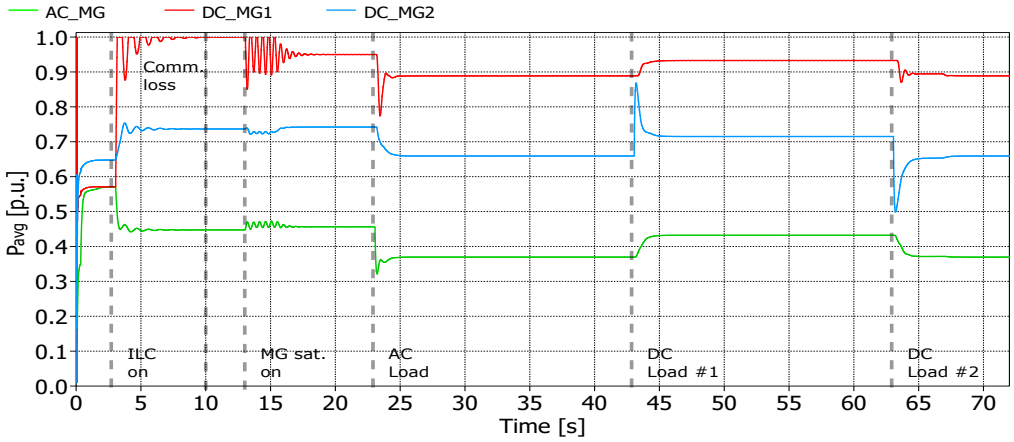

(c)

Figure 5.14: Simulation results for Case 3.c. (a) Average IC of MGs. (b) Absolute power of ILCs. (c) Average power of MGs.

Case 3.d. Economic dispatch with MG saturation constraint, ILC power-sharing and communication time delays

Simulation results using time delays in the ILC power-sharing are shown in Fig. 5.15. Overall, Fig. 5.15a, Fig. 5.15b and Fig. 5.15c expose a high level of transient and steady-state oscillations when the time delay rises close to 250 [ms]. This situation can be explained due to the initial tuning for getting a decoupling between ILC's IC consensus algorithm and ILC's power-sharing. The ILC power-sharing loop was designed to be fast, however, this fact makes the ILC stability vulnerable to time delays, especially because of the use of the distributed observer for power (which requires a fast dynamic in general).

Figure 5.15a shows initial differences in the IC consensus between MGs after each load impact; moreover, these differences are proportional to the time delay applied. This condition repeats what was seen in Chapter 4, where time delays applied to the distributed power observer create steady-state errors, which are resolved once the proposed anti-windup algorithm executes a reset. Particularly, in this case of study, the errors originated from time delays in the distributed power observer (used for ILC power-sharing) and subsequently are reflected in the IC consensus. An exception to this trend is seen at the short transient of t=13 [s], where the case with 125 [ms] seems to have a better transient state once the MG saturation control is activated. This can be explained by the errors originated by the distributed observer, which intervene and slow the control bandwidth of the IC consensus (producing a suitable amount of damping).

Despite an apparent consensus between mean steady-state values of IC being reached on every occasion, there are persistent oscillations in the steady-state for the delay of 250 [ms]. In the case with a delay of 125 [ms], the steady-state oscillations in IC are almost negligible, except for the DC MG #1. The information that can be extracted from the ICs is similar to the curves of the average power of MGs. Fig. 5.15c shows how the mean values of average power get stabilised in the steady state but with oscillations of amplitude proportional to the time delays.

The absolute powers of ILCs, shown in Fig. 5.15b, depicted with more detail the oscillatory tendency described in Fig. 5.15a. An extreme oscillatory behaviour is perceived in Cluster #3, where the time delay of 250 [ms] causes the biggest oscillation amplitude in ILC #32, followed by ILC #31. The case of the time delay of 125 [ms] presents a significant steady-state deviation compared to the base case of τ=0 [ms]. This steady-state deviation is proportional, giving roughly half of the steady-state deviation observed for the mean values of the ILC powers when compared with the case of τ=250 [ms].

Another set of charts with simulation results but with a reduction by half in the proportional gain c_C of ILC #31 and #32 is presented in Fig. 5.16. The new charts keep the curves for the τ=0[ms] and τ=125[ms] cases but update the case of τ=250[ms] with the new proportional gains. Overall, a great oscillation can still be seen during $13 < t < 23$, where the MG saturation constraint interfered with the ILC economic dispatch. The case with time delay τ=250[ms] is the only one in which the oscillations persist during this period of saturation

time. The other cases with τ=125[ms] and τ=0[ms] behave according to Case 3.a., i.e., only transient state oscillations exist. The reason for this persistency in steady-state oscillations for τ=125[ms] is attributed to couplings between economic dispatch, MG saturation and ILC power-sharing control actions. Despite the results shown, decoupling can be obtained by reducing the control bandwidth of the control loops, e.g., by reducing some of the coupling gains c_L, c_P and c_C.

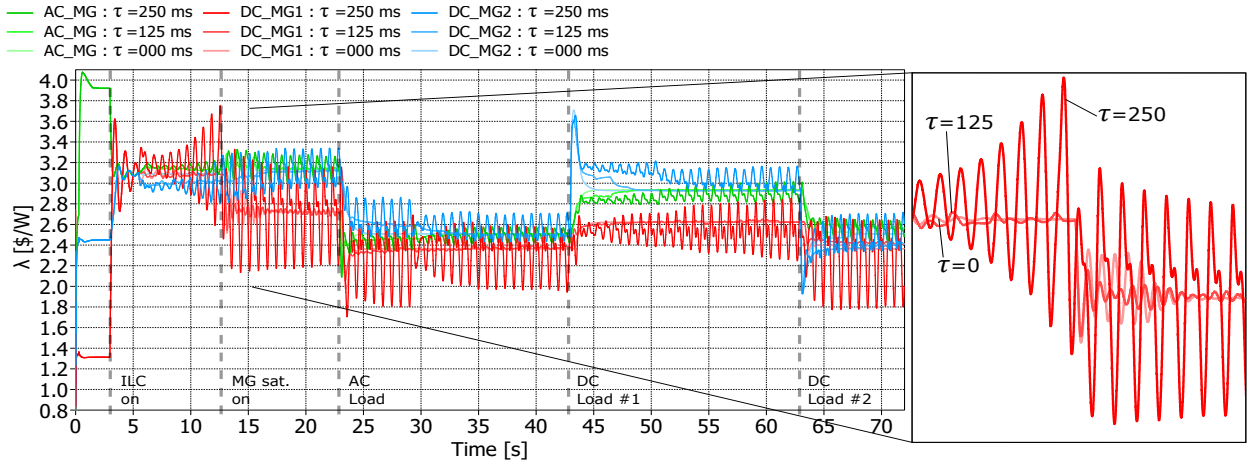

(a)

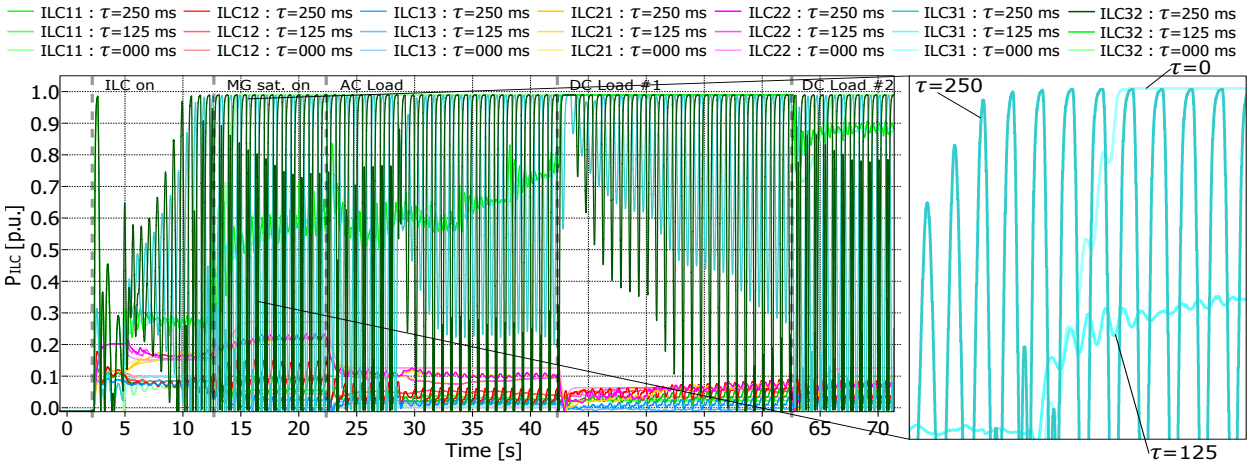

(b)

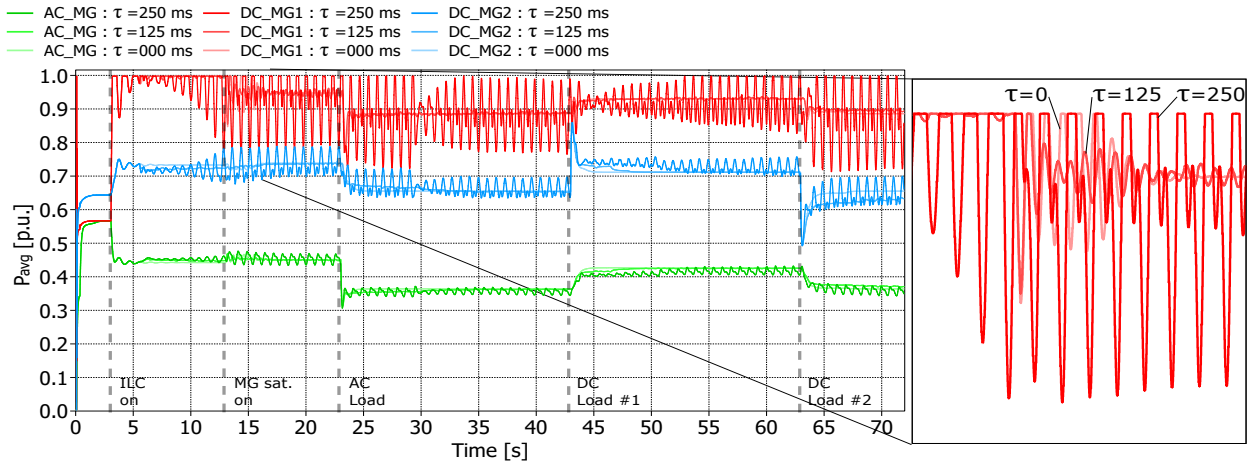

(c)

Figure 5.15: Simulation results for Case 3.d. (a) Average IC of MGs. (b) Absolute power of ILCs. (c) Average power of MGs.

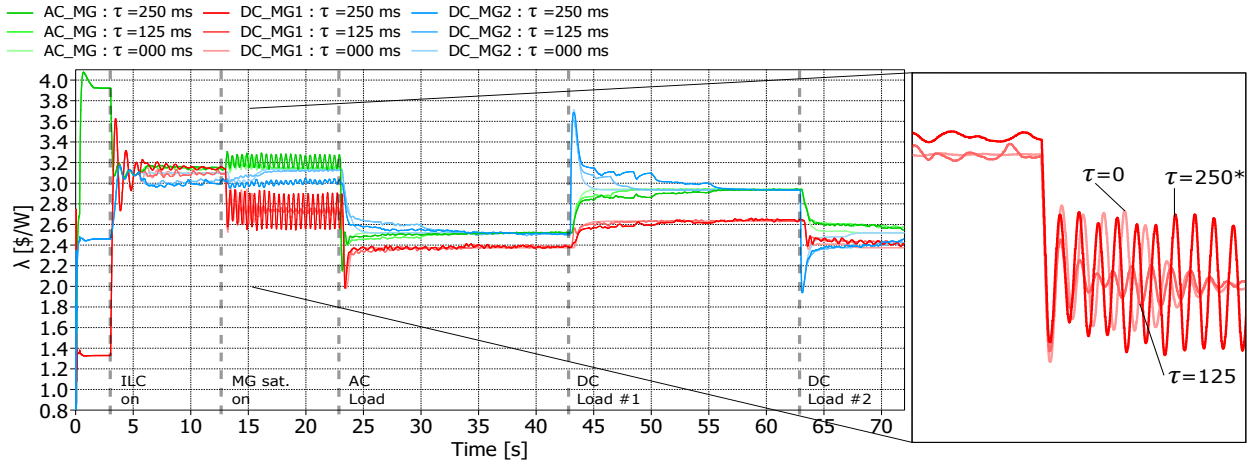

(a)

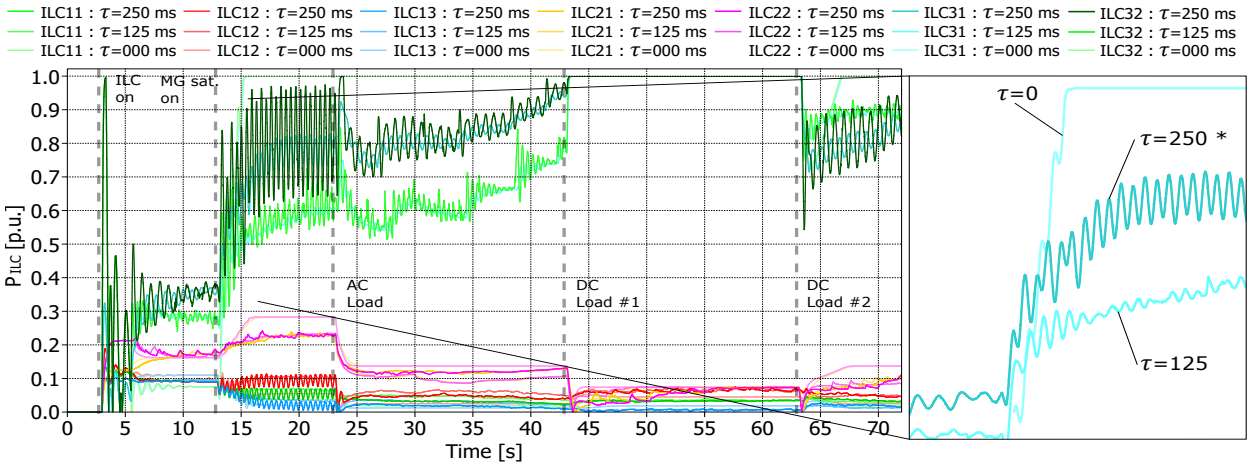

(b)

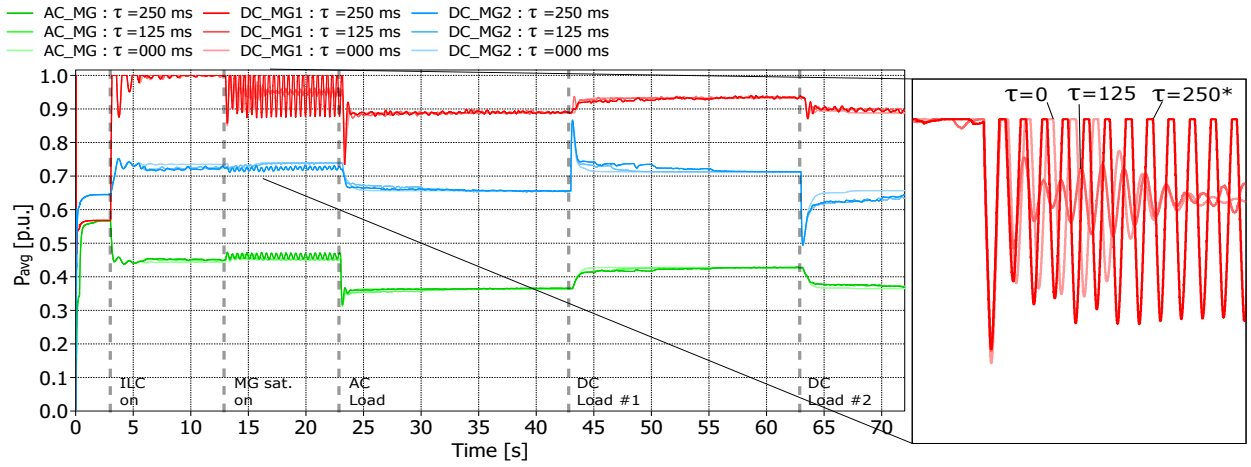

(c)

Figure 5.16: Simulation results for Case 3.d. when c_C is reduced by half in Cluster #3. (a) Average IC of MGs. (b) Absolute power of ILCs. (c) Average power of MGs.

Case 4.a. Economic dispatch with MG saturation constraint, ILC power-sharing and ILC saturation constraint

Results for the ILC cluster balancing algorithm are shown in Fig. 5.17. Overall, it can be seen oscillations when the balancing of ILC clusters is activated, at t=56 [s]. However, such transient oscillations are damped quickly by the control strategy; they do not appear again even after load changes as the one in t=63[s]. On the one hand, the effects of the ILC cluster power-sharing inside the ILC power-sharing are negligible. Whatever condition of Γ, the ILCs of the same cluster did not deteriorate their power-sharing. On the other hand, ILC cluster balancing does have a small effect on the total average power of the MGs, which inevitably deteriorates the IC synchronisation visibly.

The ICs are shown in Fig. 5.17a. After the transient oscillations got stabilised (before t=63[s]), ICs reached different steady-state values compared with Fig. 5.12a of Case 3.b., with differences near 10% depending on the Γ value. It is observed after the reset of the anti-windup (t=68[s]) that Γ=$\Gamma(P)$ obtained ICs values more similar to the condition in which the consensus between clusters is not applied (Γ=0). For the case Γ=0.5, the anti-windup's reset did not have the same effect correcting the steady-state value.

The ILC powers are shown in Fig. 5.17a. It can be seen that after the activation of the ILC cluster balancing, at t=56[s], the ILC powers get closer. In the steady-state, the results show that, in general, the ILC clusters get closer to each other the more weight the Γ coefficient gets. The biggest differences are shown in ILC #31 and ILC #32, which are part of the saturated ILC cluster.

There are transient oscillations in the average powers of Fig. 5.17c, which increased in relation to the Γ parameter. The DC MG #1 case presents the biggest oscillations, especially when $\Gamma = 0.5$. As for the steady-state values, small changes are perceived. The most significant differences appear for the DC MG #2, especially after the anti-windup reset of t=68[s].

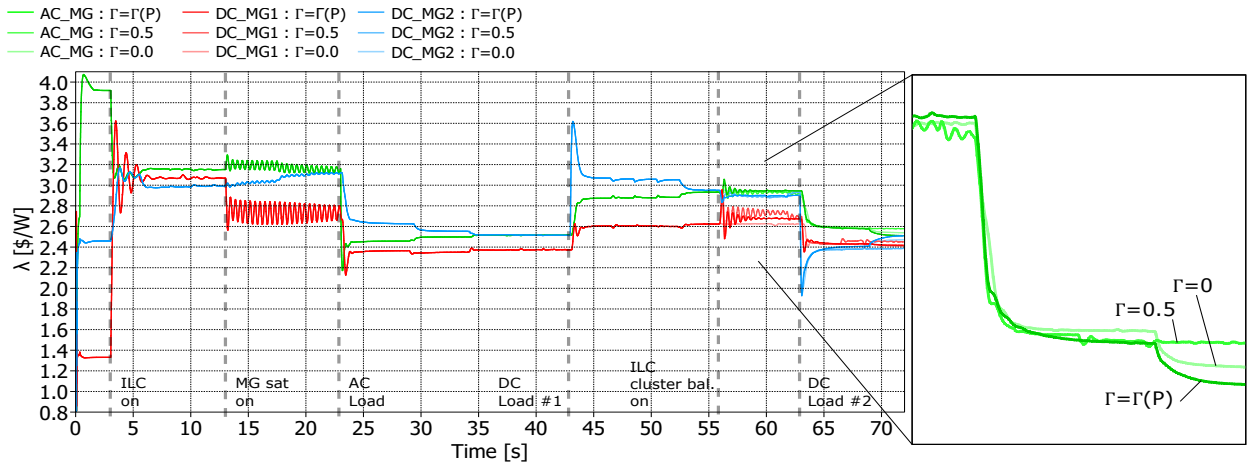

(a)

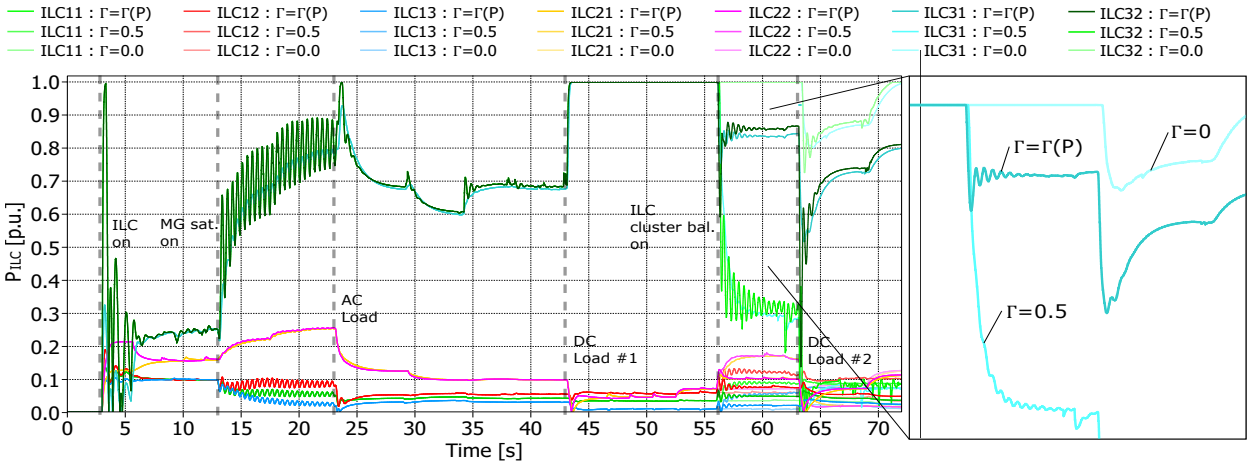

(b)

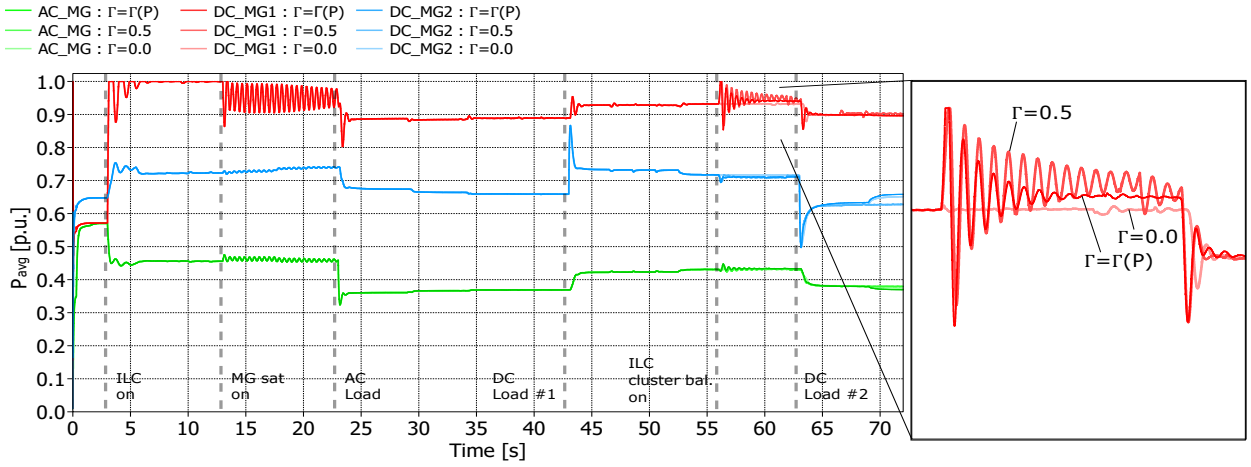

(c)

Figure 5.17: Simulation results for Case 4.a. (a) Average IC of MGs. (b) Absolute power of ILCs. (c) Average power of MGs.

Case 4.b. Economic dispatch with MG saturation constraint, ILC power-sharing, ILC saturation constraint and communication losses

The results for a complete loss of communications between the ILCs of the clusters #1 and #2 are shown in Fig. 5.18. The observed transient state and steady-state behaviours of the curves of average ICs (Fig. 5.18a), absolute power of ILCs (Fig. 5.18b), and average power of MGs (Fig. 5.18c) present no changes concerning the results of Case 4.a. with $\Gamma = \Gamma(P)$. This behaviour is expected since the communication system still has a spanning tree. In this case, the communication flows between ILC #1 and ILC #3, and consequently from ILC #3 to ILC #2 and vice-versa. Also, the relatively slow convergence time of the ILC cluster consensus concerning the ILC power-sharing consensus aid in reducing any transient state overshoot when there are changes in the communication system (like communication link failures).

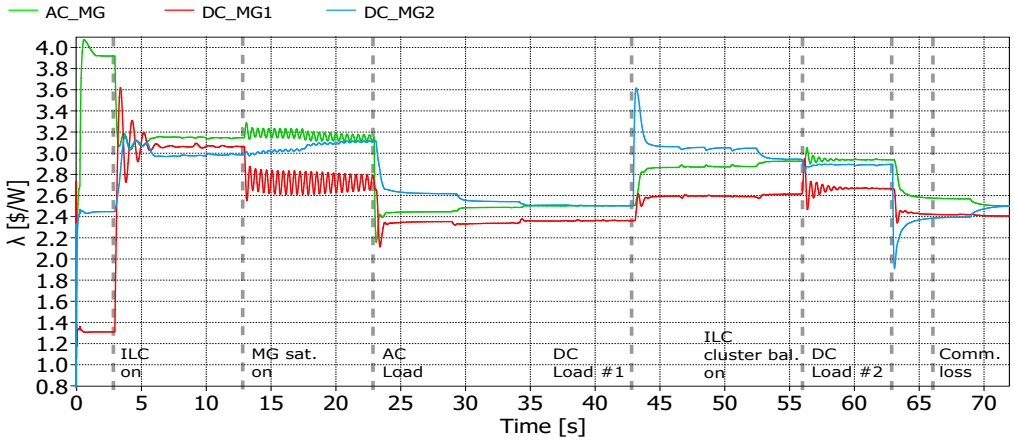

(a)

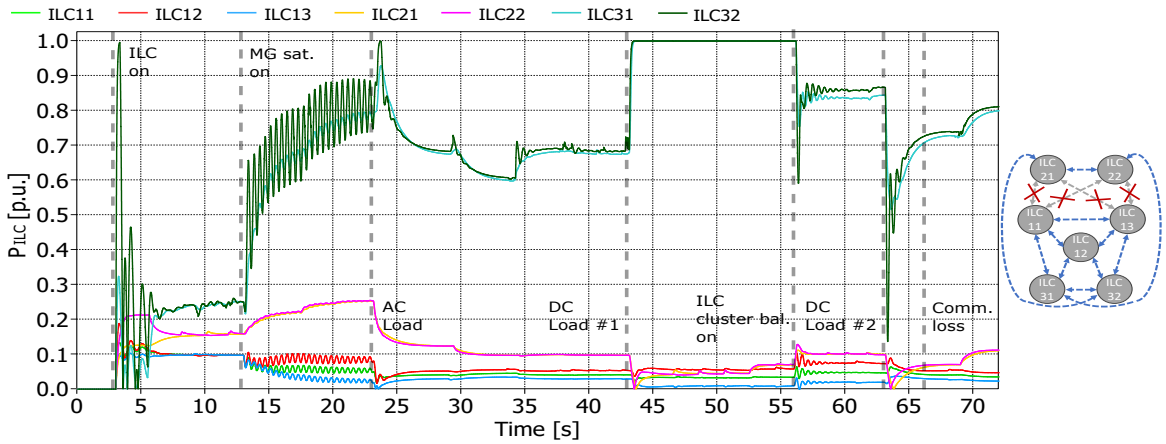

(b)

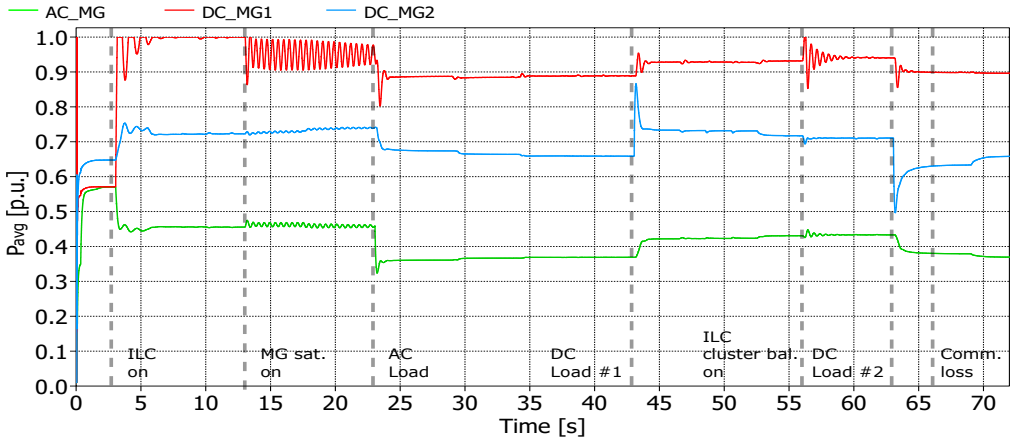

(c)

Figure 5.18: Simulation results for Case 4.b. (a) Average IC of MGs. (b) Absolute power of ILCs. (c) Average power of MGs.

Case 4.c. Economic dispatch with MG saturation constraint, ILC power-sharing, ILC saturation constraint and communication time delays

The results of the tests with time delays are shown in Fig. 5.19. In Fig. 5.19a, the average ICs present small changes during the transient states. It can be seen an increase in overshoots proportional to the time delay magnitude. At the end of the simulation, it could be seen that the case with τ=250[ms] did not get the correction caused by the anti-windup in time, as opposed to the cases τ=125[ms] and τ=0[ms]. Similar behaviour is seen for the graphs of the absolute power of ILCs, in Fig. 5.19b, and average power of MGs, in Fig. 5.19c.

Despite the similarities in the sensibility to time delays of the distributed power observers of (5.13) and (5.14), the cluster balancing can afford to face higher delays than the ILC power-sharing (see Fig. 5.15). This can be explained by the fact that the ILC cluster control has a lower control bandwidth and that the communication between ILC clusters is more robust; it does not matter which ILC shares the information since all of them transmit essentially the same ILC average power.

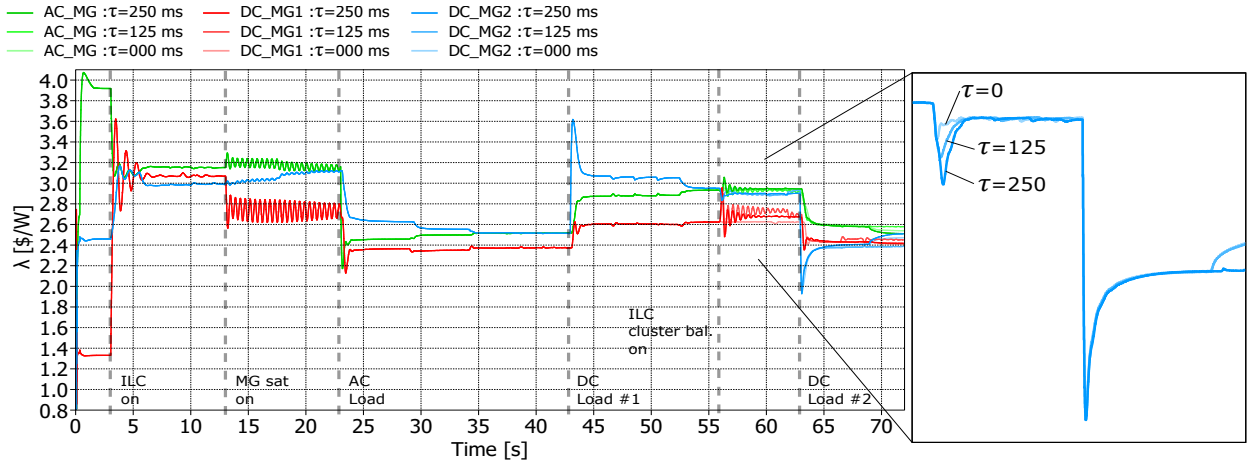

(a)

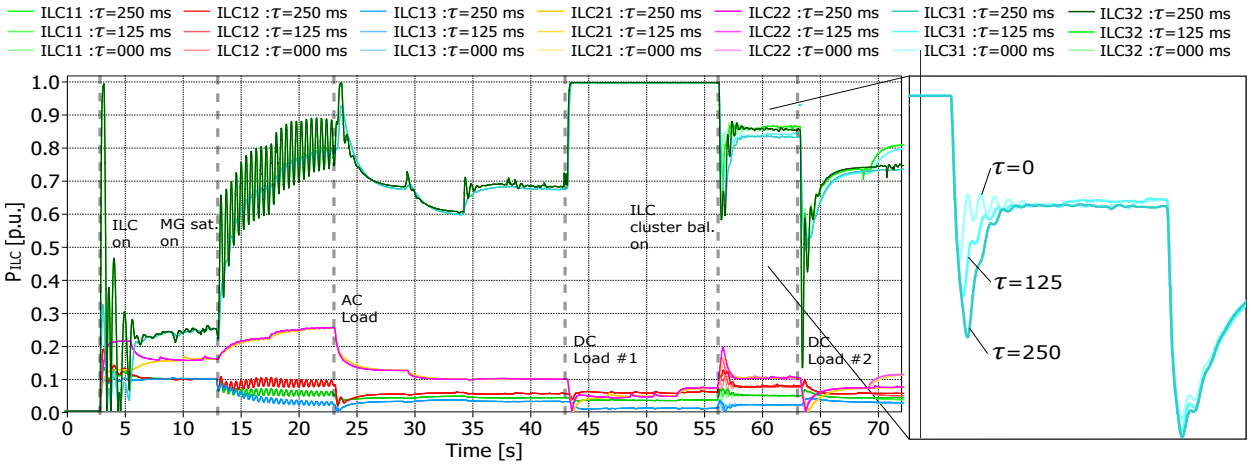

(b)

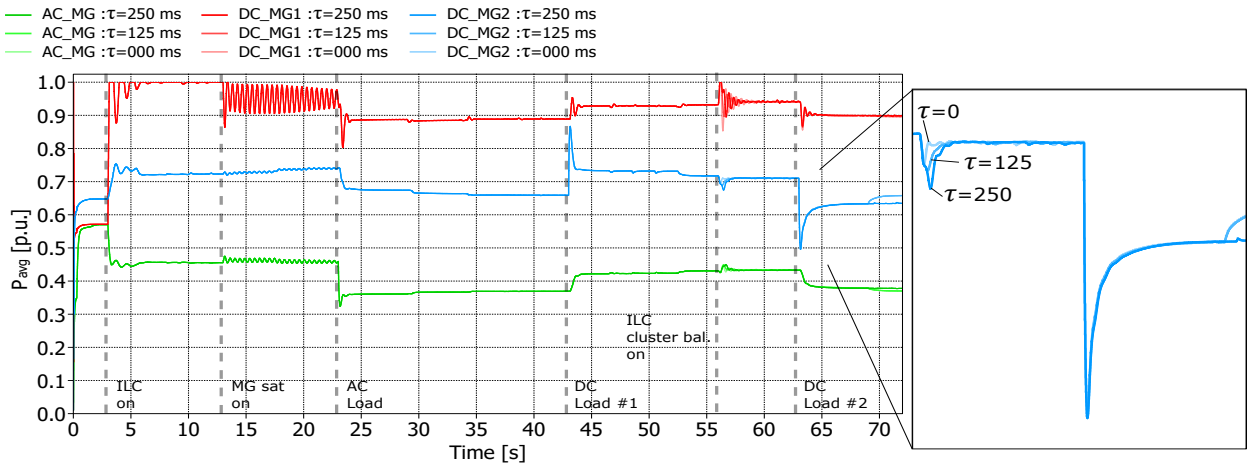

(c)

Figure 5.19: Simulation results for Case 4.c. (a) Average IC of MGs. (b) Absolute power of ILCs. (c) Average power of MGs.

5.6 Discussion

This chapter successfully described a formulation for the economic dispatch in a meshed AC/DC multi-MG with additional objectives. The formulation considered the power constraints of DGs, ILCs, MGs and clusters of ILCs, which fulfilled any critical condition that the multi-MG could face. The key factors for properly operating the proposed controller are the communication network and activation functions (h and Γ parameters).

With this approach, the economic dispatch is feasible to obtain in a robust way since there are multiple DGs located near the ILC that could bring the information of IC. Also, the ILCs do not require communication between them at all for the economic dispatch objective. Both aspects are advantages in real-world applications since they reduce the length of communication lines. Under time delays, the economic dispatch performs seamlessly with small overshoot increases.

For the ILC power-sharing, it was shown that this control objective requires a communication network with a spanning tree to work. This control objective can be executed simultaneously without altering the dynamics of the economic dispatch, MG saturation loop and the ILC cluster balancing. However, under time delays, the power observer of the ILC power-sharing introduces steady-state delays, which can be dealt with a sophisticated strategy, like the proposed anti-windup of Chapter 4, but at the cost of having to chatter in the power waveforms.

The novel proposed ILC cluster power constraint (through balancing the ILC clusters) was verified in simulations. This control goal is feasible to implement along with the IC synchronisation and the MG power balancing despite its opposition to their control actions to some degree. As mentioned in the previous paragraph, an essential element for the implementation is an adequately designed weighting factor. If this factor is constant, it always compromises the IC synchronisation; therefore, the weighting factor, Γ, must be adaptive to the system conditions to be efficient. The determination of the real utility of the ILC cluster balancing described in this chapter is still under development since there must be additional considerations in the multi-MG system to assess the advantages of giving power reserves to the ILC clusters. Among those considerations are the distribution line congestion and power quality compensations, which certainly could give directives to evaluate the performance and advantages of the control strategy. In this sense, the work of this chapter opens new lines of research concerning utilising ILCs for distributed global control goals determined by the DNO.

A final step in the discussion about the proposed control scheme is to compare. To compare the proposed control scheme against other approaches of the literature, a summary table is constructed regarding features and costs. Among the features used for the comparison are the communication topology, use of the constraints of the maximum power capacity of MGs and clusters of ILCs (all three parameters are also related to a proposed reliability feature). Regarding the costs, short-term and long-term cost components are displayed to

better understand the benefits and drawbacks of each solution.

The reason for choosing short-term and long-term costs is that the proposed strategy in this thesis promotes the deviation of ICs under certain overload/saturation conditions; the latter leads to more costs in the short term (during the overloading condition or failure), but it is sensible when replacement and unscheduled shutdowns costs are taken into account. The proposed multi-objective control safeguards critical infrastructures of the grid, such as power converters, transformers and distribution lines, which are prone to accelerate their ageing or even fail due to overloading (increase in temperature) [20, 183, 184].

The amount of savings due to the reduction in the ageing of infrastructure depends on usage, quality of materials and construction techniques. A similar uncertainty is seen regarding savings in system shutdowns due to failures. Because of this, referential symbol marks are used to demonstrate approximated differences in costs, distinguishing between short-term and long-term potential savings.

A close comparison can be made between the saturation constraint implementation proposed in this thesis and other works in the literature that use optimisers. Optimisation approaches could include penalty terms in the objective function to improve efficiency and/or avoid unsafe operation (which could be analogous to the solution proposed in this work). Unfortunately, not many works define penalties specifically for the saturation of MGs (as a whole). Also, it is worth noting a point of contrast with optimiser methods: the computation time and effort required. As demonstrated in previous chapters, the proposed distributed solution with adjustable weighting solves the economic dispatch problem seamlessly in the time/scale of secondary control whereas optimisers rely on iterative algorithms, like PSO or GA, to find the optimal after several times the secondary control timescale.

Ref.	MG type	ILC type	Comm.	Control goal	Control tech.	MG sat. const.	Cluster sat. const.	Comp. cost	ST Oper. costs	LT Oper. costs	Reliab.
[42, 182]	MM	none	centr.	ED	OPT	×	×	$ $ $	$	$ $ $	low
[43]	MM	none	centr.	ED	OPT	✓	×	$ $ $	$	$ $	low
[18]	SHM	SI	distr.	PS	ASC	×	×	$	$ $ $	$ $ $	high
[29, 30]	SHM	CI	distr.	PS	ASC	×	×	$	$ $ $	$ $ $	high
[49]	SHM	SI	mixed	ED	mixed	×	×	$ $	$ $	$ $ $	mid
[14]	SHM	SI	distr.	ED	ASC	×	×	$	$	$ $ $	high
[2]	SHM	SI	distr.	ED	FTC	✓	×	$	$ $	$	high
[4, 176], [185–187]	SHM	CI	distr.	ED	ASC	×	×	$	$	$ $ $	high
[188]	SHM	CI	distr.	ED	ASC	×	✓	$ $	$	$ $	high
[189]	SHM	SI	distr.	ED	mixed	×	×	$ $	$	$ $ $	mid
[190]	SHM	CI	distr.	ED	mixed	×	×	$ $	$	$ $ $	mid
[47]	HMM	SI	centr.	ED	OPT	✓	×	$ $ $	$	$ $	low
[24]	HMM	CI	distr.	PS	ASC	×	×	$	$ $ $	$ $ $	mid
[13, 191]	HMM	SI	distr.	ED	ASC	×	×	$	$	$ $ $	high
Chapter's proposal	HMM	CI	distr.	ED	FTC	✓	✓	$	$ $	$	high

* MM: AC multi-MG, SHM: Single hybrid AC/DC MG, HMM: Hybrid AC/DC multi-MG, SI: Single ILC, CI: Cluster of ILCs, PS: Power-sharing, ED: Economic dispatch, OPT: Optimisation, ASC: Asymptotic Consensus, FTC: Finite-Time Consensus, ST:Short-term, LT:Long-term.

Table 5.1: Comparison summary of the proposed method concerning works in the literature with multiple MGs.

Chapter 6

Conclusions, Recommendations and Future Work

The coordination of power flows in AC/DC MGs has been a challenging problem to solve by local generators and/or DNOs due to the fact that there are many conditions (constraints) to consider in order to get an optimal and safe operation. Motivated by this, this thesis helped AC/DC MGs with one and multiple ILCs, as well as AC/DC meshed multi-MGs, to get an economic dispatch under complex scenarios of power constraints. To this end, the thesis proposed hypotheses related to developing distributed control strategies on ILCs, which account for adjustable weight parameters (activation functions) and convergence improvements. When the elements of the hypotheses are combined, a distributed controller for the ILCs emerges, which looks for the economic dispatch decision-making while facing decouplings and other disturbances coming from other control loops and unmodelled dynamics.

The thesis, through its chapters, demonstrates using mathematical developments and simulations the feasibility of distributed control strategies with multiple goals applied to the ILCs of AC/DC MGs. This was tested for different topology configurations of AC/DC MGs, which cumulatively increase in complexity until the end of the thesis. In the following, there will be a listing summary of the thesis chapters and their contribution to answering the research questions imposed by the hypotheses and specific objectives.

- Chapter 2 conducted a literature review which settled the ground to understand the current developments and elements that intervene in the control and operation of MGs. Special emphasis was given to distributed control using consensus and finite-time algorithms. On its own, Chapter 2 completed Objective #i.

- It was seen from Chapter 2 that most of the literature efforts in AC/DC MGs were put in decentralised strategies relying on local droop deviations of the ILCs. Such strategies, in

general, do not take into account the dynamics of secondary control. For the economic dispatch, there are significant limitations regarding the local IC estimations that those approaches require ILCs to do; mainly, the local IC estimations are not accurate in topologies that do not use a common single bus for the interconnection of DGs and loads.

- Chapter 3 formulated the economic dispatch problem for hybrid AC/DC MGs. Then, definitions were provided to model the system and the communication network. In this case, the network was described as a combination of graphs which can operate independently. This formulation and definitions for distributed communications were essential in developing the following chapters and proving Hypothesis #i and Hypothesis #v.

- Chapter 3 also showed the design of a controller for the ILC, which sought economic dispatch and included a finite-time structure. The finite-time parameters helped to implement the economic dispatch of the ILC in the same control bandwidth as the IC consensus of DGs. Also, the finite-time structure provided robustness against disturbances, like coupling with other control loops and other unmodelled dynamics. Experimental work brought evidence of the feasibility of the ILC controller. It could be validated as an adequate operation even in the presence of time delays, which was essential for Hypothesis #i.

- Another key component developed in Chapter 3 was the MG saturation constraint. The formulation of the economic dispatch problem considering MG saturation constraints was proposed as a combined objective function with a weighting parameter to regulate the trade-off between IC consensus (economic dispatch) and MG saturation avoidance. The proposed objective function dealt with the MG saturation by balancing the average powers of MGs, which normally oppose to the IC consensus. The definition of the trade-off weighting parameter is crucial to determine the operation of the AC/DC MG. Despite that constant values could be used, during simulations, adjustable values were seen to best solve trade-offs. The combined results of this chapter allow us to prove Hypothesis #i, complete Objectives #ii and #v, and advance in the remaining hypotheses and objectives.

- Chapter 4 enlarged the formulation of the economic dispatch problem to the case of multiple ILCs for developing the Objectives #iii and #iv. Two main formulations were given: a standard implementation with an equality constraint for power-sharing between ILCs and a novel implementation with the power-sharing implemented through average powers in a new control goal inside the objective function (similar to the developments of Chapter 3, the objective function was proposed based on regularisation). In both formulations, there were included and discussed conditions for power saturation of ILCs. Also, for a generalisation of the optimisation problem, the case with fixed power commands into some of the ILCs and their stationary optimality condition were described.

- Chapter 4 also described the communication network modelling. Conversely to Chapter 3, communication links between ILCs needed to be added in order to perform the control actions proposed in the formulation. The distributed controllers that emerged from the formulation and the communication network were both conventional consensus and dynamic average consensus. Both controllers contribute to the advancement of Objective #iii and Hypothesis #ii. The dynamic average consensus was proposed as an alternative to the conventional consensus because it has the same steady-state behaviour, but it also provides an alternative method to estimate the total power of the ILC cluster and estimate the measured local power. This could be beneficial for implementing further and complex distributed control strategies with robustness features. The demonstration of the full extent of benefits of the dynamic average consensus is out of the scope of this thesis; however, a practical example was included in Chapter 3. Specifically, fixed power references were included in some of the ILCs. Such a condition overwhelmed the capabilities of the conventional consensus, whereas the proposal with the dynamic average consensus performed seamlessly, as was shown in the simulation results.

- Another feature of Chapter 4 is the proposal of a distributed anti-windup with a reset scheme, which is a crucial element to allow the deployment of the dynamic average consensus for ILC power-sharing when there is communication latency. Accordingly, Hypothesis #ii can be reinforced with the addition of this anti-windup since the condition of fixed power references in some of the ILCs (which hindered the conventional consensus) is suggested as a probable and realistic scenario in future grids which may interact with external agents, like a DNO.

- Chapter 5 combined features of Chapters 3 and 5 to formulate a multi-objective economic dispatch problem. This formulation, along with the communication network description and controller design, represents Hypothesis #i and Hypothesis #iii thoroughly. The named hypotheses were later validated in the chapter through the simulation of case studies. The effectiveness of the proposed controllers was observed, and comparisons were made when necessary.

- In Chapter 5, to demonstrate Hypothesis #iii and fulfil with Objective #iii, a controller that performs an ILC cluster balancing was derived from a regularisation of the economic dispatch objective function. To implement the controller, a weighting parameter was proposed, similar to Chapter 3. The proposed ILC cluster balancing performed as expected, with steady-state value variations depending on the weighting parameter's magnitude. Simulations have shown a higher resilience to time delays than the MG saturation control loop.

In each chapter, simulations were developed that, in sum, complete Objective #iv.

6.1 Limitations

During the realisation of this PhD thesis, some aspects could not be further studied due to time limitations, mainly caused by the COVID 2019 pandemic that desolated the world for a year and a half. Some of these pending aspects include a complete small-signal modelling of the multi-MG system and a distributed observer that takes advantage of the dynamic average consensus to increase robustness in communications. Also, there were limitations in the availability of hardware for the experimental validation of the strategies applied in the meshed AC/DC multi-MG with clusters of ILCs, mainly due to the number of DGs, ILCs and their communication network.

Limitations regarding using some of the features proposed in this thesis are summarised as follows.

- The economic dispatch by ILCs relies on communications, and the complete loss of communications with one subgrid deactivates the ILC's output for stability purposes. Also, large time delays in communications may induce significant transient state distortions (like overshoots) inherent in any distributed controller. The magnitude of the distortions depends mainly on the size of the delay and the control/coupling gain.

- The proposed power balancing between ILCs in a cluster and between clusters is sensible to time delays. Even though the proposed anti-windup with reset scheme reduces most of the steady-state errors, there is ripple and chattering in the steady-state caused by the anti-windup.

6.2 Recommendations

- The formulations of the economic dispatch problem with additional objectives presented in this thesis could be used in research works developing distributed optimisation. The proposed objective functions are a starting point to regulate the weight and penalties for achieving the same control goals. The interested reader may investigate the incorporation of absolute values or square functions inside the objective functions.

- The finite-time parameters for control should be selected according to the convergence speed needed. It is recommended to design the controller for asymptotic consensus and then use a finite-time protocol. Since the exponential parameter is the one that determines the level of non-linearity, it is recommended only to change this parameter and not the coupling gain. A methodology for fine-tuning the exponential parameter could be starting from 1 (conventional asymptotic consensus) and then gradually reducing until approximately 0.5 (values lower than 0.5 are still possible).

- The weighting parameters for dealing with the trade-offs between control objectives

are complex to design. Their recommended tunning process is similar to the finite-time exponent, i.e., starting from a neutral point, in this case, zero, and then gradually incrementing the weighting parameter until it reaches the desired operating point. The former methodology is useful for stable MGs, which do not change their power flows dramatically. In general, a more flexible method would be the proposed adjustable weightings. They provide reasonable performance in real MG systems with high load variability. Several ways to tune the adjustable weighting parameters are possible, like adaptive control. However, activation functions like the one proposed in Chapter 3 are highly recommended for control strategies that do not perform real-time optimisations.

- The proposed anti-windup is a powerful tool to deal with communication latency. It outstands when eliminating steady-state errors, although it introduces ripple/chattering in the controlled signals. Its use is not recommended in systems with minor time delays since the disadvantages in terms of signal quality surpass the aforementioned advantages. For the tuning process of Algorithm 1 parameters, starting with $T_k \approx 0.3$ and $\varepsilon = 10^{-3}$ is recommended. From there, minor adjustments could be made depending on the needs. A smaller ε will reduce the ripple of the anti-windup, but the accuracy after the resets is reduced. The value of T_k is also related to the ripple and the frequency of resets. Finally, the parameter T_{st} could be selected as needed; it is directly related to the frequency of resets. For the application presented in this thesis, selecting values of T_{st} over 5 seconds is recommended to give time for the economic dispatch to settle to equilibrium before executing a reset.

6.3 Future Work

A compilation of suggested research directions from the results presented in this thesis is described as follows.

- In terms of the ILC economic dispatch dynamic, a Taylor-made model with data-driven support could be derived to allow the ILC to operate more independently from communications (or more accurately when system failures occur).

- The economic dispatch problem could include more objectives that can be translated into ILC control actions. Examples are an objective related to SoC of BESS, or an objective related to power quality compensations in the AC subgrids.

- Robustness and resilience under cyber attacks could be added to the proposed controllers to guarantee the safe operation of the system. It is especially suggested regarding the developments in dynamic average consensus as a method to estimate systems variables.

- A methodology based on heuristic optimisation could be implemented to address the tunning process of the control parameters.

Bibliography

[1] Enrique Espina, Jacqueline Llanos, Claudio Burgos-Mellado, Roberto Cárdenas, Manuel Martínez-Gómez, and Doris Sáez. Distributed control strategies for microgrids: An overview. *IEEE Access*, 8:193412–193448, 2020.

[2] Manuel Martinez-Gomez, Alex Navas, Marcos E. Orchard, Serhiy Bozhko, Claudio Burgos-Mellado, and Roberto Cárdenas. Multi-objective finite-time control for the interlinking converter on hybrid ac/dc microgrids. *IEEE Access*, 9:116183–116193, 2021.

[3] Enrique Espina, Claudio Burgos-Mellado, Juan Gomez, Jacqueline Llanos, Erwin Rute, Alex Navas, Manuel Martinez-Gomez, Roberto Cardenas, and Doris Saez. Experimental Hybrid AC / DC-Microgrid Prototype for Laboratory Research. *22st Eur. Conf. Power Electron. and Appl. (EPE)*, pages 1–9, 2020.

[4] Manuel Martinez-Gomez, Marcos E. Orchard, and Serhiy Bozhko. Dynamic average consensus with anti-windup applied to interlinking converters in ac/dc microgrids under economic dispatch and delays. *IEEE Transactions on Smart Grid*, pages 1–1, 2023.

[5] N. Hatziargyriou, H. Asano, R. Iravani, and C. Marnay. Microgrids. *IEEE Power Energy Mag.*, 5(4):78–94, July 2007.

[6] U.S. Department of Energy Microgrid Exchange Group. Microgrid Definitions, [Online]. Available: https://building-microgrid.lbl.gov/microgrid-definitions.

[7] X Liu, P Wang, and P C Loh. A Hybrid AC/DC Microgrid and Its Coordination Control. *IEEE Transactions on Smart Grids*, 2(2):278–286, Jun 2011.

[8] Tianyang Zhao, Jianfang Xiao, Leong Hai Koh, Qianwen Xu, and Peng Wang. Distributed Energy Management for Hybrid AC/DC Microgrid Parks. In *IEEE Power and Energy Society General Meeting*, Dec 2018.

[9] Jianguo Zhou, Yinliang Xu, Hongbin Sun, Yushuai Li, and Mo Yuen Chow. Distributed Power Management for Networked AC-DC Microgrids with Unbalanced Microgrids. *IEEE Trans. Ind. Informatics*, 16(3):1655–1667, 2020.

[10] Poh Chiang Loh, Ding Li, Yi Kang Chai, and Frede Blaabjerg. Autonomous control of interlinking converter with energy storage in hybrid AC-DC microgrid. *IEEE Transactions on Industrial Applications*, 49(3):1374–1382, May 2013.

[11] Xiaonan Lu, Josep M. Guerrero, Kai Sun, Juan C. Vasquez, Remus Teodorescu, and Lipei Huang. Hierarchical control of parallel AC-DC converter interfaces for hybrid microgrids. *IEEE Transactions on Smart Grid*, 5(2):683–692, 2014.

[12] Antonis G. Tsikalakis and Nikos D. Hatziargyriou. Centralized Control for Optimizing Microgrids Operation. *IEEE Transactions on Energy Conversion*, 23(1):241–248, mar 2008.

[13] P. Lin, C. Jin, J. Xiao, X. Li, D. Shi, Y. Tang, and P. Wang. A distributed control architecture for global system economic operation in autonomous hybrid ac/dc microgrids. *IEEE Transactions on Smart Grid*, 10(3):2603–2617, 2019.

[14] Wendong Feng, Jian Yang, Zhangjie Liu, Hui Wang, Mei Su, and Xin Zhang. A unified distributed control scheme on cost optimization for hybrid AC/DC microgrid. *IEEE 4th Southern Power Electron. Conf. (SPEC)*, pages 1–6, 2018.

[15] Frank L. Lewis, Hongwei Zhang, Kristian Hengster-Movric, and Abhijit Das. *Cooperative Control of Multi-Agent Systems*. Number 3 in Communications and Control Engineering. Springer London, London, 2014.

[16] Saroja Kanti Sahoo, Avinash Kumar Sinha, and N. K. Kishore. Control Techniques in AC, DC, and Hybrid AC–DC Microgrid: A Review. *IEEE Journal of Emerging and Selected Topics in Power Electronics*, 6(2):738–759, 2018.

[17] Qianwen Xu, Jianfang Xiao, Peng Wang, and Changyun Wen. A Decentralized Control Strategy for Economic Operation of Autonomous AC, DC, and Hybrid AC/DC Microgrids. *IEEE Trans. Energy Convers.*, 32(4):1345–1355, Dec 2017.

[18] Hyeong-Jun Yoo, Thai-Thanh Nguyen, and Hak-Man Kim. Consensus-based Distributed Coordination Control of Hybrid AC/DC Microgrids. *IEEE Transactions on Sustainable Energy*, pages 629–639, Apr 2019.

[19] J. Llanos, J. Gomez, D. Saez, D. Olivares, and J. Simpson-Porco. Economic dispatch by secondary distributed control in microgrid. In *21st European Conference on Power Electronics and Applications*, 2019.

[20] J. Llanos, D. Olivares, J. Simpson-Porco, K. Mehrdad, and Doris Sáez. A novel distributed control strategy for optimal dispatch of isolated microgrids considering congestion. *IEEE Transactions on Smart Grids*, 10(6):6595 – 6606, Nov 2019.

[21] C. Chen, S. Duan, T. Cai, B. Liu, and G. Hu. Smart energy management system for optimal microgrid economic operation. *IET Renewable Power Generation*, 5(3):258–267, May 2011.

[22] Enrique Espina, Roberto Cardenas, Felipe Donoso, Matias Urrutia, and Mauricio Espinoza. A Novel Distributed Secondary Control Strategy Applied to Hybrid AC / DC Microgrids. *21st Eur. Conf. Power Electron. Appl.*, 2019. To be published.

[23] Enrique Espina. Distributed secondary control applied to hybrid ac/dc microgrids. *Tesis de la Universidad de Chile*, 2021.

[24] Jianguo Zhou, Huaguang Zhang, Qiuye Sun, Dazhong Ma, and Bonan Huang. Event-based distributed active power sharing control for interconnected AC and DC microgrids. *IEEE Transactions on Smart Grids*, 9(6):6815–6828, Nov 2018.

[25] Pengfeng Lin, Peng Wang, Chi Jin, Jianfang Xiao, Xiaoqiang Li, Fanghong Guo, and Chuanlin Zhang. A Distributed Power Management Strategy for Multi-Paralleled Bidirectional Interlinking Converters in Hybrid AC/DC Microgrids. *IEEE Trans. Smart Grid*, 10(5):5696–5711, jan 2019.

[26] Yanghong Xia, Yonggang Peng, Pengcheng Yang, Miao Yu, and Wei Wei. Distributed coordination control for multiple bidirectional power converters in a hybrid ac/dc microgrid. *IEEE Trans. Power Electron.*, 32(6):4949–4959, 2017.

[27] Saeed Peyghami, Hossein Mokhtari, and Frede Blaabjerg. Autonomous operation of a hybrid ac/dc microgrid with multiple interlinking converters. *IEEE Transactions on Smart Grid*, 9(6):6480–6488, 2018.

[28] Amr Ahmed A. Radwan and Yasser Abdel Rady I. Mohamed. Networked control and power management of AC/DC hybrid microgrids. *IEEE Systems Journal*, 11(3):1662–1673, Sep 2017.

[29] Pengfeng Lin, Peng Wang, Jianfang Xiao, Chi Jin, Junjun Wang, and Koh Leong Hai. Power management of multi-paralleled bidirectional interlinking converters in hybrid ac/dc microgrids: A dynamic consensus approach. In *2018 Asian Conf. Energy Power Transp. Electrif. (ACEPT)*, pages 1–5, 2018.

[30] Enrique Espina, Roberto Cardenas, John W. Simpson-Porco, Doris Saez, and Mehrdad Kazerani. A Consensus-Based Secondary Control Strategy for Hybrid AC/DC Microgrids with Experimental Validation. *IEEE Transactions Power Electronics*, 36(5):5971–5984, 2021.

[31] Yanghong Xia, Wei Wei, Miao Yu, Xiaoming Wang, and Yonggang Peng. Power management for a hybrid ac/dc microgrid with multiple subgrids. *IEEE Transactions on Power Electronics*, 33(4):3520–3533, 2018.

[32] Mohammad Abuhilaleh, Li Li, Jianguo Zhu, and M.J. Hossain. Distributed control and power management strategy for an autonomous hybrid microgrid with multiple sub-microgrids. In *2018 Australasian Universities Power Engineering Conference (AUPEC)*, pages 1–6, 2018.

[33] Yu Wang, Suman Mondal, Chao Deng, Kuntal Satpathi, Yan Xu, and Souvik Dasgupta. Cyber-resilient cooperative control of bidirectional interlinking converters in networked ac/dc microgrids. *IEEE Transactions on Industrial Electronics*, 68(10):9707–9718, 2021.

[34] Xiangke Li, Chaoyu Dong, Wentao Jiang, and Xiaohua Wu. Distributed control strategy for global economic operation and bus restorations in a hybrid ac/dc microgrid with interconnected subgrids. *International Journal of Electrical Power & Energy Systems*, 131:107032, 2021.

[35] Nagaraju Pogaku, Milan Prodanović, and Timothy C. Green. Modeling, analysis and testing of autonomous operation of an inverter-based microgrid. *IEEE Transactions on Power Electronics*, 22(2):613–625, 2007.

[36] Ali Bidram, Ali Davoudi, Frank L. Lewis, and Zhihua Qu. Secondary control of microgrids based on distributed cooperative control of multi-agent systems. *IET Gener. Transm. Distrib.*, 7(8):822–831, 2013.

[37] Ernane Antônio Alves Coelho, Dan Wu, Josep M. Guerrero, Juan C. Vasquez, Tomislav Dragičević, Čedomir Stefanović, and Petar Popovski. Small-Signal Analysis of the Microgrid Secondary Control Considering a Communication Time Delay. *IEEE Transactions on Industrial Electronics*, 63(10):6257–6269, 2016.

[38] Shan Zuo, Ali Davoudi, Yongduan Song, and Frank L. Lewis. Distributed Finite-Time Voltage and Frequency Restoration in Islanded AC Microgrids. *IEEE Transactions on Industrial Electronics*, 63(10):5988–5997, Oct 2016.

[39] Y. Xu, W. Zhang, W. Liu, X. Wang, F. Ferrese, C. Zang, and H. Yu. Distributed Subgradient-Based Coordination of Multiple Renewable Generators in a Microgrid. *IEEE Trans. Power Syst.*, 29(1):23–33, 2014.

[40] Huagen Xiao, An Luo, Zhikang Shuai, Guobin Jin, and Yuan Huang. An improved control method for multiple bidirectional power converters in hybrid AC/DC microgrid. *IEEE Transactions on Smart Grid*, 7(1):340–347, 2016.

[41] Hualei Zou, Shiwen Mao, Yu Wang, Fanghua Zhang, Xin Chen, and Long Cheng. A survey of energy management in interconnected multi-microgrids. *IEEE Access*, 7:72158–72169, 2019.

[42] Nima Nikmehr and Sajad Najafi Ravadanegh. Optimal power dispatch of multi-microgrids at future smart distribution grids. *IEEE Transactions on Smart Grid*, 6(4):1648–1657, 2015.

[43] Zhaoyu Wang, Bokan Chen, Jianhui Wang, Miroslav M. Begovic, and Chen Chen. Coordinated energy management of networked microgrids in distribution systems. *IEEE Transactions on Smart Grid*, 6(1):45–53, 2015.

[44] Yu Wang, Shiwen Mao, and R. M. Nelms. On hierarchical power scheduling for the macrogrid and cooperative microgrids. *IEEE Transactions on Industrial Informatics*, 11(6):1574–1584, 2015.

[45] Subham Sahoo, Sukumar Mishra, Seyed Mahdi Fazeli, Furong Li, and Tomislav Dragicevic. A Distributed Fixed-Time Secondary Controller for DC Microgrid Clusters. *IEEE Transactions on Energy Conversion*, 34(4):1997–2007, 2019.

[46] Yilin Li, Ping Dong, Mingbo Liu, and Guokang Yang. A distributed coordination control based on finite-time consensus algorithm for a cluster of dc microgrids. *IEEE Transactions on Power Systems*, 34(3):2205–2215, 2019.

[47] Haifeng Qiu, Bo Zhao, Wei Gu, and Rui Bo. Bi-level two-stage robust optimal scheduling for ac/dc hybrid multi-microgrids. *IEEE Transactions on Smart Grid*, 9(5):5455–5466, 2018.

[48] Ernauli Aprilia, Ke Meng, Mohamed Al Hosani, Hatem H. Zeineldin, and Zhao Yang Dong. Unified power flow algorithm for standalone ac/dc hybrid microgrids. *IEEE Trans. Smart Grid*, 10(1):639–649, 2019.

[49] Quan Zhou, Mohammad Shahidehpour, Zhiyi Li, and Xiaoyuan Xu. Two-Layer Control Scheme for Maintaining the Frequency and the Optimal Economic Operation of Hybrid AC/DC Microgrids. *IEEE Transactions on Power Systems*, 34(1):64–75, 2019.

[50] Pengcheng Yang, Miao Yu, Qiuwei Wu, Peng Wang, Yanghong Xia, and Wei Wei. Decentralized Economic Operation Control for Hybrid AC/DC Microgrid. *IEEE Transactions on Sustainable Energy*, 11(3):1898–1910, 2020.

[51] Josep M. Guerrero, Juan C. Vasquez, José Matas, Luis García De Vicuña, and Miguel Castilla. Hierarchical control of droop-controlled ac and dc microgrids - a general approach toward standardization. *IEEE Transactions on Industrial Electronics*, 58(1):158–172, Jan 2011.

[52] A. Bidram and A. Davoudi. Hierarchical Structure of Microgrids Control System. *IEEE Trans. Smart Grid*, 3(4):1963–1976, 2012.

[53] Daniel E Olivares, Ali Mehrizi-Sani, Amir H Etemadi, Claudio A Cañizares, Reza Iravani, Mehrdad Kazerani, Amir H Hajimiragha, Oriol Gomis-Bellmunt, Maryam Saeedifard, Rodrigo Palma-Behnke, et al. Trends in microgrid control. *IEEE Trans. Smart Grid*, 5(4):1905–1919, 2014.

[54] Fei Gao, Ren Kang, Jun Cao, and Tao Yang. Primary and secondary control in DC microgrids: a review. *Journal of Modern Power Systems and Clean Energy*, 7(2):227–242, 2019.

[55] Antonio Carlos Zambroni and Miguel Castilla. *Microgrids Design and Implementation.* Springer International Publishing, 2019.

[56] Carlos A. Hernandez-Aramburo, Tim C. Green, and Nicolas Mugniot. Fuel consumption minimization of a microgrid. *IEEE Transactions on Industry Applications*, 41(3):673–681, 2005.

[57] E. Barklund, Nagaraju Pogaku, Milan Prodanovic, C. Hernandez-Aramburo, and Tim C. Green. Energy management in autonomous microgrid using stability-constrained droop control of inverters. *IEEE Transactions on Power Electronics*, 23(5):2346–2352, 2008.

[58] Inam Ullah Nutkani, Poh Chiang Loh, Peng Wang, and Frede Blaabjerg. Cost-prioritized droop schemes for autonomous ac microgrids. *IEEE Transactions on Power Electronics*, 30(2):1109–1119, 2014.

[59] Inam Ullah Nutkani, Poh Chiang Loh, and Frede Blaabjerg. Cost-based droop scheme with lower generation costs for microgrids. *IET Power Electronics*, 7(5):1171–1180, 2014.

[60] Feixiong Chen, Minyou Chen, Qiang Li, Kaikai Meng, Yongwei Zheng, Josep M. Guerrero, and Derek Abbott. Cost-Based Droop Schemes for Economic Dispatch in Islanded Microgrids. *IEEE Transactions on Smart Grid*, 8(1):63–74, 2017.

[61] Gang Chen, Jianghong Ren, and E. Ning Feng. Distributed Finite-Time Economic Dispatch of a Network of Energy Resources. *IEEE Transactions on Smart Grid*, 8(2):822–832, 2017.

[62] Gerald B Sheblé Allen J. Wood Bruce F. Wollenberg. *Introduction to state estimation in power systems*. John Willey and Sons, 2013.

[63] Z. Zhang and Mo-Yuen Chow. Convergence analysis of the incremental cost consensus algorithm under different communication network topologies in a smart grid. *IEEE Transactions on Power Systems*, 27(4):1761 – 1768, 2012.

[64] Giulio Binetti, Mohammed Abouheaf, Frank Lewis, David Naso, Ali Davoudi, and Biagio Turchiano. Distributed solution for the economic dispatch problem. *2013 21st Mediterranean Conference on Control and Automation, MED 2013 - Conference Proceedings*, pages 243–250, 2013.

[65] W. Zhang, W. Liu, X. Wang, L. Liu, and F. Ferrese. Online optimal generation control based on constrained distributed gradient algorithm. *IEEE Transactions on Power Systems*, 30(1):35–45, 2015.

[66] Nikos Hatziargyriou. *Microgrid: Architecture and Control*. John Wiley and Sons Ltd, 2014.

[67] M. Yazdanian and A. Mehrizi-Sani. Distributed control techniques in microgrids. *IEEE Trans. Smart Grid*, 5(6):2901–2909, 2014.

[68] Kyriaki E. Antoniadou-Plytaria, Iasonas N. Kouveliotis-Lysikatos, Pavlos S. Georgilakis, and Nikos D. Hatziargyriou. Distributed and Decentralized Voltage Control of

Smart Distribution Networks. *IEEE Transactions on Smart Grid*, 8(6):2999–3008, 2017.

[69] Jeff Shamma. *Coperative Control of Distributed Multi-Agent Systems*. Wiley & Sons, 2007.

[70] Ali Bidram, Ali Davoudi, and Frank L Lewis. *Cooperative Synchronization in Distributed Microgrid Control*. Springer International, 2017.

[71] Fanghong Guo, Changyun Wen, and Yong Duan Song. *Distributed control and optimization technologies in smart grid systems*. CRC Press, 2017.

[72] Stuart Russell and Norvig Peter. *Artificial intelligence—a modern approach*. Prentice Hall, 2010.

[73] Gabriela Hug, Soummya Kar, and Chenye Wu. Consensus + Innovations Approach for Distributed Multiagent Coordination in a Microgrid. *IEEE Transactions on Smart Grid*, 6(4):1893–1903, 2015.

[74] F. Bullo. *Lectures on Network Systems*. Kindle Direct Publishing, 2019. With contributions by J. Cortes, F. Dorfler, and S. Martinez.

[75] Jiahu Qin, Qichao Ma, Yang Shi, and Long Wang. Recent advances in consensus of multi-agent systems: A brief survey. *IEEE Transactions on Industrial Electronics*, 64(6):4972–4983, 2017.

[76] Reza Olfati-Saber and R.M. Murray. Consensus Problems in Networks of Agents With Switching Topology and Time-Delays. *IEEE Trans. Automat. Contr.*, 49(9):1520–1533, Sep 2004.

[77] R. Olfati-Saber, J. Fax, and R. M. Murray. Consensus and Cooperation in Networked Multi-Agent Systems. In *Proceedings of the IEEE*, volume 95, pages 215 – 233, 2007.

[78] DP Spanos, R Olfati-Saber, and RM Murray. Dynamic consensus on mobile networks. *The 16th IFAC World Congress*, pages 1–6, 2005.

[79] Zhongkui Li, Zhisheng Duan, Guanrong Chen, and Lin Huang. Consensus of Multiagent Systems and Synchronization of Complex Networks: A Unified Viewpoint. *IEEE Transactions on Circuits and Systems I: Regular Papers*, 57(1):213–224, 2009.

[80] Jorge Cortés. Finite-time convergent gradient flows with applications to network consensus. *Automatica*, 42(11):1993–2000, Nov 2006.

[81] Suiyang Khoo, Lihua Xie, and Zhihong Man. Robust finite-time consensus tracking algorithm for multirobot systems. *IEEE/ASME Transactions on Mechatronics*, 14(2):219–228, 2009.

[82] Long Wang and Feng Xiao. Finite-time consensus problems for networks of dynamic agents. *IEEE Trans. Automat. Contr.*, 55(4):950–955, Apr 2010.

[83] Reza Olfati Saber and Richard M. Murray. Consensus Protocols for Networks of Dynamic Agents. *Proceedings of the American Control Conference*, 2:951–956, 2003.

[84] Xiaoli Wang and Yiguang Hong. Finite-Time Consensus for Multi-Agent Networks with Second-Order Agent Dynamics. *IFAC Proceedings Volumes*, 41(2):15185–15190, 2008.

[85] Leonard Weiss. Converse Theorems for Finite Time Stability. *SIAM Journal on Applied Mathematics*, 16(6):1319–1324, 1968.

[86] Sanjay P. Bhat and Dennis S. Bernstein. Finite-Time Stability of Continuous Autonomous Systems. *SIAM J. Control Optim.*, 38(3):751–766, Jul 2000.

[87] Z. Zhang and M. Chow. Incremental Cost Consensus Algorithm in a Smart Grid Environment. In *IEEE Power and Energy Society General Meeting*, pages 1–6, 2011.

[88] Gang Chen, Frank L. Lewis, E. Ning Feng, and Yongduan Song. Distributed Optimal Active Power Control of Multiple Generation Systems. *IEEE Transactions on Industrial Electronics*, 62(11):7079–7090, 2015.

[89] G. Chen, J. Ren, and E. Feng. Distributed finite-time economic dispatch of a network of energy resources. *IEEE Transactions on Smart Grid*, 8(2):822–832, 2016.

[90] C. LI, M. Savaghebi, J. Vasquez, and J. Guerrero. Multiagent based distributed control for operation cost minimization of droop controlled ac microgrid using incremental cost consensus. In *European Conference on Power Electronics and Applications (EPE'15 ECCE-Europe)*, pages 1–9, 2015.

[91] C. LI, J. Vasquez, and J. Guerrero. Convergence analysis of distributed control for operation cost minimization of droop controlled dc microgrid based on multiagent. In

IEEE Applied Power Electronics Conference and Exposition (APEC), volume 3459-3464, pages 1–9, 2016.

[92] Z. Wang, W. Wu, and B. Zhang. A fully distributed power dispatch method for fast frequency recovery and minimal generation cost in autonomous microgrids. *IEEE Transactions on Smart Grid*, 7(1):19 – 31, 2016.

[93] C. Zhao, J. He, P. Cheng, and J. Chen. Consensus-based energy management in smart grid with transmission losses and directed communication. *IEEE Transactions on Smart Grid*, 8(5):2049 – 2061, 2017.

[94] Y. Xu and Z. Li. Distributed optimal resource management based on the consensus algorithm in a microgrid. *IEEE Transactions on Industrial Electronics*, 62(4):2584 – 2592, 2015.

[95] G. Binetti, A. Davoudi, F. L. Lewis, D. Naso, and B. Turchiano. Distributed consensus-based economic dispatch with transmission losses. *IEEE Transactions on Power Systems*, 29(4):1711 – 1720, 2014.

[96] T. Yang, D. Wu, Y. Sun, and J. Lian. Minimum-time consensus-based approach for power system applications. *IEEE Transactions on Industrial Electronics*, 63(2):1318 – 1328, 2016.

[97] T. Xu, W. Wu, S. Hongbin, and L.Wang. Fully distributed multi-area dynamic economic dispatch method with second-order convergence for active distribution networks. *IET Generation, Transmission and Distribution*, 11(16):3955–3965, May 2017.

[98] R. Wang, Q. Li, B. Zhang, and L. Wang. Distributed consensus based algorithm for economic dispatch in a microgrid. *IEEE Transactions on Smart Grid*, 10(4):3630–3640, 2019.

[99] C. LI, J. Vasquez, and J. Guerrero. Convergence analysis of distributed control for operation cost minimization of droop controlled dc microgrid based on multiagent. In *European Conference on Power Electronics and Applications (EPE'15 ECCE-Europe)*, pages 3459–3464, 2016.

[100] Z. Cheng, Z. Li, J. Liang, J. Gao, J. Si, and S. Li. Distributed economic power dispatch and bus voltage control for droop-controlled dc microgrids. *Energies*, 12(12):1–22, 2019.

[101] Mohamed Zaery, Emad M. Ahmed, Mohamed Orabi, and Mohamed Youssef. Oper-

ational cost reduction based on distributed adaptive droop control technique in DC microgrids. *Energy Conversion Congr. Expo. (ECCE)*, pages 2638–2644, 2017.

[102] J. Hu, J. Duan, H. Ma, and M. Chow. Distributed adaptive droop control for optimal power dispatch in dc microgrid. *IEEE Transactions on Industrial Electronics*, 65(1):778 – 789, 2018.

[103] S. Moayedi and A. Davoudi. Unifying distributed dynamic optimization and control of islanded dc microgrids. *IEEE Transactions on Power Electronics*, 32(3):2329–2346, 2016.

[104] H. Han, H. Wang, Y. Sun, J. Yang, and Z. Liu. Distributed control scheme on cost optimisation under communication delays for dc microgrids. *IET Generation, Transmission and Distribution*, 11(17):4193–4201, 2017.

[105] Ali Bidram, Ali Davoudi, and Frank L. Lewis. Finite-time frequency synchronization in microgrids. *2014 IEEE Energy Convers. Congr. Expo. ECCE 2014*, 111:2648–2654, 2014.

[106] V. Nasirian, A. Davoudi, F. L. Lewis, and J. M. Guerrero. Distributed Adaptive Droop Control for DC Distribution Systems. *IEEE Trans. Energy Convers.*, 29(4):944–956, 2014.

[107] Vahidreza Nasirian, Seyedali Moayedi, Ali Davoudi, and Frank L. Lewis. Distributed cooperative control of dc microgrids. *IEEE Transactions on Power Electronics*, 30(4):2288–2303, 2015.

[108] Qobad Shafiee, Josep M. Guerrero, and Juan C. Vasquez. Distributed secondary control for islanded microgrids-a novel approach. *IEEE Transactions on Power Electronics*, 29(2):1018–1031, 2014.

[109] John W. Simpson-Porco, Florian Dörfler, and Francesco Bullo. Synchronization and power sharing for droop-controlled inverters in islanded microgrids. *Automatica*, 49(9):2603–2611, 2013.

[110] John W Simpson-Porco, Qobad Shafiee, Florian Dörfler, Juan C Vasquez, Josep M Guerrero, and Francesco Bullo. Secondary frequency and voltage control of islanded microgrids via distributed averaging. *IEEE Trans. Ind. Electron.*, 62(11):7025–7038, 2015.

[111] Fanghong Guo, Changyun Wen, Jianfeng Mao, and Yong Duan Song. Distributed Secondary Voltage and Frequency Restoration Control of Droop-Controlled Inverter-Based Microgrids. *IEEE Transactions on Industrial Electronics*, 62(7):4355–4364, Jul 2015.

[112] Vahidreza Nasirian, Qobad Shafiee, Josep M. Guerrero, Frank L. Lewis, and Ali Davoudi. Droop-free team-oriented control for ac distribution systems. *Conference Proceedings - IEEE Applied Power Electronics Conference and Exposition - APEC*, 2015-May(May):2911–2918, 2015.

[113] V. Nasirian, Q. Shafiee, J. M. Guerrero, F. L. Lewis, and A. Davoudi. Droop-free distributed control for ac microgrids. *IEEE Transactions on Power Electronics*, 31(2):1600–1617, 2016.

[114] Huaguang Zhang, Sunghyok Kim, Qiuye Sun, and Jianguo Zhou. Distributed Adaptive Virtual Impedance Control for Accurate Reactive Power Sharing Based on Consensus Control in Microgrids. *IEEE Trans. Smart Grid*, 8(4):1749–1761, 2017.

[115] Zhilin Lyu, Qing Wei, Yiyi Zhang, Junhui Zhao, and Emad Manla. Adaptive virtual impedance droop control based on consensus control of reactive current. *Energies*, 11(7), 2018.

[116] Baoze Wei, Albert Marzabal, Ruben Ruiz, Josep M. Guerrero, and Juan C. Vasquez. DAVIC: A New Distributed Adaptive Virtual Impedance Control for Parallel-Connected Voltage Source Inverters in Modular UPS System. *IEEE Trans. Power Electron.*, 34(6):5953–5968, 2019.

[117] Zhongguan Wang, Wenchuan Wu, and Boming Zhang. Distributed newton method for primary voltage control in Islanded DC microgrid. *IEEE Power and Energy Society General Meeting*, 2018-January(51477083):1–5, 2018.

[118] X. Lu, X. Yu, J. Lai, Y. Wang, and J. M. Guerrero. A novel distributed secondary coordination control approach for islanded microgrids. *IEEE Transactions on Smart Grid*, 9(4):2726–2740, 2018.

[119] Claudio Burgos-Mellado, Jacqueline Llanos, Roberto Cárdenas, Doris Sáez, Daniel E Olivares, Mark Sumner, and Alessandro Costabeber. Distributed control strategy based on a consensus algorithm and on the conservative power theory for imbalance and harmonic sharing in 4-wire microgrids. *IEEE Transactions on Smart Grid*, 2019.

[120] Sandeep Anand, Baylon G. Fernandes, and Josep M. Guerrero. Distributed control

to ensure proportional load sharing and improve voltage regulation in low-voltage DC microgrids. *IEEE Transactions on Power Electronics*, 28(4):1900–1913, 2013.

[121] Xiaonan Lu, Josep M. Guerrero, Kai Sun, Juan C. Vasquez, Remus Teodorescu, and Lipei Huang. Hierarchical control of parallel AC-DC converter interfaces for hybrid microgrids. *IEEE Transactions on Smart Grids*, 5(2):683–692, Mar 2014.

[122] P. Wang, X. Lu, X. Yang, W. Wang, and D. Xu. An improved distributed secondary control method for dc microgrids with enhanced dynamic current sharing performance. *IEEE Transactions on Power Electronics*, 31(9):6658–6673, 2016.

[123] S. Sahoo and S. Mishra. A distributed finite-time secondary average voltage regulation and current sharing controller for dc microgrids. *IEEE Transactions on Smart Grid*, 10(1):282–292, 2019.

[124] R. Zhang and B. Hredzak. Distributed finite-time multiagent control for dc microgrids with time delays. *IEEE Transactions on Smart Grid*, 10(3):2692–2701, 2019.

[125] Yalong Hu, Xiaoming Wang, Yonggang Peng, Ji Xiang, and Wei Wei. Distributed Finite-Time Secondary Control for DC Microgrids with Virtual Impedance Arrangement. *IEEE Access*, 7:57060–57068, 2019.

[126] Ali Bidram, Ali Davoudi, Frank L. Lewis, and Zhihua Qu. Secondary control of microgrids based on distributed cooperative control of multi-agent systems. *IET Generation, Transmission & Distribution*, 7(8):822–831, 2013.

[127] Qobad Shafiee, Vahidreza Nasirian, Juan Vasquez, Josep Guerrero, and Ali Davoudi. A Multi-Functional Fully Distributed Control Framework for AC Microgrids. *IEEE Transactions on Smart Grids*, 9(4):3247–3258, 2018.

[128] L. Meng, X. Zhao, F. Tang, M. Savaghebi, T. Dragicevic, J. C. Vasquez, and J. M. Guerrero. Distributed Voltage Unbalance Compensation in Islanded Microgrids by Using a Dynamic Consensus Algorithm. *IEEE Trans. Power Electron.*, 31(1):827–838, 2016.

[129] Fanghong Guo, Qianwen Xu, Changyun Wen, Lei Wang, and Peng Wang. Distributed Secondary Control for Power Allocation and Voltage Restoration in Islanded DC Microgrids. *IEEE Transactions on Sustainable Energy*, 9(4):1857–1869, 2018.

[130] Chendan Li, Ernane Antonio Alves Coelho, Tomislav Dragicevic, Josep M. Guerrero,

and Juan C. Vasquez. Multiagent-Based Distributed State of Charge Balancing Control for Distributed Energy Storage Units in AC Microgrids. *IEEE Transactions on Industry Applications*, 53(3):2369–2381, 2017.

[131] Cameron Nowzari, Eloy Garcia, and Jorge Cortés. Event-triggered communication and control of networked systems for multi-agent consensus. *Automatica*, 105:1–27, 2019.

[132] Zongyu Zuo, Qing Long Han, Boda Ning, Xiaohua Ge, and Xian Ming Zhang. An Overview of Recent Advances in Fixed-Time Cooperative Control of Multiagent Systems. *IEEE Trans. Ind. Informatics*, 14(6):2322–2334, 2018.

[133] Ulrich Münz, Antonis Papachristodoulou, and Frank Allgöwer. Delay robustness in consensus problems. *Automatica*, 46(8):1252–1265, 2010.

[134] N. M. Dehkordi, N. Sadati, and M. Hamzeh. Fully distributed cooperative secondary frequency and voltage control of islanded microgrids. *IEEE Transactions on Energy Conversion*, 32(2):675–685, 2017.

[135] Yinliang Xu, Hongbin Sun, Wei Gu, Yan Xu, and Zhengshuo Li. Optimal Distributed Control for Secondary Frequency and Voltage Regulation in an Islanded Microgrid. *IEEE Transactions on Industrial Informatics*, 15(1):225–235, 2019.

[136] Subham Sahoo, Deepak Pullaguram, Sukumar Mishra, Jianzhong Wu, and Nilanjan Senroy. A containment based distributed finite-time controller for bounded voltage regulation & proportionate current sharing in DC microgrids. *Appl. Energy*, 228(August):2526–2538, 2018.

[137] Renke Han, Nelson Leonardo Diaz Aldana, Lexuan Meng, Josep M. Guerrero, and Qiuye Sun. Droop-free distributed control with event-triggered communication in DC micro-grid. *Conference Proceedings - IEEE Applied Power Electronics Conference and Exposition - APEC*, pages 1160–1166, 2017.

[138] Subham Sahoo and Sukumar Mishra. An adaptive event-triggered communication-based distributed secondary control for DC microgrids. *IEEE Transactions on Smart Grid*, 9(6):6674–6683, 2018.

[139] Deepak Pullaguram, Sukumar Mishra, and Nilanjan Senroy. Event-Triggered Communication Based Distributed Control Scheme for DC Microgrid. *IEEE Trans. Power Syst.*, 33(5):5583–5593, 2018.

[140] Muhammad Tahir and Sudip K. Mazumder. Self-Triggered Communication Enabled Control of Distributed Generation in Microgrids. *IEEE Trans. Ind. Informatics*, 11(2):441–449, 2015.

[141] Jingang Lai, Hong Zhou, Xiaoqing Lu, Xinghuo Yu, and Wenshan Hu. Droop-Based Distributed Cooperative Control for Microgrids with Time-Varying Delays. *IEEE Transactions on Smart Grid*, 7(4):1775–1789, 2016.

[142] Constanza Ahumada, Roberto Cárdenas, Doris Sáez, and Josep M. Guerrero. Secondary Control Strategies for Frequency Restoration in Islanded Microgrids With Consideration of Communication Delays. *IEEE Trans. Smart Grid*, 7(3):1430–1441, 2016.

[143] M. Dong, L. Li, Y. Nie, D. Song, and J. Yang. Stability analysis of a novel distributed secondary control considering communication delay in dc microgrids. *IEEE Transactions on Smart Grid*, pages 1–1, 2019.

[144] X. Lu, X. Yu, J. Lai, J. M. Guerrero, and H. Zhou. Distributed secondary voltage and frequency control for islanded microgrids with uncertain communication links. *IEEE Transactions on Industrial Informatics*, 13(2):448–460, 2017.

[145] N. M. Dehkordi, H. R. Baghaee, N. Sadati, and J. M.Guerrero. Distributed noise-resilient secondary voltage and frequency control for islanded microgrids. *IEEE Transactions on Smart Grid*, pages 1–1, 2018.

[146] G. Lou, W. Gu, Y. Xu, M. Cheng, and W. Liu. Distributed mpc-based secondary voltage control scheme for autonomous droop-controlled microgrids. *IEEE Transactions on Sustainable Energy*, 8(2):792–804, 2017.

[147] R. Heydari, T. Dragicevic, and F. Blaabjerg. High-bandwidth secondary voltage and frequency control of vsc-based ac microgrid. *IEEE Transactions on Power Electronics*, pages 1–1, 2019.

[148] Juan S. Gomez, Doris Saez, John W. Simpson-Porco, and Roberto Cardenas. Distributed Predictive Control for Frequency and Voltage Regulation in Microgrids. *IEEE Trans. Smart Grid*, pages 1–1, 2019.

[149] A. Ingle, A. B. Shyam, S. R. Sahoo, and S. Anand. Quality-index based distributed secondary controller for a low-voltage dc microgrid. *IEEE Transactions on Industrial Electronics*, 65(9):7004–7014, 2018.

[150] S. Trip, M. Cucuzzella, X. Cheng, and J. Scherpen. Distributed averaging control for voltage regulation and current sharing in dc microgrids. *IEEE Control Systems Letters*, 3(1):174–179, 2019.

[151] Shankar Abhinav, Hamidreza Modares, Frank L. Lewis, and Ali Davoudi. Resilient Cooperative Control of DC Microgrids. *IEEE Transactions on Smart Grid*, 10(1):1083–1085, 2019.

[152] F. Guo, C. Wen, , J. Mao, and Song Yong-Duan Song. Distributed economic dispatch for smart grids with random wind power. *IEEE Transactions on Smart Grid*, 7(3):1572–1583, 2015.

[153] Z. Wang, W. Wu, and B. Zhang. A distributed control method with minimum generation cost for dc microgrids. *IEEE Transactions on Energy Conversion*, 31(4):1462–1470, 2016.

[154] Q. Li, C. Peng, M. Wang, M. Chen, J. M. Guerrero, and D. Abbott. Distributed secondary control and management of islanded microgrids via dynamic weights. *IEEE Transactions on Smart Grid*, 10(2):2196–2207, 2019.

[155] G. Binetti, A. Davoudi, F. L. Lewis, D. Naso, and B. Turchiano. Delay effects on consensus-based distributed economic dispatch algorithm in microgrid. *IEEE Transactions on Power Systems*, 33(1):602 – 612, 2018.

[156] Mohamed Zaery, Panbao Wang, Wei Wang, and Dianguo Xu. Distributed Finite-Time Coordination Control system for Economical Operation of Islanded DC Microgrids. *2019 22nd International Conference on Electrical Machines and Systems, ICEMS 2019*, 2019.

[157] Y. Xu and H. Sun. Distributed finite-time convergence control of an islanded low-voltage ac microgrid. *IEEE Transactions on Power Systems*, 33(3):2339–2348, 2018.

[158] Z. Deng, Y. Xu, H. Sun, and X. Shen. Distributed, bounded and finite-time convergence secondary frequency control in an autonomous microgrid. *IEEE Transactions on Smart Grid*, 10(3):2776–2788, 2019.

[159] Michele Cucuzzella, Sebastian Trip, Claudio De Persis, Xiaodong Cheng, Antonella Ferrara, and Arjan Van Der Schaft. A Robust Consensus Algorithm for Current Sharing and Voltage Regulation in DC Microgrids. *IEEE Transactions on Control Systems Technology*, 27(4):1583–1595, 2019.

[160] N. M. Dehkordi, N. Sadati, and M. Hamzeh. Distributed robust finite-time secondary voltage and frequency control of islanded microgrids. *IEEE Transactions on Power Systems*, 32(5):3648–3659, 2017.

[161] Yinliang Xu. Robust Finite-Time Control for Autonomous Operation of an Inverter-Based Microgrid. *IEEE Transactions on Industrial Informatics*, 13(5):2717–2725, 2017.

[162] Alessandro Pilloni, Alessandro Pisano, and Elio Usai. Robust Finite-Time Frequency and Voltage Restoration of Inverter-Based Microgrids via Sliding-Mode Cooperative Control. *IEEE Transactions on Industrial Electronics*, 65(1):907–917, 2018.

[163] Michele Cucuzzella, Sebastian Trip, Antonella Ferrara, and Jacquelien Scherpen. Cooperative Voltage Control in AC Microgrids. *Proceedings of the IEEE Conference on Decision and Control*, 2018-December(Cdc):6723–6728, 2019.

[164] Sonam Shrivastava and Bidyadhar Subudhi. Robust Finite-Time Secondary Control Scheme for Islanded Microgrid with Nonlinear Dynamics and Uncertain Disturbances. *2019 IEEE 5th International Conference for Convergence in Technology, I2CT 2019*, pages 1–6, 2019.

[165] Xiaoxiao Meng, Niancheng Zhou, Qianggang Wang, and Josep M. Guerrero. A Nonlinear, Bounded and Lipchitz Continuous Distributed Active Power Sharing Control Method for Islanded AC Microgrids. *IEEE Access*, 7:36843–36853, 2019.

[166] Pudong Ge, Xiaobo Dou, Xiangjun Quan, Qinran Hu, Wanxing Sheng, Zaijun Wu, and Wei Gu. Extended-State-Observer-Based Distributed Robust Secondary Voltage and Frequency Control for an Autonomous Microgrid. *IEEE Transactions on Sustainable Energy*, 11(1):195–205, 2020.

[167] Xueqiang Shen, Haiqing Wang, Dezhen Zhang, Jian Li, Renshu Wang, and Qingyu Su. Distributed Finite-Time Secondary Voltage Restoration of Droop-Controlled Islanded Microgrids. *IEEE Access*, pages 1–1, 2020.

[168] Wendong Feng, Jian Yang, Zhangjie Liu, Hui Wang, Mei Su, and Xin Zhang. A unified distributed control scheme on cost optimization for hybrid ac/dc microgrid. In *2018 IEEE 4th Southern Power Electronics Conference (SPEC)*, pages 1–6, 2018.

[169] G. Chen, F. Lewis, E. Ning Feng, and Y. Song. Distributed optimal active power control of multiple generation systems. *IEEE Transactions on Industrial Electronics*, 62(11):7079 – 7090, May 2015.

[170] Enrique Espina, Roberto Cardenas-Dobson, Mauricio Espinoza, Claudio Burgos-Mellado, and Doris Saez. Cooperative regulation of imbalances in three-phase four-wire microgrids using single-phase droop control and secondary control algorithms. *IEEE Transactions on Power Electronics*, 2019.

[171] Manuel Martinez Gomez, Claudio Burgos Mellado, and Roberto Cardenas Dobson. Distributed control for a cost-based droop-free microgrid. In *2020 IEEE 21st Workshop on Control and Modeling for Power Electronics (COMPEL)*, pages 1–7, 2020.

[172] Manuel Martinez-Gomez, Roberto Cardenas, Alex Navas, and Erwin Rute. A Multi-Objective Distributed Finite-Time Optimal Dispatch of Hybrid Microgrids. *46th Annu. Conf. Ind. Electron. Soc. (IECON)*, pages 3755–3760, 2020.

[173] V. V.S.N. Murty and Ashwani Kumar. Multi-objective energy management in microgrids with hybrid energy sources and battery energy storage systems. *Prot Control Mod Power Syst*, 5(2):1–20, Jan 2020.

[174] Hossein Moradian and Solmaz S. Kia. On robustness analysis of a dynamic average consensus algorithm to communication delay. *IEEE Trans. Control. Netw. Syst.*, 6:633–641, 2019.

[175] Mengxuan Shi, Xia Chen, Jianyu Zhou, Yin Chen, Jinyu Wen, and Haibo He. Pi-consensus based distributed control of ac microgrids. *IEEE Transactions on Power Systems*, 35:2268–2278, 5 2020.

[176] Jae Won Chang, Gyu Sub Lee, Seung Il Moon, and Pyeong Ik Hwang. A novel distributed control method for interlinking converters in an islanded hybrid ac/dc microgrid. *IEEE Trans. Smart Grid*, 12:3765–3779, 2021.

[177] Claudio Burgos-Mellado, Felipe Donoso, Tomislav Dragičević, Roberto Cárdenas-Dobson, Patrick Wheeler, Jon Clare, and Alan Watson. Cyber-attacks in modular multilevel converters. *IEEE Transactions on Power Electronics*, 37(7):8488–8501, 2022.

[178] Yuhua Du, Hao Tu, Hui Yu, and Srdjan Lukic. Accurate consensus-based distributed averaging with variable time delay in support of distributed secondary control algorithms. *IEEE Trans. Smart Grid*, 11(4):2918–2928, 2020.

[179] Johannes Schiffer, Thomas Seel, Jörg Raisch, and Tevfik Sezi. Voltage stability and reactive power sharing in inverter-based microgrids with consensus-based distributed voltage control. *IEEE Transactions on Control Systems Technology*, 24(1):96–109, 2016.

[180] Yang Han, Ke Zhang, Hong Li, Ernane Antônio Alves Coelho, and Josep M. Guerrero. Mas-based distributed coordinated control and optimization in microgrid and microgrid clusters: A comprehensive overview. *IEEE Trans. Power Electron.*, 33(8):6488–6508, 2018.

[181] Yeliz Yoldaş, Ahmet Önen, S.M. Muyeen, Athanasios V. Vasilakos, and İrfan Alan. Enhancing smart grid with microgrids: Challenges and opportunities. *Renew. Sust. Energ. Rev.*, 72:205–214, 2017.

[182] Seyed Ali Arefifar, Martin Ordonez, and Yasser Abdel-Rady I. Mohamed. Energy management in multi-microgrid systems—development and assessment. *IEEE Transactions on Power Systems*, 32(2):910–922, 2017.

[183] Ui-Min Choi, Frede Blaabjerg, and Kyo-Beum Lee. Study and handling methods of power igbt module failures in power electronic converter systems. *IEEE Transactions on Power Electronics*, 30(5):2517–2533, 2015.

[184] Alvaro Carreno, Marcelo Perez, Carlos Baier, Alex Huang, Sanjay Rajendran, and Mariusz Malinowski. Configurations, power topologies and applications of hybrid distribution transformers. *Energies*, 14(5), 2021.

[185] Shunwei Zheng, Kai Liao, Jianwei Yang, Zhengyou He, and Xiaofei Sun. A novel bilayer coordinated control scheme for global autonomous economic operation of islanded hybrid ac/dc microgrids. *IET Renewable Power Generation*, 15(12):2726–2739, 2021.

[186] Zhongwen Li, Zhiping Cheng, Jikai Si, and Shuhui Li. Distributed event-triggered hierarchical control to improve economic operation of hybrid ac/dc microgrids. *IEEE Transactions on Power Systems*, 37(5):3653–3668, 2022.

[187] Enrique Espina, Roberto J. Cárdenas-Dobson, John W. Simpson-Porco, Mehrdad Kazerani, and Doris Sáez. A consensus-based distributed secondary control optimization strategy for hybrid microgrids. *IEEE Transactions on Smart Grid*, 14(6):4242–4255, 2023.

[188] Jae-Won Chang, Suyong Chae, and Gyu-Sub Lee. Distributed optimal power sharing strategy in an islanded hybrid ac/dc microgrid to improve efficiency. *IEEE Transactions on Power Delivery*, 38(1):724–737, 2023.

[189] Erwin Rute-Luengo, Alex Navas-Fonseca, Juan S. Gómez, Enrique Espina, Claudio Burgos-Mellado, Doris Sáez, Mark Sumner, and Diego Muñoz-Carpintero. Distributed model-based predictive secondary control for hybrid ac/dc microgrids. *IEEE Journal*

of Emerging and Selected Topics in Power Electronics, 11(1):627–642, 2023.

[190] Alex Navas-Fonseca, Claudio Burgos-Mellado, Juan S. Gómez, Enrique Espina, Jacqueline Llanos, Doris Sáez, Mark Sumner, and Daniel E. Olivares. Distributed predictive secondary control with soft constraints for optimal dispatch in hybrid ac/dc microgrids. *IEEE Transactions on Smart Grid*, 14(6):4204–4218, 2023.

[191] Hongjun Wang, Wanfeng Li, Youjun Yue, and Hui Zhao. Distributed economic control for ac/dc hybrid microgrid. *Electronics*, 11(1), 2022.

[192] Hirofumi Akagi, Edson Hirokazu Watanabe, and Maurício Aredes. *Instantaneous Power Theory and Applications to Power Conditioning*. John Wiley & Sons, Inc., Hoboken, NJ, USA, feb 2017.

[193] Lin Xiao, Stephen Boyd, and Sanjay Lall. A Scheme for robust distributed sensor fusion based on average consensus. *2005 4th International Symposium on Information Processing in Sensor Networks, IPSN 2005*, 2005(C):63–70, 2005.

[194] Wassim M. Haddad and Andrea L'Afflitto. Finite-Time Stabilization and Optimal Feedback Control. *IEEE Transactions on Automatic Control*, 61(4):1069–1074, 2016.

[195] F. Guo, C. Wen, J. Mao, and Y. Song. Distributed secondary voltage and frequency restoration control of droop-controlled inverter-based microgrids. *IEEE Transactions on Industrial Electronics*, 62(7):4355–4364, 2015.

[196] Xiao Feng and Wang Long. Reaching agreement in finite time via continuous local state feedback. *Proceedings of the 26th Chinese Control Conference, CCC 2007*, pages 711–715, 2007.

[197] Philip Hartman. *Ordinary Differential Equations*. Society for Industrial and Applied Mathematics, Switzerland: Birkhäuser, 2 edition, 1987.

[198] Josep M. Guerrero, Luis García de Vicuna, José Matas, Miguel Castilla, and Jaume Miret. A wireless controller to enhance dynamic performance of parallel inverters in distributed generation systems. *IEEE Trans. Power Electron.*, 19(5):1205–1213, 2004.

[199] Adam Milczarek, Mariusz Malinowski, and Josep M. Guerrero. Reactive power management in islanded microgrid—proportional power sharing in hierarchical droop control. *IEEE Transactions on Smart Grid*, 6(4):1631–1638, 2015.

[200] University of Chile. Microgrids Control Laboratory, [Online]. Available: http://microgrids.ing.uchile.cl.

[201] Triphase. Triphase: Power Conversion Solutions for Test and Prototyping, [Online]. Available: https://triphase.com.

Annexes

Annex A

Extended abstract

This work focuses on developing a distributed control strategy that guarantees optimal and stable operation of multiple interconnected AC/DC hybrid microgrids. The strategy's application focuses on the isolated operation of low-voltage microgrids with distributed generators (DGs) based on renewable energy sources with power converters for interconnection and control. For the interconnection between microgrids, interlinking converters (ILCs) are used. The studied system is divided into parts in order to facilitate the analysis of the control proposals, among them are: (i) AC/DC microgrid with an ILC, (ii) AC/DC micro-grid with a cluster of multiple ILCs, and (iii) multi-microgrid AC/DC with clusters of ILCs.

The proposed control scheme is distributed and cooperative and is implemented in the ILCs. This scheme is designed to be compatible with the actions of secondary and tertiary control (economic dispatch) of the adjacent DGs. Each controller incorporates finite-time consensus algorithms to improve transient states; in addition, they use marginal generation cost variables. Additionally, multipurpose controller variants are proposed for each ILC with the ability to incorporate control actions that safeguard the saturated operation of microgrids, balance the power between ILCs in the same cluster, and avoid the saturated operation of clusters of ILCs.

The contributions of this doctoral thesis can be summarised as follows: (i) the formulation of a multi-objective strategy for hybrid AC/DC microgrids and AC/DC multi-microgrids that have clusters of ILCs. The formulation considers as an objective function the combination of economic dispatch, power balance within a cluster of ILCs, and penalty functions to avoid the saturated operation of microgrids and clusters of ILCs; (ii) the design of cooperative distributed controllers for the ILCs based on the incremental cost, average power of the microgrids, and average power of the ILC cluster; (iii) the inclusion of improvements for convergence through the tuning of finite-time algorithms, which allow economic dispatch to be executed on a time scale equivalent to that of secondary control; (iv) the development of an anti-windup method to reduce the effect of delays in communication links for a moving average consensus algorithm; (v) the experimental development of part of an AC/DC hybrid microgrid test bench prototype.

The experimental and simulation results show an adequate response of the proposed multi-objective controller, allowing global optimal dispatch in AC/DC microgrids and AC/DC multi-microgrids while taking care not to overload DGs, ILCs, subgrids, and clusters of ILCs. The simultaneous operation of the control actions of the proposed objectives is possible due to the control parameters designed to adjust the prioritisation. Thanks to the incorporation of anti-windup, steady-state errors can be reduced, and thus it is possible to operate against considerable time delays.

Annex B

Obtention of linearised relationships for the power control droop

B.1 AC Microgrid

For the AC MGs, the droop equations (2.1) are obtained by a power flow analysis from a DG connected to an AC bus bar of an MG [52]. Figure B.1 presents the unilinear diagram of the equivalent circuit, where the voltage reference $V_{com}\angle 0$ is assumed for the AC bus and that the output impedance of the converter and the transmission line are a single equivalent impedance Z.

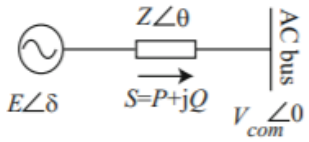

Figure B.1: Simplified diagram of a converter connected to an AC MG.

With the above, the power components are:

$$\begin{cases} P = \frac{V_{\text{com}}E}{Z}\cos(\theta-\delta) - \frac{V_{\text{com}}^2}{Z}\cos(\theta) \\ Q = \frac{V_{\text{com}}E}{Z}\sin(\theta-\delta) - \frac{V_{\text{com}}^2}{Z}\sin(\theta) \end{cases} . \tag{B.1}$$

If the effective line impedance $Z\angle\theta$ is assumed to be purely inductive, $\theta = 90°$, then (B.1) can be reduced to the relationships: $P = \frac{V_{\text{com}}E\sin(\delta)}{Z}$ and $Q = \frac{V_{\text{com}}E\cos(\delta)-V_{\text{com}}^2}{Z}$. Then if the phase difference between the converter's output and the AC bus, δ, is small enough, then $\sin(\delta) \approx \delta$ and $\cos(\delta) \approx 1$ and the relation (2.1) can be obtained.

B.2 DC Microgrid

For the DC MGs, the power droop equation of (2.2) results from the active power load flow of Fig. B.1 but considering a resistive transmission line. Alternatively, a simple derivation comes from the instantaneous power given by

$$p(t) = e(t)\, i(t) \ , \tag{B.2}$$

where $e(t)$ and $i(t)$ are the instantaneous measured voltage and current. From the conventional cascade control structure applied by the voltage-source converters, it can be assume a constant current $i(t) = I$ seen by the voltage loop. Thus, in the Laplace domain, the following relation emerges

$$E = m\, P \ , \tag{B.3}$$

where $m = 1/I$. Since there exist a linear relation between voltage and power, the coefficient m can be adjust to regulate the power-sharing ratio.

B.3 Power measurement for droop control

For DC MGs, most authors prefer to use the current-base droop curve of (2.2) due to its simplicity and accuracy. However, power-based droop is also applied in DC MGs and the power calculation is given by:

$$P_f = \frac{\omega_c}{s + \omega_c} P \ \text{ , with } \ P = EI \ , \tag{B.4}$$

where ω_c is the filter bandwidth, E and I are the converter output voltage and current, respectively.

For AC MGs, a common approach to calculate the power is through the instantaneous power theory [35, 192], resulting in the equations:

$$\begin{aligned} P_f &= \frac{\omega_c}{s + \omega_c} P \ \text{ , with } \ P = \vec{I}_{dq0} \odot \vec{E}_{dq0} = E_d I_d + E_q I_q \ , \\ Q_f &= \frac{\omega_c}{s + \omega_c} Q \ \text{ , with } \ Q = \vec{I}_{dq0} \otimes \vec{E}_{dq0} = E_q I_d - E_d I_q \ , \end{aligned} \tag{B.5}$$

where the vectors $\vec{E}_{dq0}$ and $\vec{I}_{dq0}$ are referred in a rotating reference frame coming from the application of Clarke and Park transformations [35]. The expressions shown in (B.5) are valid for a unbalanced three-phase AC MG when the zero component is considered.

Annex C

Fundamentals of consensus protocols

C.1 Graph theory

The communication topology between agents in a MAS can be represented by a communication graph [15, 69, 74]. This kind of representation allows the stability to be studied by conventional system theory tools. The graph can be expressed as $G = (V, E, A)$, where $V = \{v_1, v_2, \ldots, n\}$ represent the nodes (or DGs); $E = \{e_{ij} = (v_i, v_j)\}/E \subset V \times V$ denotes the communications links; $A = [a_{ij}]_{n\times n}/(i, j \in V)$ is the adjacency matrix whose entry a_{ij} stands for a connection weight. The relationship $(v_i, v_j) \in E \Leftrightarrow a_{ij} > 0$ implies that nodes "i" and "j" can communicate each other; otherwise, $a_{ij} = 0$. The set of neighbours of the i-th node is given by $\mathcal{N}_i = \{(i, j) \in E\}$ where j are DGs with communication links.

Define $L = D - A$ as the graph Laplacian matrix with $D = \text{diag}\{d_1, d_2, \ldots, d_n\} \in \mathbb{R}^{n\times n}$ called as in-degree matrix, where $d_i = \sum_{j=1}^{n} a_{ij}$ is the weighted in-degree of node i (that is the i-th row sum of matrix A). The Laplacian matrix L has all rows sums equal to zero. The graph G is called balanced if its Laplacian matrix L meets $1_n^T L = 0$ (all columns sums equal to zero). A balanced graph implies a bidirectional flow of information between DGs.

A necessary condition for stability is that A matrix has a spanning tree, i.e it exists a directed path from one node to any other node in the graph [15]. Because the stability and convergence of the system states depends of the communication topology, methods have been developed to optimise the adjacency matrix [193], coupling gains [194, 195] and control protocol structure [75, 132].

C.2 Linear consensus protocols

First-Order Consensus. Considering a single-integrator dynamic system where $x_i \in \mathbb{R}$ denote some variable of interest (state) and u_i is the controller input, the first-order state-space representation is given by:

$$\dot{x}_i = u_i \ . \tag{C.1}$$

From (C.1), it is said that the agents achieve a *consensus* of the states x_i if $x_i(t) - x_j(t) \to 0$ as $t \to \infty, \forall\, i, j \in N_i$. The consensus can be achieved via the following algorithm (protocol) [15, 69, 74]:

$$\dot{x}_i = -\sum_{j \in \mathcal{N}_i} a_{ij} \left(x_i - x_j\right) \ , \tag{C.2}$$

which is distributed according to the topology of the communication network. The consensus is guarantee if and only if the Laplacian matrix has a spanning tree, and the consensus value is given by:

$$\bar{x} = \frac{1}{N} \sum_{i=1}^{N} x_i(0) \ . \tag{C.3}$$

It is worth noting that the protocol (C.2) achieve the consensus asymptotically with a time-constant $\tau = 1/\lambda_{\text{Fiedler}}$, where λ_{Fiedler} is the second eigenvalue of the Laplacian matrix [15].

Second-Order Consensus. The state-space representation of the second-order (or double-integrator) system is given by:

$$\begin{aligned} \dot{x}_i &= v_i \ , \\ \dot{v}_i &= u_i \ . \end{aligned} \tag{C.4}$$

From (C.4), the protocol u_i is represented by the following equation [15]:

$$u_i = c \sum_{j \in N_i} a_{ij} \left(x_j - x_i\right) + c\gamma \sum_{j \in N_i} a_{ij} \left(v_j - v_i\right) \ , \tag{C.5}$$

where $c > 0$ is the coupling gain that gives the overall convergence speed to the system, and γ is a damping coefficient to give greater weight to the rate-change consensus. The consensus is guaranteed to $\gamma > 0$ as long as the Laplacian matrix is undirected. The final consensus values are given by:

$$\bar{x} = \frac{1}{N} \sum_{i=1}^{N} x_i(0) + t\, \frac{1}{N} \sum_{i=1}^{N} v_i(0) \ . \tag{C.6}$$

For initial values $v_i(0) = 0$ (a reasonable assumption), the rate-change consensus tends to zero and the steady-state consensus value $\bar{x}$ is identical to the first-order consensus, but with a modified dynamic behaviour. This structure can be interpreted as a variant of the classical proportional-derivative (PD) controller [15].

Annex D

Finite-time convergence and stability analysis

D.1 Definitions and lemmas

In order to develop the stability analysis of the finite-time controllers, the following definitions and lemmas are introduced [82].

Definitions:

Infinity vector norm: It is defined as $\|\vec{x}\|_\infty = \max\left(|x_1|, |x_2|, \ldots, |x_n|\right) = \max_{i\in\{1,\ldots,n\}} |x_i|$, where $\boldsymbol{x} = (x_1, x_2, \ldots, x_n)$ is a vector space.

Right continuity: A function f and a real number c are considered such that f is defined in c and not to the immediate right of c. F is said to be continuous on the right in c if the right limit of f in c exists and is equal to $f(c)$, that is, $\lim_{x\to c^+} f(x) = f(c)$.

Unique linear combination subspace: We consider the vector $\mathbf{1} = [1, 1, \ldots, 1]^T \in \mathbb{R}^n$, then the unique linear combination subspace is defined by $\text{span}(\mathbf{1}) = \{\boldsymbol{\xi} \in \mathbb{R}^n : \boldsymbol{\xi} = r\mathbf{1}, r \in \mathbb{R}\}$.

Lemmas:

Lemma 1 (from [82]) *Under a consensus protocol u_i, the set of equilibrium points of the differential equation $\dot{x}_i = u_i$ is* $\text{span}(\mathbf{1})$*, provided that the graph, $\mathcal{G}$, has a spanning tree.*

Lemma 2 (from [76]) *Provided the Laplacian matrix of the graph $\mathcal{G}$ is positive semi-defined, it is fulfilled the relation $\boldsymbol{\xi}^T L\, \boldsymbol{\xi} = (1/2)\sum_{i,j=1}^{n} a_{ij}\left(\xi_j - \xi_i\right)^2$, for any $\boldsymbol{\xi} = [\xi_1, \xi_2, \ldots, \xi_n]^T \in \mathbb{R}^n$.*

Furthermore, the second eigenvalue of the Laplacian matrix is $\lambda_2 = \min_{\xi \notin 0} \boldsymbol{\xi}^T L\, \boldsymbol{\xi} / \boldsymbol{\xi}^T \boldsymbol{\xi}$*, and if* $\mathbf{1}^T \boldsymbol{\xi} = 0$*, then* $\boldsymbol{\xi}^T L\, \boldsymbol{\xi} \geq \lambda_2(L) \boldsymbol{\xi}^T \boldsymbol{\xi}$.

Lemma 3 (from [196]) *For any non-negative real numbers* $\xi_1, \ldots, \xi_N$ *and* $0 < p < 1$*, the inequality* $\sum_{i=1}^{N} \xi_i^p \geq \left(\sum_{i=1}^{N} \xi_i \right)^p$ *holds.*

Lemma 4 (from [86]) *Suppose that a function* $V(t) : [0, \infty) \to [0, \infty)$ *is differentiable (the derivative of V(t) at 0 is in fact its right derivative) and* $\dot{V}(t) \leq -K \left(V(t)\right)^{\alpha}$*, where* $K > 0$ *and* $0 < \alpha < 1$*. Then* $V(t) = 0,\ \forall\ t \geq T$.

D.2 Stability of finite-time protocol

It is considered a first-order multi-agent system implementing the protocol in (2.15)

$$u_i = \sum_{j \in \mathcal{N}_i} a_{ij} \text{sig}\, |x_j - x_i|^{\alpha_i} \tag{D.1}$$

The communications topology is assumed to be time-invariant with a bidirectional flow of information between agents ($a_{ij} = a_{ji}\ \forall i, j \in \mathcal{I}_n$). The protocol (D.1) will reach consensus in finite time $t^* \leq V(0)^{1-\alpha_i} / (K(1-\alpha_i))$ for all $t \geq t^*$, where V(t) is a candidate function of Lyapunov.

Remark: Providing $\alpha_i > 0$, $\text{sig}(r)^{\alpha}$ is a continuous function with respect to r, which leads to the continuity of the protocol in (D.1).

Property 1 (from [197]). If the communication topology is time invariant, then when applying the protocol (D.1) the differential equations of the system are continuous to the right, and there is at least one solution in [0, ∞) for any initial state $x(0)$. Furthermore, $\|\boldsymbol{x}(t)\|_\infty$ is non-increasing and holds $\|\boldsymbol{x}(t)\|_\infty \leq \|\boldsymbol{x}(0)\|_\infty$ for all $t \geq 0$.

Proof. Based on [82], the protocol (D.1) is equivalent to:

$$\sum_{i=1}^{n} \dot{x}_i(t) = 0 \tag{D.2}$$

Let $x^* = (1/n) \sum_{i=1}^{n} x_i(t)$ be the average value of the states, the following relationship is defined:

$$x_i(t) = x^* + \delta_i(t) \tag{D.3}$$

with $\delta(t) = [\delta_1(t), \delta_2(t), \ldots, \delta_n(t)]^T$ referring the disagreement vector. It is obtained that when updating the state $x_i(t)$ of (D.3) according to (D.2), x^* is time invariant and $\dot{\delta}_i(t) = \dot{x}_i(t)$.

Then, let a function $V(t)$: $[0,\infty) \to [0,\infty)$ be a Lyapunov candidate defined as

$$V_1(\delta(t)) = \frac{1}{2}\sum_{i=1}^{n} \delta_i^2(t)$$

which is non-negative over all its domain and codomain. The function $V(t)$ is differentiable and its time derivative is

$$\begin{aligned}
\frac{dV_1(t)}{dt} &= \sum_{i=1}^{n} \delta_i(t)\dot{\delta}_i(t) \\
&= \sum_{i=1}^{n} \delta_i(t) \sum_{j=1}^{n} a_{ij} \operatorname{sig}(x_j - x_i)^{\alpha_i} \\
&= \sum_{i=1}^{n} \delta_i(t) \sum_{j=1}^{n} a_{ij} \operatorname{sig}(\delta_j - \delta_i)^{\alpha_i} \\
&= \sum_{i=1}^{n}\sum_{j=1}^{n} \frac{1}{2}(\delta_i - \delta_j)\, a_{ij} \operatorname{sig}(\delta_j - \delta_i)^{\alpha_i} \\
&= \frac{1}{2}\sum_{i,j=1}^{n} a_{ij}(\delta_i - \delta_j) \operatorname{sig}(\delta_j - \delta_i)^{\alpha_i} - \frac{1}{2}\sum_{i,j=1}^{n} \left(a_{ij}^{\frac{2}{1+\alpha_0}} \left((\delta_j - \delta_i)^2\right)^{\frac{1+\alpha_i}{1+\alpha_0}} \right)^{\frac{1+\alpha_0}{2}}
\end{aligned}$$

Recalling $0 < \alpha_i < 1$, the above was algebraically arranged using the inequality $1/2 < (1+\alpha_0)/2 < 1$, where $\alpha_0 = \max(\alpha_i)$.

Assuming $V_1(t) \neq 0$, we have through **Lemma 3** the following expression:

$$\frac{dV_1(t)}{dt} \leq -\frac{1}{2}\left(\frac{\sum_{i,j=1}^{n} a_{ij}^{\frac{2}{1+\alpha_0}} \left((\delta_i - \delta_j)^2\right)^{\frac{1+\alpha_i}{1+\alpha_0}}}{\sum_{i,j=1}^{n} a_{ij}^{\frac{2}{1+\alpha_0}} (\delta_i - \delta_j)^2} \cdot \frac{\sum_{i,j=1}^{n} a_{ij}^{\frac{2}{1+\alpha_0}} (\delta_i - \delta_j)^2}{V_1(t)} V_1(t) \right)^{\frac{1+\alpha_0}{2}} \tag{D.4}$$

The lower limits of the first two terms are then estimated:

For the first term of (D.4), given **Lemma 1** and $\max_i x_i - \min_i x_i$ non-growing, then for any $i, j \in \mathcal{I}_n$ it is had $|\delta_i(t) - \delta_j(t)| \leq \max_k x_k(t) - \min_k x_k(t) \leq \max_k x_k(0) - \min_k x_k(0)$.

Let

$$K_1 = \frac{1}{\sum_{i,j=1}^{n} a_{ij}^{\frac{2}{1+\alpha_0}}} \cdot \min_{\substack{i,j\in\mathcal{I}_n \\ a_{ij}\neq 0}} a_{ij}^{\frac{2}{1+\alpha_0}} \left(\max_k x_k(0) - \min_k x_k(0) \right)^{2\left(\frac{1+\alpha_i}{1+\alpha_0} - 1\right)}$$

be a positive value, and considering $(i_0, j_0) = \arg\max_{i,j\in\mathcal{I}_n} (\delta_i - \delta_j)^2$, and the relation $\left(\frac{(1+\alpha_i)}{1+\alpha_0} - 1\right) \leq 0$, it is had:

$$K_1 \leq \frac{a_{i_0 j_0}^{\frac{2}{1+\alpha_0}} \left((\delta_{i_0} - \delta_{j_0})^2\right)^{\frac{1+\alpha_{i_0}}{1+\alpha_0}}}{\left(\sum_{i,j=1}^{n} a_{ij}^{\frac{1}{1+\alpha_0}}\right)(\delta_{i_0} - \delta_{j_0})^2} \leq \frac{\sum_{i,j=1}^{n} a_{ij}^{\frac{2}{1+\alpha_0}} \left((\delta_i - \delta_j)^2\right)^{\frac{1+\alpha_i}{1+\alpha_0}}}{\sum_{i,j=1}^{n} a_{ij}^{\frac{2}{1+\alpha_0}} (\delta_i - \delta_j)^2} \tag{D.5}$$

For the second term of (D.4), **Property 1** is used. It is denoted $B = \left[a_{ij}^{2/(1+\alpha_0)}\right] \in \mathbb{R}^{n\times n}$, with what it is had $\sum_{i,j=1}^{n} a_{ij}^{\frac{2}{1+\alpha_0}} (\delta_i - \delta_j)^2 = 2\boldsymbol{\delta}^T L(\boldsymbol{B})\boldsymbol{\delta}$ (noting $\delta \perp \mathbf{1}$). Then:

$$\frac{\sum_{i,j=1}^{n} a_{ij}^{\frac{2}{1+\alpha_0}} (\delta_i - \delta_j)^2}{V_1(t)} = \frac{2\boldsymbol{\delta}^T L(\boldsymbol{B})\boldsymbol{\delta}}{\frac{1}{2}\boldsymbol{\delta}^T\boldsymbol{\delta}} \geq 4\lambda_2(L(\boldsymbol{B})) > 0 \tag{D.6}$$

where $L(\boldsymbol{B})$ is the Laplacian matrix of the graph $\mathcal{G}(\boldsymbol{B})$ and λ_2 is the 2nd eigenvalue of $L(\boldsymbol{B})$.

Therefore, rewriting (D.4) using the lower limits determined in (D.5) and (D.6), it finally results

$$\frac{dV_1(t)}{dt} \leq -\frac{1}{2}\left(4K_1\lambda_2(L(B))\right)^{\frac{1+\alpha_0}{2}} V_1(t)^{\frac{1+\alpha_0}{2}}$$

where it is followed that $V_1(t)$ satisfies the conditions of **Lemma 4**. Also, the final state is x^*, i.e. the average of the initial agent's states. Consequently, $V(t)$ will reach zero at a finite-time $t^* \leq V(0)^{1-\alpha}/(K(1-\alpha))$.

■

Annex E

Numeric verification of steady state errors in dynamic average consensus

For a numerical verification of the performance of dynamic average consensus under time delays (τ), let us assume 5 agents using the protocol:

$$\overline{P}_i(t) = \begin{cases} P_i(t) + \int_0^t \sum_{j=1}^N a_{ij}(\overline{P}_j(0) - \overline{P}_i(t))dx & , \text{ if } 0 < t \leq \tau \ , \\ P_i(t) + \int_0^t \sum_{j=1}^N a_{ij}(\overline{P}_j(t-\tau) - \overline{P}_i(t))dx & , \text{ if } t > \tau \ , \end{cases} \tag{E.1}$$

with $\overline{P}_j(0)$ as initial values $\forall j \in \mathcal{N}$, and the communication matrix using a binary weighting, i.e. $a_{ij} = 1$ when there is communication between agents i and j, and $a_{ij} = 0$ otherwise. Let us assume

$$A = \begin{bmatrix} 0 & 1 & 1 & 0 & 0 \\ 1 & 0 & 1 & 1 & 0 \\ 1 & 1 & 0 & 1 & 1 \\ 0 & 1 & 1 & 0 & 1 \\ 0 & 0 & 1 & 1 & 0 \end{bmatrix} .$$

Then, from (3.43), one has for $0 < t \leq \tau$ the following equations:

$$\begin{aligned} \overline{P}_1(t) &= (1-2)^s \, P_1 \ , \\ \overline{P}_2(t) &= (1-3)^s \, P_2 \ , \\ \overline{P}_3(t) &= (1-4)^s \, P_3 \ , \\ \overline{P}_4(t) &= (1-3)^s \, P_4 \ , \\ \overline{P}_5(t) &= (1-2)^s \, P_5 \ . \end{aligned} \tag{E.2}$$

It can be seen that the values $\overline{P}_i$ will deviate overtime from their local measurements P_i,

violating the required "initial" condition for consensus with the true average value [78, 174, 175]. The algorithm starts to work properly with neighbouring measurements after $t > \tau$. More mathematical developments about this issue were also presented by authors in [175].

Simulations using the previous example are presented next, considering both constant (step) and time-varing (triangular) values of P_i. The frequency of triangular signals is the same for all agents, equal to 0.1 [Hz]. The magnitude of Triangular modulation is 10 for agent # 1, 20 for agent # 2, 30 for agent # 3, 40 for agent # 4 and 50 for agent # 5. The offsets are different for every agent, and they change over time, simulating "load impacts". Details of the offset values are summarised in the next table.

Agent	$0 < t < 20$	$20 < t < 40$	$40 < t < 60$	$60 < t < 80$	$80 < t < 100$
1	40	100	70	-50	100
2	30	130	130	23	130
3	30	120	90	3	120
4	20	150	120	8	150
5	10	170	140	20	170

Table E.1: Offset values ("load impacts") for simulation.

The results of simulations are shown in Fig. E.1 and Fig. E.2 for the base case without communication delays using step and triangular signals, respectively, and in Fig. E.3 and Fig. E.4 for the case with 300 [ms] of constant delays in all of the communication links, with step and triangular references, respectively.

It can be seen from Fig. E.1b that under the step references, the dynamic average consensus can successfully achieve consensus when there is no delay in the communications. However, in Fig. E.3b, the estimated average value is less than half the true average value. A similar behaviour is observed for the comparison between Fig. E.2b and Fig. E.4b. It is worth also noting that in the presence of ramp (or triangular) shapes, the dynamic average consensus presents small deviations between the local estimations of $\overline{P}_i$, which has already been reported in [78]. However, despite the small deviations, the average between the estimations $\overline{P}_i$ is still equal to the true average, at least at the no-delay case (Fig. E.2c).

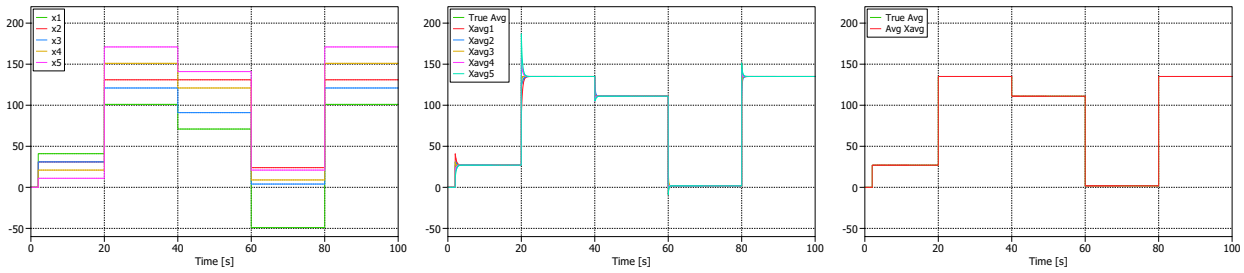

(a) (b) (c)

Figure E.1: Simulation results using step local values and no delays. (a) Local value of agents over time. (b) Local estimated average value of agents over time, also including the true average value. (c) Comparison between true average value and average between the estimated average values.

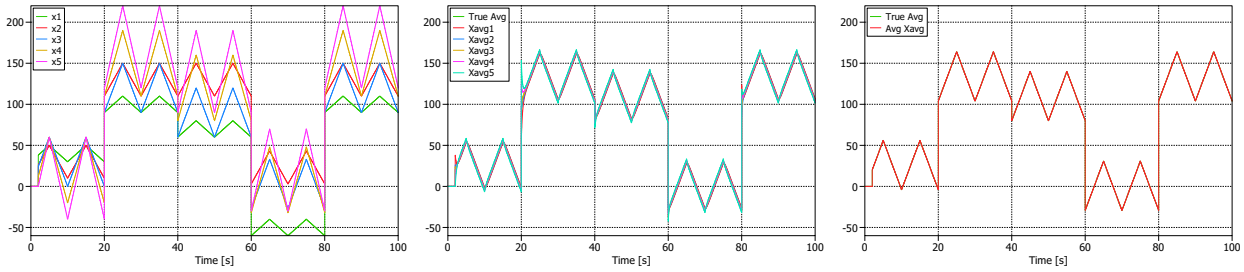

(a) (b) (c)

Figure E.2: Simulation results using triangular local values and no delays. (a) Local value of agents over time. (b) Local estimated average value of agents over time, also including the true average value. (c) Comparison between true average value and average between the estimated average values.

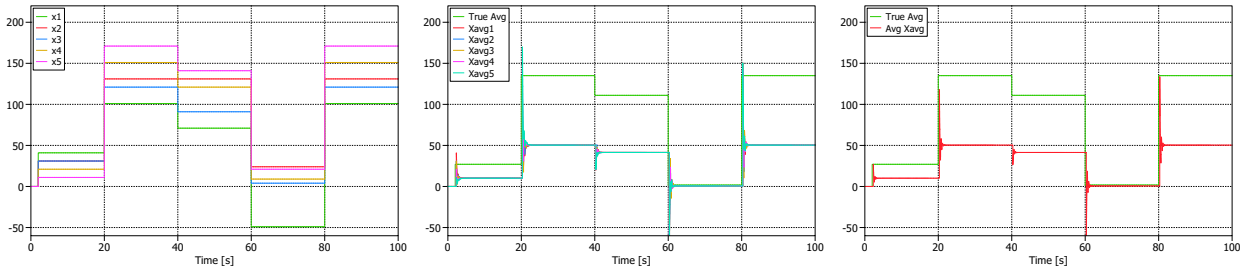

(a) (b) (c)

Figure E.3: Simulation results using step local values and delays of 300 [ms]. (a) Local value of agents over time. (b) Local estimated average value of agents over time, also including the true average value. (c) Comparison between true average value and average between the estimated average values.

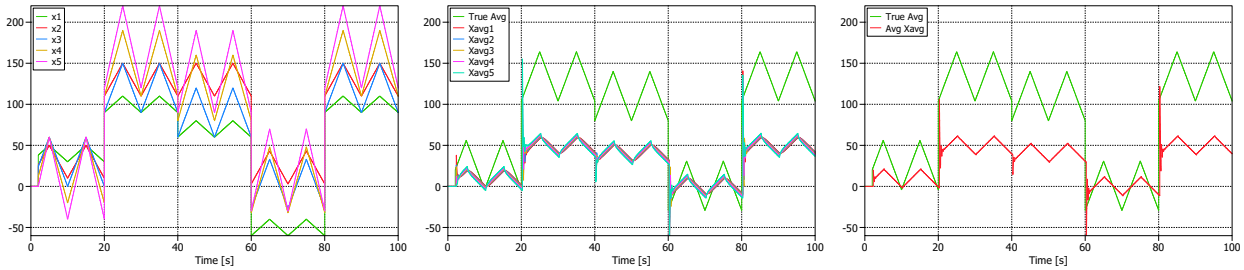

(a) (b) (c)

Figure E.4: Simulation results using triangular local values and delays of 300 [ms]. (a) Local value of agents over time. (b) Local estimated average value of agents over time, also including the true average value. (c) Comparison between true average value and average between the estimated average values.

Annex F

Control scheme for distributed generators

F.1 Distributed cooperative control of DC MGs

This section describes the procedure to obtain a distributed controller for the DC MG that aims for the economic dispatch of power while coping with fast transient dynamics. This controller performs the control action of tertiary and secondary control levels of the hierarchical control structure [51].

Design of a distributed finite-time controller for the economic dispatch in DC MGs

The design begins by choosing a proper control law for the voltage regulation. Based on (2.2), let us consider the voltage reference for the i-th DG unit represented by:

$$E_i^{\text{ref}} = E_{\text{DC}}^* - n^{\text{DC}} P_i + n_d^{\text{DC}} \dot{P}_i + \delta E_i^1 + \delta E_i^2 \ , \tag{F.1}$$

where E_{DC}^* is the MG's nominal voltage and n^{DC} is the droop coefficient. The terms δE_i^1 and δE_i^2 are compensations coming from secondary control that intervene in the voltage dynamics. By assuming that the converter's inner dynamic is fast enough (i.e. $E_i = E_i^{\text{ref}}$ where E_i is the converter output voltage) and that there exists a linear relationship between the converter's voltage and IC [58, 99], the terms δE_i^1 and δE_i^2 of (F.1) can be obtained by combination of a feedback linearisation and consensus protocols [36, 88]. This procedure results in the following set of equations:

$$\begin{aligned} \delta \dot{E}_i^1 &= c_1 \left(E_{\text{DC}}^* - \overline{E}_i \right) \ , \\ \overline{E}_i &= E_i + \int_0^t \left(\textstyle\sum_{j \in \mathcal{N}_i} a_{ij} \ \left(\overline{E}_j - \overline{E}_i \right) \right) d\tau \ , \end{aligned} \tag{F.2}$$

$$\delta \dot{E}_i^2 = c_2 \textstyle\sum_{j \in \mathcal{N}_i} a_{ij} \ (\lambda_j - \lambda_i) \ , \tag{F.3}$$

where λ_i is the local IC, $\overline{E}_j$ is the output average voltage from the j-th DG, and $\{c_1, c_2\} > 0$ are local convergence coefficients The term δE_i^1 is the result of an average voltage observer, which allow to handle the inherent trade-off between voltage and power regulation [106]. In steady-state, the MG achieves an average voltage equals to reference E_{DC}^*. Similarly, the compensation term δE_i^2 is obtained from a consensus but of ICs, which ensures the fulfilment of economic dispatch [63] distributing the power according to the cost coefficients [60]. The IC is measured locally as (2.9); Lagrange multipliers σ_i^+ and σ_i^- are calculated decentralised as in [20].

Additionally, in order to improve the convergence, and thus the transient operation of (F.2)-(F.3), a finite-time protocol is incorporated as in (2.15); A slight modification of the protocol is used in the voltage observer to reduce steady-state errors, i.e. the sig[·] function is inside the summation. Also, the protocols are modified with a proportional integral (PI) structure to correct the tracking error signals from consensus protocols [106], giving the following equations:

$$\left.\begin{aligned} \delta E_i^1 &= k_p^E \left(u_i^E\right) + k_i^E \int_0^t \left(u_i^E\right) d\tau \ , \\ u_i^E &= E_{\text{DC}}^* - \overline{E}_i \ , \\ \overline{E}_i &= E_i + \int_0^t \left(\sum_{j \in \mathcal{N}_i} a_{ij} \ \text{sig}\left[\overline{E}_j - \overline{E}_i\right]^{\nu^1} \right) d\tau \ , \end{aligned} \right\} \begin{array}{c} \text{Average} \\ \text{voltage} \\ \text{regulator} \end{array} \tag{F.4}$$

$$\left.\begin{aligned} \delta E_i^2 &= k_p^\lambda (u_i^\lambda) + k_i^\lambda \int_0^t (u_i^\lambda) d\tau \ , \\ u_i^\lambda &= c_\lambda \ \text{sig} \left[\sum_{j \in \mathcal{N}_i} a_{ij} \left(\lambda_j - \lambda_i\right) \right]^{\nu^2} \ , \end{aligned} \right\} \begin{array}{c} \text{Incremental} \\ \text{cost} \\ \text{regulator} \end{array} \tag{F.5}$$

where $\{k_p^E, k_i^E, k_p^\lambda, k_i^\lambda\} > 0$ are parameters of PI controllers, $\{\nu^1, \nu^2\} \in (0, 1)$ and $c_\lambda > 0$ are convergence speed parameters.

Remark 9 The PI controller structure for the regulators was selected instead of the single integrator used in DAPI [110] due to its flexibility in the design, which is being able to achieve fast response with proper damping. However, stability proofs for PI structure are more complex, and the tuning more challenging because of the number of parameters.

F.2 Distributed cooperative control of AC MGs

Following the same trend as the design for the DC MG, this section will describe the control strategy used by the DGs in the AC MG.

Design of a distributed finite-time controller for the economic dispatch of AC MGs

Conventional frequency and voltage droop equations in (2.1) allow to obtain the control laws that relate the variables of power with the converter-controlled variables (voltage magnitude and frequency). In this subsection, droop dynamics for voltage and frequency are proposed based on distributed control of DGs.

Voltage Loop

Based on the voltage control loop of DC MG, (2.1), [198] and [110], we propose the following droop dynamics:

$$E_{di}^{\text{ref}} = E_{\text{AC}}^{*} - n^{\text{AC}} Q_i + n_d^{\text{AC}} \dot{Q}_i + \delta E_i^1 + \delta E_i^2 \ , \tag{F.6}$$

where E_{di} is the local voltage in the direct axis of a d-q reference frame, E_{AC}^{*} is the MG reference voltage (assuming a leaderless strategy), and n_d^{AC} is a damping coefficient to improve transient dynamics. For the voltage loop, similar to the DC MG, the control effort can be divided into two: compensation for the average voltage (δE_i^1) and for the reactive power (δE_i^2). As in the DC MG formulation, it is assumed that the converter's inner dynamic is fast enough, such that $E_{di} = E_{di}^{\text{ref}}$ where E_{di} is the converter output voltage and E_{di}^{ref} is the reference of the internal voltage controller. Including a finite-time consensus protocol with a PI structure results in the following equations:

$$\left.\begin{aligned} \delta E_i^1 &= k_p^E \left(u_i^E\right) + k_i^E \int_0^t \left(u_i^E\right) d\tau \ , \\ u_i^E &= E_{\text{AC}}^{*} - \overline{E}_i \ , \\ \overline{E}_i &= E_{di} + \int_0^t \left(\sum_{j \in \mathcal{N}_i} a_{ij} \ \text{sig}\left[\overline{E}_j - \overline{E}_i\right]^{\mu^1} \right) d\tau \ , \end{aligned} \right\} \ \begin{array}{c}\text{Average} \\ \text{voltage} \\ \text{regulator}\end{array} \tag{F.7}$$

$$\left.\begin{aligned} \delta E_i^2 &= k_p^Q (u_i^Q) + k_i^Q \int_0^t (u_i^Q) d\tau \ , \\ u_i^Q &= c_Q \sum_{j \in \mathcal{N}_i} a_{ij} \left(\frac{Q_j}{Q_j^{\max}} - \frac{Q_i}{Q_i^{\max}} \right) \ , \end{aligned} \right\} \ \begin{array}{c}\text{Reactive} \\ \text{power} \\ \text{regulator}\end{array} \tag{F.8}$$

where $\overline{E}_i$ and Q_i are the local average voltage and reactive powers of the i-th DG, $k_p^E > 0$ and $k_i^E > 0$ are the parameters of a PI controller whose input is u_i^E, $k_p^Q > 0$ and $k_i^Q > 0$ are the parameters of a PI controller whose input is u_i^Q, $0 < \mu^1 < 1$ is fractional exponent, and $c_Q > 0$ is a convergence speed gain.

Remark 10 The use of reactive power-sharing (in this case in secondary control) could be relaxed (or omitted) to simplify the system's dynamics [171, 199], reducing prioritising the

active power-sharing while reducing the coupling with other control loops, like voltage and frequency restorations.

Frequency Loop

For the frequency loop, based on (2.1), [198] and [110], the following droop dynamics is proposed:

$$\omega_i = \omega^* - m^{\mathrm{AC}} P_i + m_d^{\mathrm{AC}} \dot{P}_i + \delta\omega_i^1 + \delta\omega_i^2 \ , \tag{F.9}$$

where ω_i is the DG's output frequency, ω^* is the MG's frequency reference, and m_d^{AC} is a damping factor to improve transient dynamics. Also, $\delta\omega_i^1$ and $\delta\omega_i^2$ are secondary control compensations for the frequency restoration and disagreement of IC, respectively. The compensations $\delta\omega_i^1$ and $\delta\omega_i^2$ are obtained by:

$$\left.\begin{aligned} \delta\omega_i^1 = c_\omega \int_0^t \left((\omega^* - \omega_i) + \sum_{j\in\mathcal{N}_i} a_{ij} \left(\delta\omega_j^1 - \delta\omega_i^1 \right) \right) , \end{aligned}\right\} \ \text{Frequency regulator} \tag{F.10}$$

$$\left.\begin{aligned} \delta\omega_i^2 = c_\lambda \int_0^t \mathrm{sig} \left(\sum_{j\in\mathcal{N}_i} a_{ij} \left(\lambda_j - \lambda_i \right) \right)^{\mu^2} , \end{aligned}\right\} \ \text{Incremental cost regulator} \tag{F.11}$$

where the parameter $0 < \mu^2 < 1$ is a fractional exponent of the finite-time protocol and $c_\lambda, c_\omega > 0$ are convergence coupling gain. The MG's frequency reference ω^* can be considered coming from a DNO as a tertiary control variable, or in a grid-connected application, ω^* can be obtained through a PLL applied to the grid side. For simplicity, it is assumed that all DGs have access to this reference, i.e. a leaderless synchronisation problem is assumed for the consensus protocols.

F.3 Control strategy and parameters used for DGs in Chapter 3

The control used for experimental setup of DGs in AC MG: $\omega_c^{\mathrm{AC}} = 6.28$, $m^{\mathrm{AC}} = 2.8\text{x}10^{-3}$, $m_d^{\mathrm{AC}} = 0$, μ^1=1, μ^2=1, $c_\omega = 1/0.15$, $c_\lambda^{\mathrm{AC}} = 0.14$, $n^{\mathrm{AC}} = 1.4\text{x}10^{-2}$, n_d^{AC} =0, $k_p^E = 0$, $k_i^E = 47.12$, $c_Q = 12$, $k_p^Q = 0.05$, $k_i^Q = 1.57$. For the DGs in DC MG: ω_c^{DC} =18.85, $m^{\mathrm{DC}} = 3.0\text{x}10^{-3}$, ν^1=1, ν^2=1, $k_p^E = 0$, $k_i^E = 4.71$ $c_\lambda^{\mathrm{DC}} = 400$, $k_p^\lambda = 0.28$, $k_i^\lambda = 0.54$.

The control used for simulation setup of DGs in AC MG: $\omega_c^{\mathrm{AC}} = 6.28$, $m^{\mathrm{AC}} = 2.8\text{x}10^{-3}$, $m_d^{\mathrm{AC}} = 0$, μ^1=1, μ^2=1, $c_\omega = 1/0.15$, $c_\lambda^{\mathrm{AC}} = 9.8$, $n^{\mathrm{AC}} = 1.4\text{x}10^{-2}$, n_d^{AC} =0, $k_p^E = 0.041$, $k_i^E = 47.12$, $c_Q = 9$, $k_p^Q = 0.075$, $k_i^Q = 1.885$. For the DGs in DC MG: ω_c^{DC} =18.85, $m^{\mathrm{DC}} = 3.0\text{x}10^{-3}$, ν^1=1, ν^2=1, $k_p^E = 0.75$, $k_i^E = 4.71$ $c_\lambda^{\mathrm{DC}} = 100$, $k_p^\lambda = 0.28$, $k_i^\lambda = 0.54$.

F.4 Control strategy and parameters used for DGs in Chapter 4

The control used for simulation setup of DGs in AC MG: $\omega_c^{\text{AC}} = 6.28$, $m^{\text{AC}} = 0.94\text{x}10^{-3}$, $m_d^{\text{AC}} = 0.1$, μ^1=1, μ^2=1, $c_\omega = 1/0.15$, $c_\lambda^{\text{AC}} = 0.95$, $n^{\text{AC}} = 1.4\text{x}10^{-2}$, n_d^{AC} =0.1, $k_p^E = 2$, $k_i^E = 37.77$, $c_Q = 8.8$, $k_p^Q = 0.05$, $k_i^Q = 1.04$. For the DGs in DC MG: ω_c^{DC} =18.85, $m_i^{\text{DC}} = 1.6\text{x}10^{-3}$ (for DGs 1 and 2) and $m_i^{\text{DC}} = 1.0\text{x}10^{-3}$ (for DGs 3, 4 and 5), ν^1=1, ν^2=1, $k_p^E = 0.25$, $k_i^E = 4.71$ $c_\lambda^{\text{DC}} = 28.8$, $k_p^\lambda = 0.05$, $k_i^\lambda = 0.94$.

F.5 Control strategy and parameters used for DGs in Chapter 5

The control used for simulation setup of DGs in AC MG: $\omega_c^{\text{AC}} = 6.28$, $m^{\text{AC}} = 0.94\text{x}10^{-3}$, $m_d^{\text{AC}} = 0.01$, μ^1=0.5, μ^2=0.5, $c_\omega = 1/0.15$, $c_\lambda^{\text{AC}} = 0.95$, $n^{\text{AC}} = 1.4\text{x}10^{-2}$, n_d^{AC} =0.1, $k_p^E = 2$, $k_i^E = 37.77$, $c_Q = 8.8$, $k_p^Q = 0.05$, $k_i^Q = 1.04$. For the DGs in DC MG: ω_c^{DC} =18.85, $m_i^{\text{DC}} = 1.6\text{x}10^{-3}$, ν^1=0.5, ν^2=0.5, $k_p^E = 0.25$, $k_i^E = 4.71$ $c_\lambda^{\text{DC}} = 16$, $k_p^\lambda = 0.05$, $k_i^\lambda = 0.94$.

Annex G

Experimental set-up

A validation step of the proposed controllers is performed by experimental prototypes at laboratory level. The prototypes of AC, DC and hybrid AC/DC MGs are being constructed in the MGs Control Laboratory of the University of Chile [200]. Each experimental set-up allows to test the efficiency of the proposed controllers under real conditions.

The prototypes' to be constructed will use racks with the corresponding set-up, i.e. protection system and interconnections between loads and generators. For implement the generators, the equipment available in the laboratory corresponds to integrated embedded systems with power electronics modules constructed and commercialised by *Triphase* company [201].

Triphase units are a scalable, flexible and open platform for rapid prototyping and power-hardware-in-the-loop testing of power system applications. Each Triphase unit compounds an arrangement of converters fed by the main grid including its own measurement and signal processing system. The units account with an embedded target PC, which has a dedicated operating system that enables the real time operation. The interface for developing and running the programs is through *Matlab/Simulink* ©. The communications between modular converters and target PCs is performed by optical fibre with a custom communication protocol (elaborated by the manufacturer).

G.1 Triphase generation units

To feed the rack loads, the converter outputs from Triphase units are used to emulate DGs. The equipment considered for the development of this thesis are the following.

(i) Unit PM15I60F06

The unit schematic is shown in Figure G.1. This unit is configured as an AC/DC back-to-back converter with 1 AC-input and 6 DC-outputs. Its nominal power is 30.0 [kW].

(a) Hardware of PM15I60F06 unit.

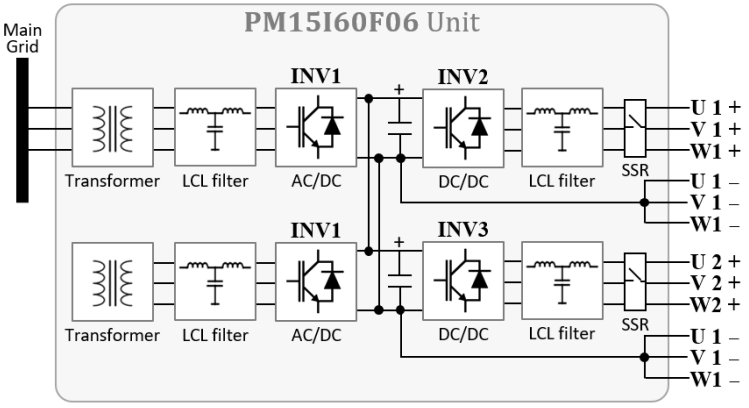

(b) Schematic of PM15I60F06 unit.

Figure G.1: Triphase unit PM15I60F06.

(ii) Unit PM15I30F60

The hardware and topology of this unit are shown in Figure G.2. This unit will be configured as an AC/AC back-to-back converter with 1 AC-input and 2 AC-outputs. Its nominal power is 15.0 [kW].

(a) Hardware of PM15I30F60 unit.

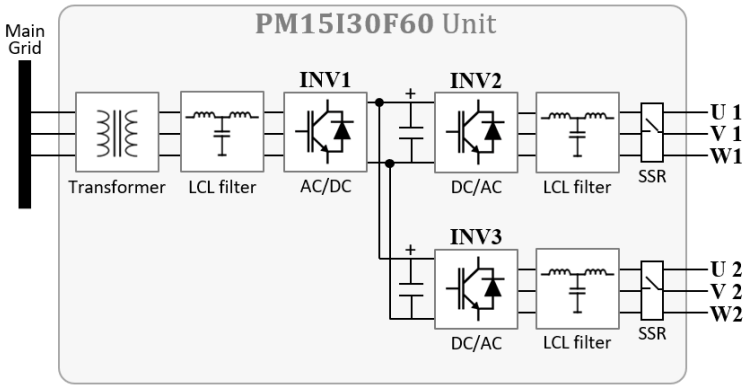

(b) Schematic of PM15I30F60 unit.

Figure G.2: Triphase unit PM15I30F60.

(iii) Unit PM15F120C

The hardware and topology of this unit are shown in Figure G.3. This unit will be configured as an AC/AC back-to-back converter with 2 AC-input and 2 AC-outputs. Its nominal power is 11.5 [kW].

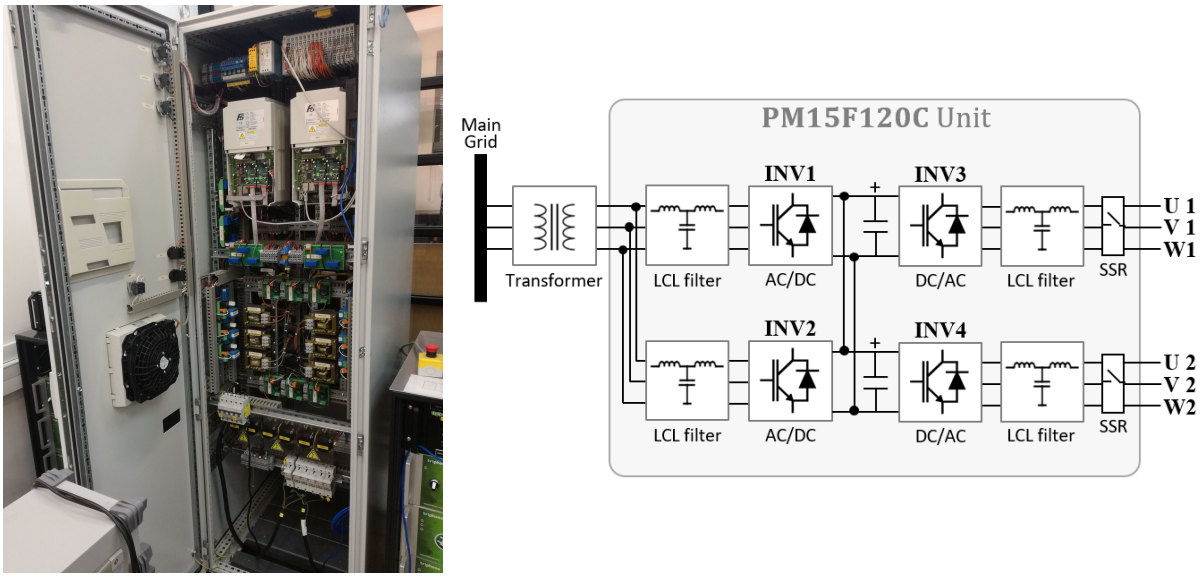

(a) Hardware of PM15F120C unit. (b) Schematic of PM15F120C unit.

Figure G.3: Triphase unit PM15F120C.

(vi) Unit PM5F60R

The hardware and topology of this unit are shown in Figure G.4. This unit will be configured as an AC/AC back-to-back converter with 1 AC-input and 1 AC-outputs. Its nominal power is 5.0 [kW].

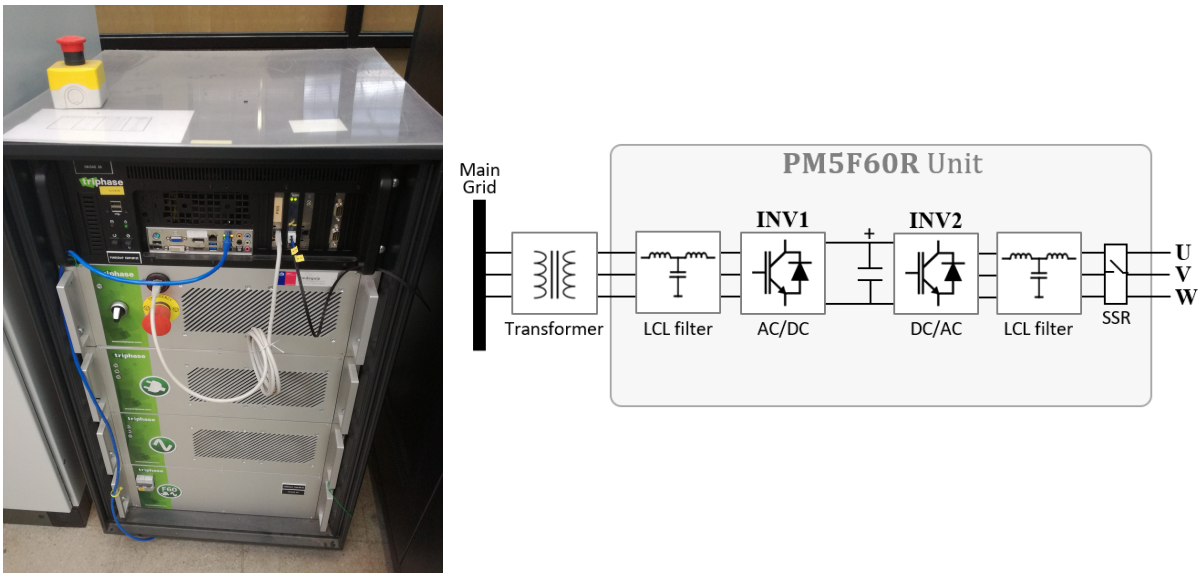

(a) Hardware of PM5F60R unit. (b) Schematic of PM5F60R unit.

Figure G.4: Triphase unit PM5F60R.

(v) Unit PM5F42R

The hardware and topology of this unit are shown in Figure G.5. This unit will be configured as an AC/DC back-to-back converter with 1 DC-input and 1 AC-outputs. Its nominal power is 5.0 [kW].

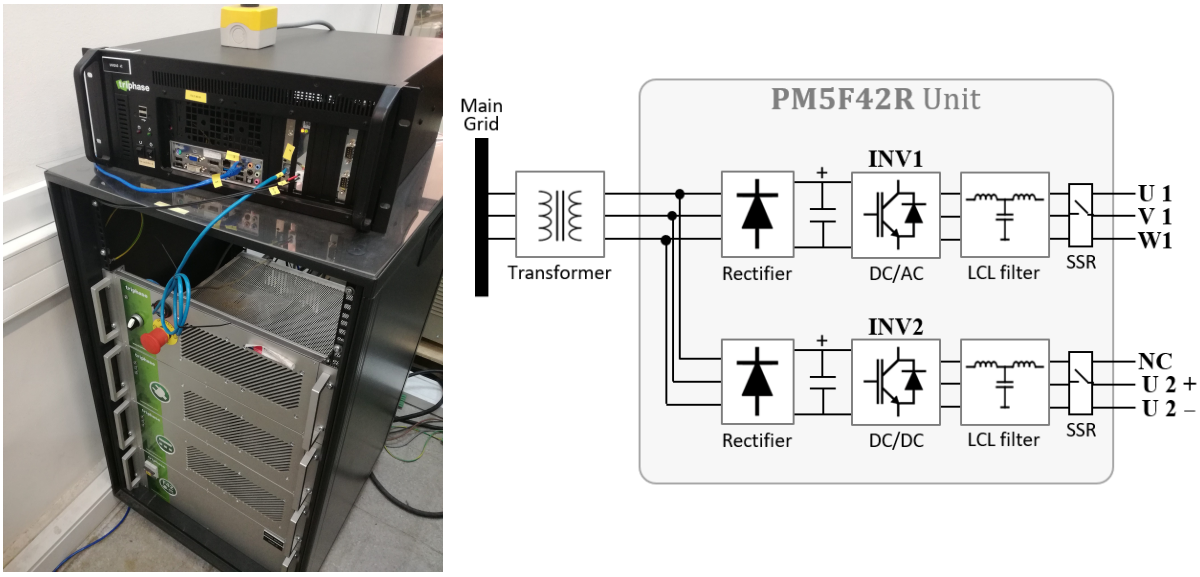

(a) Hardware of PM5F42R unit.

(b) Schematic of PM5F42R unit.

Figure G.5: Triphase unit PM5F42R.

G.2 Prototype of DC-MG

The experimental prototype for the DC MG presented in this section was build by the author of this thesis as part of the subject "ED785-1 Trabajo de Investigación Dirigido". The set-up is a rack consisting of trays and rails that contain thermomagnetic switches, line resistors and inductances, and the MG loads. The experimental set-up and schematic with details about the implemented elements are shown in Fig. G.6.

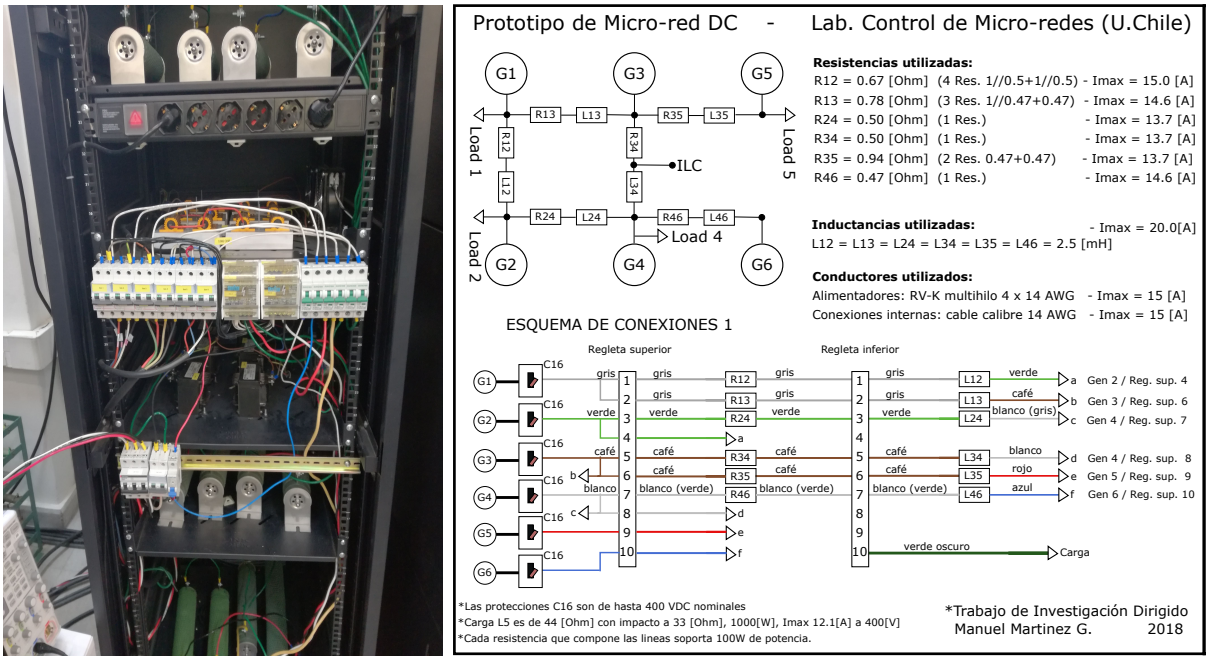

(a) Experimental set-up in rack. (b) Schematic of experimental DC MG.

Figure G.6: Built prototype of DC MG used for this thesis.

The prototype considers 6 DG emulated from the Triphase unit PM15I60F06. The communication is through a fibre optic ring that connects all the Triphase units. The communication architecture considers a master CPU, in this case of the PM5F60 unit, which receives and transmits the consensus variables. Inside the software model of the master, the proposed communication topology is configured.

G.3 Prototype of AC-MG

The experimental prototype for the AC MG will be based on existing topologies already available in the MG Control Lab. The basic design consider 5 DGs emulated from the Triphase units M15I30F60 (2 DGs), PM15F120C (2 DGs) and PM5F60R (1 DG). The experimental set-up for the AC MG is shown in Fig.G.7

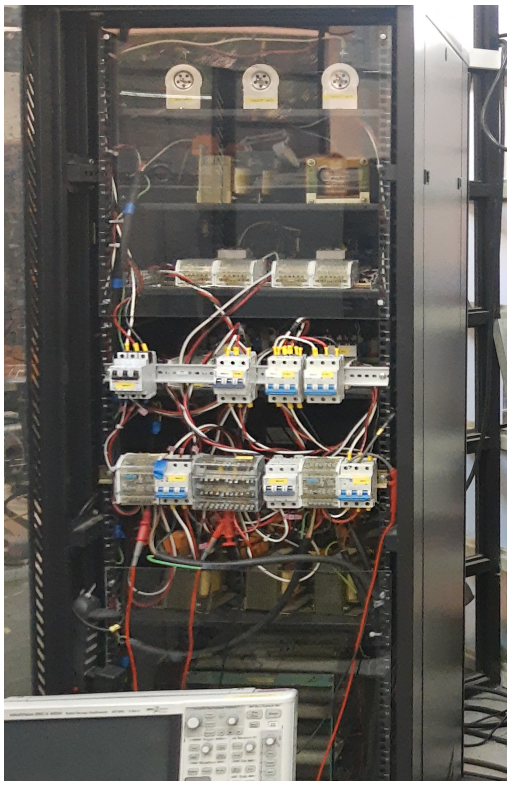

Figure G.7: Prototype of AC MG used for this thesis.

G.4 Hybrid AC/DC MG prototype

The experimental prototype for the hybrid AC/DC MG considers the combinations of the two previous developments, AC and DC MG set-ups. To complete the hybrid MG an additional Triphase unit is considered as an ILC to interfacing both AC and DC sides. The ILC will be emulated via the Triphase PM5F42R unit, which acts as a grid feeding (current-source) converter for both sides. For cooperative control of the ILC, it is considered a communication between two units; The Triphase PM5F60R unit communicates the ILC with the AC side while the Triphase PM15I60F06 unit communicates the DC side DGs. The strategy is summarised in Figure G.8

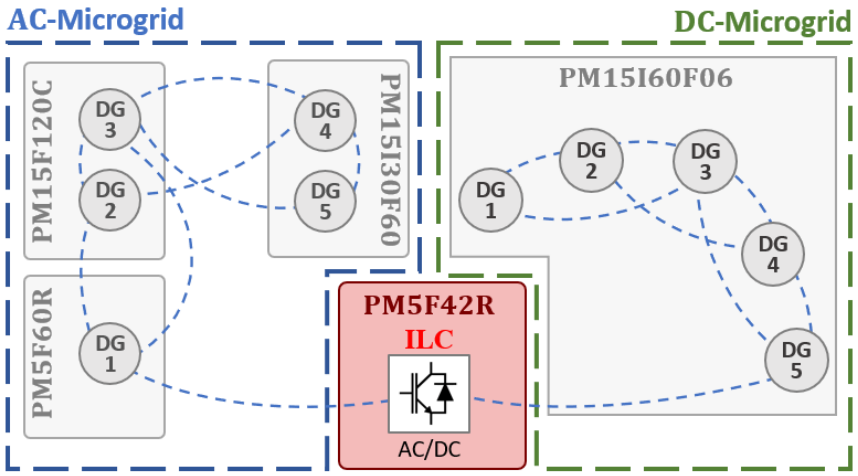

Figure G.8: Diagram of proposed experimental setup for hybrid AC/DC MG.